Garnet Systematics of Subducted Continental Margins

Dissertation

zur

Erlangung des Doktorgrades (Dr. rer. nat.)

der

Mathematisch-Naturwissenschaftlichen Fakultät

der

Rheinischen Friedrich-Wilhelms-Universität Bonn

vorgelegt von

Sascha Sandmann

aus

Dinslaken

Bonn, Januar 2015

Angefertigt mit Genehmigung der Mathematisch-Naturwissenschaftlichen Fakultät
der Rheinischen Friedrich-Wilhelms-Universität Bonn

1. Gutachter: PD Dr. Thorsten J. Nagel
2. Gutachter: Prof. Dr. Nikolaus Froitzheim

Tag der Promotion: 12. Juni 2015

Erscheinungsjahr: 2015

Table of Contents

1 Introduction

1.1 Tectonics of continental margins

Continental margins separate the two types of crust that build up the earth's solid shell: (1) Oceanic crust is up to 7 km thick and located beneath an average water depth of 4.5 km (Kearey et al., 2009). Oceanic lithosphere and crust is formed by sea floor spreading, i.e. the upwelling and partial melting of material from the asthenosphere at ocean ridges (e.g. Dietz, 1961; Whitehead et al., 1984). It's typical internal structure is a top to bottom sequence of pelagic sediments, basaltic pillow lavas, a basaltic sheeted dike complex, layered gabbroic rocks, and ultrabasic cumulates. At magma poor, slow spreading ridges lithospheric mantle can be exhumed at the sea floor. The progressive growth of oceanic lithosphere is compensated by the consumption of lithosphere in subduction zones. (2) Continental crust is up to 70 km thick with an average thickness of c. 41 km (Christensen and Mooney, 1995) and of andesitic or granodioritic average composition (McLennan and Taylor, 1996). Continental and oceanic crust are in isostatic equilibrium. Since oceanic crust is much thinner than continental crust, these two types consequently differ in their specific density. The mean density of oceanic crust is c. 2890 kg/m^3 (Carlson and Raskin, 1984) while the mean density of continental crust is c. 2830 kg/m^3 (Christensen and Mooney, 1995). The oldest in-situ preserved oceanic crust is located in the Ionian Sea and the east Mediterranean basin and ranges in age from c. 270 to c. 230 Ma (Müller et al., 2008). In contrast, continental crust can reach ages of over 3 billion years (e.g. Qiu et al., 2000; Zhang et al., 2006).

Passive continental margins result from rifting of continental lithosphere that leads to the formation of oceanic basins between the resulting margins. They outline regions of extended continental crust where the thickness of the continental crust is gradually reduced towards the ocean. As a result of isostatic compensation these margins subside below sea level (Kearey et al., 2009). The thinning of the crust is caused by movement of tilted blocks on oceanward dipping faults (Fig. 1.1). Single blocks may even be positioned as isolated allochthons with exhumed mantle on their continentward side (e.g. Manatschal, 2004). The width and steepness of these margins depend on strength and rheology of the lithosphere. Thick, cool, and strong lithosphere produces rather narrow margins during rifting while thin, hot, and weak lithosphere tends to form wide margins where deformation is distributed across zones of several hundreds of kilometres (Kearey et al., 2009). Figure 1.1 illustrates a schematic transect through a non-volcanic passive continental margin. This series can be covered by deposits of volcanic material and added by gabbroic intrusions

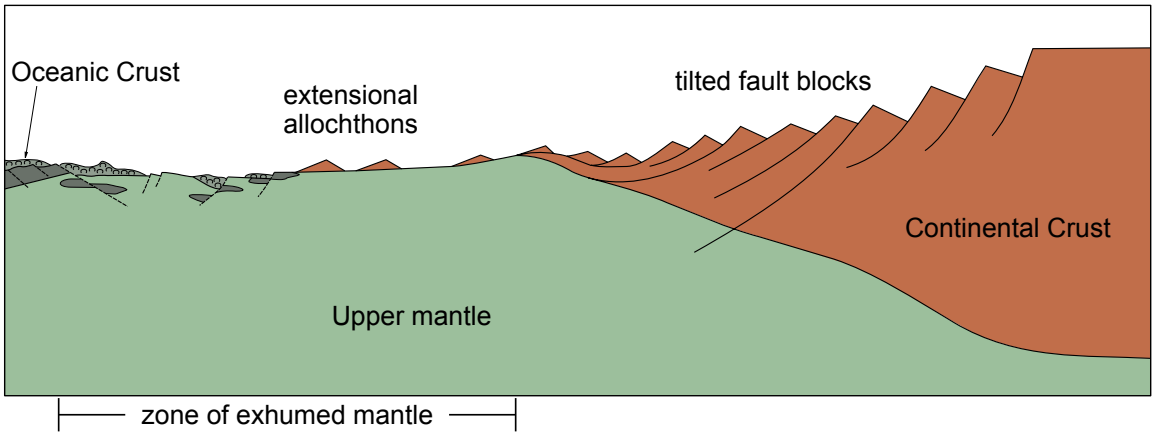

Figure 1.1: Schematic transect of a non-volcanic passive continental margin (not to scale; compiled after Louden and Chian, 1999 and Manatschal, 2004).

into the lower crust if volcanism proceeded during rifting.

Active continental margins are zones of convergent movement of tectonic plates where the upper plate is continental (Wilson, 2000). An oceanic lower plate is typically subducted into the mantle (Fig. 1.2). Excess density in the down going slab is the driving force for movement of plates towards subduction zones and causes mid-ocean ridges to spread (Stern, 2002). As a result, formation and recycling of oceanic crust is a cyclic process that is observable e.g. in the pacific, where the oldest oceanic crust is c. 180 Ma old (Müller et al., 2008). Caused by progressive cooling and accretion of asthenospheric mantle to the bottom of the lithosphere oceanic lithosphere becomes negatively buoyant during its movement from a mid-ocean ridge towards a subduction zone.

If consumption of oceanic crust is followed by the advent of continental crust the geometry of a subduction zone changes fundamentally (Warren et al., 2008; Agard et al., 2009). Continent-continent collision causes intense deformation of both upper and lower plate and formation of a collisional orogen. Ultimately, the convergent plate movement comes to a standstill. Alpine-type orogens represent collision zones of passive continental margins that formed during the breakup of Pangea. If distal portions of the lower plate continental crust remain coupled to the down going oceanic slab they can be transferred to mantle depth.

At subduction zones temperature isopleths are bent downwards because cold material is transported into the mantle. The subducted slab is affected by heating and compression. As long as rocks are coupled to the downgoing slab they are affected by raising pressure and temperature (PT) conditions (e.g. Spear et al., 1984). If they are decoupled from the slab and transported towards the surface before they completely equilibrated to mantle temperatures they can be affected by a phase of

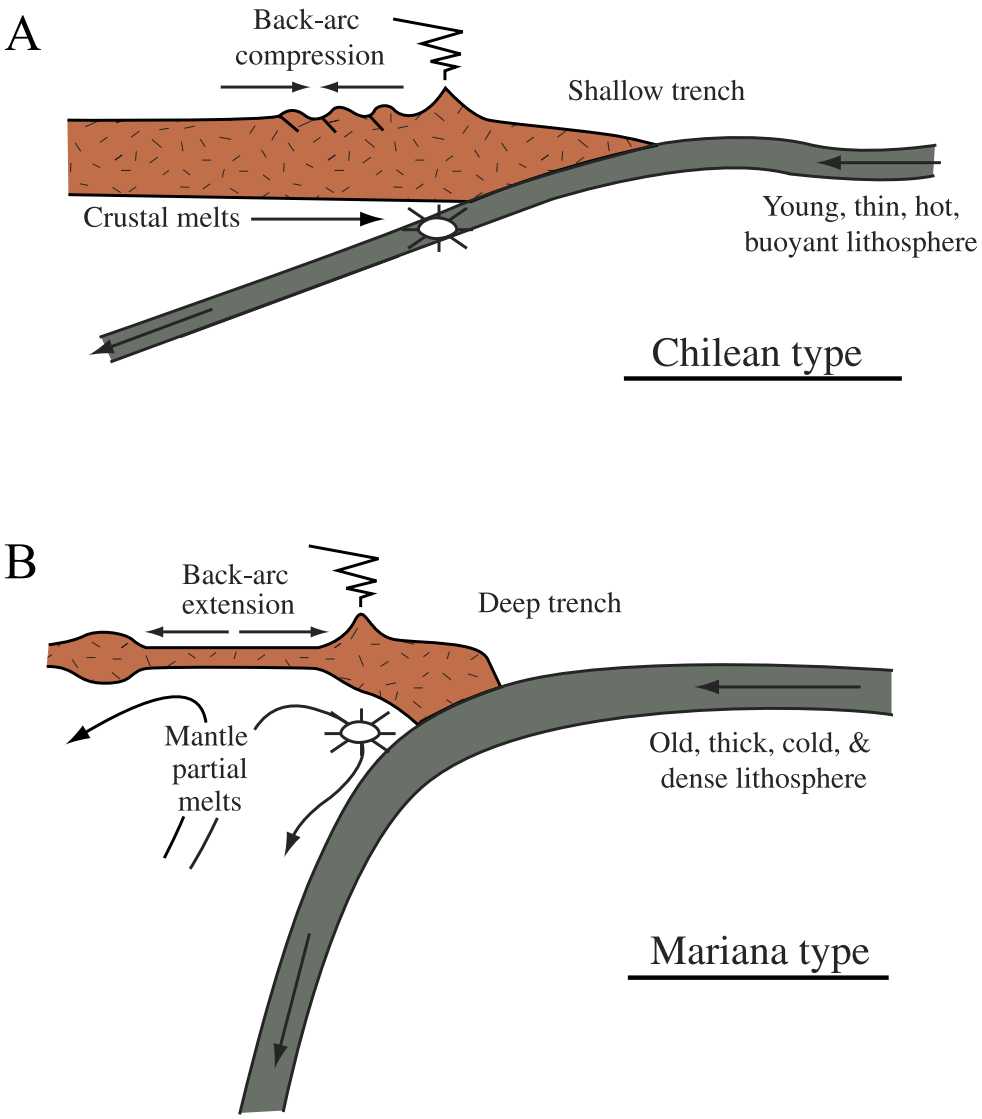

Figure 1.2: Two end-member types of subduction zones with continental upper plates (after Stern, 2002). A: Shallow dipping lower plate with compression in the upper plate; B: Steeply dipping lower plate with extension in the upper plate.

continuing heating contemporaneous with incipient decompression or by isothermal uplift and decompression (e.g. Ernst and Liou, 2008; Hacker et al., 2010). Finally, exhumation of rocks to the surface causes cooling along with decreasing pressure conditions. This sequence can be visualized in PT-space (Fig. 1.3). Rocks may be buried repeatedly before they are exhumed to the surface (for example by circulation inside a subduction channel) and, thus, run through several PT paths.

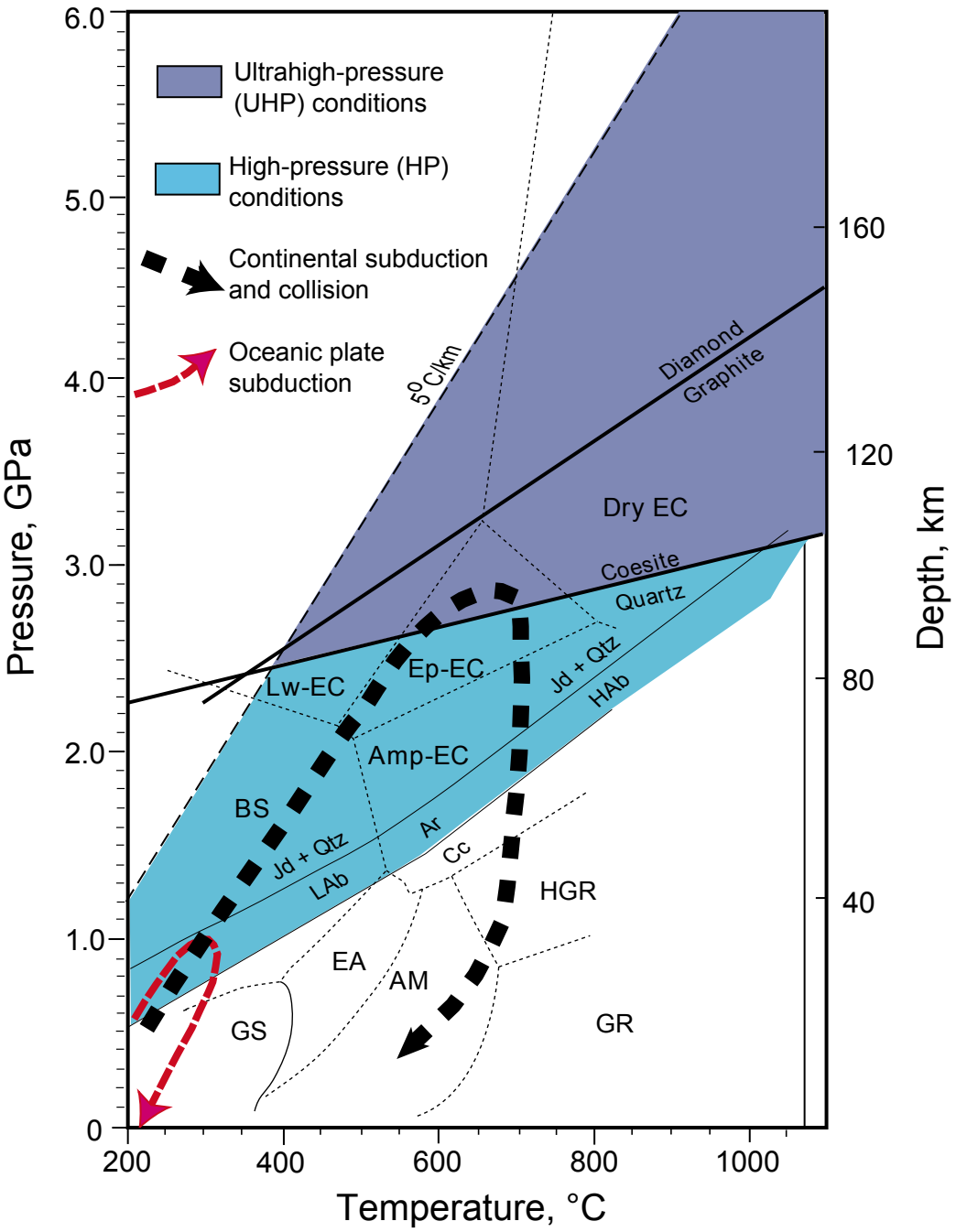

Figure 1.3: Schematic P-T paths of subducted and exhumed continental and oceanic rocks (modified from Ernst and Liou, 2008). Thick-dashed black line: P-T path of continental UHP rocks from the Kaghan Valley, western Himalaya. Raising PT conditions are followed by near isothermal decompression after peak pressure conditions. Thin red line: P-T path of oceanic rocks from the Franciscan HP belt, Diablo Range, western California. A subduction-zone geothermal gradient of 5°C/km is shown for reference. Mineral abbreviations: Ar = aragonite; Cc = calcite; Jd = jadeite; Qtz = quartz; LAb = low albite; and HAb = high albite. Metamorphic-facies abbreviations: AM = amphibolite; Amp-EC = amphibolite-eclogite; BS = blueschist; EA = epidote amphibolite; EC = eclogite; Ep-EC = epidote-eclogite; GR = sillimanite-granulite; GS = greenschist; HGR = kyanite-granulite; Lw-EC = lawsonite-eclogite; and Px-Hf = pyroxene hornfels.

1.2 Subduction of continental rocks

In contrast to oceanic crust continental crust is positively buoyant with respect to the mantle (Massonne et al., 2007). Phase transformations of minerals to high-pressure phases seemingly has no effect on this buoyancy (Chopin, 2003; Peterman et al., 2009). Only if melting occurs and the melt migrates out of the subducting unit, the buoyancy of the remaining residue is reduced (Hacker et al., 2011). Nevertheless, findings of high-pressure (HP) polymorphs of silica and carbon, coesite and diamond, respectively, in dominantly felsic continental units proof that these can be subjected to ultrahigh-pressure (UHP) metamorphic conditions in depths exceeding 120 km (e.g. Chopin, 2003 and references therein). Metastable coesite and diamond survive up to surface conditions as inclusions in mechanically strong host minerals like garnet and zircon. However, significant rock volumes of (U)HP units may escape mineral equilibration to (U)HP metamorphic conditions (Jolivet et al., 2005). Crystal nucleation and mass transfer is often hampered because the required fluid flow is generally limited in HP and UHP bodies (Rumble, 1998; Chopin, 2003). Especially granitic orthogneisses often retain their original mineral assemblage through entire subduction-exhumation cycles and do not equilibrate to the high pressure and temperature conditions they were subjected to (e.g. Bruno et al., 2001).

Hacker and Gerya (2013) summarised six tectonic settings that can cause burial of continental rocks to ultrahigh-pressure metamorphic conditions (Fig. 1.4). Intracontinental subduction can occur in a weak zone inside a purely continental realm. Possible examples are the early Palaeozoic orogen of southeastern China (Faure et al.,

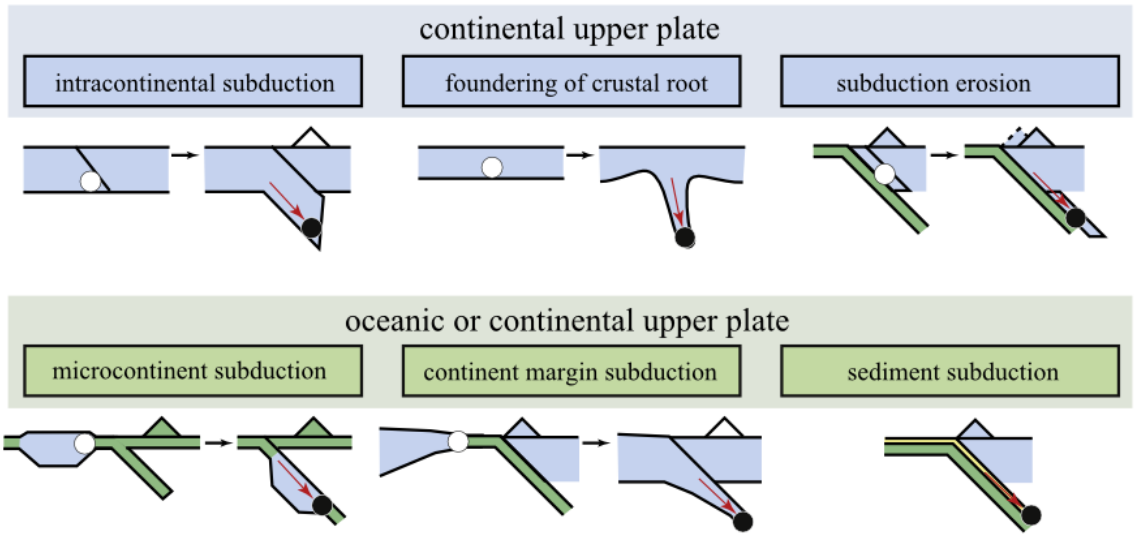

Figure 1.4: Six tectonic settings in which felsic rocks can be subjected to ultrahigh-pressure metamorphic conditions (from Hacker and Gerya, 2013).

2009) and the Pamir in central Asia (Burtman and Molnar, 1993). Gravitational foundering of crustal rocks to great depth was proposed beneath a thick orogenic root (Burtman and Molnar, 1993). Subduction erosion refers to abrasion of upper plate units that are carried to greater depth by incorporation into the down going slab (Cloos and Shreve, 1988; van Huene et al., 2004; Gerya and Stöckhert, 2006). Microcontinents can be subducted if they remain coupled with the surrounding less buoyant oceanic crust (e.g. Kylander-Clark et al., 2012). A continental margin that enters a subduction zone after consumption of an oceanic basin can be transferred to UHP conditions (Chopin, 2003). Felsic sediments that rest on top of oceanic crust can be subducted together with the underlying basic lithologies (Cloos and Shreve, 1988).

1.3 Exhumation mechanisms

A number of different mechanisms have been proposed for the exhumation of continental high-pressure metamorphic rocks (e.g. Warren, 2013; Hacker and Gerya, 2013; and references therein). There are models that predict semi-coherent exhumation of continental terranes with only little internal deformation, while other models propose mélange-like exhumation inside a subduction channel with intense internal deformation. Kylander-Clark et al. (2012) compared the characteristics of continental UHP terranes worldwide and concluded that thin, distal continental margins are generally subducted and exhumed faster than thick, proximal continental portions. Similar results were inferred from thermo-mechanical numerical modelling (Burov et al., 2014). Exhumation rates rather resemble plate velocities (up to 1-2 cm/yr) than erosion rates (e.g. Hermann et al., 2001; Chopin, 2003).

Eduction refers to exhumation of a subducted unit by reversed plate motion along with minor internal deformation (Andersen et al., 1991). In this case exhumation doesn't require a thrust fault at the base of the exhumed unit. If the force that pulls the slab into the mantle exceeds the internal strength of the slab, necking of the slab initiates (van Hunen and Allen, 2011; Fig. 1.5A). This process detaches the continental part of the slab from the negatively buoyant oceanic portion. The positive

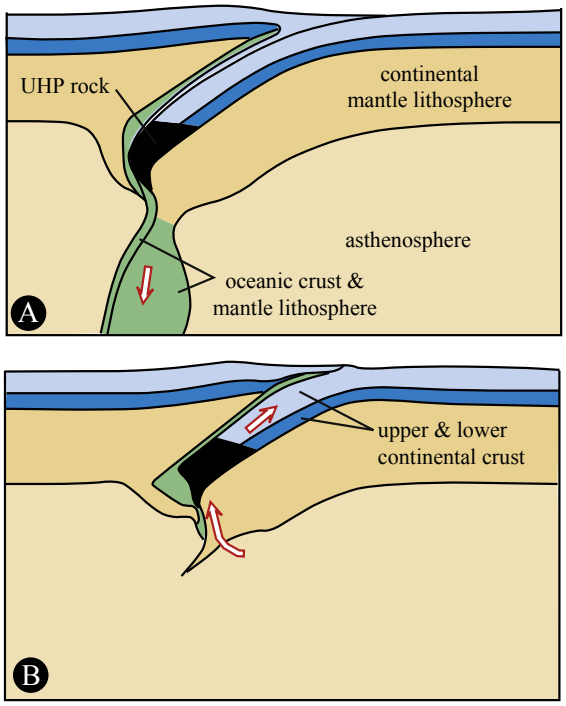

Figure 1.5: Tectonic model for the exhumation of subducted continental crust by eduction (from Hacker and Gerya, 2013; after Andersen et al., 1991 and Duretz et al., 2012). A: A continent attached to an oceanic slab follows the latter to great depth. If the force that pulls the slab into the mantle exceeds the internal strength of the slab, necking of the slab initiates. B: The positively buoyant continental portion then moves upwards.

buoyancy of the continental slab then causes upward movement contemporaneous with orogenic extension in the upper plate (Duretz et al., 2012; Fig. 1.5B). Eduction is a favoured process if the continental crust is strongly coupled to the underlying mantle lithosphere (Duretz and Gerya, 2013).

In contrast, **extrusion** is a proposed exhumation mechanism for continental crust that is not strongly coupled to the underlying mantle lithosphere (Fig. 1.6). When the buoyancy force exceeds slab pull the buoyant crust may detach from the lithospheric mantle and extrude upwards while subduction of the lithosphere continues (Chemenda et al., 1995; Fig. 1.6C).

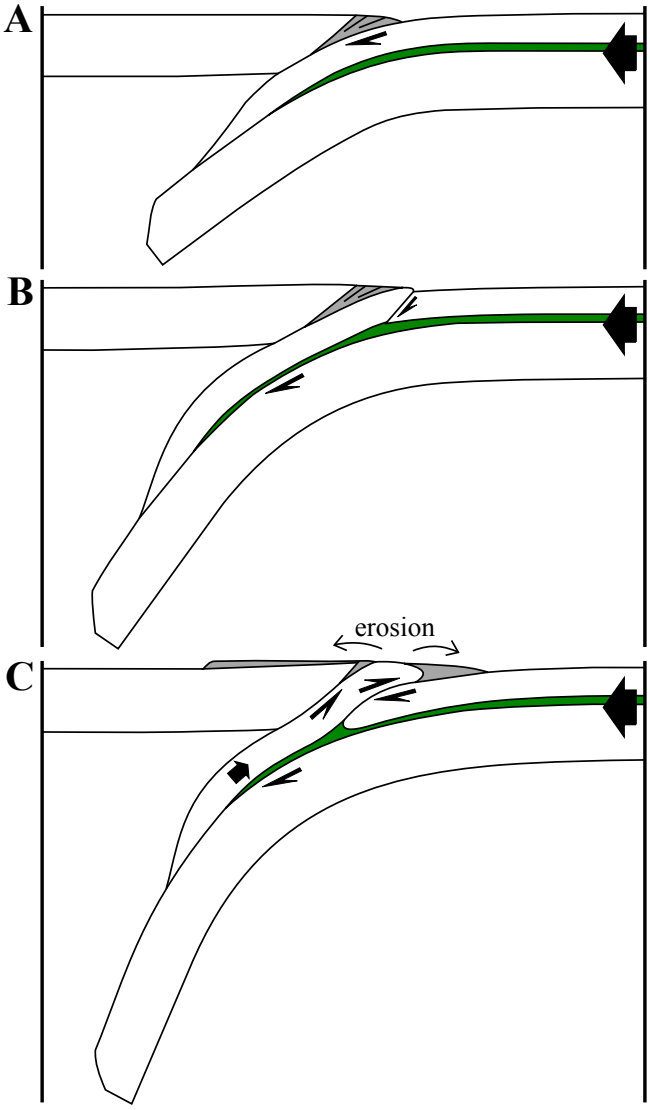

Figure 1.6: Tectonic model for exhumation of subducted continental crust by extrusion (from Chemenda et al., 1995). A: A continental margin is subducted beneath a continental upper plate. B: The buoyancy force exceeds the slab pull and the crust detaches from the lithospheric mantle. C: The crust extrudes upwards while subduction of the lithosphere continues. Proximal continental crust underplates the extruded unit.

The mechanism of **slab extraction** was first proposed for the exhumation of the Adula Nappe (Froitzheim et al., 2003), which is investigated in chapter 2 of this study. For this mechanism to apply two consecutive subduction zones that dip in the same direction are required where the exhumed crustal rocks are originally part of the lowermost plate (Fig. 1.7A). When the superimposed slab of the middle plate is removed by sinking into the mantle, the underlying high-pressure rocks are isostatically uplifted (Fig. 1.7B). In this case, buoyancy of the crustal high-pressure rocks does not cause exhumation but the negative buoyancy of the extracted slab (Froitzheim et al., 2003).

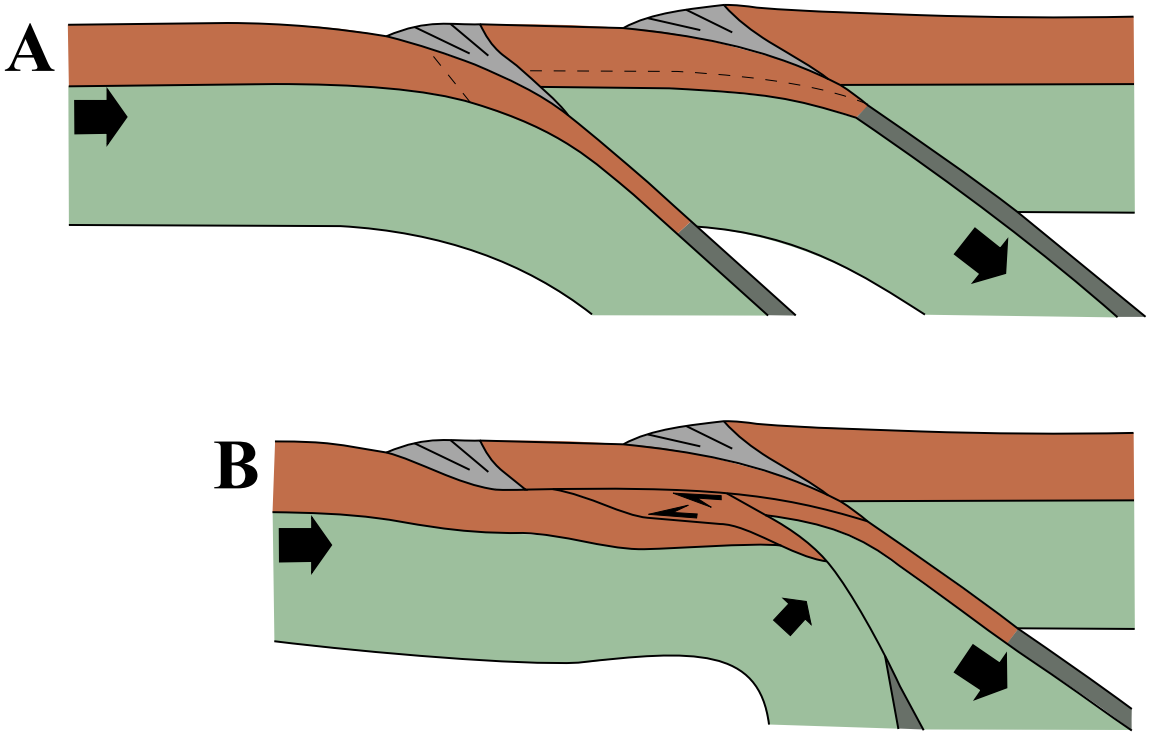

Figure 1.7: Tectonic model for exhumation of subducted continental crust by slab extraction (simplified after Froitzheim et al., 2003). A: Two consecutive subduction zones dip in the same direction. B: When the slab of the middle plate is extracted, the underlying high-pressure rocks are uplifted to fill the arisen void.

Subducted small continental terranes can be exhumed by the process of **slab rollback** (Brun and Faccenna, 2008; Husson et al., 2009; Vogt and Gerya, 2014). When a buoyant terrane enters the subduction zone it slows rollback of the lower plate and causes steepening of the slab (Hacker and Gerya, 2013; Fig. 1.8B). If the terrane detaches from the slab rollback quickens. This fast rollback enables extension in the upper plate that, in turn, can provide room for the continental terrane to lift up (Fig. 1.8C).

Hacker et al. (2000) proposed that the UHP terrane of Dabie Shan in eastern China was exhumed by **rotation** of the subducted continental unit. This unit is underlain

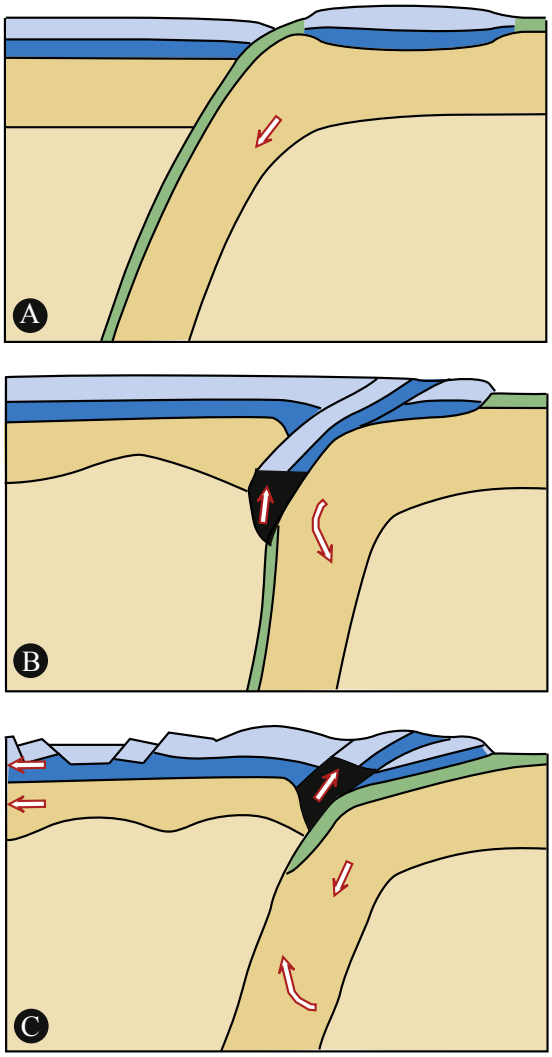

Figure 1.8: Tectonic model for exhumation of subducted continental crust by slab rollback (from Hacker and Gerya, 2013). A: Initial tectonic situation with a shallow dipping slab. B: The continental terrane slows rollback and steepens the slab. C: The detached terrane exhumes and slab rollback quickens.

by a thrust fault with increasing offset parallel to an increase in metamorphic pressure that affected the unit. Exhumation related stretching lineations and the metamorphic pressure gradient indicate clockwise rotation of this unit (Hacker et al., 2000; Hacker and Gerya, 2013). Subduction of an oblique continental margin might be required to enable this exhumation process (Fig. 1.9).

If the continental material is subducted inside a confined **subduction channel**, it tends to be affected by circulation that is driven by traction at the base of the channel and upward movement of the enclosed material caused by buoyancy (e.g. Cloos and Shreve, 1988; Raimbourg et al., 2007; Hacker and Gerya, 2013; Burov et al., 2014). The material inside the channel can be exhumed if newly subducted material pushes older material up (Li and Gerya, 2009), when buoyancy inside the channel exceeds

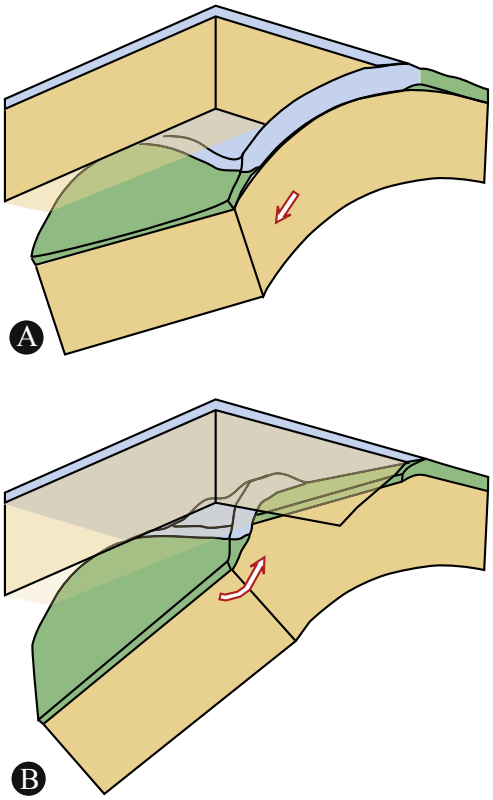

Figure 1.9: Tectonic model for exhumation of subducted continental crust by microplate rotation (from Hacker and Gerya, 2013; after Hacker et al., 2000). A: A continental microplate is subducted in an oblique angle. B: Rotation of the microplate exhumes that part of the unit that was subjected to greatest depth.

traction (Warren et al., 2008), or if a subducted indenter squeezes the channel (Gerya et al., 2008). Metamorphic terranes that formed by this process should then be characterised by various rock types of which only small portions display (U)HP assemblages (e.g. Jolivet et al., 2005; Krebs et al., 2011) and by scattered isotopic ages related to HP conditions (e.g. Federico et al., 2007).

1.4 Radiometric dating

Different radiometric dating methods were developed to reveal absolute ages that can be assigned to metamorphic stages of subduction-exhumation cycles. Parent isotopes decay with an individual constant (λ) that is independent from external chemical and physical factors and daughter isotopes are enriched over time in closed systems. Because of differing partition coefficients parent isotopes are incorporated into natural minerals in different amounts. The isochron dating method takes advantage of this circumstance (Fig. 1.10; Nicolaysen, 1961). It is used for Rb-Sr, Sm-Nd, and Lu-Hf dating. But for this method to apply the analysed phases have to be part of the HP mineral assemblage and they have to be in chemical equilibrium at the time that is to be dated. Lu-Hf garnet geochronology was applied to the samples of this study. If minerals are affected by raising temperatures, they may pass a temperature limit where their rare earth element (REE) content becomes mobile (i.e. diffusion from the lattice site) and the daughter isotopes of a radiometric decay are lost by

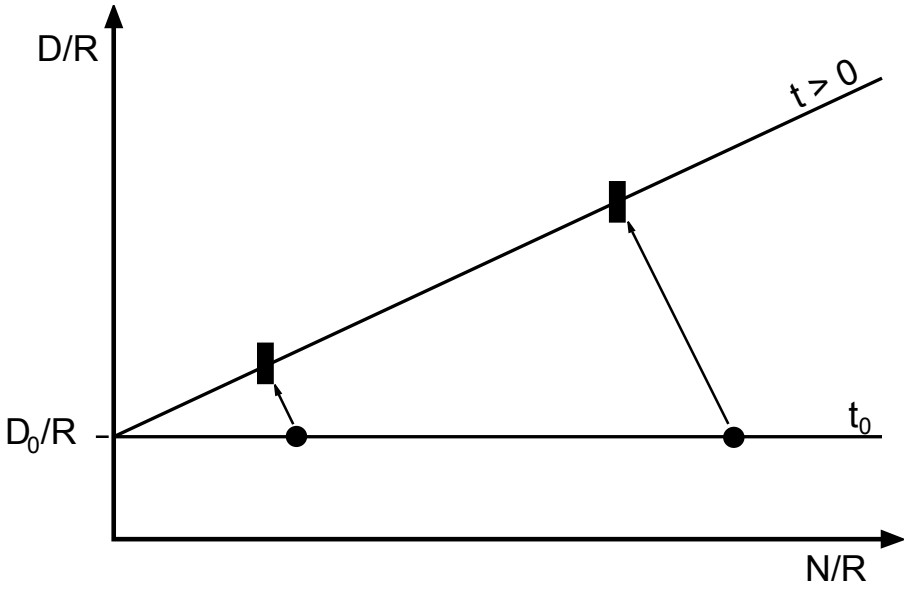

Figure 1.10: Schematic isochron plot after Nicolaysen (1961). The ratio of parent isotope and reference isotope (N/R) is shown on the x-axis and the ratio of daughter isotope and reference isotope (D/R) is given on the y-axis. The reference isotope cannot be the product of a decay system and is typically from the same element as is the daughter isotope. Partition coefficients determine the amount of parent isotopes that are incorporated in natural minerals. At the time of chemical equilibrium (t_0) ratios of parent and reference isotopes of all investigated phases define a line without a slope. When the system is closed (i.e. the investigated isotopes are immobile) the amount of parent and daughter isotopes in a phase is solely triggered by the decay of parent isotopes. After a given time ($t > 0$) the mineral phases define a line with a positive slope. This slope is directly proportional to the time that elapsed since the system was closed (i.e. the metamorphic age of the sample). These ages are particularly well defined if one phase is characterised by extraordinary high partition coefficients for the parent isotope's element (e.g. Lu in garnet).

equilibration with the rocks matrix (Dodson, 1973). Revealed ages then represent that point in time when the mineral cooled below its specific closure temperature (T_C) and mobile daughter isotopes became completely immobile during retrograde metamorphism (i.e. the exhumation of metamorphic rocks).

1.4.1 Methods for dating high-pressure metamorphism

K-Ar and ^{40}Ar-^{39}Ar dating of mica (Merrihue and Turner, 1966) has been applied for decades in order to date high grade metamorphic processes (e.g. Raith et al., 1978; Chopin and Maluski, 1980; Kligfield et al., 1986; Treloar et al., 1989; Ratschbacher et al., 2004). Some of these data later turned out to be geological insignificant due to excess argon (e.g. Ruffet et al., 1997; Sherlock et al., 1999). Diffusive transported ^{40}Ar that was incorporated into the analysed minerals during the metamorphic cycle can result in too high apparent K-Ar ages (Li et al., 1994; Arnaud and Kelley, 1995; Ruffet et al., 1995; Scaillet, 1996). This problem often arises when a metamorphic unit is affected by temperature dominated metamorphism subsequent to high pressure metamorphism.

The Rb-Sr method utilises mineral phases that were in isotopical equilibrium when the analysed sample was affected by high grade metamorphic conditions. A preferred phase is white mica with its high content of Rb (e.g. Sherlock et al., 1999; Li et al., 2000). But the closure temperature of the Rb-Sr system is considerably lower than that of the Sm-Nd and Lu-Hf systems making this method preferably used to date retrograde cooling of high grade metamorphic cycles (e.g. Li et al., 2000).

Uranium-Pb geochronometry of zircon is a proven method to date HP metamorphic events in a huge variety of lithologies since zircons atomic structure remains stable over long periods of geological time (Harley and Kelly, 2007; and references therein). Similar to garnet zircon often preserves growth zones within single grains. Zircon in HP rocks can form over a wide range of conditions, i.e. prograde subduction, peak pressure and temperature conditions, and post-peak exhumation (Harley et al., 2007). Thus, zircon domains need to be assigned to metamorphic stages by in situ trace element analysis (Rubatto, 2002). Seemingly, the presence of fluids or melt is required to enable crystallization of zircon in metamorphic rocks (Rubatto and Hermann, 2003, 2007) and preservation of older zircon is the rule in HP metamorphic rocks that were affected by temperatures of less than c. 650 °C (Hermann et al., 2001; Katayama et al., 2001). Hence, subduction related metamorphism under blueschist- or lower eclogite-facies conditions may remain undetected by zircon geochronometry (Liati et al., 2009).

Phase transformations to HP mineral assemblages enable the formation of garnet in nearly all lithologies. Garnet establishes compositional core-to-rim gradients of its major elements Ca, Fe, Mg, and Mn which are controlled by diffusional element supply towards the nucleating crystal and chemical equilibrium between the crystal and its surrounding matrix (Spear and Daniel, 2001; Konrad-Schmolke et al., 2005). Decreasing grossular and spessartine components along with a decreasing iron-magnesium ratio from core to rim are indicative for a preserved growth zoning. Progressive heating can cause diffusional homogenisation of this original garnet growth zoning (Carlson and Schwarze, 1997; Caddick et al., 2010). Similar to major element zoning, garnet establishes characteristic zoning patterns in its rare earth element budget (e.g. Skora et al., 2006). When garnet starts to grow it tends to incorporate high amounts of available Lu (Konrad-Schmolke et al., 2008b). Thus, garnet that retained its initial prograde growth zoning is characterised by highly elevated concentrations of Lu in the crystals cores with decreasing Lu content towards garnets rims (Skora et al., 2006). In contrast, Sm is incorporated at later stages of garnet growth and, thus, concentrated close to garnet rims (Skora et al., 2006). Diffusion coefficients of bivalent elements in garnet are generally one order of magnitude larger than those of trivalent REEs (Carlson, 2012). Hence, garnet's prograde zoning in REEs can be preserved even when major elements are already re-equilibrated.

Temperature estimations for the diffusive closure temperature of the Lu-Hf system inside garnet range from 600 °C to 970 °C (e.g. Duchêne et al., 1997; Skora et al., 2008; Schmidt et al., 2011) with the rule that larger grains and faster cooling rates push the estimations towards higher values (Scherer et al., 2000; Skora et al., 2008). These values are greater than or equal to those of the Sm-Nd system (Scherer et al., 2000 and references therein). Since the temperatures that affect subducted continental rocks are often smaller than the above given estimations, Lu-Hf geochronology carried out on garnet and mineral phases that were in chemical equilibrium with garnet at HP conditions is a perfect tool to reveal absolute ages that can be attributed to the initiation of prograde garnet growth (e.g. Ague and Carlson, 2013; Baxter and Scherer, 2013).

Scherer et al. (2000) showed that monazite and apatite inclusions inside garnet may bias Sm-Nd data while they have little or no influence on the Lu-Hf system. In contrast, inclusions of Hf-rich zircon can affect Lu-Hf data. Lagos et al. (2007) presented a method to effectively remove the Hf-rich phases zircon and rutile during garnet digestion.

Resorption of garnet can affect the geological significance of obtained Lu-Hf garnet

ages. During resorption Lu migrates into the remaining garnet crystals while Hf is lost into the rocks matrix (Kelly et al., 2011). The absolute age bias is controlled by the degree of garnet resorption and the time difference between growth of garnet and resorption. The age effect may be negligible when resorption happened shortly after garnet growth. But Lu-Hf garnet ages are biased towards younger apparent ages when resorption took place considerably later than garnet growth.

1.4.2 Lu-Hf garnet geochronology

The samples that were selected for Lu-Hf geochronometry were crushed and separated into two splits. One split was powdered and used for bulk rock analyses. The second split was used for mineral separation. Mineral separates were cleaned in an ultrasonic bath in 2.5 M HCl and rinsed twice with deionised water. A mixed ^{176}Lu-^{180}Hf tracer was added to all samples before digestion. Two digestion methods were applied: (1) Mineral separates and selected whole rock powders were dissolved by applying the "table top" procedure that was first described by Lagos et al. (2007). This method leaves behind the Hf-rich minerals rutile and zircon that can preserve isotope signatures that did not equilibrate under HP conditions. These samples were digested with HF-HNO_3-$HClO_4$ in closed Teflon vials on 120 °C hotplates and subsequently dried down followed by addition of 6 N HCl. The undigested phases were then removed by centrifugation. (2) Some selected whole rock powders were dissolved by applying a method that ensures complete digestion. These samples were stored inside steel-jacketed PARR bombs with HF-HNO_3 for 5 days at 180 °C. Subsequently, $HClO_4$ was added to the samples. The samples were dried down and re-dissolved in 6 N HCl. Finalising, sample solutions of both methods were then dried down and re-dissolved in 3 N HCl.

Lutetium and Hf were separated from matrix elements by applying the single-column element separation procedure that was developed by Münker et al. (2001): Sample solutions were loaded onto columns of Eichrom® Ln-spec resin and rinsed with 10 ml of 3 N HCl. Lu was then eluted using 10 ml 6 N HCl and the columns were rinsed with two additional resin-bed volumes of 6 N HCl. Ti was removed using a mixture of 0.09 N citric acid, 0.4 N HNO_3, and 1% H_2O_2. Subsequently, Hf was eluted using 2 N HF. All Hf-cuts were further purified by an additional clean-up procedure: They were dried down and re-dissolved in 6 N HCl. The solutions were loaded onto the columns again. Remaining matrix elements and especially remains of Lu were removed using four resin-bed volumes of 6 N HCl. Finally, Hf was eluted using 2 N HF.

Lutetium and Hf measurements were carried out on a Thermo Neptune MC-

ICPMS. Instrumental mass bias on Hf isotope ratios was corrected by using $^{179}Hf/^{177}Hf$ and the exponential law. Measured $^{176}Hf/^{177}Hf$ ratios are given relative to $^{176}Hf/^{177}Hf$ = 0.282160 for the Münster Ames Hf standard, which is isotopically identical to the JMC-475 standard. The external reproducibility was estimated by the empirical relationship 2σ external reproducibility $\approx 4\sigma m$ (σm = standard error of a single analysis; e.g. Bizzarro et al., 2003). Hafnium compositions were calculated using both the tracers and the natural Lu compositions (Amelin et al., 2011). The difference between the two was then added to the external reproducibilities used for the isochron calculations. Isobaric interferences on ^{176}Hf and ^{180}Hf were corrected by monitoring ^{173}Yb, ^{175}Lu, ^{181}Ta, and ^{183}W and their natural isotope compositions. Naturally occurring Yb in the Lu cuts was used for mass bias correction on Lu isotope ratios (Vervoort et al., 2004; Lagos et al., 2007). Interferences on ^{176}Lu were corrected by monitoring ^{173}Yb and ^{177}Hf and the natural isotope compositions.

Regressions of isochrons and ages were obtained using ISOPLOT v. 2.49 (Ludwig, 2001) and a decay constant of $\lambda = 1.867 \times 10^{-11} yr^{-1}$ for the decay of ^{176}Lu (Scherer et al., 2001; Söderlund et al., 2004).

1.5 Aim of this study

The aim of this study is to present Lu-Hf garnet ages of continental units from different tectonic settings. These ages are combined with major element and Lu characterisations of selected garnet grains in order to pin point the age information with metamorphic stages. On the basis of these data and additional literature data a tectonic model for each location is developed. The presented four case studies contribute to the discussion of the following questions:

- What is the duration of subduction-exhumation cycles of continental margins?
- Were the investigated continental units subducted and exhumed as cohesive terranes or were they dismembered inside subduction channels?

1.5.1 Case studies

The Adula Nappe in the eastern Central Alps (Chapter 2) represents that part of the former European passive continental margin that was subjected to highest pressure and temperature conditions following consumption of the Penninic ocean basins (Fig. 1.11; Froitzheim et al., 1996; Schmid et al., 2004). It comprises a mixture of various continental gneisses with local occurrences of metabasic, metaultrabasic, and Mesozoic metasedimentary rocks. Only the metabasics, metaultrabasics, and some garnet-mica schists unambiguously record HP conditions and it is disputed if the bulk of the felsic lithologies underwent the same Alpine subduction history. The unit has been among the first proposed to represent a chaotic subduction channel mélange (Trommsdorff, 1990) and has become a prime subject in the debate about mechanisms that drive exhumation of subducted continental crust. Some studies came to the conclusion that it represents a mélange from rocks of different paleogeographic provenances and/or with different subduction histories (Trommsdorff, 1990; Toth et al., 2000; Engi et al., 2001; Brouwer et al., 2005; Berger et al., 2005) while other studies propose a more or less coherent character of the basement unit at least since peak-pressure conditions (Heinrich, 1982; Dale and Holland, 2003; Froitzheim et al., 2003; Nagel, 2008; Carry et al., 2009; Herwartz et al., 2011; Cavargna-Sani et al., 2014). A major obstacle in unravelling the subduction history of continental units in Alpine-type orogens is that they by definition largely consist of old basement, which likely records previous tectonometamorphic events. Heinrich (1982) and Dale and Holland (2003) presented southward increasing pressure and temperature conditions in the Adula Nappe and attributed these data to the Alpine subduction-exhumation event. However, garnet in a sample from the northern Adula Nappe displays a single growth cycle and yields a Variscan age of 323.8 ± 6.9 Ma. In

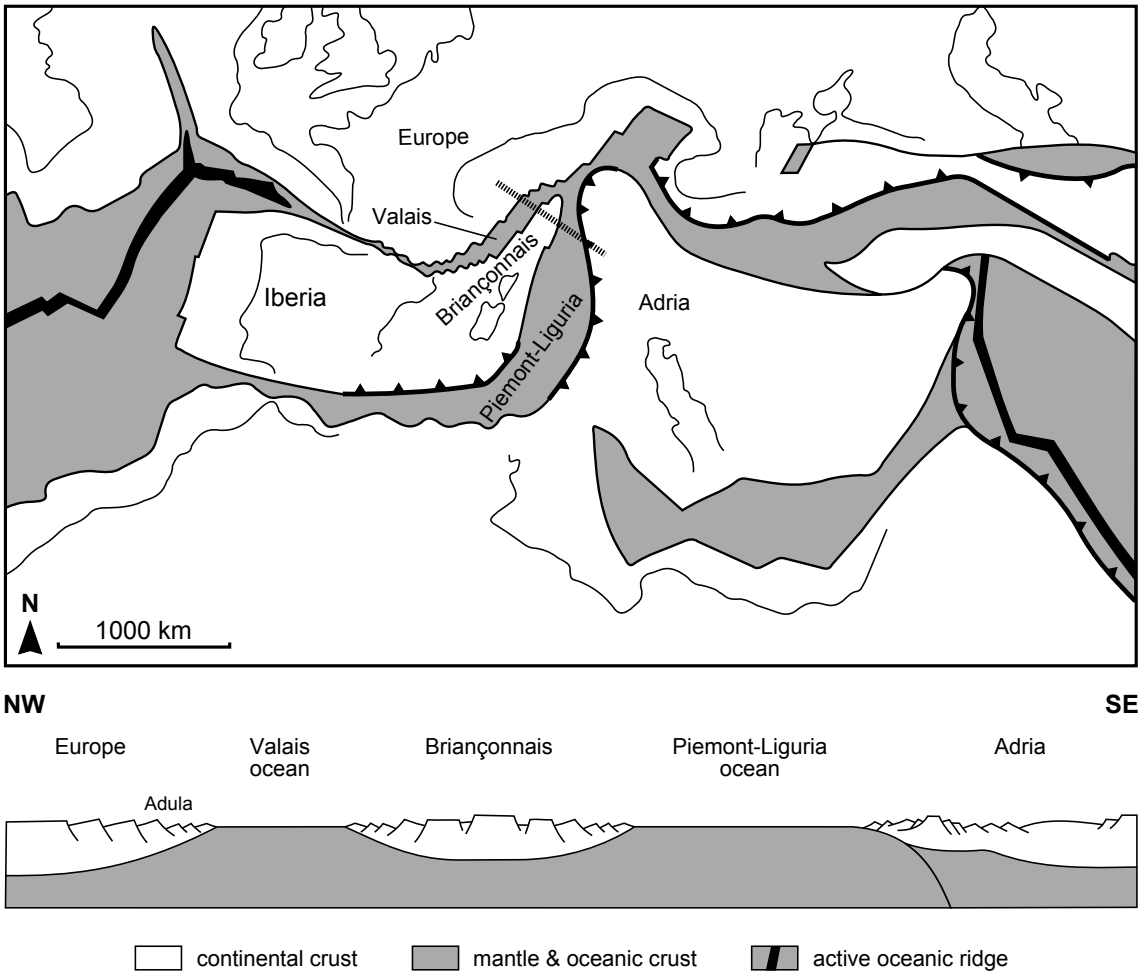

Figure 1.11: Paleogeographic map of the Alpine realm and adjacent areas in the Late Cretaceous (modified from Schmid et al., 2004). The dashed line in the map marks the location of the cross-section in the lower panel. Valais and Piemont-Liguria represent the Penninic Oceans. Both oceanic basins were consumed by subduction towards the southeast. The Adula Nappe represents the most distal part of the European continental margin.

contrast, a sample from the southern part of the nappe contains unzoned garnet that fully equilibrated to high-pressure metamorphic conditions unrevealing a slightly retrograde age of 34.1 ± 2.8 Ma. A third sample from the central Adula Nappe contains separable Alpine and Variscan garnet populations. The Alpine population yields a maximum age of 38.8 ± 4.3 Ma which is in line with a previously published garnet maximum age from the central nappe of 37.1 ± 0.9 Ma (Herwartz et al., 2011). Hence, from north to south, eclogites display an increasing degree of Alpine metamorphic overprint on top of garnet-bearing, Variscan high-grade assemblages. This fits well into the view of the Adula Nappe representing a coherent piece of pre-Mesozoic basement that underwent subduction and exhumation as a whole. The unit was affected by a single, short-lived Eocene subduction and exhumation event

during the Alpine cycle. Exhumation from peak-pressure conditions occurred within few Ma since the entire nappe pile was established before 32 Ma (Nagel, 2008; Berger et al., 2011).

The nappe stack of the Eastern Alps that is subdivided from bottom to top into the Lower Austroalpine, the Lower Central Austroalpine, and the Upper Central Austroalpine (Janák et al., 2004) was established by thrusting towards the NW during the Cretaceous Eo-Alpine orogenic cycle (e.g. Schmid et al., 2004; Handy et al., 2010). The metamorphic series of southeastern Pohorje in Slovenia (Chapter 3) represents that part of the Lower Central Austroalpine that was subjected to the highest pressure and temperature conditions beneath the Upper Central Austroalpine in a setting of intracontinental subduction. The Slovenska Bistrica Ultramafic Complex is an 8 km wide body of mainly serpentinite that is embedded in a series of metapelitic gneisses and orthogneisses. Eclogites are associated with the ultramafic as well as the felsic rocks. Lu-Hf garnet chronometry was applied to two ultramafic samples and to two eclogites. One eclogite was sampled inside the ultramafic body while the other was located in direct contact with felsic lithologies. The eclogites yield ages of 96.6 ± 1.2 Ma and 94.8 ± 5.1 Ma that can be attributed to prograde garnet growth due to preserved Lu-zoning. In contrast, Lu content is unzoned in garnet of the ultramafic samples. One ultramafic sample yielded 91.6 ± 4.1 Ma while the other gave no geological reasonable age. The Lu-Hf ages of eclogites can be attributed close to the initial stages of garnet formation on the prograde path of the subduction cycle. Also, the Lu-Hf age of 91.6 ± 4.1 Ma that was inferred from an ultramafic sample is interpreted to represent a minimum age for garnet growth. These data indicate that the ultramafic body and its felsic host rocks were subjected to eclogite facies conditions in a single tectonic event between c. 97 and 90 Ma. Hence, eclogites, ultramafic rocks, and felsic country rocks shared a common PT path during the Cretaceous subduction cycle. Furthermore, there is a marked synchroneity of eclogite metamorphism in the different parts of the Austroalpine high-pressure belt (Thöni, 2006). Intra-continental subduction was possibly localized at a Permian-aged rift within the Austroalpine realm (Janák et al., 2004). The new Lu-Hf garnet ages reveal that subduction related garnet growth in southeastern Pohorje is contemporaneous with major out-of-sequence thrusting in the Northern Calcareous Alps which is kinematically linked to subduction of the Lower under the Upper Central Austroalpine.

Blueschist-facies metamorphic rocks in the Yuli Belt of Taiwan's Central Range (Chapter 4) record ongoing subduction of the Eurasian plate beneath the Philippine Sea plate. Collision between the passive continental margin of China and the Luzon

Island Arc proceeds from south to north because the continental margin is oblique to the plate boundary. A south-to-north sequence of sections across Taiwan can be viewed as a time sequence, with the southernmost located sections showing the earliest stages of the evolution (Suppe, 1984). Metamorphic rocks of the Yuli Belt are juxtaposed to unmetamorphic sedimentary and volcanic rocks of the Luzon Island Arc as well as accreted unmetamorphic forearc sediments of the Coastal Range. The dated sample TW1 is a garnet-amphibole schist that contains three distinct generations of amphibole. These generations of amphibole record successive stages of blueschist-, epidote-amphibolite-, and greenschist-facies metamorphic conditions. The occurrence of garnet inside glaucophane and major element zoning of garnet show that garnet growth was prograde. Lu-Hf geochronology applied to sample TW1 revealed a garnet-whole-rock age of 5.1 ± 1.7 Ma. Stratigraphic data indicate that collision of the continental margin with the Luzon Island Arc started around 6.5 Ma at the latitude of Taiwan (Lin et al., 2003). Thus, garnet growth in sample TW1 postdates arc-continent-collision and rocks of the Yuli Belt could have reached their maximum burial depth of about 35 km within less than one Ma. Rocks from the Yuli belt remained only very shortly at their maximum depth and were exhumed rapidly during ongoing convergence. The lithosphere of the upper plate failed in the area of the island arc when the Chinese continental margin entered the subduction zone and was removed by sinking off into the mantle (Chemenda et al., 2001; Shyu et al., 2011). This extraction process (Froitzheim et al., 2003) removed overburden above the subducted Yuli Belt and triggered its rapid exhumation. Further shortening enabled basal accretion of more external continental units of the Eurasian margin that were affected by lower pressure conditions below the exhumed Yuli Belt.

The Theodul Glacier Unit in the western Central Alps (Chapter 5) is a continental outlier inside the ophiolitic Zermatt-Saas Zone. It represents a fragment of the distal margin of the Cervinia microcontinent that was originally located close to the southeastern end of the Piemonte-Liguria Ocean. The investigated samples are eclogites that are framed by various types of high-pressure schists. Their chemical characteristics indicate a within-plate basalt signature that is similar to those found in other continental outliers. Garnet in both samples retained its prograde chemical growth zoning: It constitutes a bell-shaped distribution of Mn, Ca and Fe/(Fe+Mg) with high contents of Mn and Ca in the core and decreasing contents towards the rim. In addition, high amounts of Lu are evident in the cores of garnet and they also decrease towards the rims. Lu-Hf garnet dating yielded ages of 56.5 ± 2.7 Ma and 58.2 ± 1.4 Ma. These ages fall into the so-called “Paleocene restoration phase” (e.g. Trümpy, 1973). A reduction in clastic sediment deposition, a lack of folds and

thrusts, and almost a termination of convergence between Africa and Europe are characteristics of this period of time. However, the new Lu-Hf ages indicate that subduction continued in the Paleocene. The new ages also differ from subduction related ages of other continental outliers that are located inside the Zermatt-Saas Zone (e.g. Duchêne et al., 1997; Lapen et al., 2003). Thus, they support the conclusion that the Zermatt-Saas Zone is a composition of units with different tectonic histories rather than a single coherent body (Rebay et al., 2012). Since convergence between Africa and Europe was small in the Paleocene (Trümpy, 1973; Frisch, 1979; Rosenbaum and Lister, 2005; Schettino and Turco, 2011) subduction was probably balanced by extension of the upper plate. This process typically appears during roll-back of a subduction zone (e.g. Rosenbaum and Lister, 2005).

2 Lu-Hf garnet systematics of a polymetamorphic basement unit: New evidence for coherent exhumation of the Adula Nappe (Central Alps) from eclogitefacies conditions

Sascha Sandmann[1], Thorsten J. Nagel[1], Daniel Herwartz[2], Raúl O.C. Fonseca[1], Robert M. Kurzawski[3], Carsten Münker[2], Nikolaus Froitzheim[1]

[1] Steinmann-Institut für Geologie, Mineralogie und Paläontologie, Universität Bonn, Meckenheimer Allee 169, D-53115 Bonn, Germany

[2] Institut für Geologie und Mineralogie, Universität Köln, Greinstr. 4-6, D-50939 Köln, Germany

[3] Geomar, Helmholtz Centre for Ocean Research, Wischhofstr. 1-3, D-24148 Kiel, Germany

Abstract

The Adula Nappe in the Central Alps is a mixture of various pre-Mesozoic continental basement rocks, metabasics, ultrabasics, and Mesozoic cover rocks, which were pervasively deformed during Alpine orogeny. Metabasics, ultrabasics and locally garnet-mica schists preserve eclogite-facies assemblages while the bulk of the nappe lacks such evidence. We provide garnet major-element data, Lu profiles and Lu-Hf garnet geochronology from eclogites sampled along a north-south traverse. A southward increasing Alpine overprint over pre-Alpine garnets is observed throughout the nappe. Garnets in a sample from the northern Adula Nappe display a single growth cycle and yield a Variscan age of 323.8 ± 6.9 Ma. In contrast, a sample from Alpe Arami in the southernmost part contains unzoned garnets that fully equilibrated to Alpine high-pressure metamorphic conditions with temperatures exceeding 800 ºC. We suggest that the respective Eocene Lu-Hf age of 34.1 ± 2.8 Ma is affected by partial re-equilibration after the Alpine pressure peak. A third sample from the central part of the nappe contains separable Alpine and Variscan garnet populations. The Alpine population yields a maximum age of 38.8 ± 4.3 Ma in line with a previously published garnet maximum age from the central nappe of 37.1 ± 0.9 Ma.

The Adula Nappe represents a coherent basement unit which preserves a continuous Alpine high-pressure metamorphic gradient. It was subducted as a whole in a single, short-lived event in the upper Eocene. Controversial high-pressure ages and conditions in the Adula Nappe may result from partly preserved Variscan assemblages in Alpine metamorphic rocks

2.1 Introduction

The exhumation of high-pressure (HP) and ultra-high-pressure (UHP) metamorphic rocks in collision orogens has been a major subject in tectonic research for several decades, yet, very different concepts about geometry and driving forces are still discussed (e.g. Hacker and Gerya, 2013 and references therein). One ongoing controversy is about the degree of tectonic ordering found in HP terranes. Many apparently coherent HP units have been proposed to actually represent tectonic mélanges mixed inside a subduction channel until relatively late in the subduction-exhumation history. These units would consist of potentially small pieces with very different pressure-temperature time paths and even repeated subduction-exhumation events of the same subunit within a few Million years (e.g. Gerya et al., 2002; Rubatto et al., 2011). This scenario has mainly been supported by numerical modelling studies which propose vigorous, more or less steady-state return flow in the subduction channel coeval to ongoing subduction (e.g. Gerya et al., 2002; Burov et al., 2014). The main field observations supporting this scheme are that (1) HP and UHP units often consist of various rock types of which only a small portion displays (U)HP assemblages (e.g. Jolivet et al., 2005; Krebs et al., 2011) and/or (2) HP units often appear to show scattered isotopic ages related to HP conditions (e.g. Federico et al., 2007). Other tectonic schemes propose more distinct exhumation events driven or at least triggered by changes in the tectonic framework such as the advent of continental crust in the subduction zone and these models typically predict exhumation of coherent units, which would display continuous metamorphic gradients and ages. Coherency of HP units has mainly been favoured by field-based studies (e.g. Agard et al., 2009), but has also been reproduced by physical or numerical modelling approaches (e.g. Chemenda et al., 1995; Warren et al., 2008). Accordingly, the observation of variable metamorphic conditions or scattered ages within a single unit have to be attributed to incomplete prograde mineral reactions, variable metamorphic retrogression, disturbed isotopic systems, or inherited mineral assemblages of previous metamorphic cycles. Models proposing chaotic mixing have been favoured in oceanic HP units, which often display a mechanically soft serpentinite matrix and/or display incorporated slices of continental origin (e.g. Gerya et al., 2002; Federico et al., 2007; Krebs et al.,

2011; Rebay et al., 2012), even though also for oceanic units like the Zermatt-Saas Zone in the western Central Alps very different magnitudes of tectonic mixing have been proposed (Angiboust et al., 2009; Rebay et al., 2012). For continental HP units it is more questionable whether mélange-forming subduction-channel models apply and exhumation events affecting entire cohesive (U)HP terranes have been proposed in models (e.g. Chemenda et al., 1995) and case studies (e.g. Chopin, 2003; Nagel, 2008; Hacker et al., 2010).

The Adula Nappe in the eastern Central Alps is a mixture of various continental gneisses with local occurrences of metabasics, metaultrabasics, and Mesozoic metasediments. Only the metabasics, metaultrabasics, and some garnet-mica schists unambiguously record HP conditions and it is unclear if the bulk of the felsic lithologies underwent the same Alpine subduction history. The unit has been among the first proposed to represent a chaotic subduction channel mélange (Trommsdorff, 1990) and has become a prime subject in the mentioned debate with some studies concluding that it would represent a mélange from rocks of different paleogeographic provenances and/or with different subduction histories (Trommsdorff, 1990; Toth et al., 2000; Engi et al., 2001; Brouwer et al., 2005; Berger et al., 2005) and others proposing a more or less coherent basement unit at least since peak-pressure conditions Heinrich (1982); Dale and Holland (2003); Nagel (2008); Carry et al. (2009); Herwartz et al. (2011); Cavargna-Sani et al. (2014, subm). A major obstacle in unravelling the subduction history of continental units in Alpine-type orogens is that they by definition largely consist of old basement, which likely records previous tectonometamorphic events. The geology of the Adula Nappe, described in detail in the next paragraph, is no exception. Heinrich (1982) and Dale and Holland (2003) presented southward increasing pressure and temperature conditions and attributed these data to the Alpine subduction event. Here, we present chemical data and Lu-Hf geochronology from three eclogites sampled parallel to this inferred Alpine pressure gradient. Major element data are used to identify different growth generations and intra-garnet diffusion of Lu is additionally monitored by LA-ICPMS analyses. Together with microprobe data from three additional samples and the abundant literature data we come to the conclusions that (1) the Adula Nappe represents a coherent piece of pre-Mesozoic basement that underwent subduction and exhumation as a whole, (2) from north to south, eclogites display an increasing degree of Alpine metamorphic overprint on top of garnet-bearing, Variscan high-grade assemblages, and (3) the Adula Nappe experienced a single, short-lived Eocene subduction and exhumation event during the Alpine cycle.

2.2 Geological setting

The Adula Nappe is part of the Lepontine Dome in southeastern Switzerland and adjacent Italy. The core of this structural half-window consists of basement-cover nappes derived from the subducted European continental margin. These nappes are surrounded by the overlying remnants of the partly oceanic Penninic units, which were subducted to the southeast prior to the Eo-Oligocene collision of Europe and Adria (e.g. Froitzheim et al., 1996; Schmid et al., 2004; Handy et al., 2010). In the present nappe edifice, the structurally highest units represent the paleogeographically southernmost parts of the pre-collisional Alpine realm. Since tectonic boundaries on the eastern flank of the Lepontine Dome dip towards east, a transit from east to west corresponds to a transit from paleogeographically southern to northern units (Fig. 2.1). From top to bottom, these units are: (1) the Austroalpine Nappes representing the northern margin of the Adriatic continent, (2) Arosa Zone and Platta Nappe, strongly dismembered remnants of the Piemont-Liguria Ocean which opened in the Jurassic (Trümpy, 1975), (3) the Schams-, Suretta- and Tambo Nappes representing

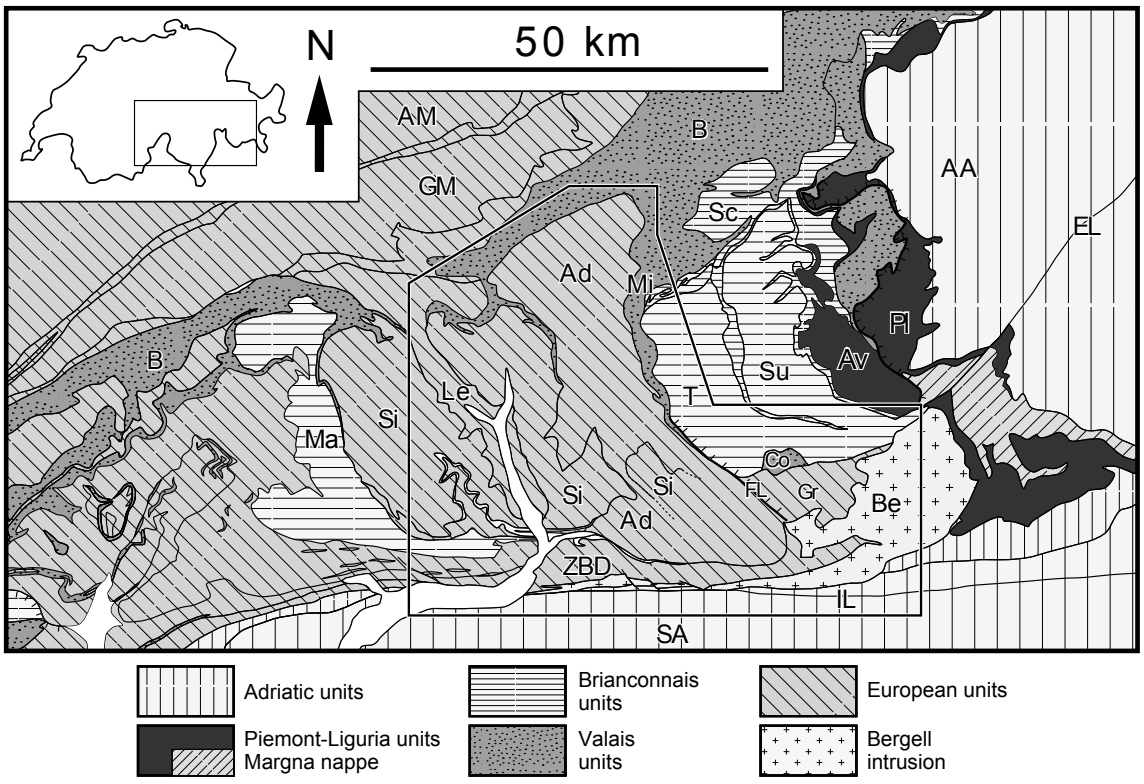

Figure 2.1: Tectonic sketch map of the central Alps (after Spicher, 1980; Froitzheim et al., 1996). The inset frame outlines the area of Figure 2.2. AA, Austroalpine Nappes; Ad, Adula Nappe; AM, Aare Massif; Av, Avers Unit; B, Bündnerschiefer; Be, Bergell Intrusion; Co, Chiavenna Ophiolite; EL, Engadin Line; FL, Forcola Line; GM, Gotthard Massif; Gr, Gruf Complex; IL, Insubric Line; Ma, Maggia Nappe; Le, Leventina Nappe; Mi, Misox Zone; Pl, Platta Nappe; SA, Southern Alps; Sc, Schams Nappes; Si, Simano Nappe; Su, Suretta Nappe; T, Tambo Nappe; ZBD, zone of Bellinzona-Dascio.

the Briançonnais microcontinent, an eastward extension of the Iberian continent, (4) the Misox Zone consisting of metasediments of the Valais Ocean that opened in the Cretaceous (Stampfli, 1993; Florineth and Froitzheim, 1994), and (5) the Subpenninic Nappes derived from the subducted European continental margin. The Adula Nappe represents the highest of the Subpenninic Nappes. Towards south, the entire nappe pile is folded into a vertical to overturned (i.e. north-dipping) orientation by a series of large backfolds. The southern limb of this fold array is called the Southern Steep Belt or "Root Zone" and consists of highly-sheared mylonites commonly regarded as the strongly thinned extensions of the nappes exposed further north. This complex mylonite belt accommodates a few tens of kilometres north-block-up vertical offset at high amphibolite-facies conditions and a disputed greenschist-facies dextral offset in mapview (e.g. Schmid et al., 1987, 1996). The southern termination of this mylonite belt and of the entire Lepontine halfwindow is a distinct brittle fault also associated with dextral offset.

The Adula Nappe rests on top of the underlying Subpenninic Simano Nappe which consists of a coherent pre-Mesozoic gneiss core and enveloping remnants of Mesozoic sediments (e.g. Rütti et al., 2005). The frontal part of the Adula Nappe is wrapped by metasediments of the Valais oceanic basin, the so-called Bündnerschiefer. These metasediments are interlayered with metabasic rocks of oceanic affinity and slivers of continental basement (Steinmann, 1994). East of the Adula Nappe this unit extends into the Misox Zone. The Misox Zone terminates to the south as it is cut by an east-dipping Late Oligocene to Miocene normal fault, the Forcola Line (Meyre et al., 1998; Ciancaleoni and Marquer, 2006). Further south, the Forcola Line defines the boundary between the Adula Nappe and the next-higher Tambo Nappe, which is derived from the Briançonnais microcontinent (Marquer et al., 1998). The Gruf Complex to the southeast is often considered as an extension of the Adula Nappe, but several studies consider it as an independent lower crustal unit (e.g. Galli et al., 2012). Sandwiched between Tambo Nappe and Gruf Complex, at the same structural level as the Misox Zone is the Chiavenna Ophiolite, a complex of oceanic basement and part of the Valais Ocean (Liati et al., 2003). The Bergell Intrusion forms the southeastern border of the Gruf Complex. This Tertiary (30-32 Ma; Van Blanckenburg, 1992) granodioritic to tonalitic body intruded subsequent to nappe stacking and thus also subsequent to HP-metamorphism (Rosenberg et al., 1995; Davidson et al., 1996). The portion of the Southern Steep Belt south of the Adula Nappe is called Zone of Bellinzona-Dascio (ZBD). Schmid et al. (1996) view this zone as structurally higher than the Adula Nappe and as the continuation of the Upper Penninic Misox Zone. Stucki et al. (2003) report metaophiolitic remnants

inside the ZBD, which might be derived from the Piemont-Liguria Ocean. However, as the ZBD is a direct continuation of the Adula Nappe and comprises very similar lithologies including HP and UHP metamorphic rocks, we follow Berger et al. (2005), who consider it as a southward continuation of the Adula Nappe. The Cima Lunga Unit west of the Ticino Valley (Valle Leventina) represents a lithologically and structurally identical westward extension of the Adula Nappe (e.g. Trommsdorff, 1990; Maxelon and Mancktelow, 2005).

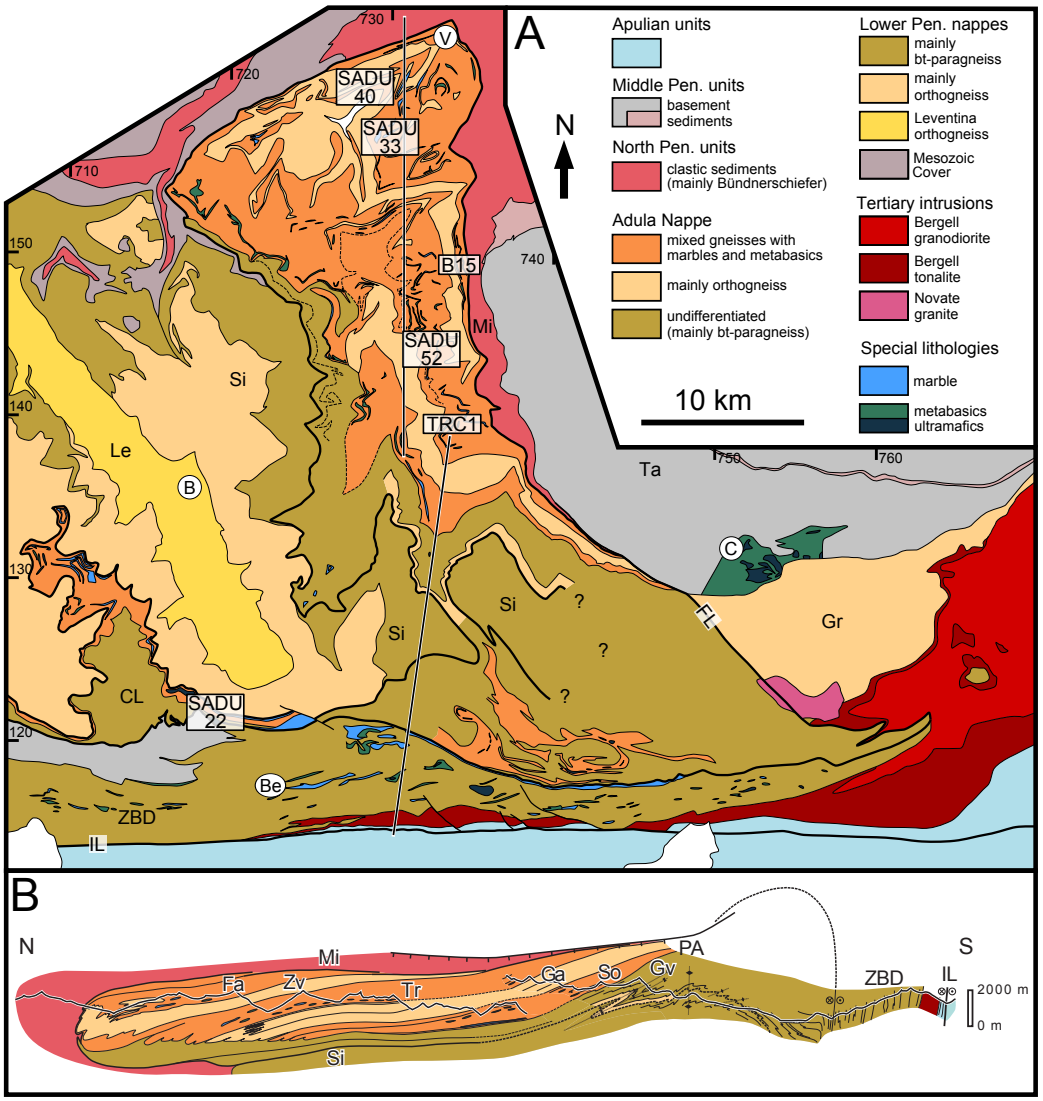

Figure 2.2: (A) Tectonic map of the Adula Nappe and adjacent units (from Nagel, 2008; with modifications after Galli et al., 2012) with sample locations of this study. The outline of the map is illustrated in Figure 2.1. (B) Tectonic cross-section through the Adula Nappe (Nagel, 2008). B, Biasca; Be, Bellinzona; C, Chiavenna; CL, Cima Lunga Unit; Fa, Fanella Lobe; FL, Forcola Line; Ga, Ganan Lobe; Gr, Gruf Complex; Gv, Groveno Lobe; IL, Insubric Line; Le, Leventina Nappe; Mi, Misox Zone; PA, Paglia Antiform; Si, Simano Nappe; So, Soazza Lobe; Ta, Tambo Nappe; Tr, Trescolmen Lobe; V, Vals; ZBD, zone of Bellinzona-Dascio; Zv, Zervreila Lobe. Coordinates are Swiss coordinates.

Different to the underlying lower Subpenninic Nappes, the Adula Nappe displays a pervasive internal mylonitisation, subparallel to the lithological boundaries, referred to as Zapport foliation (Löw, 1987; Partzsch, 1998; Nagel et al., 2002a; Pleuger et al., 2003). The Alpine age of this foliation has recently been confirmed by the identification of a Permian protolith age of the Zervreila Gneiss of the northern Adula Nappe, which is affected by the Zapport foliation (Cavargna-Sani et al., 2014). The nappe comprises several lobes, which are arranged in a forward-dipping duplex geometry (Frischknecht et al., 1923; Fig. 2.2). The backbone of this architecture are lobes of orthogneisses like the Zervreila Gneiss, which can be traced for tens of kilometres (Frischknecht et al., 1923; Cavargna-Sani et al., subm; Fig. 2.2B). These orthogneiss lobes are interlayered with mixed units of dominantly paragneisses and mica schists containing layers and lenses of marble, metabasics, and metaultrabasics. Metabasic rocks are mainly amphibolites but many boudins preserve pristine eclogite (Fig. 2.3). While marbles and some associated metasediments are clearly Mesozoic (Galster et al., 2012), the remaining basement including most of the basic rocks now appears to be of pre-Mesozoic origin (Liati et al., 2009; Cavargna-Sani et al., 2014).

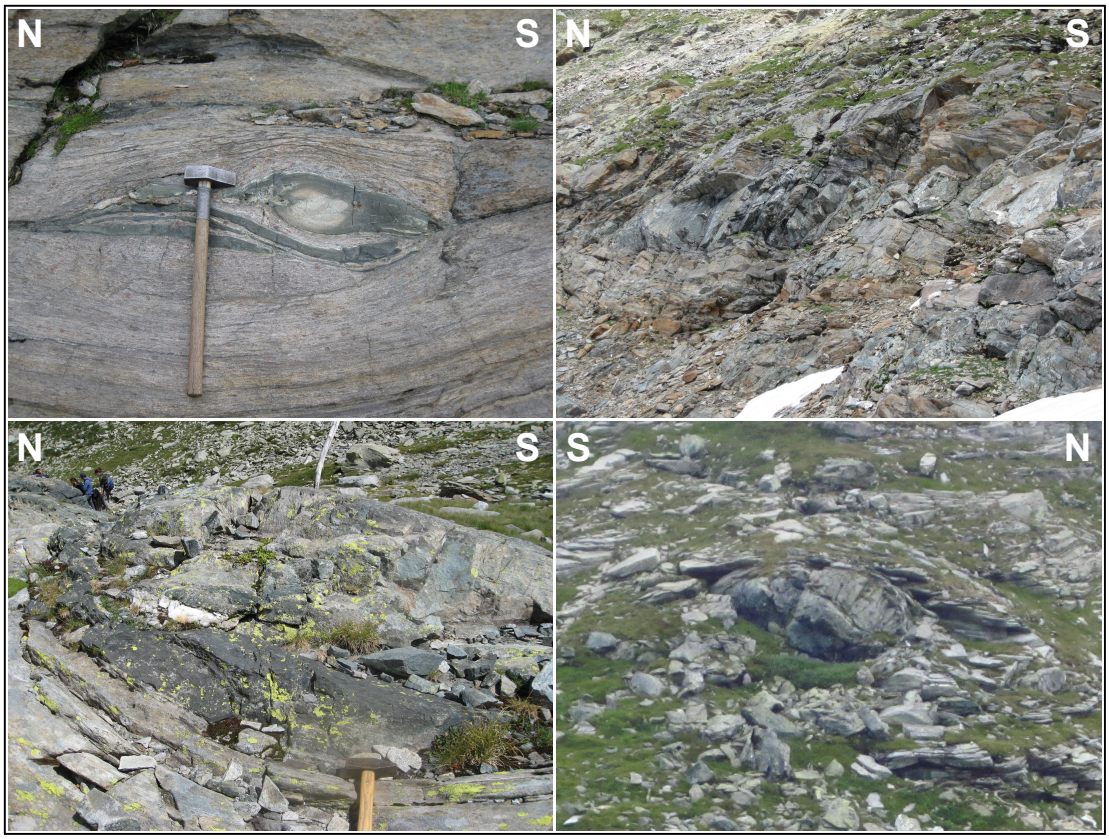

Figure 2.3: Appearance of metabasic lithologies in the field. Metabasics are present as elongated boudins that mainly consist of amphibolite but occasionally contain pristine eclogite in their inside. These boudins are embedded in garnet-mica schist layers of the metasedimentary lobes of the Adula Nappe.

Of all nappes on the eastern flank of the Lepontine halfwindow, only the Adula Nappe experienced at least in parts unambiguous HP and even UHP conditions during the Alpine Orogeny. The underlying as well as the overlying continental nappes experienced peak-pressures of around 12 kbar (Irouschek, 1985; Baudin and Marquer, 1993). Peak-pressure conditions in the North-Penninic Misox Zone immediately on top of the Adula Nappe are somewhat disputed. A low-temperature, high pressure stage at blueschist-facies conditions in the Upper-Penninic sedimentary rocks further north is well established (Bousquet et al., 2002), yet, there is also a clear metamorphic break to higher conditions towards the Adula Nappe (Wiederkehr et al., 2011). The entire nappe pile was subjected to Barrovian metamorphism under southward increasing, greenschist- to amphibolite-facies conditions subsequent to nappe stacking as isograds of this metamorphic stage clearly crosscut nappe boundaries (e.g. Niggli and Niggli, 1965; Todd and Engi, 1997; Nagel et al., 2002b; Berger et al., 2011).

Within the Adula Nappe, HP metamorphic assemblages are restricted to local occurrences of eclogites, garnet peridotites, and HP garnet mica schists, while the bulk of the gneisses does not record such conditions. For the HP rocks, Heinrich (1982) proposed a pressure gradient from 9-13 kbar/450-550 °C in the north to 18-35 kbar/750-900 °C in the south. These estimations are in line with later findings of Löw (1987); Meyre et al. (1999); Nimis and Trommsdorff (2001), and Nagel et al. (2002b) and such a gradient would strongly suggest a coherent character of the Adula Nappe during the Alpine subduction cycle. The associated metamorphic field gradient would exceed the lithostatic pressure gradient implying N-S shortening of the nappe after peak-pressure conditions, an event apparently at odds with the observed subhorizontal N-S stretching during internal mylonitisation (Nagel, 2008; Pleuger and Podladchikov, 2014). Pleuger and Podladchikov (2014) proposed a period of local tectonic overpressure that affected the Adula Nappe during its maximum burial stage. However, the pressure gradient itself has also been challenged in several studies. Dale and Holland (2003) proposed peak-pressure conditions of about 17 kbar/640 °C and Zulbati (2010) proposed conditions of 19 kbar/580 °C for eclogites from the northernmost Adula Nappe, i.e. conditions much higher than inferred by Heinrich (1982). Another possible outlier not consistent with the mentioned gradient is the ultrabasic complex of Alpe Arami located in the very south of the nappe. Estimations for the peak pressure conditions of this complex range from 32 kbar/840 °C (Nimis and Trommsdorff, 2001) to 50 kbar/1120 °C (Brenker and Brey, 1997) and even more than 100 kbar (e.g. Dobrzhinetskaya et al., 1996). Also, Toth et al. (2000) proposed different PT paths for generally high-grade eclogites in the southern part of the

nappe supporting the view of a mélange formation after peak-pressure conditions.

The age of HP metamorphism in the Adula Nappe has been the target of several studies. An Eocene age is obtained by various chronometers for the southernmost part of the nappe: Sm-Nd dating of garnet peridotites and eclogites from the Cima Lunga Unit yielded ages of 37-44 Ma (Becker, 1993). U-Pb zircon dating of samples from the same area led to ages of c. 44 Ma, that are interpreted to reflect melting and/or subsolidus re-equilibration at (U)HP conditions and ages of c. 35 Ma, which are interpreted to be related to decompression after peak-pressure conditions (Gebauer et al., 1992a; Gebauer, 1996). Lu-Hf garnet dating of eclogites from the Southern Steep Belt performed by Brouwer et al. (2005) yielded ages from c. 36 Ma to more than 70 Ma and were interpreted to reflect different HP events in individual samples and thus to support a mélange model for the Adula Nappe. For the bulk of the Adula Nappe, however, the Alpine age of eclogite-facies conditions is less-well established. Liati et al. (2009) identified HP zircon ages of c. 370 Ma for the central Adula Nappe and of 330 to 340 Ma for the northern Adula Nappe, but did not find evidence for an Eocene HP event in their samples. Herwartz et al. (2011) separated and dated two garnet generations from an eclogite sample from Trescolmen in the central Adula Nappe using Lu-Hf chronology. Relic cores in large garnets yielded a minimum age of 333 Ma, while a second generation as part of the Alpine HP assemblage turned out to be younger than 38 Ma old.

2.3 Methods

Garnet is an excellent and widely used recorder of metamorphic history and especially suitable to study HP processes (Baxter and Scherer, 2013). It can preserve information about distinct metamorphic stages via chemical growth zoning, multiple growth domains, preserved HP and UHP inclusions or reset chemical signatures (e.g. Carlson and Schwarze, 1997; Konrad-Schmolke et al., 2008a; Whitney and Seaton, 2010; Faryad, 2012; Ague and Carlson, 2013; Baxter and Scherer, 2013). Garnet can be dated robustly by Lu-Hf chronology, which is now established as one of the most reliable tools to date subduction histories (e.g. Duchêne et al., 1997; Kylander-Clark et al., 2007, 2009; Schmidt et al., 2011; Baxter and Scherer, 2013). We measured the distribution of major bivalent cations and Lu in garnets from eclogite samples by electron microprobe and LA-ICPMS analyses, respectively. The diffusion coefficients of bivalent elements in garnet are generally an order of magnitude larger than those of trivalent REEs (Carlson, 2012). Hence, prograde zoning in REEs can be preserved when major elements are already re-equilibrated. While bivalent elements provide fundamental insight into the growth history, the Lu distribution allows to

identify, which part of garnet crystals actually control the isotopic age. The closure temperature of the Lu-Hf system in garnet appears to be higher than the one for Sm-Nd (Scherer et al., 2000; Lapen et al., 2003), certainly above 630 °C (Skora et al., 2008), but probably much higher (Schmidt et al., 2011; Shu et al., 2014).

2.3.1 Electron microprobe and LA-ICPMS analysis

Electron microprobe analyses were achieved using the JEOL Superprobe JXA 8200 at the Steinmann-Institut, Bonn. Configuration was set to a beam current of 15 nA and an acceleration voltage of 15 kV. Dwell time of single spot analyses during map scans was between 100 and 200 msec depending on the size of the scanned grain. Laser ablation analyses were carried out at the Steinmann-Institut using a Resonetics M50-E ATL Excimer 193 nm laser system coupled to a Thermo-Finnigan X-series 2 quadrupole ICP-MS, following the routine described in Kirchenbaur et al. (2012). Spot sizes were set to 55 µm. Laser fluence at the sample surface was measured between 4 and 7 J/cm^{-2}. The laser repetition rate was set to 10 Hz. Count rates were normalized using ^{29}Si as the internal standard and NIST-SRM 612 as the external standard (Jochum et al., 2011). Measurement accuracy was checked using NIST-SRM 610 as an external reproducibility standard and was found to be between 5-15 % of the preferred values (as described in Jochum et al., 2011). Count rates monitored during 20 seconds for background, and 40 seconds during ablation. Oxide production rates were monitored using ThO_2/Th ratios and kept below 0.5 % in order to avoid oxide molecular interferences on the REE nuclides. Data reduction and evaluation followed the procedure of Longerich et al. (1996).

2.3.2 Sample digestion and MC-ICPMS analysis

We followed the routine that has previously been established by several studies (e.g. Lagos et al., 2007; Herwartz et al., 2011; Kirchenbaur et al., 2012; Nagel et al., 2013). The samples selected for Lu-Hf chronometry were crushed and separated into two splits. One split was powdered and used for bulk rock analyses. The second was used for mineral separation. Mineral separates were cleaned in an ultrasonic bath in 2.5 M HCl and rinsed twice with deionised water. A mixed ^{176}Lu-^{180}Hf tracer was added to all samples before digestion. Two digestion methods were applied: (1) Mineral separates and whole rock powder of sample SADU22 were dissolved by using the "table top" procedure described by Lagos et al. (2007). This method leaves behind Hf-rich phases (rutile and zircon) that might preserve unequilibrated isotope signatures. The samples were digested with HF-HNO_3-$HClO_4$ in closed Teflon vials on 120 °C hotplates and subsequently dried down followed by addition of 6N HCl.

The undigested minerals (rutile and zircon) were removed by centrifugation before the solutions were loaded onto cation exchange columns. (2) Whole rock powders of samples SADU40 and B15 were dissolved inside steel-jacketed PARR bombs with HF-HNO_3 for 5 days. Subsequently $HClO_4$ was added to the samples. The samples were dried down and re-dissolved in 6N HCl. A clear solution indicated complete digestion of each sample. Sample solutions were dried down and re-dissolved in 3N HCl. The solutions of both methods were further treated with the single-column element separation procedure of Münker et al. (2001) in order to separate Lu and Hf from the matrix elements. The Hf-cuts were additionally purified. These were dissolved in 6N HCl and loaded onto the columns again. Remaining matrix elements and especially Lu were removed using several resin-bed volumes of 6N HCl. Subsequently Hf was eluted using 2N HF. Lu and Hf measurements were carried out on a Finnigan Neptune MC-ICPMS at the Steinmann-Institut in Bonn. Instrumental mass bias on Hf isotope ratios was corrected by using $^{179}Hf/^{177}Hf$ and the exponential law. Measured $^{176}Hf/^{177}Hf$ ratios are given relative to $^{176}Hf/^{177}Hf = 0.282160$ for the Münster Ames Hf standard, which is isotopically identical to the JMC-475 standard (Table 2.1).

Table 2.1: Lu-Hf isotope data of whole rock samples and mineral separates used for the calculation of isochrons.

Sample		ppm Lu	ppm Hf	$^{176}Lu/^{177}Hf$	Error	$^{176}Hf/^{177}Hf$	Error
B15	WR	0.431	2.68	0.02281	0.00006	0.282980	0.000047
	Grt1	5.40	0.0959	8.057	0.020	0.326795	0.000099
	Grt2	4.26	0.0678	8.057	0.020	0.326795	0.000039
	Grt3	4.54	0.0678	8.992	0.022	0.325351	0.000153
	Omph	0.0309	0.230	0.01911	0.00005	0.283292	0.000160
	small Grt1	0.939	0.0452	2.947	0.007	0.284822	0.006396
	small Grt2	1.01	0.0515	2.775	0.007	0.285289	0.000161
SADU22	WR	0.508	0.359	0.2006	0.0005	0.283277	0.000066
	Grt1	0.944	0.0916	1.463	0.004	0.284074	0.000051
	Grt2	0.904	0.0893	1.437	0.004	0.284047	0.000051
	Grt3	0.880	0.0713	1.751	0.004	0.284275	0.000060
SADU40	WR	0.586	3.00	0.02770	0.00007	0.283028	0.000039
	Grt1	2.09	0.0619	4.819	0.012	0.312729	0.000197
	Grt2	2.14	0.0765	3.994	0.010	0.308104	0.000024
	Grt3	2.23	0.0957	3.316	0.008	0.303717	0.000053

The external reproducibility was estimated by the empirical relationship 2σ external reproducibility ≈ 4σm (σm = standard error of a single analysis; e.g. Bizzarro et al., 2003). Isobaric interferences on ^{176}Hf and ^{180}Hf were corrected by monitoring ^{173}Yb, ^{175}Lu, ^{181}Ta, and ^{183}W and their natural isotope compositions. Naturally occurring Yb in the Lu cuts was used for mass bias correction on Lu isotope ratios (Vervoort et al., 2004; Lagos et al., 2007). Interferences on ^{176}Lu were corrected by monitoring ^{173}Yb and ^{177}Hf and the natural isotope compositions. Regressions of isochrons and ages were obtained using ISOPLOT v. 2.49 (Ludwig, 2001) and a decay constant of λ^{176}Lu = 1.867 x 10^{-11}yr^{-1} (Scherer et al., 2001; Söderlund et al., 2004). Procedural blanks were <24 pg for Lu and <43 pg for Hf and thus insignificant.

2.4 Characterization of metamorphic episodes

Three samples from the southern, central and northern Adula Nappe were analysed including the collection of Lu-Hf data as well as major element and Lu concentrations in garnet. In addition, the major element zoning of garnets from two further eclogite samples and one garnet-mica schist was obtained (Appendix 7). We now first present and discuss each of the three samples analysed in detail. Representative electron microprobe analyses are given in Table 7.1 and Table 7.2. Coordinates of the sample locations can be found in Table 2.2 and the locations are also marked in Figure 2.2A. Mineral abbreviations used in the following are after Whitney and Evans (2010).

Table 2.2: Coordinates of sampling locations of the presented samples.

Sample	Location	UTM coordinates	Swiss coordinates
B15	Passo del San Bernardino	32T 513968 5149671	E733821 N151393
SADU8	Passo del San Bernardino	32T 513994 5149074	E733859 N150795
SADU22	Alpe Arami	32T 498728 5119544	E719177 N120954
SADU33	Fanellahorn	32T 510726 5155408	E730464 N157066
SADU40	Lake Zervreila	32T 508957 5158701	E728629 N160324
SADU52	Piz d'Arbeola	32T 512444 5141964	E732450 N143653
TRC1	Alp de Trescolmen	32T 513654 5137902	E733741 N139614

2.4.1 Alpe Arami (southern Adula Nappe)

Sample SADU22 is a medium grained eclogite from a body located in direct contact to the UHP garnet peridotite complex of Alpe Arami (e.g. Dobrzhinetskaya et al., 1996; Bozhilov et al., 1999; Nimis and Trommsdorff, 2001; Paquin and Altherr, 2001). The (U)HP mineral assemblage is Omp + Grt + Ky + Qz + Rt + Zrn. A weak

metamorphic layering is defined by layers enriched in garnet. The matrix minerals partly show symplectitic retrogression products like amphibole, potassic feldspar, plagioclase, Na-poorer pyroxene, or spinel. Garnets are anhedral and contain sparse inclusions of rutile and kyanite. They display a homogeneous composition with virtually no zoning of major elements ($Alm_{40}Prp_{30}Grs_{29}Sps_1$; Fig. 2.4A, B). Also the Lu concentration is more or less constant, i.e. around 0.8 ppm with a possible slight rise to 1.1 ppm towards one rim (Fig. 2.4C). During garnet crystallisation HREEs strongly fractionate into garnet, which results in an enrichment of Lu in the centre of garnet grains (Skora et al., 2006; Konrad-Schmolke et al., 2008b). Hence, flat Lu profiles point towards diffusional redistribution of Lu in garnet. However, Lu peaks

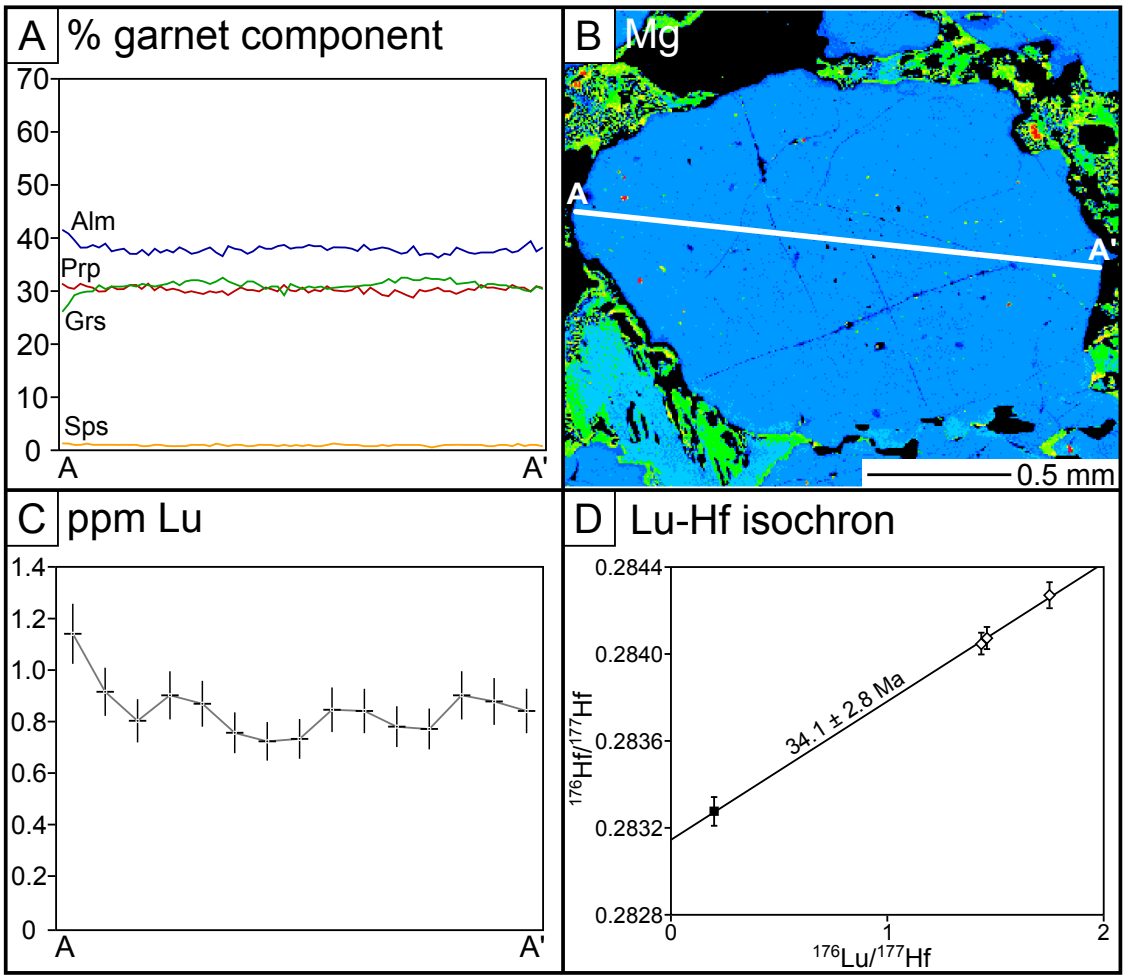

Figure 2.4: (A) Compositional profile through a representative garnet grain of eclogite sample SADU22 from Alpe Arami in the southern Adula Nappe. (B) Elemental map of Mg distribution in the same garnet. The white line indicates the trace of the profiles of A and C. Blue, garnet; light blue and green, omphacite; black, feldspar. (C) Lu concentration profile. The indicated errors on the x-axis are spot diameters of LA-ICPMS analyses. The errors on the y-axis are 10 % of the measured value. (D) Lu-Hf whole rock-garnet isochron of sample SADU22. Filled square, whole rock analysis; white diamonds, garnet analyses.

in garnet can be restricted to the very core of garnet and therefore it remains unclear if this peak exists or not. Reported (U)HP conditions in samples from the Alpe Arami basic-ultrabasic body are particularly diverse, but temperatures associated with (U)HP conditions generally exceed 800 °C for these rocks. Thus, redistribution of Lu is feasible.

The Lu-Hf garnet-whole rock age obtained from this sample is 34.1 ± 2.8 Ma (MSWD 0.27, n=4; Fig. 2.4D). Despite the low MSWD, suggesting that this age is of geological significance, we caution that it may be affected by re-equilibration and we interpret it as a minimum age for peak metamorphic conditions. Effects of resorption (Kelly et al., 2011) and contamination by older garnet are probably insignificant (see section 2.5.1).

The observed Lu-Hf age of sample SADU22 is in good agreement with previous age constraints. Gebauer (1996) suggested a retrograde age close to peak metamorphic conditions of 35.4 ± 0.5 Ma for metabasic and metaultrabasic rocks from Alpe Arami by applying U-Pb zircon chronometry. Lu-Hf dating of another eclogite sample from Alpe Arami (36.6 ± 8.9 Ma) and a garnet amphibolite sample from Gorduno located c. 4 km east of Alpe Arami (38.1 ± 2.9 Ma) performed by Brouwer et al. (2005) yielded ages that overlap within error with our age. Both samples of Brouwer et al. (2005) display a homogeneous distribution of major and, in the case of the eclogite sample, trace elements. Sm-Nd garnet dating of an eclogite and several ultrabasic lithologies from Alpe Arami yielded ages ranging from 37.5 ± 2.2 Ma to 43.9 ± 5.7 Ma (Becker, 1993).

2.4.2 Passo del San Bernardino & Alp de Trescolmen (Central Adula Nappe)

Sample B15 comes from a metabasic boudin located east of the Passo del San Bernardino (Fig. 2.2A). The mineral assemblage is Grt + Omp + Amp + Zo + Qz + Cal + Ph + Rt + Zrn. There are two populations of garnet present in this sample, which can easily be distinguished optically by grain size. Population 1 is up to 3 mm in diameter with irregular shapes, whereas grains from population 2 are up to a maximum of 0.2 mm in diameter and euhedral. Different to sample SADU22, garnets in this sample preserve chemical gradients. Inner parts of grains from population 1 gradually evolve from a core composition of $Alm_{53}Grs_{28}Prp_{11}Sps_{8}$ to a rim composition of $Alm_{56}Grs_{28}Prp_{11}Sps_{5}$. To the outermost rim the composition changes abruptly into a zone poor in almandine and spessartine component but enriched in pyrope component ($Alm_{46-48}Grs_{20-31}Prp_{20-29}Sps_{1}$; Fig. 2.5A, B).

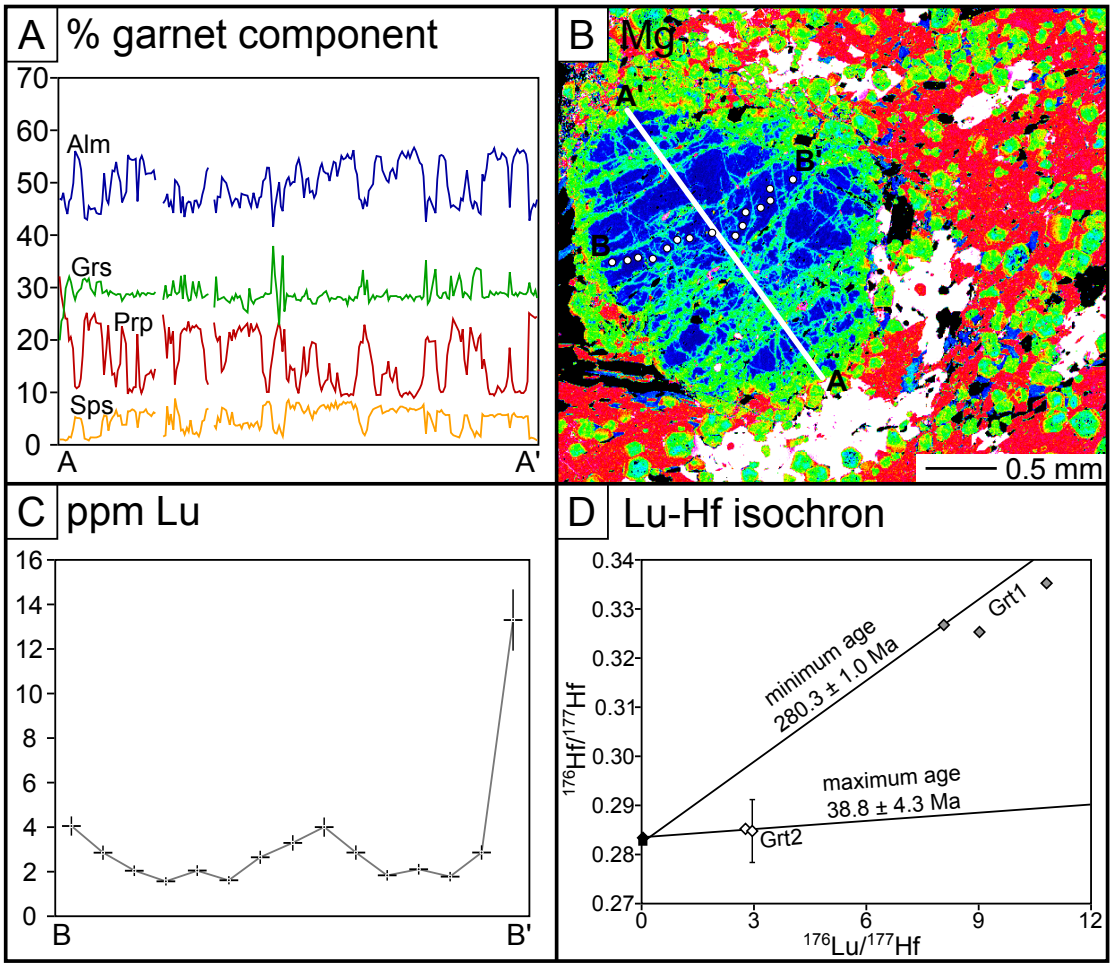

Figure 2.5: (A) Compositional profile through a representative garnet grain of eclogite sample B15 from the Passo del San Bernardino in the central Adula Nappe. (B) Elemental map of Mg distribution in the same garnet. The white line indicates the trace of the profile of A. White spots show locations of LA-ICPMS analyses. Blue, pyrope-poor garnet; green, pyrope-rich garnet; red, omphacite; white, amphibole; black, zoisite. (C) Lu concentration profile crossing that part of the grain that is attributed to the first event of garnet growth. The indicated errors on the x-axis are spot diameters of LA-ICPMS analyses. The errors on the y-axis are 10 % of the measured value. (D) Lu-Hf isochrons of sample B15. Filled square, whole rock analysis; black diamond, omphacite analysis; grey diamonds, analyses of large garnets; white diamonds, analyses of small garnets.

The inner area is ragged with fissures filled by garnet of the same composition as the outermost rim. Small euhedral garnet grains exhibit a zoning from grossular-rich core ($Alm_{50}Grs_{27}Prp_{22}Sps_1$) to a grossular-poor rim ($Alm_{49}Grs_{22}Prp_{28}Sps_1$). Altogether the composition of small garnets resembles the one from the outer rim and fissures in the large garnets (Fig. 2.5B, Table 7.1 and 7.2). We interpret this microstructure to result from two growth events separated by a phase of resorption during which fissures formed in large garnets. These fissures were annealed during a second growth event, which also lead to the nucleation of new small garnets. A profile of Lu-concentration through the inner part of a large garnet grain that can be

attributed to the first growth event displays a more or less bell-shaped distribution through most of the grain as would be expected for growth zoning. A particularly high concentration is observed at one rim of the inner, early garnet generation (Fig. 2.5C). This likely represents a phase of backward diffusion into the remaining grain during garnet consumption (Kelly et al., 2011) and supports the view that the early garnet generation was affected by a period of resorption before overgrowth by garnet 2 took place.

The two populations of garnet are clearly distinguishable in Lu-Hf space (Fig. 2.5D): The population of large garnets is characterised by higher $^{176}Lu/^{177}Hf$ and $^{176}Hf/^{177}Hf$ ratios than the population of small euhedral garnets and garnet separates of population 1 contain approximately five times more Lu than garnet separates of population 2 (Table 2.1). A completely digested whole rock sample and all separates of large garnets yield an age estimation of 265 ± 59 Ma (MSWD 2300, n=4). The scatter results from differing amounts of overgrowth of garnet 2. A two-point isochron that is defined by the whole rock sample and the garnet separate with the most radiogenic $^{176}Hf/^{177}Hf$ ratio yields an age of 280.3 ± 1.0 Ma. This age is still affected by younger overgrowth domains and is thus distorted towards a younger apparent age (see discussion 2.5.1). Also garnet 1 was affected by resorption prior to overgrowth by garnet 2, which can lead to too young apparent Lu-Hf garnet ages (Kelly et al., 2011). As a result, we regard 280.3 ± 1.0 Ma as a minimum age for the formation of the early garnet generation in sample B15. For analysis of garnet generation 2, euhedral garnets were separated from a grain size fraction of less than 0.25 mm diameter. Two analysed separates of these small garnets together with a separate of omphacite produced an age of 38.8 ± 4.3 Ma (MSWD 0.034, n=3) and we interpret this age to be related to Alpine HP metamorphism. Omphacite in this sample is in equilibrium with garnet generation 2 and, thus, alpine (Fig. 2.5B). Though garnet generation 1 typically forms large relic grains, we cannot rule out that some of the small garnet grains might have crystallized around tiny fragments of garnet generation 1, i.e. that the separate of garnet generation 2 is completely free of contamination with garnet generation 1. Obviously, such a contamination would distort the age towards older apparent ages and the age of 38.8 ± 4.3 Ma strictly represents a maximum age for the formation of the small garnets in sample B15. The age data from the two populations of garnet present in sample B15 show that this sample was affected by two phases of garnet growth, which can be attributed to two orogenic cycles of Alpine and pre-Alpine age (Biino et al., 1997; Herwartz et al., 2011).

Sample B15 is very similar to a sample from Alp de Trescolmen further south in the Central Adula Nappe (TRC1 in Fig. 2.2A) presented by Herwartz et al. (2011).

Sample TRC1 also shows chemically zoned relics of garnet 1 overgrown by a second generation of garnet 2, which also nucleates as euhedral small grains. These two generations yielded minimum 332 Ma and maximum 37.1 ± 0.9 Ma, respectively.

2.4.3 Lake Zervreila (Northern Adula Nappe)

Sample SADU40 was taken from a metabasic body close to the northern front of the Adula Nappe. Its mineral assemblage comprises Omp + Grt + Qz + Amp + Rt + Zrn. Garnets are subhedral, contain inclusions of amphibole, quartz, epidote, rutile, and omphacite, and display pronounced zoning with respect to their major elements (Fig. 2.6A, B). The spessartine and grossular components as well as the Fe/(Fe+Mg)

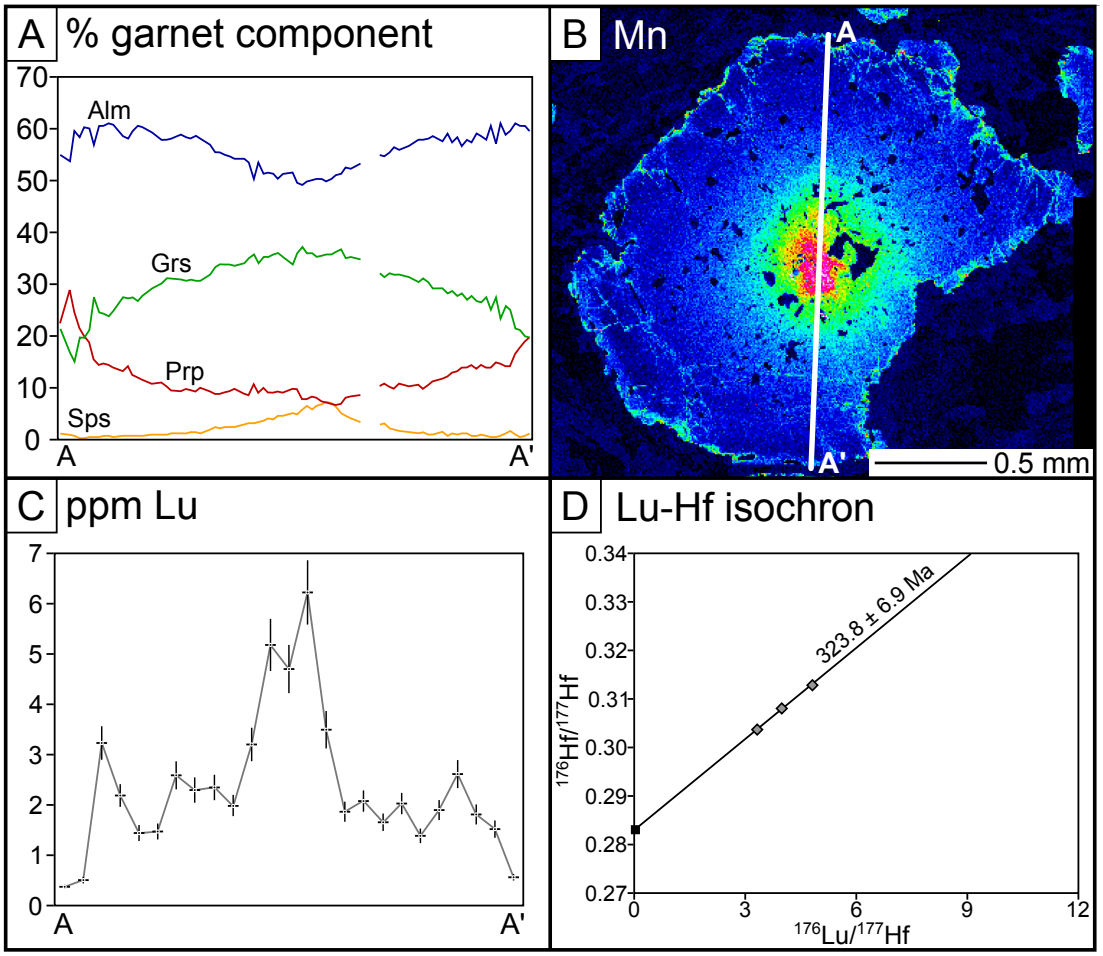

Figure 2.6: (A) Compositional profile through a representative garnet grain of eclogite sample SADU40 from Lake Zervreila in the northern Adula Nappe. (B) Elemental map of Mn distribution in the same garnet. The white line indicates the trace of the profiles of A and C. From red to dark blue: Mn-rich garnet to Mn-poor garnet. (C) Lu concentration profile. The indicated errors on the x-axis are spot diameters of LA-ICPMS analyses. The errors on the y-axis are 10 % of the measured value. (D) Lu-Hf whole rock-garnet isochron of sample SADU40. Filled square, whole rock analysis; grey diamonds, garnet analyses.

ratio and the Lu concentration (Fig. 2.6C) describe bell-shaped patterns, which are all typical for prograde growth zoning. A slight enrichment of the spessartine component at the outermost rim probably indicates minor resorption after garnet growth. We consider the obtained Lu-Hf garnet-whole rock age of sample SADU40 of 323.8 ± 6.9 Ma (MSWD 14, n=4) as a garnet formation age. This age corresponds to previously published radiometric age estimations for metamorphism in this part of the Adula Nappe. Liati et al. (2009) reported metamorphic U-Pb zircon ages in an orthogneiss and a garnet amphibolite from localities close to the sample location of SADU40 and obtained ages of 331 ± 4 Ma and 309 ± 36 Ma, respectively. Based on REE patterns in zircon domains, they attributed these ages to a HP metamorphic stage. An Alpine garnet generation was not identified in this sample.

2.4.4 Characterization of garnet from complementary samples

Sample SADU33 is an eclogite from the northern flank of the Fanellahorn located north of the sample location of sample B15. It also contains a population of large garnets up to 2.5 mm in diameter and a population of small garnets not larger than 0.2 mm in diameter. Chemical zoning of large garnets is again characterized by an abrupt change in composition (Fig. 2.7A), which is interpreted as to reflect two distinct growth stages. The inner zone has a core enriched in spessartine

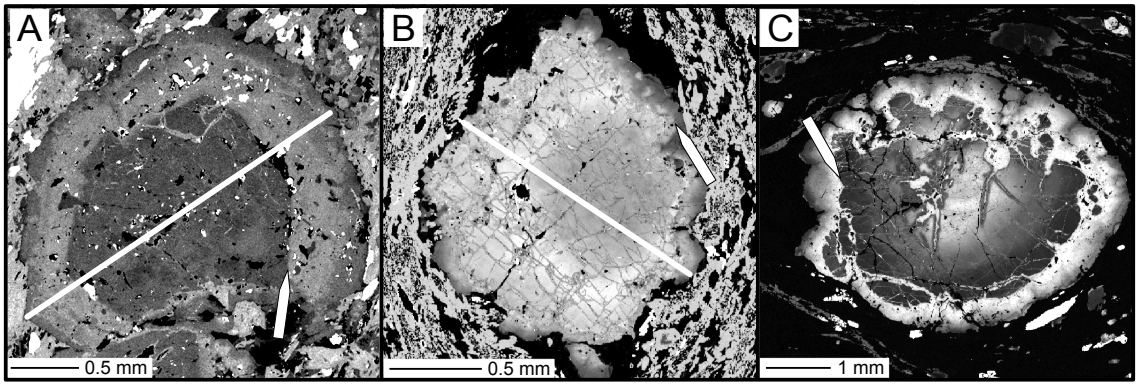

Figure 2.7: Ca zoning maps of garnets from (A) eclogite SADU33, (B) eclogite SADU52, and (C) garnet-mica schist SADU8. The white arrows mark the transition from the inner zone of garnet, which formed during a first metamorphic cycle, to the overgrowth zone of the second event. Detailed garnet compositions are given in Table 7.1 and 7.2.

($Alm_{54}Grs_{25}Prp_{6}Sps_{15}$), which evolves gradually towards a spessartine-poorer rim ($Alm_{58}Grs_{26}Prp_{10}Sps_{6}$), while almandine and pyrope increase. Grossular component shows minor variation. Indicators of garnet resorption are nearly absent in this zone (except for a small healed fissure at the top of figure 2.7A). The outer zone is grossular-rich and pyrope-poor at the border to the inner zone ($Alm_{58}Grs_{35}Prp_{6}Sps_{1}$) but becomes grossular-poorer and pyrope-richer towards the rims ($Alm_{58}Grs_{27}Prp_{15}Sps_{0}$).

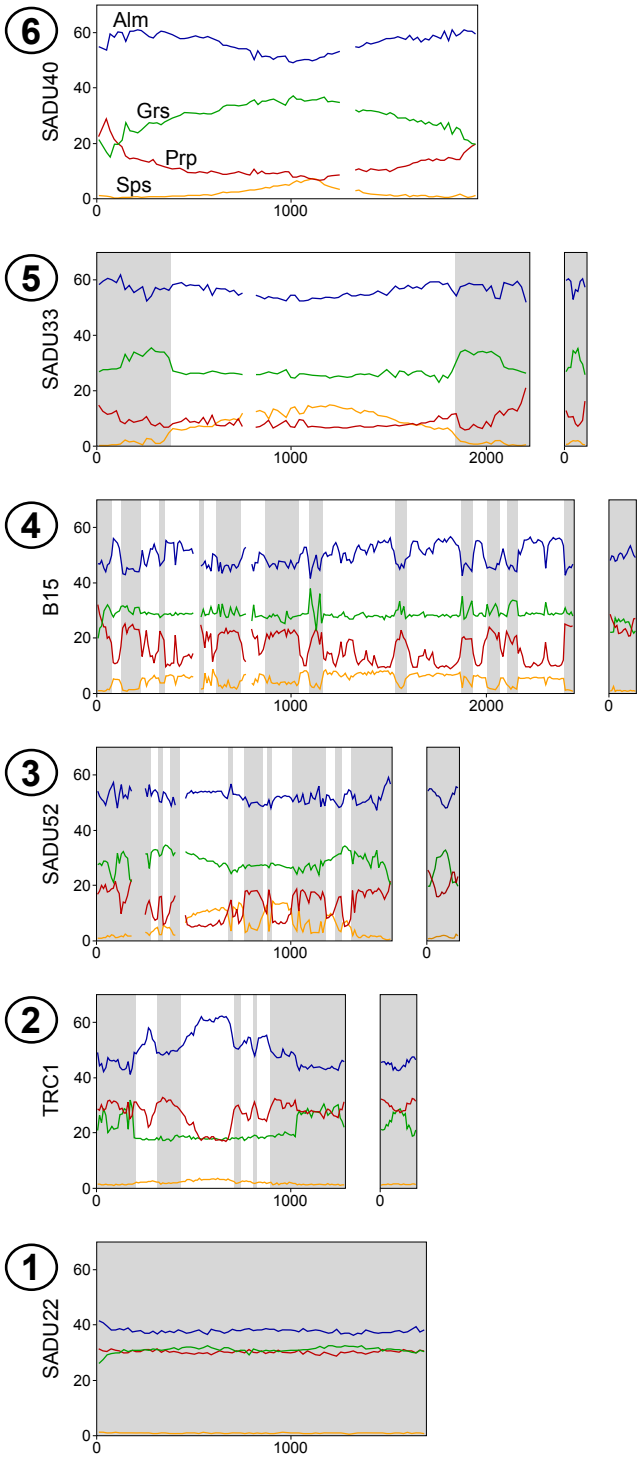

Figure 2.8: Representative compositional profiles through single garnet grains of eclogite samples from several locations. Sample locations are marked in Figure 2.2. The zones of garnet that are shaded in grey are attributed to re-equilibration or growth of garnet during the Alpine subduction event. Alpine metamorphic overprint apparently becomes less intense from the south to the north and is absent in garnets of eclogites from the northernmost part of the Adula Nappe. Locations: (1) Alpe Arami, SADU22; (2) Alp de Trescolmen, TRC1; (3) Piz d'Arbeola, SADU52; (4) Passo del San Bernardino, B15; (5) Fanellahorn, SADU33; (6) Lake Zervreila, SADU40.

Small garnets display one stage of garnet growth, which shows the same chemical attributes as the outer zone of the large garnets (Fig. 2.8). Eclogite sample SADU52 stems from the north-western flank of Piz d'Arbeola located south of the sample location of sample B15. Also this sample contains the same two populations of garnet (Fig. 2.8). Large garnets are reticulately fissured and exhibit two growth stages (Fig. 2.7B) while small garnets are monocyclic. The early generation evolves gradually from the composition $Alm_{52}Grs_{29}Prp_{6}Sps_{13}$ in the core to the composition $Alm_{57}Grs_{31}Prp_{9}Sps_{3}$ towards the rim. Again, garnet generation 2 fills the fissures, forms rims, and is also present as small euhedral grains. It has a distinct spessartine-poor and pyrope-rich composition with a decrease in grossular-component and a corresponding increase in almandine- and pyrope-component from core to rim (Fig. 2.8). In summary, these two samples display petrological appearances very much alike the sample from Passo del San Bernadino above and the sample from Trescolmen (Herwartz et al., 2011). They confirm the concept that eclogites in much of the central and northern Adula Nappe contain Variscan and Alpine garnet generations. The observation of similar distinct garnet generations defined by grain size and/or chemistry has been made in several studies in the Adula Nappe not just on eclogites, but also on garnet-mica schists (Meyre et al., 1997, 1999; Nagel et al., 2002b; Zulbati, 2008, 2010). Especially Zulbati (2008, 2010) suspected that the early generation might be pre-Alpine. As an example, we present one element distribution map of garnet from a garnet-mica schist (SADU8) from the Passo del San Bernardino (Fig. 2.7C and 7.6), where these schists constitute the host rocks of metabasic boudins. Like the eclogite samples, SADU8 contains a bimodal grain size distribution with large garnets up to 5.5 mm and small ones of up to 0.75 mm in diameter. The inner domain of large garnets preserve zoning, which evolves from $Alm_{69}Grs_{15}Prp_{13}Sps_{3}$ in the core to $Alm_{76}Grs_{3}Prp_{18}Sps_{3}$ at the rim. At the rim of this domain, the composition changes abruptly to $Alm_{71}Grs_{18}Prp_{10}Sps_{1}$ and then evolves to $Alm_{74}Grs_{4}Prp_{21}Sps_{1}$ at the grain boundary (Fig. 2.7C, Table 7.1 and 7.2). Small garnets display a chemical pattern that is similar to the outer rim of the large garnet grains.

2.5 Discussion

In the following sections we discuss several aspects of the presented data: the effect of biphasic garnet growth on Lu-Hf systematics (2.5.1), the significance of the obtained Lu-Hf ages (2.5.2), the timing of Alpine and pre-Alpine metamorphism (2.5.3), and consequences of the gradually southward increasing Alpine metamorphic overprint (2.5.4).

2.5.1 Biphasic garnet growth

Lu-Hf (or Sm-Nd) isotope data for polymetamorphic samples is rarely published because individual components scatter in $^{176}Lu/^{177}Hf$ vs. $^{176}Hf/^{177}Hf$ space (Brueckner et al., 2010; Herwartz et al., 2011; Nagel et al., 2013). Thus various unequilibrated reservoirs exist within single samples. For example, the $^{176}Hf/^{177}Hf$ isotopic reservoir of the first garnet generation did not re-equilibrate with the bulk rock after it formed. This first garnet generation may also shield inclusions, which then also preserve their original $^{176}Hf/^{177}Hf$ isotopic composition (Herwartz et al., 2011). During the second metamorphic event a sample may then partly equilibrate to the respective PT conditions. In our case, the samples from the central Adula Nappe partly equilibrated to alpine HP conditions. Only phases that are in equilibrium with each other should be used for isochron regressions, such as garnet 2 and omphacite. The by far largest error on the apparent isochron ages is induced due to mixing of unequilibrated phases, such as the imperfect separation of garnet generations 1 and 2 from each other. Lu-Hf ages of garnet 1 that formed during the older event is biased towards younger apparent ages when garnet of the second event is present in the analysed mineral fraction. Likewise, fractions of garnet 2 from the second event that inherit some older garnet would provide age information that is distorted towards older apparent ages. Because such cross contamination cannot be excluded the Lu-Hf ages of polymetamorphic samples represent maximum and minimum values. Figure 2.9 visualizes the expected evolution of isotopic reservoirs during two stages of garnet growth of different age.

2.5.2 Significance of Lu-Hf ages

Besides cross contamination, several other processes such as garnet resorption, re-equilibration and inclusions can bias Lu-Hf ages (Fig. 2.10). Especially the Variscan garnet generation is strongly resorbed, with Lu being partitioned into the relict garnet. Kelly et al. (2011) quantified these resorption effects and their models predict an age bias exclusively towards younger apparent ages. The degree of garnet resorption and the time difference between garnet growth and garnet resorption (Δtres) control the absolute age bias. A garnet that is resorbed by 50 % should be biased 4 to 14 % of Δtres (Kelly et al., 2011). For the samples studied by Kelly et al. (2011), the time interval between garnet growth (at 1850 Ma) and garnet resorption (at 1320 Ma) was large (Δtres = 530 Ma). Hence, Kelly et al. (2011) observed a large age effect for strongly resorbed garnet. For the Variscan samples studied herein, garnet was resorbed either within the same metamorphic cycle (Δtres $\leq$ 10 Ma) or in the Permian (Δtres $\approx$ 50 Ma). The age bias predicted from various models (Kelly et al.,

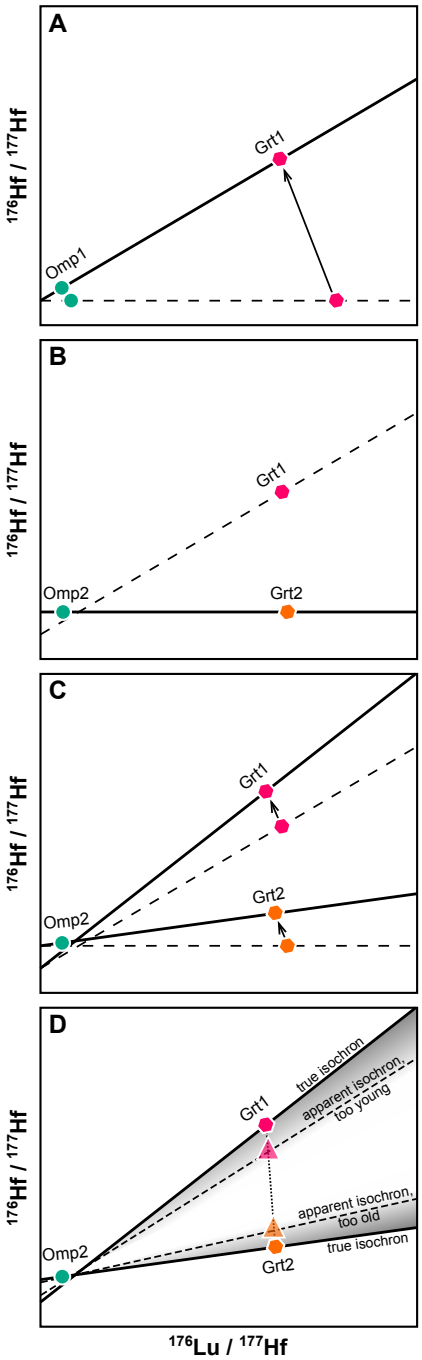

Figure 2.9: Schematic isochron plot illustrating the evolution of isochrons during two distinct metamorphic events. (A) Following the first metamorphic event the present mineral phases evolve towards lower $^{176}Lu/^{177}Hf$ and higher $^{176}Hf/^{177}Hf$. (B) During the second metamorphic event the new forming mineral phases establish a new $^{176}Hf/^{177}Hf$ initial while unequilibrated garnet remains decoupled from this process and retains its elevated $^{176}Hf/^{177}Hf$ value. (C) Following the second metamorphic event all present mineral phases evolve towards lower $^{176}Lu/^{177}Hf$ and higher $^{176}Hf/^{177}Hf$. The solid lines indicate the isochrons that represent the true ages for the two events. (D) Mixing of garnet that formed during the first event and garnet that formed during the second event produces younger apparent ages for the first metamorphic event and older apparent ages for the second metamorphic event. Triangles describe $^{176}Lu/^{177}Hf$-ratios and $^{176}Hf/^{177}Hf$-ratios that could be obtained today.

2011) and Δtres is 0.4 to 7 Ma. This could be significant for single stage garnet, but in our case, cross contamination by younger garnet is more important. In any case, the Variscan ages represent minimum ages. Because the Δtres of Alpine garnet is likely only a few million years, alpine ages are not biased by more than 0.4 Ma towards younger apparent ages.

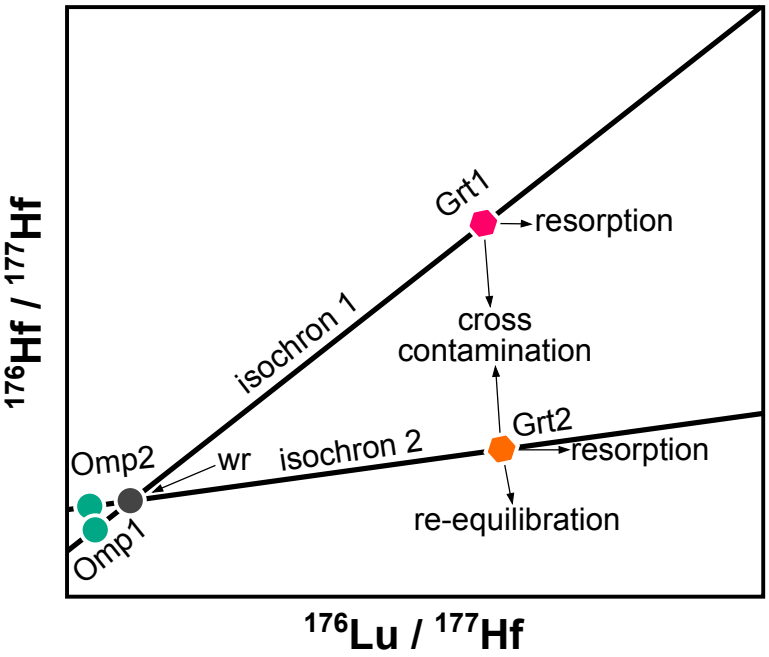

Figure 2.10: Schematic isochron plot illustrating how cross contamination, resorption, and re-equilibration can bias Lu-Hf garnet ages. Mixing of two garnet generations produces younger apparent ages for the first metamorphic event and older apparent ages for the second metamorphic event. Cross contamination is probably small or absent for garnet 2 of our sample B15 because only small euhedral garnet crystals were handpicked. Separation of garnet 1 was certainly imperfect. Hence, we expect a large cross contamination effect for garnet 1 of sample B15 from the central Adula Nappe. Resorption of garnet also leads to younger apparent Lu-Hf ages. For garnet 1 resorption may be significant (up to 7 Ma) but for garnet 2 resorption effects are small (c. 0.4 Ma; see section 2.5.2). Re-equilibration may be significant for sample SADU22 from the southern Adula Nappe, where temperatures were high. The figure does not consider inclusions as a source of error, nor does it consider potential disequilibrium between garnet and omphacite.

For the southern Adula Nappe, temperatures in excess of 800 °C and flat Lu profiles suggest that sample SADU22 may have been partially re-equilibrated. Redistribution of Lu within garnet, would lead to flat Lu profiles. Because garnet partition coefficients for Lu are high no Lu is lost to the matrix and bulk Lu-Hf ages are not affected by this process. Restricted mobility of trivalent REE is supported by the similar or slightly older Sm-Nd ages within the same area (Becker, 1993), implying that tetravalent Hf was largely immobile. However, we cannot exclude restricted re-equilibration of $^{176}Hf/^{177}Hf$ between garnet and matrix, which would lead to a

younger apparent age (see Fig. 2.10). Therefore, the age of sample SADU22 is interpreted as a minimum age.

Inclusions may bias ages towards either older or younger apparent ages and dissolution of protolith zircon cores is especially problematic for the Lu-Hf system (Scherer et al., 2001). We therefore applied the dissolution method of Lagos et al. (2007) were zircon is not dissolved to all mineral separates. Age bias due to inclusions is thus unlikely for our samples and certainly subordinate to cross contamination, re-equilibration, and resorption.

2.5.3 Timing of tectonic events recorded in the Adula Nappe

Eclogites from the Adula Nappe record age clusters of two distinct orogenic cycles: The first cycle is Variscan and in our study recorded by zoned garnets from the northernmost Adula Nappe and by relic domains enclosed in large garnets from the central Adula Nappe (Zulbati, 2010; Herwartz et al., 2011; this study). During a second orogenic cycle in the Eocene these rocks were subducted to upper blueschist and eclogite-facies conditions again. In that process rocks in the central and southern Adula Nappe experienced growth of a second generation of garnet, represented by overgrowth rims and new monocyclic garnets in eclogites. This event occurred under southward increasing PT conditions and possibly led to re-equilibration of the Lu-Hf isotopic system in our sample from the southern Adula Nappe.

2.5.3.1 Variscan HP-metamorphism

Sample SADU40 from the northern Adula Nappe does not contain obvious Alpine garnet and since Lu is strongly fractionated into the large Variscan grains (Fig. 2.5C and 2.6C), we propose that the Lu-Hf age of 323.8 ± 6.9 Ma is a garnet formation age. This Variscan age is close to metamorphic U-Pb SHRIMP zircon ages of 340-330 Ma in samples from the northern Adula Nappe (Liati et al., 2009). 340-320 Ma is a well-known Variscan metamorphic age found at many places in Central Europe (e.g. Schmädicke et al., 1995; Todt et al., 1995; Giorgis et al., 1999). Inclusions of omphacite inside garnet are a clear indicator that the formation of Variscan garnet occurred under eclogite-facies conditions. Variscan eclogites are well known in several basement units of the Alps which were less affected by Alpine overprint (Biino et al., 1997). In sample SADU40, matrix minerals like omphacite may also represent pre-Alpine relics and, finally, zircon from that age cluster apparently formed under eclogite-facies conditions. REE patterns in zircon indicate formation above the stability field of plagioclase and contemporaneous with garnet (Liati et al., 2009).

The partial resorption of the Variscan garnet generation observed in many samples

in the Adula Nappe either took place during isothermal decompression on the retrograde path of the Variscan pressure-temperature cycle or may be related to the Permian high-temperature metamorphism also widely distributed in the Alps (Schuster and Stüwe, 2008). In any case, the imbricated Triassic to Jurassic sedimentary cover rocks (Galster et al., 2012) indicate a near-surface position of the basement rocks of the Adula Nappe before Alpine subduction. Therefore, Alpine assemblages clearly formed during an entirely new metamorphic cycle.

2.5.3.2 Alpine HP-metamorphism

Maximum ages for the alpine HP event are 38.8 ± 4.3 Ma (this study) and 37.1 ± 0.9 Ma (Herwartz et al., 2011), while our Lu-Hf age from the southern Adula Nappe of 34.1 ± 2.8 Ma is probably a minimum age (see above). We suggest that these ages bracket the age of Alpine HP metamorphism between c. 34 and c. 38 Ma. This estimation is consistent with classic Rb-Sr ages from the northern Adula Nappe of c. 38 Ma (Jäger et al., 1967; Jäger, 1973) and U-Pb Zircon ages from the southern Adula Nappe of 35 Ma, possibly dating a slightly retrograde stage (Gebauer et al., 1992a; Gebauer, 1996). The Rb-Sr ages were interpreted as the age of formation of white mica and attributed to the post-nappe-stacking Barrovian stage of metamorphism. However, white mica often forms during prograde HP metamorphism (Guidotti and Sassi, 1998) and we propose that this age also reflects a metamorphic stage close to peak-pressure conditions even in the lower Lepontine Nappes (Nagel, 2008).

Brouwer et al. (2005) obtained Lu-Hf garnet ages between 35 and 79 Ma for 2-point isochrons defined by different garnet separates and non-garnet separates/whole rocks in eclogites and garnet amphibolites from the southern Adula Nappe. They interpreted this as indication for a long lasting record of HP metamorphism in the studied rocks. Considering that eclogites in the Adula Nappe often comprise Variscan garnet relics, we suspect that the scattering age record of Brouwer et al. (2005) results from contamination of Alpine garnet separates with Variscan garnet. Very similar scattering 2-point isochrons are recorded from the Eclogite Zone in the Tauern Window in eclogite samples that appear to be monocyclic (Nagel et al., 2013). A lack of full equilibration to Alpine (U)HP conditions may have produced the scattering ages observed by Brouwer et al. (2005). If so, not all samples in the southern Adula Nappe are fully equilibrated to alpine conditions. Hence, an age bias towards older apparent ages cannot be excluded for the samples of Becker (1993), some of which give rather old ($\geq$ 40 Ma) Sm-Nd ages. We propose that the existing age record in the Adula Nappe is consistent with a short lived and uniform (U)HP event 36-38 Ma ago. This event occurred under southward increasing conditions and is associated

with a southward increasing degree of Alpine overprint on top of Variscan high-grade assemblages. This interpretation also leads to the conclusion that the Adula Nappe represents a coherent piece of basement that experienced the Alpine subduction history as a whole at least from peak conditions onward. Kylander-Clark et al. (2012) summarized that microcontinents and thin continental margins undergo short lived (< 10 Ma) subduction cycles and we can now confirm that this is also true for the Adula Nappe with regard to the Alpine cycle.

2.5.4 Gradual character of Alpine metamorphic overprint

The Adula Nappe documents a southward increasing degree of Alpine overprint over Variscan assemblages. While sample SADU40 from the northernmost nappe is hardly affected by Alpine overprint sample SADU22 from the southernmost part of the nappe is fully equilibrated to Alpine conditions. Through most of the nappe, two distinct growth events can be distinguished. This confirmation of the metamorphic gradient is a strong argument for the Adula Nappe being a coherent piece of basement at least from the time of peak-pressure conditions onward. The view of a strongly-deformed, yet continuous, pre-Mesozoic Adula Nappe with isoclinal folds of Mesozoic cover rocks is also supported by zircon chronology and lithostratigraphic observations (Cavargna-Sani et al., 2014, subm).

Our data further offer an explanation for the diverging peak-pressure conditions published for the northern Adula Nappe. While the conservative estimation of 12 kbar/500 °C of Heinrich (1982, 1986) is based on mineral assemblages in a series of glaucophane-bearing metabasic rocks and schists, the higher estimations around 17-20 kbar (Dale and Holland, 2003; Zulbati, 2010) are derived from thermobarometry in solitary occurrences of true eclogites. We propose that eclogites from the northernmost part of the Adula Nappe are Variscan remnants. Zulbati (2010) already discussed the possibility that the discrepancy may result from the fact that high-grade conditions found in eclogites would actually be pre-Alpine. We agree with the peak-pressure estimations for the northern Adula Nappe that were presented by Heinrich (1982, 1986) because they are based on truly Alpine phases. In contrast, Alpine garnet clearly formed in equilibrium with omphacite and other HP matrix minerals in the central Adula Nappe (Fig. 2.5B; Meyre et al., 1997). Hence, eclogites and associated published PT estimates of 20-25 kbar/600-700 °C (e.g. Heinrich, 1986; Meyre et al., 1997; Dale and Holland, 2003) clearly reflect Alpine conditions. As a consequence, we favour a regional gradient from 12 kbar in the north to > 30 kbar in the south, the largest of proposed regional gradients (Heinrich, 1986; Dale and Holland, 2003; Carry et al., 2009). As mentioned above,

the associated field gradient exceeds the lithostatic pressure gradient. The internal mylonitisation suggests north-south stretching rather than shortening subsequent to peak-pressures. As a consequence, the Adula Nappe might have experienced enormous internal deformation, pronounced vertical flattening and a complete shape change (Nagel, 2008), yet it remained a continuous piece of basement.

A coherent character of the Adula Nappe implies that the felsic gneiss masses building the bulk of the nappe were subjected to the same HP metamorphism as the metabasics and metaultrabasics. In the northern Adula Nappe, gneisses and the so-called phengite schists often display high silica contents in white mica and assemblages in line with the conditions obtained for the Alpine HP stage (e.g. Heinrich, 1982; Löw, 1987). In the central and southern Adula Nappe, however, the much higher peak-pressure conditions of eclogites have not been identified in felsic rocks so far, except for trace element compositions in metamorphic zircon suggesting formation under eclogite-facies conditions (Liati et al., 2009). Hence, we have to assume that these rock types were completely retrogressed. In the southern Adula Nappe, the question arises if peak-pressure conditions in excess of 800 °C should not cause massive melting in gneisses. This should certainly happen if water is added during HP conditions. If, however, rocks remain anhydrous or water-undersaturated in the subducting slab (Ono, 1998; Spandler et al., 2010), melting is not expected to occur at temperatures less than 950 °C (Hermann and Green, 2001; Spandler et al., 2010).

Burial depths down to the transition zone proposed for the Alpe Arami ultrabasic complex in some studies (e.g. Dobrzhinetskaya et al., 1996; Bozhilov et al., 1999) exceed pressure estimations of all surrounding lithologies and are beyond any reasonable depth for crustal rocks. Hence, these conditions certainly do not represent regional HP metamorphism. They may, however, not be related to Alpine subduction. If the Alpe Arami complex belonged to the Adula Nappe already before the Alpine orogenic cycle, then the indicators for UHP metamorphism could be relics of a pre-Alpine mantle history. As an alternative, the ultrabasic complex may have been incorporated as a piece from the overlying mantle wedge to the deeply subducted European continental margin during the Alpine subduction cycle (Nimis and Trommsdorff, 2001), a scenario that was also proposed for the exhumation of the Otrøy UHP peridotites in western Norway (Van Roermund and Drury, 1998). This scenario is also supported by the southward increasing frequency of ultramafic bodies observed in the Adula Nappe. In that case, the ultrabasic complex of Alpe Arami and the continental Adula Nappe were indeed welded together in the subduction channel close to peak-pressure conditions but still underwent the subsequent stages

of the Alpine metamorphic cycle as a coherent unit. Nevertheless, the extremely high peak pressure prediction proposed by Dobrzhinetskaya et al. (1996) and Bozhilov et al. (1999) itself has been doubted by several authors (e.g. Hacker et al., 1997; Nimis and Trommsdorff, 2001; Risold et al., 2001) and its geological significance remains disputable.

2.5.5 Outlook

Our results imply that the felsic bulk of the Adula Nappe was subjected to HP metamorphic conditions together with the basic lithologies. It still needs to be evaluated if the gneisses record direct information about their HP history or show indications of retrogression following HP metamorphism. The Adula Nappe constitutes a suitable surrounding for further examinations on the characteristics of the Lu-Hf garnet geochronometer. The southernmost part of the unit features redistributed Lu patterns of garnet in eclogites, while further to the north garnet with preserved Lu zoning is found. A combined study of Lu and Hf distributions inside garnet with pressure and temperature estimations could lead to an improved determination of the actual temperature above which Lu and Hf are able to re-equilibrate.

2.6 Conclusions

The presented evidence argues for an origin of the Adula Nappe as a coherent part of pre-Mesozoic continental basement from the distal European continental margin, which was subducted to mantle depth during the Eocene orogenic cycle but already recorded Variscan high-pressure metamorphic conditions. Alpine HP metamorphism was coeval and short lived. The Adula Nappe shows a continuous gradient of Alpine metamorphic conditions from north to south, which exceeds the lithostatic pressure gradient. Today, this metamorphic gradient corresponds to a gradient of increasing Alpine overprint of Variscan relics, which are relatively well preserved in the North but mainly obliterated in the South. Exhumation from peak-pressure conditions occurred within few Ma as the entire nappe pile was established before 32 Ma.

Annotations

This chapter is published in *Contributions to Mineralogy and Petrology* (2014, 168:1075). T. Nagel, R. Kurzawski, and I collected the samples. I performed all microprobe analyses and Lu-Hf garnet dating. R. Fonseca and I carried out the LA-ICPMS analyses. T. Nagel, D. Herwartz, and C. Münker contributed to the interpretation of garnet analyses. T. Nagel and N. Froitzheim contributed to the tectonic interpretation. I wrote the manuscript and produced all figures.

3 Timing of eclogite-facies metamorphism of mafic and ultramafic rocks from the Pohorje Mountains (Eastern Alps, Slovenia) based on Lu-Hf garnet geochronometry

Sascha Sandmann[1], Daniel Herwartz[2], Frederik Kirst[1], Nikolaus Froitzheim[1], Thorsten J. Nagel[1], Raúl O.C. Fonseca[1], Carsten Münker[2], Marian Janák[3]

[1] Steinmann-Institut für Geologie, Mineralogie und Paläontologie, Universität Bonn, Meckenheimer Allee 169, D-53115 Bonn, Germany

[2] Institut für Geologie und Mineralogie, Universität Köln, Greinstr. 4-6, D-50939 Köln, Germany

[3] Geological Institute, Slovak Academy of Sciences, Dúbravská 9, 840 05 Bratislava 45, Slovak Republic

Abstract

The metamorphic series of the Pohorje Mountains represents that part of the Lower Central Austroalpine that was subjected to the highest pressure and temperature conditions during the Cretaceous Eo-Alpine metamorphic cycle. The Slovenska Bistrica Ultramafic Complex is an 8 km wide body of mainly serpentinite enclosing lenses of garnet-bearing ultramafites. It is surrounded by eclogites, metapelitic gneisses, and orthogneisses. We applied Lu-Hf garnet chronometry on two eclogite samples and two garnet-bearing ultramafites. Intra-garnet zoning of major elements and Lu was examined via electron microprobe and laser ablation ICPMS analyses. Lu-Hf garnet ages of 96.6 ± 1.2 Ma and 94.8 ± 5.1 Ma were obtained from eclogites. Garnets in these eclogites show growth zoning for Lu while major element contents are homogeneous due to diffusive equilibration. One ultramafic sample yielded 91.6 ± 4.1 Ma. Garnets in this sample show homogeneous Lu and major element contents. The other ultramafic sample gave no reasonable age. Together with previously published age data our results reveal that the ultramafic body and surrounding high grade metamorphic rocks were subjected to eclogite facies conditions in a single tectonic event between c. 97 and 90 Ma. This is contemporaneous with major out-of-sequence

thrusting in the Northern Calcareous Alps which is kinematically linked to subduction of the Lower under the Upper Central Austroalpine.

3.1 Introduction

The Pohorje Mountains in the Eastern Alps (Slovenia) are formed by three tectonic nappes of the Austroalpine mega-unit. The lowermost nappe (Pohorje Nappe after Janák et al., 2006) encompasses a variety of metamorphic rocks overprinted by orogenic high-pressure (HP) to ultrahigh-pressure (UHP) metamorphism. Although eclogite facies conditions were followed by regional amphibolite facies overprint, rocks from several locations still exhibit their primary HP and UHP mineral assemblages (Hinterlechner-Ravnik, 1987; Sassi et al., 2004; Janák et al., 2004, 2006; Kirst et al., 2010; Vrabec et al., 2012). The Pohorje Nappe represents a part of the Lower Central Austroalpine (Janák et al., 2004), a tectonic level that includes several eclogite facies metamorphic complexes (e.g. Saualpe, Koralpe, Fig. 3.1). Based on the collection of datasets summarized below, the age of HP and UHP metamorphism in the Austroalpine is generally accepted to be Eo-Alpine (i.e. Cretaceous). The metamorphic series of the Pohorje Nappe comprises mafic and ultramafic rocks embedded in orthogneisses and metasediments (e.g. Sassi et al., 2004; Janák et al., 2004; Kirst et al., 2010).

Peak pressure and temperature (PT) conditions of the Cretaceous metamorphism in the Pohorje region, whether HP or UHP, have been discussed controversially. Hinterlechner-Ravnik et al. (1991) and Visona et al. (1991) determined conditions of 750-1050 °C and 2.4-3.6 GPa for garnet peridotites from the SBUC, i.e. HP to UHP conditions. However, these authors assumed that the metamorphism of the garnet peridotites was pre-Alpine. Sassi et al. (2004) and Miller et al. (2005) determined peak PT conditions of the eclogites from Pohorje of 1.8-2.6 GPa and 600-740 °C, i.e. in the quartz stability field. In contrast, Janák et al. (2004, 2006) and Vrabec et al. (2012) derived conditions in the coesite stability field, i.e. 3.5-3.7 GPa at 800-940 °C for eclogites and 3.4-4 GPa at 890-960 °C for garnet peridotites, respectively. The lower conditions determined by Sassi et al. (2004) and Miller et al. (2005) may be explained by retrogression during exhumation. On the other hand, neither coesite nor diamond have been reported from Pohorje so far.

The timing of Eo-Alpine metamorphism in the Pohorje Mountains has been addressed in several studies. U-Pb zircon ages of eclogites and metapelites are c. 93-90 Ma (Miller et al., 2005; Janák et al., 2009). This is identical to Sm-Nd garnet ages and one Lu-Hf garnet age of eclogites (Miller et al., 2005; Thöni et al., 2008). These ages are in line with ages of HP metamorphism in the adjacent Koralpe and Saualpe

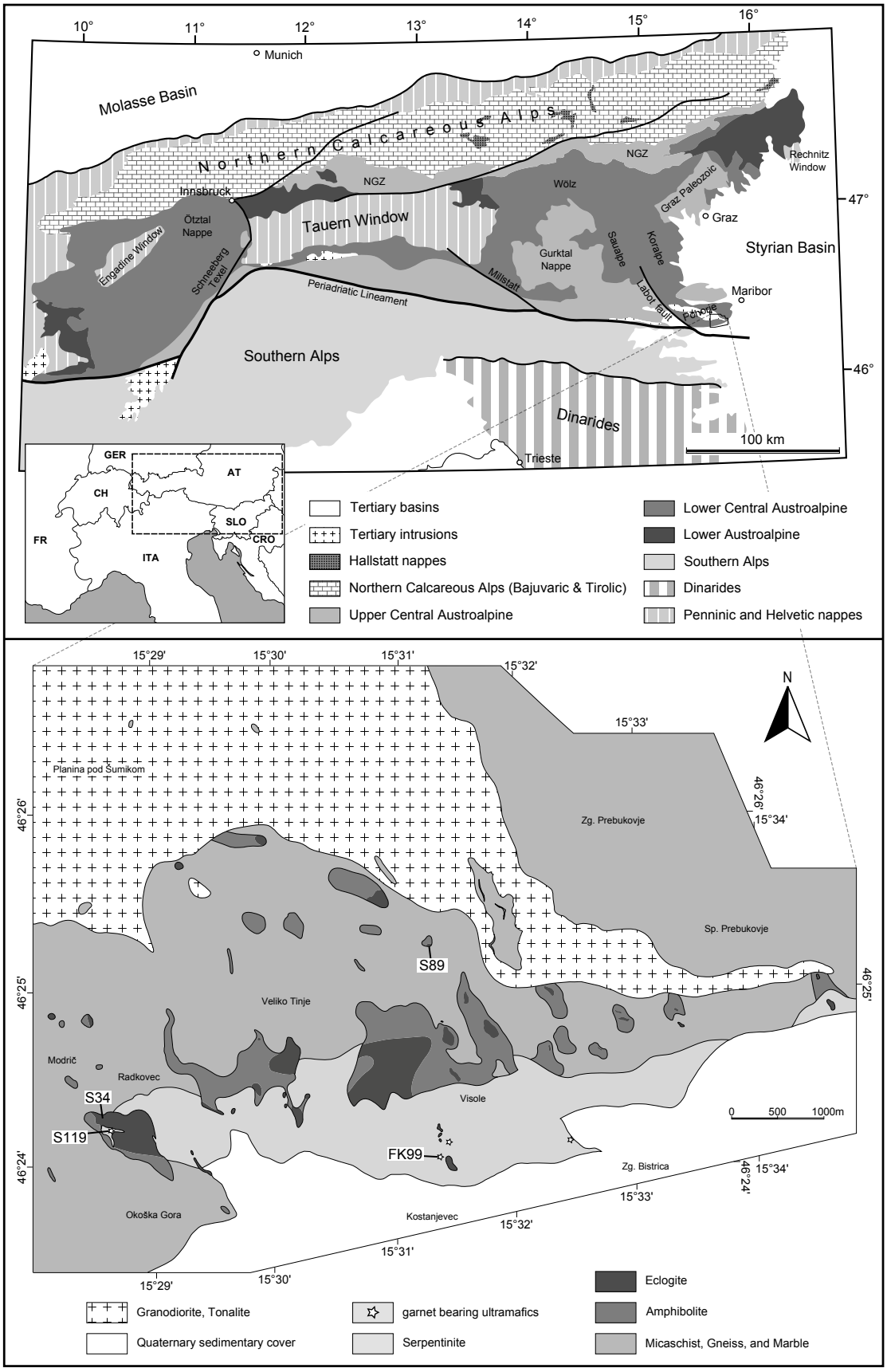

Figure 3.1: Tectonic map of the eastern Alps after Janák et al. (2004) and Vrabec et al. (2012). NGZ, Northern Grauwacke Zone; (B) Geological map of the southeastern part of the Pohorje Mountains with sample locations (simplified after Kirst et al., 2010).

(e.g. Thöni, 2006). HP and UHP metamorphism of ultramafic rocks have not been dated so far, neither in Pohorje nor in other parts of the Lower Central Austroalpine. Considering the high temperatures presented above, it is uncertain if these ages represent garnet growth or re-equilibration. Here we present new age constrains on garnet-bearing ultramafites and associated eclogites from the southeastern Pohorje Mountains by applying Lu-Hf garnet geochronometry. In situ LA-ICPMS Lu-profiles are employed to monitor intra-garnet diffusion, so that Lu-Hf ages can be attributed to garnet growth or re-equilibration. We argue that the closure temperature (T_C) was exceeded in one ultramafic sample, while the other samples give ages close to garnet formation.

3.2 Geological setting

The Austroalpine units represent the former northwestern continental margin of Apulia. They were thrust upon each other towards the NW during the Cretaceous Eo-Alpine orogeny (e.g. Schmid et al., 2004; Handy et al., 2010). The nappe stack can be subdivided from bottom to top into the thrust sheets of the Lower Austroalpine, the Lower Central Austroalpine and the Upper Central Austroalpine (Janák et al., 2004; Fig. 3.2). The former Permian to Mesozoic sedimentary cover of the Lower and Upper Central Austroalpine is represented by the allochthonous nappes of the Northern Calcareous Alps (Janák et al., 2004). Following Schmid et al. (2004), the metamorphic series of the Pohorje area, together with the Koralpe, Saualpe, Wölz, Millstatt, Schneeberg, and Texel complexes, belongs to the Koralpe-Wölz nappe system, a subunit of the Lower Central Austroalpine. During the Upper Cretaceous, these rocks were subducted towards the SE beneath the units of the Upper Central Austroalpine. The polarity of subduction is indicated by a southeastward increase in peak pressures along the Koralpe/Pohorje traverse (Hoinkes et al., 1999; Tenczer and Stüwe, 2003; Janák et al., 2004; Bruand et al., 2010).

The Pohorje Mountains in NE Slovenia represent the southeasternmost exposure of Austroalpine high-grade metamorphic assemblages (Fig. 3.1). They are located at the southeastern margin of the Eastern Alps just north of the Periadriatic Line and are bordered by the Miocene Ribnica Trough to the North and the Miocene to Pleistocene Styrian Basin to the East and South (Sachsenhofer et al., 1998). The Labot Fault defines the western and southwestern border of the Pohorje Mountains. The uppermost nappe in the Pohorje Mountains comprises Permo-Triassic sedimentary rocks, the next deeper one low-grade metamorphic Paleozoic metasediments. They are both restricted to the northwestern part of the Pohorje Mountains and belong to the Upper Central Austroalpine. The metamorphic series of the underlying Pohorje

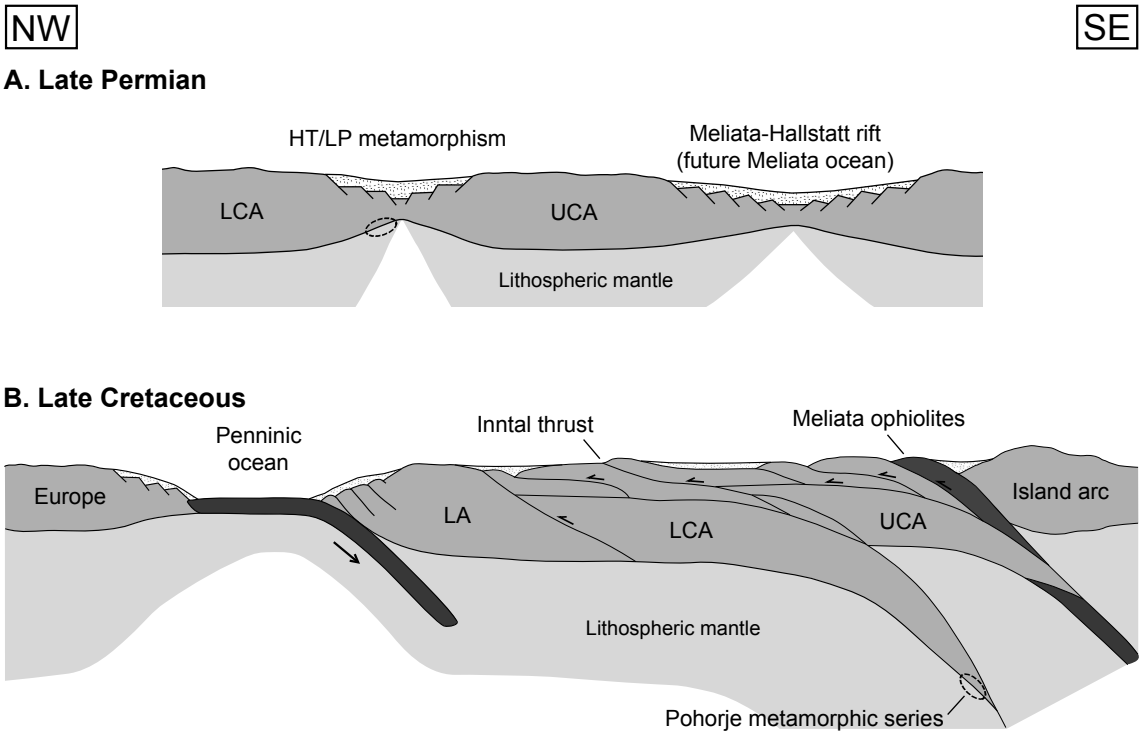

Figure 3.2: Tectonic model for the evolution of the Austroalpine realm. (A) Late Permian (modified after Kirst et al., 2010): The development of a rift between the Lower Central Austroalpine and the Upper Central Austroalpine causes HT/LP metamorphism. The Meliata ocean opens later in a rift SE of the Upper Central Austroalpine. (B) Late Cretaceous (modified after Janák et al., 2004): Already in the Jurassic, arc-continent collision after closure of the Meliata Ocean caused imbrication of Meliata ophiolites. The Pohorje eclogites and ultramafites were enclosed in an intracontinental subduction zone (e.g. Stüwe and Schuster, 2010) that formed in a more external position between the Lower and Upper Central Austroalpine. Albian-Cenomanian out-of-sequence thrusting along the Inntal Thrust coincides in time with c. 96 Ma eclogite metamorphism in Pohorje. LA, Lower Austroalpine; LCA, Lower Central Austroalpine; UCA, Upper Central Austroalpine.

Nappe mainly comprises gneisses and schists with minor marbles and quartzites as well as embedded bodies and lenses of eclogite and amphibolite. At the southeastern end of the Pohorje Mountains, the Slovenska Bistrica Ultramafic Complex (SBUC) extends over 8 km in E-W direction. This body consists of serpentinized ultramafites, eclogites and amphibolites as well as some garnet-bearing ultramafic rocks (Janák et al., 2006; Kirst et al., 2010). It forms the core of an isoclinal, recumbent, northward closing antiform, the Slovenska Bistrica Antiform (Kirst et al., 2010), which is mantled by the gneiss-dominated metamorphic series. The origin of eclogites and ultramafites is still under debate. Kirst et al. (2010) demonstrated that an unfolded Slovenska Bistrica Antiform resembles crust-mantle boundary complexes (e.g. the Ivrea Zone in the Western Alps) by displaying the tectonostratigraphic series of (1) ultramafic rocks with incorporated eclogite lenses at the base, (2) larger eclogite

bodies connected with the internal eclogites of the SBUC in the middle part, and (3) ortho- and paragneisses interlayered with schists, marbles, and smaller mafic lenses at the top. They proposed that the SBUC represented the uppermost mantle in a Permian-age rift and already belonged to the down-going plate during Eo-Alpine subduction. In contrast, Janák et al. (2006) proposed that the ultramafites were incorporated into the subducting slab from the upper-plate mantle wedge before subduction to UHP depth. De Hoog et al. (2009, 2011), based on major and trace element data, argued that the ultramafic rocks are of oceanic origin. Hence, the origin of the ultramafic rocks and their relation to the mafic eclogites are still debated and await clarification.

The central part of the Pohorje Mountains is built by a granodioritic to tonalitic intrusion with an early Miocene crystallization age of c. 18.6 Ma (Fodor et al., 2008; Trajanova et al., 2008). Still in the Neogene, the intrusion and the overlying metamorphic rocks were folded into a large, open, WNW-ESE trending antiform, the Pohorje Antiform (Kirst et al., 2010). At the same time, the Pohorje Massif was tectonically exhumed as a metamorphic core complex.

3.3 Analytical methods

Lu-Hf garnet geochronology has been established as a robust tool to date subduction processes (e.g. Duchêne et al., 1997; Lapen et al., 2003; Herwartz et al., 2011). The distribution of the bivalent major elements Ca, Fe, Mg, and Mn inside garnet crystals provides insight into the growth history of garnet. The isotopic age of garnet is controlled by the distribution of Lu in garnet crystals. Since diffusion coefficients of bivalent elements in garnet are generally higher than those of trivalent REEs (Carlson, 2012), garnet may preserve a prograde zoning of Lu while the major elements have already been re-equilibrated.

3.3.1 Electron microprobe and LA-ICPMS analysis

Electron microprobe analyses were carried out on a JEOL Superprobe JXA 8200 at the Steinmann-Institut in Bonn, using a beam current of 15 nA and an acceleration voltage of 15 kV. Dwell time of single spot analyses during map scans was set between 100 and 200 msec depending on the size of the scanned grain. Laser ablation analyses were carried out at the Steinmann-Institut using a Resonetics M50-E ATL Excimer 193 nm laser system coupled to a Thermo-Finnigan X-series 2 quadrupole ICP-MS, following the routine described by Kirchenbaur et al. (2012). Spot sizes were set between 55 and 75 µm depending on grain size and the amount of

visible inclusions. Laser fluency at the sample surface was measured between 4 and 7 J/cm^{-2}. The laser repetition rate was set to 10 Hz. Count rates were normalized using ^{29}Si as the internal standard and NIST-SRM 612 as the external standard (Jochum et al., 2011). Measurement accuracy was checked using NIST-SRM 610 as an external reproducibility standard and was found to be between 5-15 % of the preferred values (as described in Jochum et al., 2011). Count rates for ^{175}Lu were monitored during 20 seconds for background, and 40 seconds during ablation (Fig. 3.3). Oxide production rates were monitored using ThO_2/Th ratios and kept below 0.5 % in order to avoid oxide molecular interferences on the REE nuclides. Data reduction and evaluation followed the procedure presented by Longerich et al. (1996).

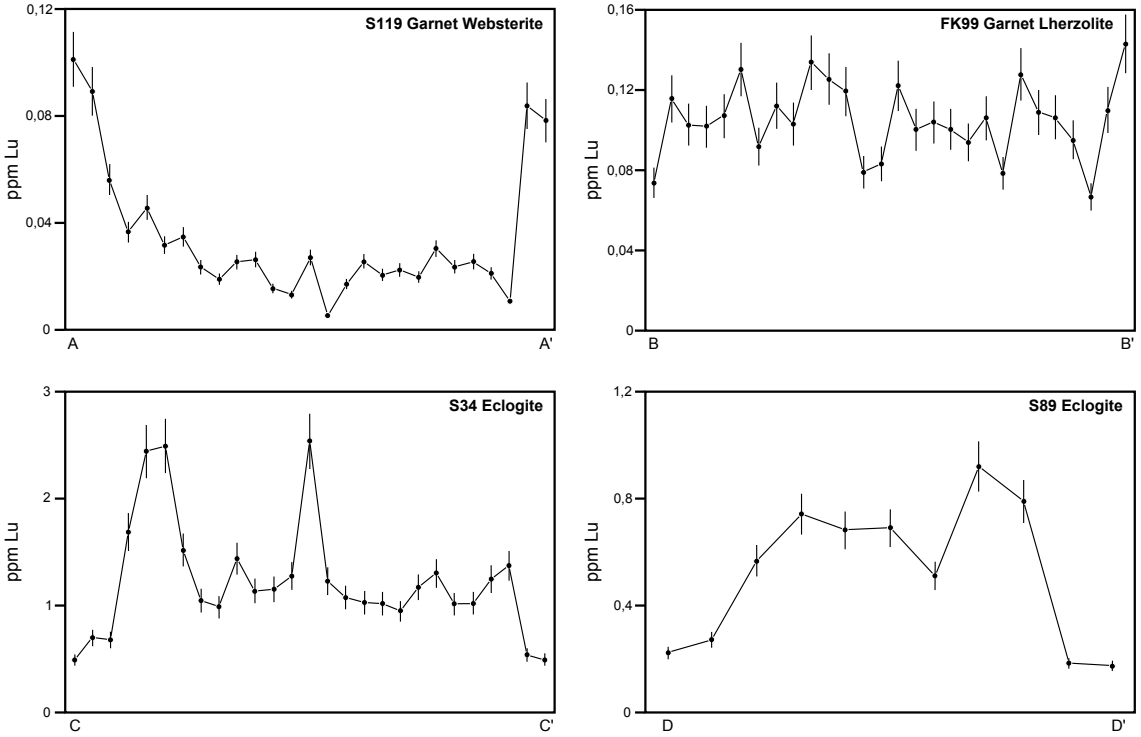

Figure 3.3: Element profiles for Lu obtained by laser ablation analyses. The indicated errors are 10 % of the measured value. The eclogite samples S34 and S89 comprise inherited garnet growth zonation with high content of Lu in the core of garnet which is decreasing towards the rims. Highly elevated peak values of Lu observable in sample S34 may be caused by undetected, Lu-rich microinclusions. Ultramafic sample FK99 is characterised by the absence of a preferential zonation of Lu. Ultramafic sample S119 comprises enriched garnet rims relative to a plateau poor in Lu in the core.

3.3.2 Sample digestion and MC-ICPMS analysis

For mineral separation, crushed samples were split into grain size fractions by dry sieving. A garnet-rich fraction was separated using a Frantz L-1® magnetic separator.

Garnet separates were then handpicked under a stereo microscope. From each sample three garnet fractions have been extracted with each of the fraction containing c. 100 mg. In addition, one fraction of c. 100 mg of omphacite was handpicked from samples S89 and S34. From sample FK99 one fraction of c. 100 mg clinopyroxene was separated. All mineral separates were cleaned with 2.5 M HCl in an ultrasonic bath and rinsed twice with deionised water. A mixed ^{176}Lu-^{180}Hf tracer was added to all samples prior to digestion. All mineral separates were dissolved by using the selective digestion procedure of Lagos et al. (2007) leaving behind Hf-rich phases (rutile and zircon), which might comprise unequilibrated isotope signatures. The separates were digested in Savillex screw-top PFA beakers by addition of HF-HNO_3-$HClO_4$ (4:2:1) and adjacent dry down followed by addition of 6N HCl (see Lagos et al., 2007 for details). A clear solution indicated complete digestion of mineral grains, whereas unclear solutions were processed a second time. Whole-rock powders of all samples were dissolved inside steel-jacketed Teflon PARR® bombs for five days at 180 °C in order to ensure complete sample dissolution. Lu and Hf were separated from the matrix elements using Eichrom® Ln-Spec resin and the method described by Münker et al. (2001). The Hf cuts were additionally purified following the clean-up procedure of Lagos et al. (2007) by repeating the Ln spec column chemistry using 48 ml of 6N HCl to remove remaining matrix elements and especially Lu. Subsequently Hf was eluted using 2N HF.

Lu and Hf measurements were obtained on a Finnigan Neptune MC-ICPMS at the Steimann-Institut in Bonn. Naturally occurring Yb in the Lu cuts was used for mass bias correction on Lu isotope ratios (Vervoort et al., 2004; Lagos et al., 2007) and interferences on ^{176}Lu were corrected by monitoring ^{173}Yb and ^{177}Hf and applying the natural isotope compositions (Vervoort et al., 2004). Instrumental mass bias on Hf isotope ratios were corrected by using the exponential law and a ^{179}Hf/^{177}Hf of 0.7325. Measured ^{176}Hf/^{177}Hf ratios presented in this work are given relative to a ^{176}Hf/^{177}Hf ratio of 0.282160 for the Münster Ames Hf standard, which is isotopically identical to the JMC-475 standard. Isobaric interferences on ^{176}Hf and ^{180}Hf were corrected by monitoring ^{173}Yb, ^{175}Lu, ^{181}Ta, and ^{183}W and their natural isotope compositions (Vervoort et al., 2004). In case of significant Lu impurities that sometimes remained even after the clean-up procedure, Hf compositions were calculated using both the spiked and the natural Lu compositions (Amelin et al., 2011). The difference between the two was then added to the external reproducibilities used for the isochron calculations, which were estimated by the empirical relationship 2σ external reproducibility ≈ 4σm (σm = standard error of a single analysis; e.g. Bizzarro et al., 2003). The given 2σ external reproducibility for ^{176}Lu/^{177}Hf includes

an error propagation for over- or under-spiked samples. Typical errors for $^{176}Lu/^{177}Hf$ were 0.2538 % of the measured ratio. The errors of single analyses are given in Table 3.1. Regressions of isochrons and ages were calculated using ISOPLOT v. 2.49 (Ludwig, 2001) and a decay constant of $\lambda^{176}Lu = 1.867 \times 10^{-11} yr^{-1}$ (Scherer et al., 2001; Söderlund et al., 2004). Blanks were 3-25 pg for Lu and 13-42 pg for Hf and were always insignificant.

Table 3.1: Lu-Hf isotope data of whole rock samples and mineral separates used for the isochrons.

Sample		ppm Lu	ppm Hf	$^{176}Lu/^{177}Hf$	Error	$^{176}Hf/^{177}Hf$	Error
S119	WR	0.0404	0.0949	0.06043	0.00015	0.283343	0.000034
	Grt1	0.0498	0.0417	0.1697	0.0004	0.283314	0.000113
	Grt2	0.0451	0.0424	0.151	0.0004	0.283469	0.000037
FK99	WR	0.0566	0.0824	0.09748	0.00024	0.283404	0.000025
	Grt1	0.131	0.0145	1.282	0.003	0.285388	0.000137
	Grt2	0.141	0.0142	1.411	0.004	0.285648	0.00009
	Grt3	0.142	0.0139	1.45	0.004	0.285748	0.000064
	Cpx	0.00931	0.208	0.006347	0.000016	0.283264	0.000098
S34	WR	0.44	1.78	0.03501	0.00009	0.283138	0.000016
	Grt1	1.07	0.0884	1.722	0.004	0.286281	0.000046
	Grt2	1.01	0.076	1.883	0.005	0.286528	0.000027
	Grt3	1.04	0.0777	1.896	0.005	0.286553	0.000027
	Omph	0.0592	0.535	0.0157	0.00004	0.283163	0.000037
S89	WR	0.118	0.244	0.06871	0.00017	0.283289	0.000016
	Grt1	0.302	0.0538	0.7969	0.002	0.284589	0.000045
	Grt2	0.305	0.0532	0.8146	0.002	0.284601	0.000032
	Grt3	0.296	0.0535	0.7862	0.002	0.284555	0.000032
	Omph	0.137	0.167	0.1167	0.0003	0.28337	0.000064

3.4 Sample description

The eclogite sample S34 and the garnet-bearing ultramafic samples S119 and FK99 belong to the SBUC. Eclogite S89 was sampled c. 1 km north outside the SBUC (Fig. 3.1). Sample coordinates are given in Table 3.2 and representative mineral analyses are presented in Table 7.3 and 7.4. Mineral abbreviations follow Whitney and Evans (2010).

Table 3.2: UTM coordinates of sample locations.

Sample	Location	UTM Coordinates
S119	Radkovec	33T 536667 5138931
FK99	Kostanjevec	33T 539820 5138338
S34	Radkovec	33T 536612 5139064
S89	Jurišna Vas	33T 540062 5140956

3.4.1 Ultramafic rocks

Sample S119 contains the HP-mineral assemblage garnet + clinopyroxene + olivine + amphibole. This HP-mineral assemblage is partly replaced by secondary amphibole, serpentine, green spinel, talc, and chlorite. The sample contains a significant modal proportion of garnet (~35 vol %) and only minor olivine and can therefore be classified as a garnet websterite. Garnet forms subhedral grains up to 5 mm in size and has a composition of $Prp_{58-67}Alm_{17-23}Grs_{13-22}Sps_{0-1}$. It does not show any concentric chemical zoning with respect to the major elements Fe, Mg, Ca, and Mn (Fig. 3.4). Garnet contains inclusions of clinopyroxene, spinel, and pargasite which are mostly located close to the crystal rims. Although garnets display an apparent resorption texture there is no significant enrichment of Mn towards the rims. Olivine forms subhedral to anhedral grains with a composition of Fo_{90-92}. Clinopyroxene is diopsidic and some of the grains contain exsolutions of orthopyroxene, amphibole, and rutile. Pargasitic amphibole replaces diopside but also occurs as idiomorphic crystals. It is rich in Al (up to 13.5 wt% Al_2O_3) and Cr (up to 1 wt% Cr_2O_3). Tremolitic amphibole occurs as corona around diopside and pargasite. Sample S119 was taken from the same block like sample 119 of Janák et al. (2006). These authors determined peak conditions of c. 4 GPa and 900 °C for their sample.

Sample FK99 consists of the mineral assemblage garnet + clinopyroxene + orthopyroxene + amphibole + olivine, which is to some extent replaced by secondary amphibole. Thus, this sample can be classified as a garnet lherzolite. Subhedral garnet is up to 4 mm in size and has a composition of $Prp_{56-60}Alm_{25-30}Grs_{13-18}Sps_{0-1}$. It does not show a chemical zoning of the major elements (Fig. 3.4). Garnet contains inclusions of clinopyroxene and pargasite. Olivine forms subhedral to anhedral grains with the composition Fo_{84-85}. Orthopyroxene has the composition En_{85-90} and in some cases shows a slight increase of Al towards the rims. Diopsidic clinopyroxene sometimes contains exsolutions of amphibole and spinel. Matrix amphibole is pargasitic while tremolitic amphibole occurs as corona around diopside.

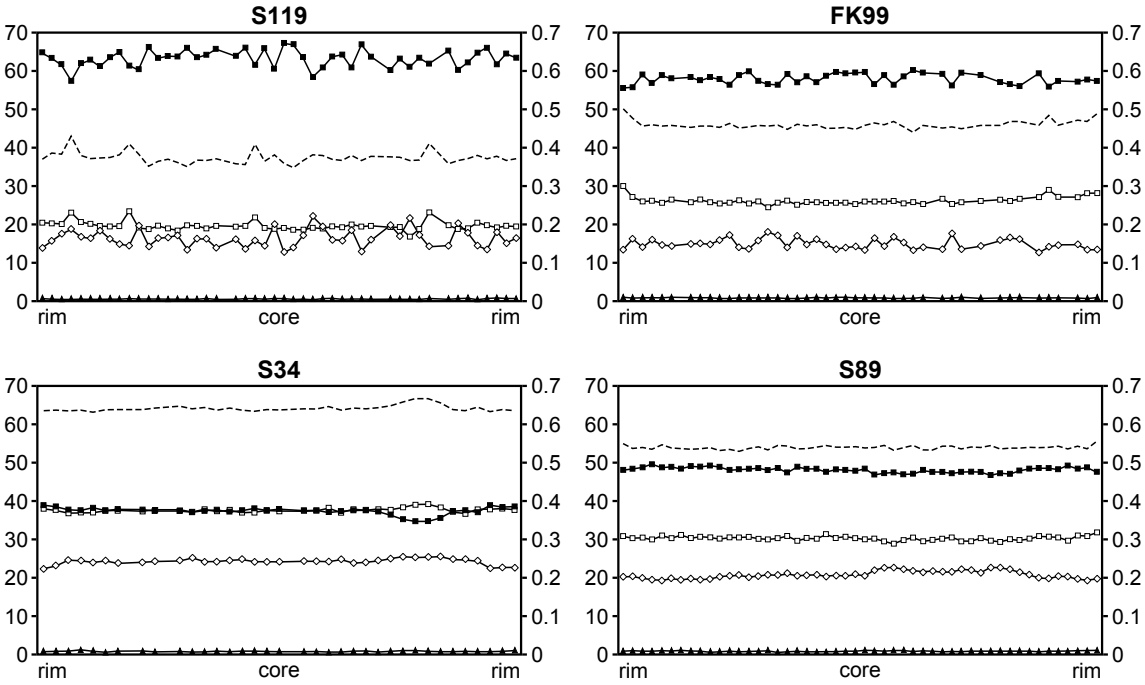

Figure 3.4: Representative compositional profiles of garnet from the four samples dated in this study. A prograde growth zoning of garnets major element composition is absent in all samples. Black squares, pyrope component; White squares, almandine component; White diamonds, grossular component; Black triangles, spessartine component; dashed line, FeO/(FeO+MgO).

3.4.2 Eclogites

The peak-pressure mineral assemblage of eclogite sample S34 consists of garnet + omphacite + kyanite + zoisite + quartz + rutile. Retrograde phases are amphibole, plagioclase, and diopsidic clinopyroxene as well as some chlorite, spinel, and sapphirine. Garnet grains are mostly euhedral with sizes of up to 7 mm. Garnet has the composition $Alm_{37-39}Prp_{35-39}Grs_{22-26}Sps_{0-1}$ and lacks a zoning of major elements (Fig. 3.4). Inclusions inside garnet are omphacite, quartz, rutile, and zircon. Omphacite contains 22-32 mol% jadeite component, the rest is mainly diopside. Anorthite-rich plagioclase partly replaces zoisite and garnet is sometimes rimmed by retrograde chlorite. Symplectites of sapphirine, spinel, plagioclase and amphibole occur around kyanite in contact with omphacite.

The peak-pressure mineral assemblage of sample S89 is identical to the one of sample S34. Euhedral garnet is up to 3 mm in size. Garnet is not zoned and has the composition $Prp_{47-49}Alm_{29-32}Grs_{19-23}Sps_{0-1}$ (Fig. 3.4). There are sparse inclusions of omphacite and rutile in garnet. The retrogression of the primary mineral assemblage is less pronounced than in sample S34. Sample S89 is identical to sample JV03 of Janák et al. (2004). They determined peak PT conditions of 3.1 GPa and 762-767 °C for this sample.

3.5 Results

3.5.1 Zoning of Lu contents in garnet

Lu-concentration profiles of single garnet grains obtained by laser ablation analyses are presented in Figure 3.3. Lu in garnet of the eclogite samples S34 and S89 is accumulated in the cores with decreasing Lu content towards the rims. Conversely, garnet from the ultramafic sample S119 is enriched in Lu along the rims relative to a plateau poor in Lu in the core. Ultramafic sample FK99 shows no preferential distribution of Lu contents.

3.5.2 Lu concentrations and Lu-Hf ages

Bulk Lu concentrations in the ultramafic samples S119 (0.0404 ppm) and FK99 (0.0566 ppm) are about one order of magnitude lower than the respective concentrations in eclogite samples S34 (0.440 ppm) and S89 (0.118 ppm). A similar relation is evident for Hf (Table 3.1). $^{176}Lu/^{177}Hf$ ratios of garnet from eclogite sample S34 range from 1.72 to 1.89 and $^{176}Lu/^{177}Hf$ ratios of garnet from eclogite sample S89 range from 0.814 to 0.786. Garnet of ultramafic sample FK99 yields high $^{176}Lu/^{177}Hf$ ratios between 1.28 and 1.45, but garnet from ultramafic sample S119 exhibits extremely low $^{176}Lu/^{177}Hf$ ratios (0.150 and 0.170), making this sample less suitable for Lu-Hf geochronology. In this sample, the spread in $^{176}Lu/^{177}Hf$ ratios between whole rock and garnet is too small to define an age and the slope of a correlated isochron would even be negative (Fig. 3.5). The three other samples returned data sufficient to infer well-defined ages. The clinopyroxene-garnet age of ultramafic sample FK99 is 91.6 ± 4.1 Ma (MSWD 0.55, n=4; Fig. 3.5). The omphacite-garnet ages for the eclogite samples are 96.6 ± 1.2 Ma (MSWD 1.5, n=4; Fig. 3.5) for S34 and 94.8 ± 5.1 Ma (MSWD 0.25, n=4; Fig. 3.5) for S89. All three ages are identical within error with their error bars overlapping between 95.4 and 95.7 Ma.

3.6 Discussion

In the following we discuss the zoning of major elements and Lu in garnet of our samples (3.6.1). We compare our new Lu-Hf ages with previously published metamorphic age data from the Pohorje Mountains (3.6.2) and draw tectonic implications for the Austroalpine realm which follow from these data (3.6.3).

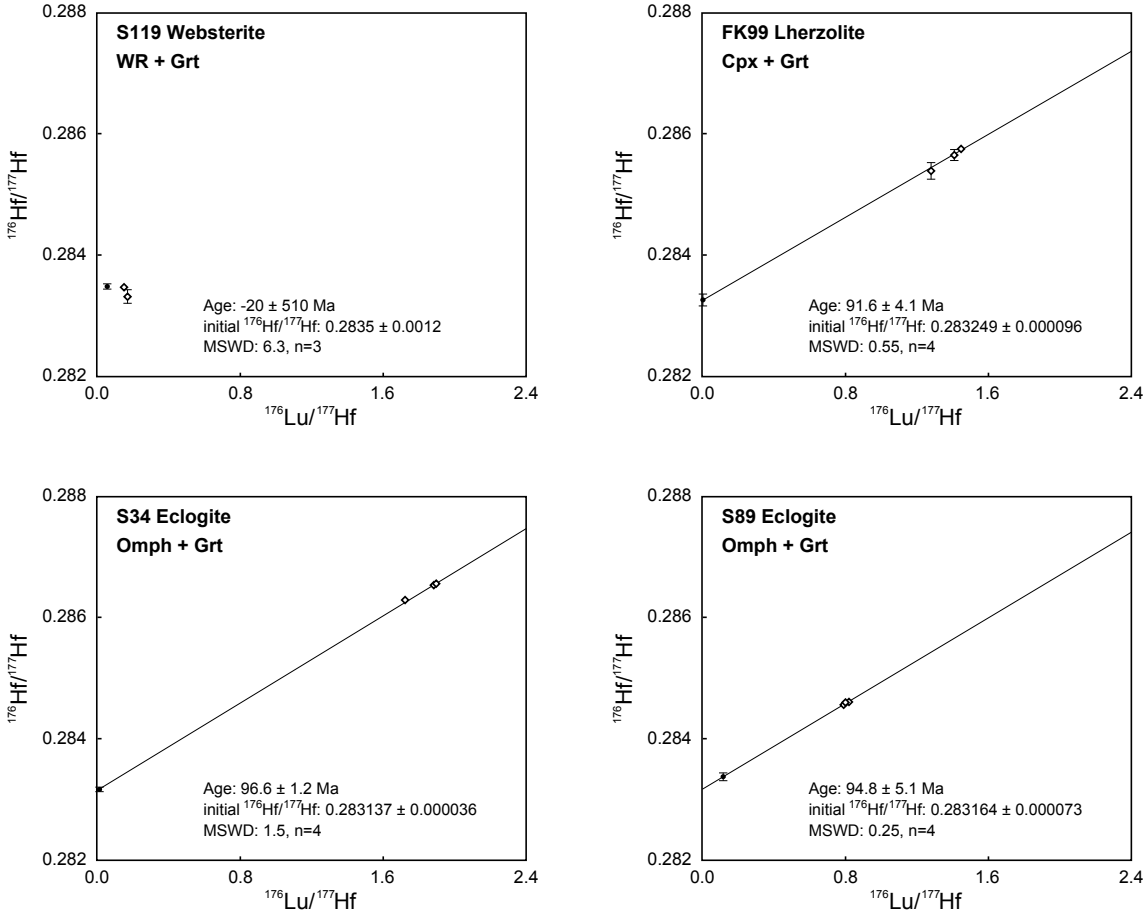

Figure 3.5: Lu-Hf isochron plots of eclogite samples (S34 and S89) and ultramafic samples (FK99 and S119). If not indicated error bars are smaller than the icons. Peridotite sample S119 comprises low $^{176}Lu/^{177}Hf$ ratios, hampering this sample to be used for Lu-Hf geochronology.

3.6.1 Element distribution in garnet and its implications for the Lu-Hf closure temperature

The 2D maps of garnets for the major elements Fe, Mg, Ca, and Mn and the flat Fe/(Fe+Mg) profiles illustrate that the samples of this study were affected by temperatures allowing diffusional re-equilibration of these bivalent cations in garnet. Re-equilibration of major elements in garnet is expected to occur at temperatures above 600 to 650 °C depending on the length of time that the rock is affected by these temperatures (Caddick et al., 2010). In contrast, diffusional re-equilibration of trivalent cations in garnet requires higher temperatures (Carlson, 2012).

An approximately flat pattern for Lu is observed in ultramafic sample FK99 which yields the youngest Lu-Hf age (Fig. 3.3). This sample may have been affected by temperatures that enabled diffusion of Lu inside garnet resulting in an equilibrated concentration pattern. Ultramafic sample S119 exhibits enriched garnet rims relative to a plateau poor in Lu in the core, which can be explained by garnet resorption.

Consumption of the outer grain parts causes migration of Lu into the remaining garnet (Kelly et al., 2011). Unfortunately, the spread in $^{176}Lu/^{177}Hf$ for this sample is too low to examine any effect on the Lu-Hf age. In contrast to the ultramafic samples, Lu content in garnet grains of eclogite samples S34 and S89 is characterised by roughly bell-shaped distributions with high concentrations of Lu in the core and a decrease towards the rims (Fig. 3.3). This is a characteristic primary pattern that establishes during garnet growth (e.g. Lapen et al., 2003; Kohn, 2009; Skora et al., 2009; Kirchenbaur et al., 2012). Schmidt et al. (2011) observed similar patterns in garnet of eclogite samples that were subjected to temperatures of up to 800-850 °C and, like in our study, the bivalent cations in garnet had been re-equilibrated. Hence, we attribute the Lu-Hf ages of the eclogite samples (96.6 ± 1.2 Ma, 94.8 ± 5.1 Ma) to the initial stages of garnet formation on the prograde path of the subduction cycle. Diffusion of Lu seems to be negligible and an effect of resorption is also not identified in these samples. In contrast, we consider the Lu-Hf age of sample FK99 to possibly be distorted towards a slightly younger apparent age. The Lu profile in this sample is flat and, thus, Lu was likely mobile. Because Lu fractionates into garnet and is not lost into the rocks matrix the Lu-Hf age is not affected by the mobility of Lu. However, if Hf was also mobile diffusional re-equilibration of $^{176}Hf/^{177}Hf$ between garnet and matrix would lead to a younger apparent age. Consequently, we interpret the age of 91.6 ± 4.1 Ma as a minimum age for garnet formation in this sample. Still, this age overlaps within error with the garnet growth ages inferred from the eclogite samples.

The calculated temperature that affected the ultramafic rocks (890-960 °C; Janák et al., 2006) in the southeastern Pohorje Mountains slightly exceeds the maximum temperature that was attributed to the eclogites of the same area (800-940 °C; Janák et al., 2004; Vrabec et al., 2012), although both spans overlap with each other. The Lu-distribution inside garnet of the ultramafic sample FK99, along with the circumstance that this sample gives the youngest age of this study, suggests that this sample was affected by temperatures transcending its T_C for the Lu-Hf isotope system. In contrast, a prograde growth zoning of Lu is preserved in garnet of the eclogite samples, indicating that these samples did not exceed their T_C for Lu-Hf. If mafic and ultramafic samples were affected by the same temperatures during metamorphism, then diffusive re-distribution would have been less effective in the eclogites than in the ultramafic rocks, resulting in a higher T_C for garnets in the eclogites which do have different compositions with respect to major elements. In contrast, if all samples have a similar T_C, then the eclogites of this study may have been affected by lower temperatures than the ultramafites during metamorphism.

We regard this as unlikely for tectonic reasons, since the two ultramafic samples and one of the eclogites were taken within the structurally and lithologically coherent body of the SBUC.

3.6.2 Comparison of Lu-Hf garnet ages to literature data

Our new Lu-Hf garnet ages of eclogites are identical within error with a Lu-Hf two-point isochron (whole rock-garnet) of an eclogite sample from a location close to the sampling area of our study (93.3 ± 2.8 Ma; Thöni et al., 2008), implying that this age is also prograde. Sm-Nd garnet dating of eclogites from southeastern Pohorje yielded ages of 90.7 ± 3.9 and 90.1 ± 2.0 Ma (Miller et al., 2005). Garnet is known to incorporate most of the matrix' Lu during the earliest stages of garnet growth. Lu is therefore highly concentrated in garnet cores. Sm, however, is incorporated into garnet during later stages of garnet growth and is therefore more concentrated in outer parts of garnet grains (e.g. Lapen et al., 2003; Skora et al., 2006). Since garnets in our eclogite samples preserved their initial growth zoning in REE, it is likely that Sm-Nd ages of eclogites reflect a later stage of garnet growth. U-Pb zircon geochronometry of an eclogite sample yielded an age of 90.7 ± 1.0 Ma (Miller et al., 2005), which is identical with the Sm-Nd garnet ages mentioned above. This points towards a contemporaneous formation of metamorphic zircon and garnet.

Thöni (2002) presented Sm-Nd two-point (whole rock-garnet) isochrons of felsic host rocks that enclose the mafic and ultramafic lithologies of Pohorje. One sample of leucocratic gneiss gave an age of 87.0 ± 3.1 Ma while a garnet micaschist was dated at 93.0 ± 1.8 Ma. The latter is identical with a 92.0 ± 0.5 Ma U-Pb zircon age from a metapelitic kyanite-bearing gneiss (Janák et al., 2009). The formation of metamorphic zircon also occurred at HP or UHP conditions, contemporaneously with garnet growth in adjacent rocks. The estimated metamorphic ages of felsic lithologies do not differ from the ages of eclogites from the same region. Thus, eclogites and their felsic host rocks were likely subjected to UHP metamorphic conditions together and share a common PT history.

All these age data point towards garnet formation in southeastern Pohorje between c. 97 and 90 Ma. Our new Lu-Hf garnet age of an ultramafic sample from the SBUC also falls into this time frame. Thus, we argue that the SBUC is a primary part of the metamorphic series of the Pohorje Mountains that was affected by high grade metamorphic conditions contemporaneous with the associated eclogites and their felsic host rocks. Therefore, the metamorphic series of southeastern Pohorje represents an assemblage of high grade metamorphic rocks that was exhumed from eclogite facies conditions as a coherent unit.

3.6.3 Tectonic implications

We attribute our Lu-Hf garnet ages of eclogites (96.6 ± 1.2 Ma, 94.8 ± 5.1 Ma) to initial garnet formation in the subducting slab, whereas our Lu-Hf garnet age of the ultramafic sample FK99 (91.6 ± 4.1 Ma) rather dates a later phase of the subduction cycle or is shifted towards a younger age by subsequent loss of Hf. The subduction occurred between 97 and 90 Ma. The data give no upper limit for the speed of subduction because all three are identical within error. The new age data support the inference already drawn in earlier papers (Miller et al., 2005; Janák et al., 2006; Kirst et al., 2010; Vrabec et al., 2012) that the Pohorje eclogites, ultramafites, and their felsic country rocks shared a common tectonometamorphic history during the Cretaceous. Thöni (2006) reviewed existing age data for eclogite-facies metamorphism in the entire Austroalpine high-pressure belt and found that peak metamorphism and initial decompression occurred everywhere "close to 90 Ma". As shown by Thöni (2006), there is a marked synchroneity of eclogite metamorphism in the different parts of the Austroalpine high-pressure belt. This would be in line with subduction of a narrow ocean basin or, alternatively, with intra-continental subduction localized in a Permian-aged rift within the Austroalpine realm, as suggested by Janák et al. (2004). The upper panel of Figure 3.2 shows such a scenario with two Permian rifts. The southeastern one located in the Hallstatt-Meliata zone is documented by thick Permian evaporites (e.g. at Hallstatt) whereas the northwestern one, between the Lower and Upper Central Austroalpine, is mainly known from gabbroic intrusions (e.g. in Koralpe and Saualpe) and HT/LP metamorphism (Schuster and Stüwe, 2008). The southeastern rift developed into the Meliata Ocean after breakup in the Anisian, whereas the northwestern one failed. In Pohorje, the association of mafic and ultramafic rocks with felsic gneisses, including Permian to Triassic zircon cores (Janák et al., 2009), is interpreted to represent a near-MOHO part of the thinned crust in the northwestern rift.

The Cretaceous orogenic processes within the Austroalpine can be divided into two phases (Kurz and Fritz, 2003). The first is the formation of a thin-skinned, foreland fold-and-thrust belt related to the collision of the Austroalpine continental margin with an island arc after subduction of the Meliata Ocean. The thrust system formed in sequence from southeast to northwest, beginning in the Jurassic (e.g. Missoni and Gawlick, 2011) and continuing in the Early Cretaceous, e.g. with the formation of the basal thrust of the Lechtal Nappe in the western Northern Calcareous Alps during the Aptian/Albian (Ortner, 2003). This process stopped when too thick crust of the Austroalpine margin entered the southeast-dipping subduction zone. A new lithosphere-cutting thrust formed in the failed rift between the Lower and Upper

Central Austroalpine, and evolved into an intracontinental subduction zone. Since the front of the thin-skinned Meliata-related thrust belt had already advanced from southeast over the failed rift, the new subduction zone resulted in out-of-sequence thrusting in shallow crustal levels (Fig. 3.2, lower panel).

Subduction of the Lower Central Austroalpine reaching eclogite facies conditions at c. 97 Ma fits well into the framework of tectonic processes as provided by the synorogenic sediments of the Northern Calcareous Alps. From biostratigraphic evidence in synorogenic sediments, the thrust of the Tirolic over the Bajuvaric nappes, located at the base of the Inntal Nappe in the western part of the Northern Calcareous Alps (Inntal Thrust, Fig. 3.2), was active as an out-of-sequence thrust in the Albian to Cenomanian (Ortner, 2003), that is, between 112.0 and 93.5 Ma. Since the Tirolic Nappes are connected with the Upper Central Austroalpine and the Bajuvaric Nappes with the Lower Central Austroalpine (Janák et al., 2004; Fig. 3.2), the burial of the Lower Central Austroalpine in the intracontinental subduction zone should be contemporaneous with the activity of the Inntal Thrust, which is indeed the case according to our new age data. Growth of garnet in mafic and ultramafic rocks occurs only after significant subduction, when the rocks reach the necessary depth, which is in good agreement with the fact that garnet ages fall into the last part of the time span for thrusting.

3.7 Conclusions

Lu-Hf garnet geochronometry on eclogite and ultramafic samples from the Pohorje Mountains, Eastern Alps, can provide new insight into the tectonic history of the Eastern Alps. In situ LA-ICPMS Lu-profiles were employed to attribute Lu-Hf ages to garnet growth or re-distribution, respectively. Garnet in two dated eclogite samples retained a zonation of Lu established during growth of garnet. Garnet in two ultramafic samples was affected by re-distribution of Lu and partly by resorption of garnet. We infer that our eclogite samples date a point close to garnet formation when these rocks were subjected to eclogite facies conditions. In contrast, our ultramafic sample FK99 probably dates a later stage of the PT loop, which is still under UHP metamorphic conditions, possibly close to the pressure and temperature peak. All our garnet ages are in line with previously published ages of eclogites and their felsic host rocks that were interpreted to reflect the age of UHP metamorphism. Thus, we conclude that the metamorphic series of the Pohorje Mountains, including the ultramafic body at its southeastern border, underwent UHP metamorphic conditions between 97 and 90 Ma within a single PT loop.

Annotations

An earlier version of this chapter was submitted to *Lithos*. This version will be resubmitted to *Lithos*. Lu-Hf data of whole rock samples and garnet separates are taken from my diploma thesis. Lu-Hf analysis of pyroxenes were produced for this Ph.D. thesis. All LA-ICPMS and microprobe analysis presented here were exclusively performed for this Ph.D. thesis. The entire text is new, since the results from LA-ICPMS analysis fundamentally changed the interpretation of the Lu-Hf data. I performed all microprobe analyses and Lu-Hf garnet dating. R. Fonseca and I carried out the LA-ICPMS analyses. D. Herwartz, T. Nagel, and C. Münker contributed to the interpretation of garnet analyses. F. Kirst, N. Froitzheim, and M. Janák contributed to the tectonic interpretation. I wrote the manuscript and produced all figures.

4 Late Miocene to Early Pliocene blueschist from Taiwan and its exhumation via forearc extraction

Sascha Sandmann[1], Thorsten J. Nagel[1], Nikolaus Froitzheim[1], Kamil Ustaszewski[2], and Carsten Münker[3]

[1] Steinmann-Institut für Geologie, Mineralogie und Paläontologie, Universität Bonn, Meckenheimer Allee 169, D-53115 Bonn, Germany

[2] Institute for Geoscience, Aarhus Universitet, Høegh-Guldbergs Gade 2, 8000 Aarhus C, Denmark

[3] Institut für Geologie und Mineralogie, Universität Köln, Greinstr. 4-6, D-50939 Köln, Germany

Abstract

Taiwan is a perfect natural laboratory to investigate recent subduction-exhumation processes. Blueschist-facies metamorphic rocks in the Yuli Belt of Taiwan's Central Range record ongoing subduction of the Eurasian plate beneath the Philippine Sea plate. We present a Lu-Hf garnet-whole-rock age of 5.1 ± 1.7 Ma from a retrogressed blueschist in the Yuli Belt. The age reflects prograde garnet growth during subduction. It is considerably younger than the previously assumed age of 14-8 Ma for high-pressure metamorphism in the Yuli Belt and to our knowledge the youngest ever recorded age for blueschist-facies metamorphism worldwide. The age sheds new light on the paleogeographic origin and the exhumation scenario of the Yuli belt. We propose that the Yuli Belt originated from the ocean-continent boundary of the Chinese passive margin. It was subducted eastward during collision of the margin with the Luzon island arc and rapidly exhumed during downward removal (extraction) of forearc lithosphere.

4.1 Introduction

Continental high-pressure rocks in collisional orogens are typically derived from the distal margin of the subducting plate. Over the past decades, improving techniques for dating metamorphic minerals have led to the general conclusion that exhumation

of subducted continental material back to mid-crustal levels and to the surface occurs at velocities similar to subduction (Rubatto and Hermann, 2001; Jolivet et al., 2003). The kinematics of exhumation events and the involved forces, however, are matters of ongoing debate and reconstructions are often still limited by uncertainties about the precise timing of high-pressure metamorphism.

Taiwan is a perfect area to study the exhumation of high-pressure rocks and arc- continent collision for two main reasons: Firstly, collision between the passive continental margin of China and the Luzon Island Arc at the western border of the Philippine Sea Plate proceeds from south to north as the passive continental margin is oblique to the subducting plate boundary (Fig. 4.1A). Hence, a south-to-north sequence of sections across Taiwan can be viewed as a time sequence, with more southerly located sections showing earlier stages of the evolution (Suppe, 1984). Secondly, well-preserved, young blueschist-facies rocks, which are arguably derived from the Chinese margin (see below), are exposed in the Central range of Taiwan where collision is mature and uplift rates are high (Willet et al., 2003). Hence, the tectonics of high-pressure exhumation are potentially active.

Associated with collision in Taiwan is the disappearance of the forearc lithosphere along strike of the orogen. It is about 100 km wide south of Taiwan (Lundberg et al., 1997), but progressively removed by sinking off into the mantle further north (Chemenda et al., 2001; Shyu et al., 2011). This process leaves behind an extraction fault in the Longitudinal Valley of Eastern Taiwan, along which blueschist-facies metamorphic rocks of the subducted eastern Central Range (Yuli Belt) to the West are juxtaposed to unmetamorphic sedimentary and volcanic rocks of the arc as well as accreted unmetamorphic forearc sediments of the Coastal Range to the East (Fig. 4.1A and B). The Yuli Belt is a key element for any reconstruction of the collision process but its evolution is still incompletely understood. It comprises blocks of serpentinite, metagabbro, rodingite, garnet-epidote amphibolite, glaucophane schist, and meta-plagiogranite in a matrix of metapelitic schists (Liou and Ernst, 1984; Yui and Lo, 1989). Peak metamorphic conditions were 1.0 to 1.2 GPa and c. 550 °C (Beyssac et al., 2008; Tsai et al., 2013). Earlier attempts at dating metamorphism of the belt yielded ages from 12 to 1 Ma using K-Ar (Juang and Bellon, 1986; Tsao et al., 1996), from 110 to 4.4 Ma using ^{40}Ar-^{39}Ar (Lo and Yui, 1996), and from 79 to 4.6 Ma using Rb-Sr (Jahn and Liou, 1977; Jahn et al., 1981). In order to explain the Cretaceous ages, most authors assume that the Yuli Belt is partly derived from the Chinese passive continental margin (e.g. Lo and Yui, 1996) and that the blueschist-facies pressure peak was reached at around 14 to 8 Ma (Beyssac et al., 2008; Ota and Kaneko, 2010). Conversely, the beginning of arc-continent

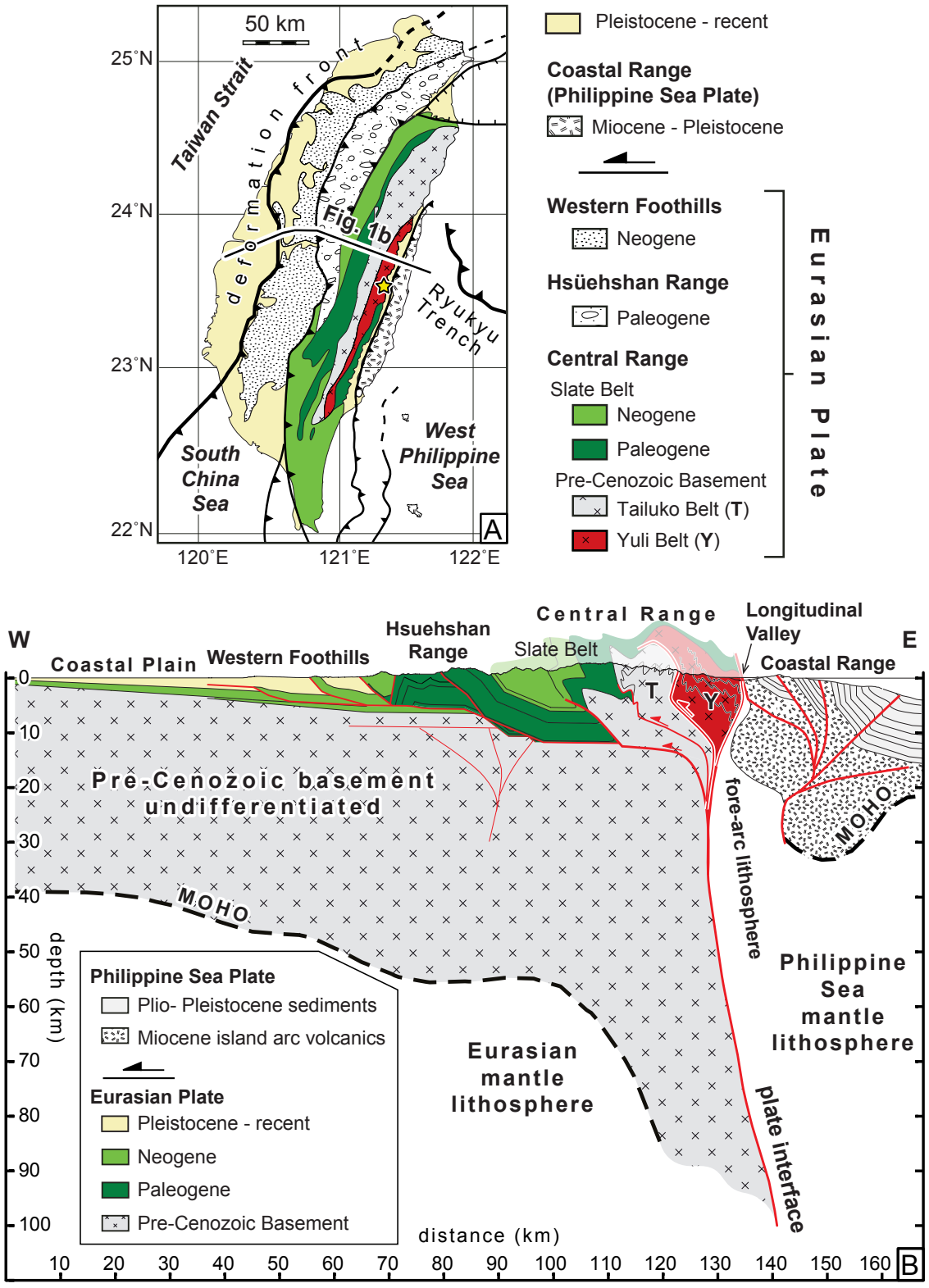

Figure 4.1: Tectonic overview of Taiwan. A: Tectonic map of Taiwan with sample location (starred). B: Crustal scale cross section through the Taiwan fold-and-thrust belt, modified and extended after Yue et al. (2005). Crust-mantle boundaries (Moho and plate interface) are from Ustaszewski et al. (2012).

collision in Taiwan is dated at about 6.5 Ma by stratigraphy and subsidence history (Lin et al., 2003). This would mean that the Yuli Belt rocks were subducted and reached peak pressure conditions before arc-continent collision started, which is in conflict with the derivation of the Yuli Belt from the Chinese margin. We dated prograde metamorphism of the Yuli Belt using Lu-Hf chronometry on garnet. This method avoids problems with excess daughter isotopes or confusion of metamorphic and protolith ages because garnet growth can well be attributed to discrete steps of the metamorphic evolution. Our analysis yielded a well-defined isochron with an age of 5.1 ± 1.7 Ma, to our knowledge the youngest age for blueschist-facies metamorphism ever recorded. This result supports a model where the Yuli Belt originates from the most distal part of the Chinese continental margin, was subducted immediately after the arc-continent collision started, and subsequently exhumed during forearc extraction.

4.2 Sample Petrology

The dated sample TW1 is a garnet-amphibole schist collected as float in a small riverbed within the Tamayen mélange at the eastern margin of the Yuli Belt (starred location in Fig. 4.1A and in Fig. 7.7 in the supplemental material, sampling coordinates are 121°20'58.2'' E, 23°30'55.7'' N). The Yuli Belt forms the tectonically highest Eurasian-derived thrust sheet in the Taiwan orogen (Fig. 4.1B). The Tamayen mélange itself consists of predominantly greenschist and metapelite with varying amounts of garnet-epidote amphibolite, glaucophane-bearing rocks and serpentinite (Tsai et al., 2013). Sample TW1 perfectly corresponds to type 1 blueschists described in Tsai et al. (2013). As major components it contains garnet, amphibole, quartz, chlorite, and epidote/clinozoisite (Fig. 4.2A). Minor phases are albite, phengite, titanite, Fe-Cu-sulfides, and late calcite veins. Amphiboles, epidote/clinozoisite, and quartz ribbons define a weak foliation. There are three distinct generations of amphibole (Table 7.5). Pargasitic hornblende (Fig. 4.2; Am_2 in Table 7.5) contains inclusions of Fe-Mg-glaucophane (Am_1) and frequent rims of actinolite/tremolite (Am_3). Hence, amphibole records successive stages of blueschist-, epidote-amphibolite-, and greenschist-facies metamorphic conditions. Rare phengite flakes contain up to 6.9 Si p.f.u., indicating formation under high pressures. Feldspar is consistently pure albite. Euhedral garnet of 20-100 micron is Mn-rich and perserves concentric growth zoning only weakly zoned (Fig. 4.2; Table 7.5). Even the largest garnets are present as inclusions in hornblende, but garnet also occurs in glaucophane (Fig. 4.2). This indicates that garnet growth started before the pressure peak was reached and terminated before growth of hornblende took place. This notion is also supported

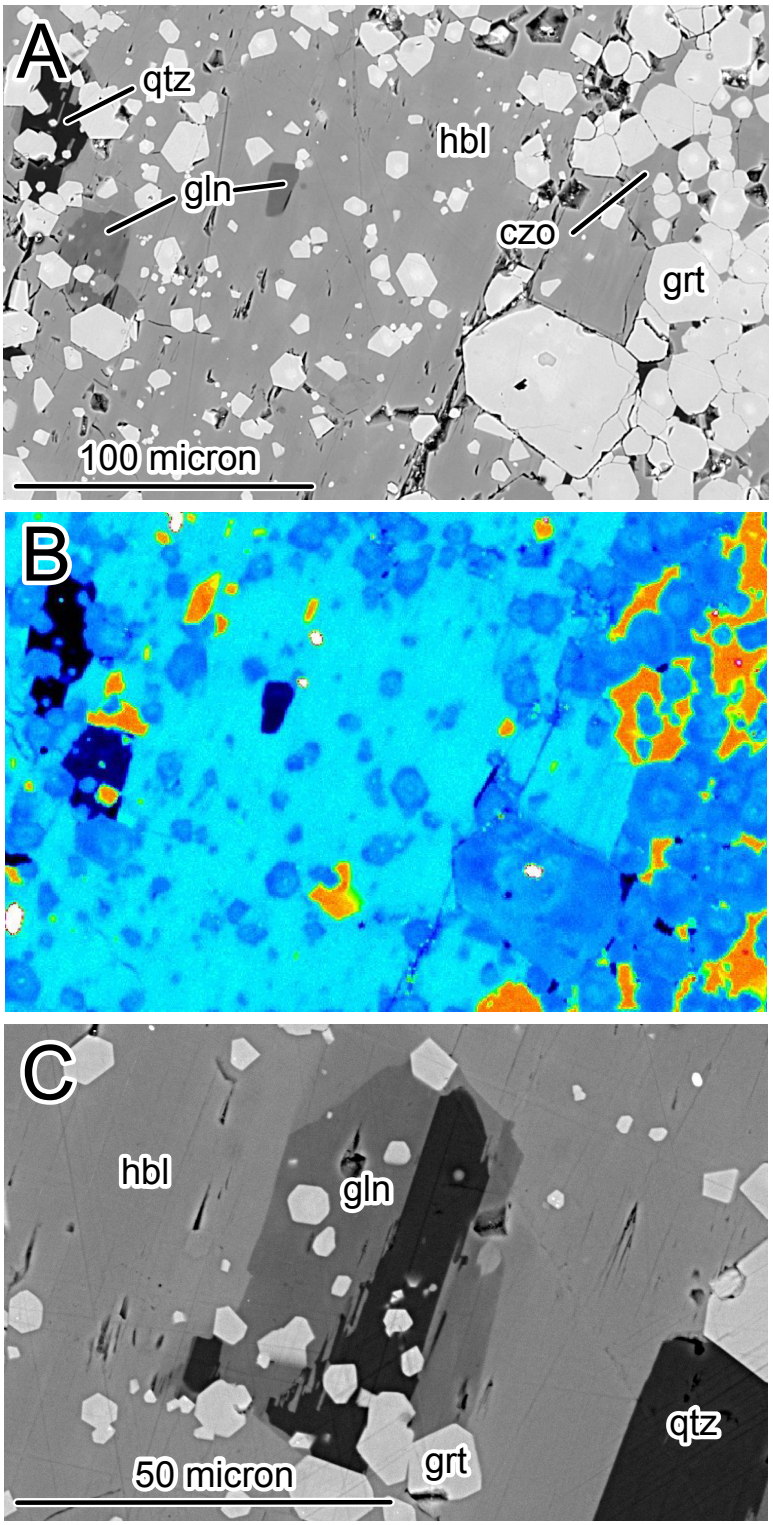

Figure 4.2: Petrological observations in sample TW1. A: Backscattered image of main assemblage. B: Element distribution map of Ca of the area displayed in Fig. 2A. Garnet preserves concentric growth zoning. Inclusions of glaucophane-rich amphibole in hornblende contain almost no calcium. C: Backscattered image showing garnet inclusions in glaucophane, indicating high-pressure growth of garnet before or at peak pressure conditions.

by the abundance of manganese in the sample and consequently in garnet (Fig. 4.2; Table 7.5). Because manganese strongly fractionates into garnet it enlarges the garnet stability field and, thus, promotes early garnet growth. Thermodynamic modelling of sample TW1 presented in the supplementary material (Fig. 7.8) reproduces the observed assemblages and inferred garnet growth stages along a pressure-temperature path similar to the one presented by Tsai et al. (2013) for nearly identical samples.

4.3 Lu-Hf Dating

Despite the extremely small grain size of 20-80 micron, final garnet separation was performed by laborious handpicking and resulted in pure garnet separates of c. 30 mg. The applied digestion method leaves behind refractory, Hf-rich phases like zircon that might preserve inherited isotope signatures (Lagos et al., 2007). The garnet separation procedure and the analytical protocol are described in the appendix and references therein. Measurements of Lu and Hf were obtained with a Thermo Neptune MC-ICPMS. Procedural blanks of garnet analyses were less than 12 pg for Lu and less than 30 pg for Hf. Blanks of the whole rock analysis were 5 pg for Lu and 71 pg for Hf. All sample-to-blank ratios are in excess of 500 and, thus, the effect of blank uncertainties on isochron ages is negligible. Isotope compositions and concentrations of TW1 and the associated age are presented in Figure 4.3 and Table 7.6. Three garnet and one whole rock analysis define an isochron of 5.1 ± 1.7 Ma (MSWD 1.9). The three garnet analyses alone yield an age of 6.1 ± 1.2 Ma (MSWD 0.001) which is identical within error with the 4-point isochron including the whole rock analysis.

4.4 Discussion

Phase relations and mineral chemistry show that garnet in TW1 grew at blueschist-facies metamorphic conditions. The maximum temperature that affected the sample (500-550 °C) is well below the closure temperature of the Lu-Hf system, which is at least 630 °C (Skora et al., 2008). Since Lu strongly fractionates into garnet and is, thus, typically concentrated in the core of crystals, Lu ages are considered to capture a relatively early stage of the metamorphic history (Skora et al., 2006). Hence, the obtained age of 5.1 ± 1.7 Ma records prograde garnet growth during subduction-related burial of TW1 and the result indicates a very young age for blueschist-facies metamorphism in Taiwan. The scattering and often higher K-Ar and ^{40}Ar-^{39}Ar ages from the Yuli Belt may be partly influenced by excess argon, and the widely scattering Rb-Sr ages probably reflect a mixture of protolith, metamorphic, and deformation ages.

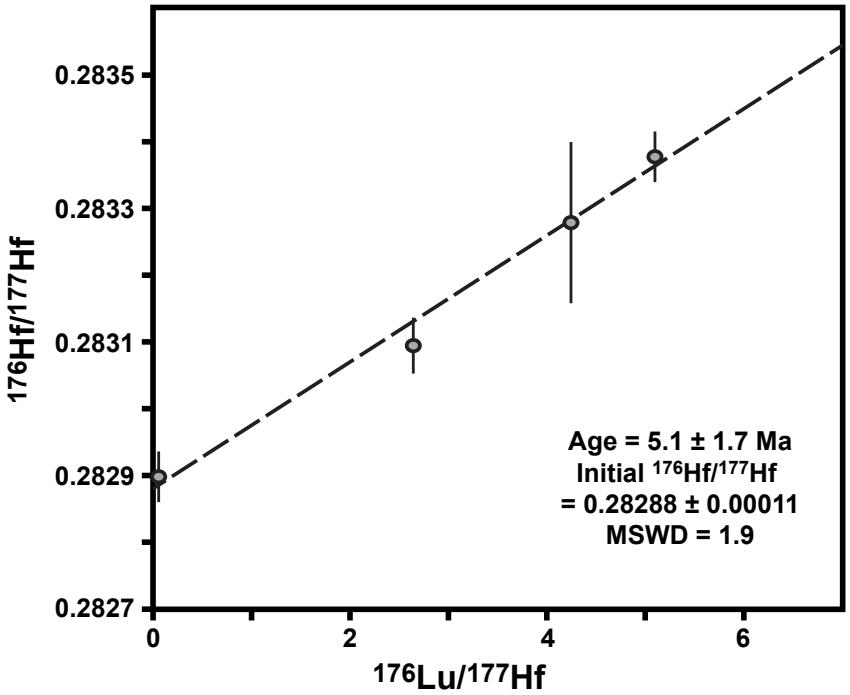

Figure 4.3: Lu–Hf isochron plot for sample TW1. Error bars indicate 2σ uncertainties. Error of the $^{176}Lu/^{177}Hf$ ratio is smaller than the symbol size. The Program 'ISOPLOT v. 2.49´ (Ludwig, 2001) was used to calculate isochron regressions using the errors reported in Table 7.6. Ages are based on $\lambda^{176}Lu = 1.867 \times 10^{-11}yr^{-1}$ (Scherer et al., 2001; Söderlund et al., 2004).

Subduction at c. 5 Ma, as indicated by our dating, solves the dilemma described above, i.e. that subduction of rocks derived from the continental margin appeared to predate arc-continent collision. Our result is in accordance with the hypothesis that rocks of the Yuli Belt were indeed located at the most distal part of the Chinese continental margin. Such an origin is required by the Cretaceous Rb-Sr ages from the Yuli Belt, because the subducted ocean floor of the South China Sea, from which the Yuli Belt could alternatively be derived, is younger than 30 Ma (Lin et al., 2003). Stratigraphic data indicate that collision of the Chinese margin with the Luzon arc started around 6.5 Ma at the latitude of Taiwan (Lin et al., 2003). Assuming (1) a convergence velocity similar to the present-day rate of 8 cm/a, (2) a direction slightly oblique to the plate boundary, and (3) a subduction angle of 45°, the tip of the margin was buried at a rate of about 5 cm/a or 50 km/Ma. Hence, rocks of the Yuli Belt could have reached their maximum burial depth of about 35 km within less than one Ma after the onset of collision, which is perfectly within error of our new Lu-Hf garnet age of 5.1 ± 1.7 Ma.

We follow the concept that the lithosphere of the upper plate failed in the area of the island arc due to an increase in horizontal stress when the Chinese continental margin entered the subduction zone (Chemenda et al., 2001). This led to detachment

of the forearc lithosphere from the Philippine Sea Plate. In the following, the forearc lithosphere started to sink independently into the mantle by extraction (Froitzheim et al., 2003, 2006). This process removed overburden above the subducted trailing edge of the continent and, thus, triggered rise of the Yuli Belt (Fig. 4.4). Such a suction-driven exhumation scheme was recently proposed for UHP metamorphic units in the Swedish Caledonides (Majka et al., 2014). The trailing edge of the descending forearc block is presently imaged by earthquake foci and seismic tomography below the Longitudinal Valley, and opposite motion senses on seismogenic faults delineating the trailing edge of the block indicate downward extraction (Shyu et al., 2011). Ongoing shortening led to basal accretion of more external continental units of the Eurasian margin below the exhumed Yuli Belt. These units were affected by considerably lower pressures (Tailuko belt, Fig. 4.1).

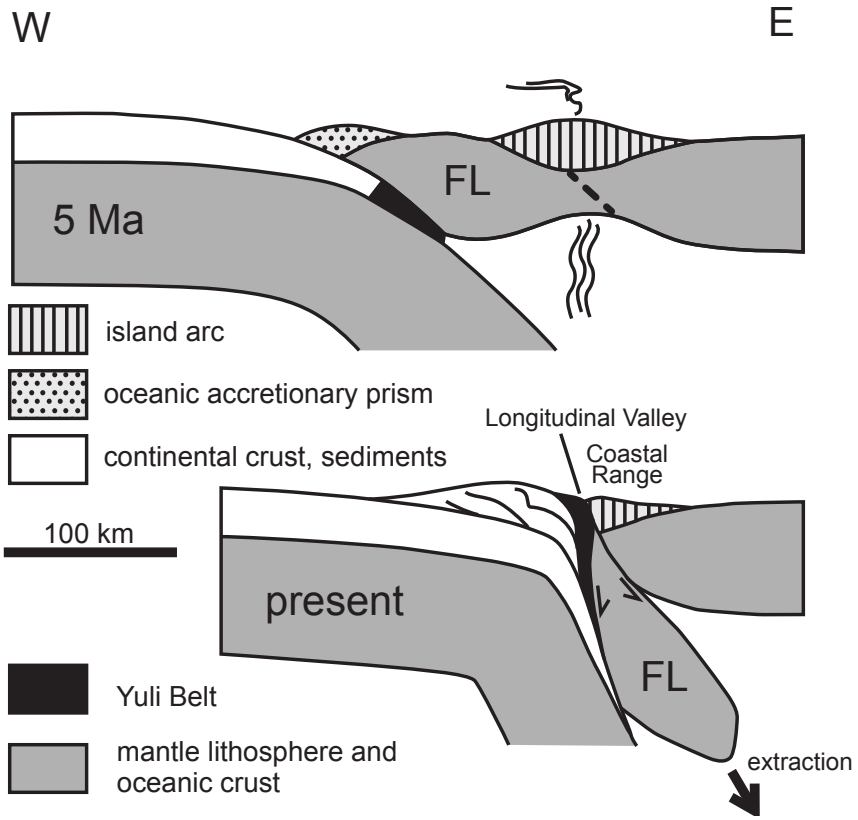

Figure 4.4: Proposed tectonic evolution during collision of the Eurasian margin with the Luzon Arc. Rocks in the Yuli Belt are derived from the distal continental margin and entered the subduction zone about 6 Ma ago. Subsequent exhumation occurred via differential sinking (extraction) of the forearc lithospheric mantle, which led to the juxtaposition of high-pressure rocks of the Yuli Belt next to unmetamorphic arc-derived rocks in the Coastal Range.

4.5 Summary

The Lu-Hf garnet age of 5.1 ± 1.7 Ma shows that the Yuli Belt was subducted after the beginning of arc-continent collision at about 6.5 Ma and, hence, very likely originates from the distal Chinese passive continental margin. Rocks from the Yuli belt remained only very shortly at their maximum depth of about 35 kilometers and were exhumed rapidly during ongoing convergence. We explain this by downward removal (extraction) of the overlying forearc lithosphere and associated rise of deeply subducted soft material.

Annotations

This chapter was submitted to *Terra Nova*. I carried out the Lu-Hf dating. T. Nagel and I performed the microprobe analyses. T. Nagel and C. Münker contributed to the interpretation of garnet analyses. N. Froitzheim and K. Ustaszewski contributed to the tectonic interpretation. T. Nagel calculated and interpreted the phase relations that are presented in the Appendix.

5 Dating the initiation of Piemonte-Liguria Ocean subduction: Lu-Hf garnet chronometry of eclogites from the Theodul Glacier Unit

Sebastian Weber[1], Sascha Sandmann[2], Raúl O. C. Fonseca [2], Nikolaus Froitzheim[2], Carsten Münker[3], Kurt Bucher[1]

[1] Institut für Geo- und Umweltnaturwissenschaften, Albert-Ludwigs-Universität, Albertstraße 23b, D-79104 Freiburg, Germany

[2] Steinmann-Institut für Geologie, Mineralogie und Paläontologie, Universität Bonn, Meckenheimer Allee 169, D-53115 Bonn, Germany

[3] Institut für Geologie und Mineralogie, Universität Köln, Greinstr. 4-6, D-50939 Köln, Germany

Abstract

The Penninic nappe stack in the Central and Western Alps was formed in a collision zone environment during the closure of the Penninic oceans in the Paleogene. This study reports Lu-Hf garnet-whole rock isochron ages of 56.5 ± 2.7 Ma and 58.2 ± 1.4 Ma for two eclogite samples from the Theodul Glacier Unit, which is inserted within the structurally uppermost parts of the ophiolitic Zermatt-Saas Zone. The distribution of major elements, Y, and Lu in garnet, and specifically an enrichment of Lu in the cores, indicate that the ages record 30 prograde growth of garnet during pressure increase. They provide direct evidence for the continuation of subduction during the "Paleocene restoration phase", often regarded as a tectonically quiescent period due to a reduction in clastic sediment deposition, lack of folds and thrusts of this age, and a cessation of Africa-Europe convergence as derived from the magnetic anomaly pattern in the Atlantic Ocean. The evidence for ongoing subduction in the absence of Africa-Europe convergence suggests that the subduction system was driven by gravity acting on the downgoing slab in a rollback setting, and that subduction was balanced by extension of the upper plate. The overlap of the Lu–Hf ages of both samples from the Theodul Glacier Unit show that this tectonic element represents a relative coherent body. However, the difference with respect to the 48 Ma Lu-Hf age of the Lago di Cignana Unit, another element of the

Zermatt-Saas Zone, suggests that the Zermatt-Saas Zone was not subducted in one coherent slab but represents an assemblage of slivers subducted at different times. The exhumation, however, probably occurred as an assembled complex without further modification.

5.1 Introduction

The Western and Central Alps represent a classical arc-shaped orogen assembled by subduction and collision. Tectonic models that attempt to reconstruct their evolution (e.g. Laubscher, 1988, 1991; Schmid et al., 1996; Michard et al., 1996; Escher et al., 1997; Schmid and Kissling, 2000; Stampfli et al., 1998, 2002; Rosenbaum and Lister, 2005; Handy et al., 2010) showed that the deformation and metamorphism migrated from internal to external parts, that is, mostly towards northwest. It is not clear to what extent this migration was continuous or episodic (Lister et al., 2001). Trümpy (1973) found that the Cretaceous deformation, mostly recorded in the Austroalpine nappes, did not simply continue into the Eocene to Oligocene main deformation phases of the Central and Western Alps but that the two were separated by a period of relative tectonic quiescence, uplift and erosion during the Paleocene, i.e. 65 to 56 Ma ("Paleocene restoration"; Trümpy, 1973; Schettino and Turco, 2011). Later, the analysis of plate motions from magnetic anomaly patterns in the Atlantic showed that the rate of Europe-Africa convergence at the longitude of the Alps was only c. 0.22 cm yr^{-1} between 65 and 55 Ma and c. 0.4 cm yr^{-1} between 55 and 51 Ma (Schmid et al., 1996, using rotation parameters of Dewey et al., 1989; see also Rosenbaum et al., 2002; Jolivet et al., 2003; Rosenbaum and Lister, 2005; Schettino and Turco, 2011). Convergence rates were considerably higher before and after this period. This slow-down of convergence coincides with the "Paleocene restoration". So far, the geochronological record for subduction-related metamorphism also shows a gap between c. 65 and 50 Ma (see below). This may indicate that subduction stopped at that time. However, using semi-quantitative profile balancing, Schmid et al. (1996) derived significantly higher convergence rates across the Alps of 1.33 cm yr^{-1} for 65 to 50 Ma, and assumed continuing subduction during the Paleocene. In order to better constrain the subduction history of the Central and Western Alps, and to answer the question of continuous versus discontinuous subduction, more geochronological data for high-pressure units are needed.

The Penninic nappe stack of the Western and Central Alps (Figure 5.1) consists of both oceanic and continental units subducted to various depths, which were then juxtaposed together and subsequently exhumed to the surface. This is reflected by a large spectrum of mineral assemblages, which developed under low-temperature/high-

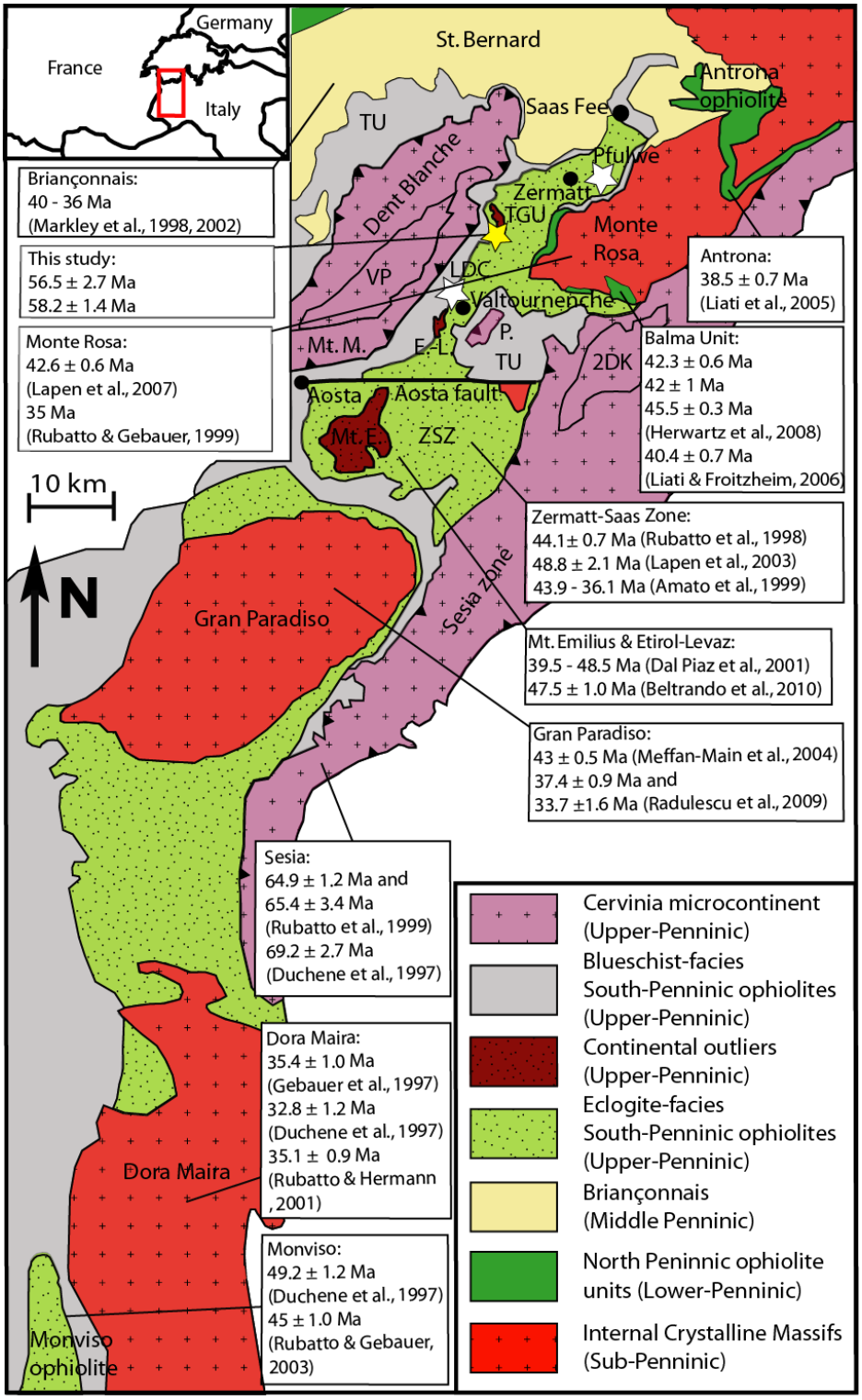

Figure 5.1: Tectonic map of the Western Alps, showing distribution of HP ages for metamorphic rocks (modified after Rosenbaum and Lister, 2005). White stars indicate the location of Pfulwe pass area, where eclogite facies rocks preserved pillow textures and the Lago di Cignana coesite locality (LDC). Dent-Blanche nappe, Sesia zone and Pillonet klippe are considered as derived from the Cervinia microcontinent. Although the continental outliers were probably also part of Cervinia, they are designated as a separate unit. TGU = Theodul Glacier Unit, LDC = Lago di Cignana Unit, E. L. = Etirol-Levaz sliver, Mt. E. = Mont Emilius, Mt. M. = Mont Mary, P. = Pillonet klippe, VP = Valpelline Series, 2DK = Seconda Zona Dioritico-Kinzigitica.

pressure conditions and afterwards were overprinted by a Barrovian-type metamorphism (Bearth, 1967; Reinecke, 1991; Dal Piaz, 1999; Bousquet et al., 2004; Bucher et al., 2005; Frezzotti et al., 2011; Gasco et al., 2013). The eclogite-facies mineral assemblage is extensively preserved in the Sesia zone, in the ophiolites and continental outliers of the Zermatt-Saas Zone (ZSZ), in the structurally deeper Antrona and Balma ophiolites, and in the "Internal Massives" of Monte Rosa, Dora-Maira and Gran Paradiso (Figure 5.1).

The ZSZ, one of the most intensively studied subducted ophiolite complexes worldwide, has been investigated in numerous works by various geochronological methods (e.g. Bowtell et al., 1994; Rubatto et al., 1998; Amato et al., 1999; Dal Piaz et al., 2001; Lapen et al., 2003). These dating techniques constrain the timing of formation and subduction of the Piemonte-Liguria Ocean. Although the ZSZ has received a lot of attention during the past years, most geochronological studies dealt with only a few localities. U-Pb zircon, Sm-Nd garnet, and Lu-Hf garnet data for the subduction-related metamorphism exist only for the ultrahigh-pressure (UHP) locality Lago di Cignana (Figure 5.1: LDC; Rubatto et al., 1998; Amato et al., 1999; Lapen et al., 2003) and the locality Pfulwe further north (Figure 5.1; Bowtell et al. 1994). However, the ZSZ is a complex, about 60 km long, dismembered ophiolite sequence including also rock slivers of continental affinity (Figure 5.1: continental outliers). Some authors suggested that these continental slivers were emplaced as extensional allochthons already during pre-oceanic rifting (Dal Piaz et al., 2001; Beltrando et al., 2010) and that the ZSZ was subducted in one piece (e.g. Angiboust et al., 2009), whereas others assumed that it is composed of several tectonic slices with their own metamorphic histories (e.g. Negro et al., 2013). The geochronological record is still not sufficient to distinguish between these alternatives. In this article, we present two new age determinations from the Theodul Glacier Unit (TGU) in the Zermatt-Saas Zone, a unit that has not been dated so far.

In early works, the ^{40}Ar-^{39}Ar technique was used to date high-pressure metamorphic events in the Western and Central Alps (Chopin and Maluski, 1980; Monié and Chopin, 1991; Hunziker et al., 1992) but it has been shown that ^{40}Ar-^{39}Ar ages of high-pressure rocks are often affected by the presence of excess argon, making them too old (Li et al., 1994; Arnaud and Kelley, 1995; Ruffet et al., 1997; Warren et al., 2012). Rb-Sr isochrons from phengitic mica (Paquette et al., 1989; Ruffet et al., 1997; Dal Piaz et al., 2001) are unaffected by this problem and date the high-pressure metamorphism provided that the closure temperature of the Rb-Sr system in white mica (c. 500°C ± 50; Jäger, 1979; Inger and Cliff, 1994) was not exceeded (Dodson, 1973; Ganguly and Tirone, 1999).

U-Pb zircon geochronology has the advantage of a high closure temperature and the possibility of spot dating using SHRIMP or LA-ICPMS. In mafic lithologies of ophiolites, however, zircon is rare. Furthermore, it is often difficult to correlate the growth or recrystallization of zircon to a certain step of the P-T evolution (Rubatto et al., 2001; Hermann et al., 2001; Rubatto, 2002; Rubatto and Hermann, 2007). In spite of these problems, U-Pb dating of metamorphic zircon domains has been successfully applied in the Western and Central Alps (Tilton et al., 1991; Gebauer et al., 1992b, 1997; Gebauer, 1996, 1999; Rubatto and Gebauer, 1999; Rubatto et al., 1999; Rubatto and Hermann, 2003; Liati et al., 2003; Hermann et al., 2006).

Garnet can be dated by the ^{147}Sm to ^{143}Nd and ^{176}Lu to ^{176}Hf decay systems, where the Lu-Hf chronometer seems to be the more suitable system to date prograde metamorphism in eclogite rocks due to the higher closing temperature (Duchêne et al., 1997; Ganguly and Tirone, 1999; Herwartz et al., 2008, 2011; Schmidt et al., 2011; Kirchenbaur et al., 2012; Nagel et al., 2013; Smit et al., 2013). Moreover, the Lu-Hf garnet-whole rock ages are affected by epidote-zoisite-phosphate inclusions only to a minor extent when compared to the Sm-Nd system (Zhou and Hensen, 1995). The only critical types of inclusions are zircon and rutile. Their high Hf content can strongly influence the Lu-Hf system (Scherer et al., 2000). This problem can be minimized by the selective dissolution procedure for garnet of Lagos et al. (2007).

The aim of this contribution is to present Lu-Hf isotope data for whole rocks and garnet mineral separates for two eclogite samples belonging to the Theodul Glacier Unit. The Lu-Hf data are combined with element mapping of single garnet grains, in order to correlate the age information with the metamorphic path. By using the TGU as a case study, the present geochronological results contribute to discussing the following questions:

1. Was subduction in the Alps continuous or episodic?
2. What is the significance of plate tectonics for the Paleocene restoration?
3. Was the Zermatt-Saas Zone subducted in one piece or is it a composite of units subducted at different times?

5.2 Regional geological setting and previous dating

The western Alpine orogenic wedge consists of a sequence of continental and ophiolite thrust sheets which are aligned parallel to the main strike of the Alpine orogen. From the base to the top, the following structural domains can be subdivided: (1) the European margin, represented by tectonic units of the Helvetic nappes, Dauphinois, External Crystalline Massives (e.g. Aiguilles Rouges, Montblanc), and Internal Crystalline Massives (Monte Rosa, Gran Paradiso and Dora Maira), (2) units from a northern ocean basin, the Valais Ocean (Lower Penninic Nappes), (3) the St. Bernard multi-nappe system derived from the Briançonnais continental zone (Middle Penninic nappes), (4) units from the southern ocean basin, the Piemonte ocean (Upper Penninic nappes), and (5) units from the Cervinia Microcontinent (Pleuger et al., 2007) or Margna-Sesia Fragment (Schmid et al., 2004), represented by the Sesia Zone, Dent-Blanche Nappe, Mt. Mary, and Pillonet Klippen (Upper Penninic Nappes; Figure 5.1). In addition, small fragments which show lithological and metamorphic features similar to those of the Sesia Zone occur between the different Upper Penninic ophiolite units Ballèvre et al. (1986). All nappes have been thrust towards NW over the Molasse Basin and European basement and record a decrease in metamorphic grade from SE to NW (Berger and Bousquet, 2008).

Apart from the Internal Crystalline Massives, the European domain is overprinted by sub-greenschist to greenschist-facies metamorphism without any evidence for a HP metamorphic imprint (Frey et al., 1999). The origin of the Internal Crystalline Massives (Dora Maira, Gran Paradiso, and Monte Rosa) is still a matter of debate (Figure 5.1). They are considered to derive from continental crust of the Briançonnais terrane (Escher et al., 1997; Schmid and Kissling, 2000; Schmid et al., 2004), from the Adria domain (Stampfli et al., 1998), or from the distal margin of Europe (Sub-Penninic nappes; Gebauer, 1999; Froitzheim, 2001). We follow the latter interpretation because it is in line with the young ages of HP/UHP metamorphism in these units (see below). In the case of the Dora-Maira Massif, the presence of coesite shows UHP metamorphism at depths of more than 100 km (Chopin, 1984), dated around 35 Ma (Duchêne et al., 1997; Gebauer et al., 1997; Gebauer, 1999). A U-Pb rutile age for eclogite-facies metamorphism in the Monte Rosa nappe is 42.6 ± 0.6 Ma (Lapen et al., 2007). The eclogite-facies imprint of the Gran Paradiso nappe was dated at 43.0 ± 0.5 Ma using Rb-Sr on apatite and phengite (Meffan-Main et al., 2004), but this result was called into question by Radulescu et al. (2009) who interpreted 37.4 ± 0.9 Ma and 33.7 ± 1.6 Ma (U-Pb SHRIMP on monazite and allanite, respectively) as dating the high-pressure metamorphism.

Within the Lower Penninic Nappes (Valais Ocean), the subduction history is

relatively weakly constrained because they are flysch-dominated with minor intercalated ophiolite material (Ziegler, 1956; Trümpy, 1980; Coward and Dietrich, 1989). Recently published radiometric ages for the Antrona ophiolite and the Balma Unit, which are assigned to the Valais Ocean using structural arguments (Froitzheim, 2001), yielded 40 to 37 Ma for the high pressure metamorphism (Liati et al., 2003, 2005; Liati and Froitzheim, 2006). Herwartz et al. (2008) dated garnet growth in the Balma Unit at 45 to 40 Ma using Lu-Hf.

The Briançonnais high, consisting of pre-Mesozoic basement with a sedimentary cover, is generally considered to represent the eastern prolongation of Iberia, separating Valais and Piemonte-Liguria ocean basins (Frisch, 1979). The Briançonnais nappes display an Alpine metamorphism grading eastward from HP greenschist facies to blueschist facies (Bearth, 1963; Goffé, 1977; Bucher et al., 2003; Oberhänsli et al., 2004; Bousquet et al., 2004; Bucher and Bousquet, 2007). The Briançonnais reached peak pressure during the Middle Eocene between 50 and 43 Ma as indicated by Ar/Ar data on HP-phengites (Markley et al., 1998, 2002).

The Zermatt-Saas Zone and other equivalent units further south (e.g. Monviso Ophiolite) comprises eclogite-facies metamorphosed ophiolites derived from the Middle to Late Jurassic sea floor spreading of the Piemonte-Liguria ocean, as indicated by U-Pb (SHRIMP) ages of magmatic zircon between 166 and 160 Ma (Rubatto et al., 1998; Rubatto and Hermann, 2003; Beltrando et al., 2010). The magmatic origin is also documented by locally well-preserved pillow structures, e.g. at the Pfulwe locality (Bearth, 1967; Barnicoat, 1988). Sm-Nd garnet-whole rock dating of metabasaltic rocks from Pfulwe yielded 50 $\pm$ 18 Ma (Bowtell et al., 1994). More precise data were obtained using U-Pb zircon on rocks from the Lago di Cignana Unit (44.1 $\pm$ 0.7 Ma; Rubatto et al., 1998) and the Monviso ophiolite (45.1 $\pm$ 1 Ma; Rubatto and Hermann, 2003). The zircon data are broadly consistent with Lu-Hf ages of 48.8 $\pm$ 2.1 Ma for the LDC Unit (Lapen et al., 2003) and 49.1 $\pm$ 1.2 Ma for Monviso (Duchêne et al., 1997). The eclogite-facies ophiolites are overlain by the Combin Zone, which consists of similar rocks derived from the Piemonte-Liguria Ocean but metamorphosed at lower P-T conditions (blueschist facies; Reddy et al., 1999). The age of Alpine subduction related metamorphism in the Combin Zone is not well constrained.

The Sesia-Dent Blanche nappe system, located in the highest structural position, is either assigned to the Austroalpine (Staub, 1938) or is treated as Upper Penninic continental nappes derived from the Cervinia microcontinent (Trümpy, 1992; Froitzheim and Manatschal, 1996; Pleuger et al., 2007). The rocks of the Sesia Zone were subducted to eclogite facies conditions during the Late Cretaceous around

79-65 Ma (Duchêne et al., 1997; Rubatto et al., 1999, 2011), and subsequently added to the accretionary prism. Rubatto et al. (2011) distinguished two periods of HP metamorphism, at 79-75 Ma and at 70-65 Ma, separated by a low-pressure stage, based on U-Pb dating of zircon and allanite. By contrast, the Dent Blanche Nappe experienced only greenschist to blueschist metamorphic conditions (Compagnoni et al., 1977; Dal Piaz, 1999; Bousquet et al., 2004). Previously, these basement rocks had partly been affected by a (Late?) Variscan granulite facies overprint, recorded in both the Valpelline series of the Dent-Blanche nappe and in the 2DK in the Sesia nappe (Figure 5.1). Continental basement rocks similar to the Sesia Zone are also found at a deeper tectonic level, embedded as tectonic slivers along the contact between the ZSZ and the Combin Zone or within the uppermost part of ZSZ (e.g. Mt. Emilius, Etirol-Levaz; Ballèvre et al., 1986; Dal Piaz, 1999), and metamorphosed under eclogite-facies conditions. Rb-Sr phengite ages from these units are 49 to 40 Ma (Dal Piaz et al., 2001). These results are consistent with SHRIMP U-Pb zircon ages of 47.5 ± 1.0 Ma from Etirol-Levaz (Beltrando et al., 2010).

5.3 Field relations and sample description

In this study, Lu-Hf isotope data are presented for two eclogite samples (SW9 and SW14) from the Theodul Glacier Unit. It crops out at the Upper Theodul Glacier, near "Trockener Steg" in the southern part of the Zermatt valley (Figure 5.2). The TGU appears as a coherent body with a NW-SE extension of 2 km and a thickness of several tens of meters. The samples were taken at a distance of 1.5 km on opposite ends of the TGU. The TGU comprises eclogites interlayered with various types of high-pressure schists: garnet-phengite schists, biotite schists, and metapelitic schists with Ca-poor garnets. The eclogites and schists from the TGU differ from the adjacent ZSZ rocks in terms of mineral paragenesis and trace element composition but share many characteristics with the Sesia-type continental outliers (Weber, 2013).The well-preserved basal contact of the TGU is parallel to the foliation inside the TGU. The TGU is dissected by several faults, each of them forming the base of an imbricate thrust sheet. Two of these are shown on the map (Figure 5.2). Serpentinite is intimately associated with the TGU not only by enveloping but also occuring along faults within the TGU. Since serpentinite within the TGU is restricted to these faults, it may be assumed that the TGU formed as a duplex above a layer of serpentinite serving as décollement horizon.

Both samples in this study are eclogites with a clearly developed foliation. In hand specimen, garnet, omphacite, phengite and green amphibole are visible. Their HP mineral assemblages comprise garnet + omphacite + glaucophane + phengite

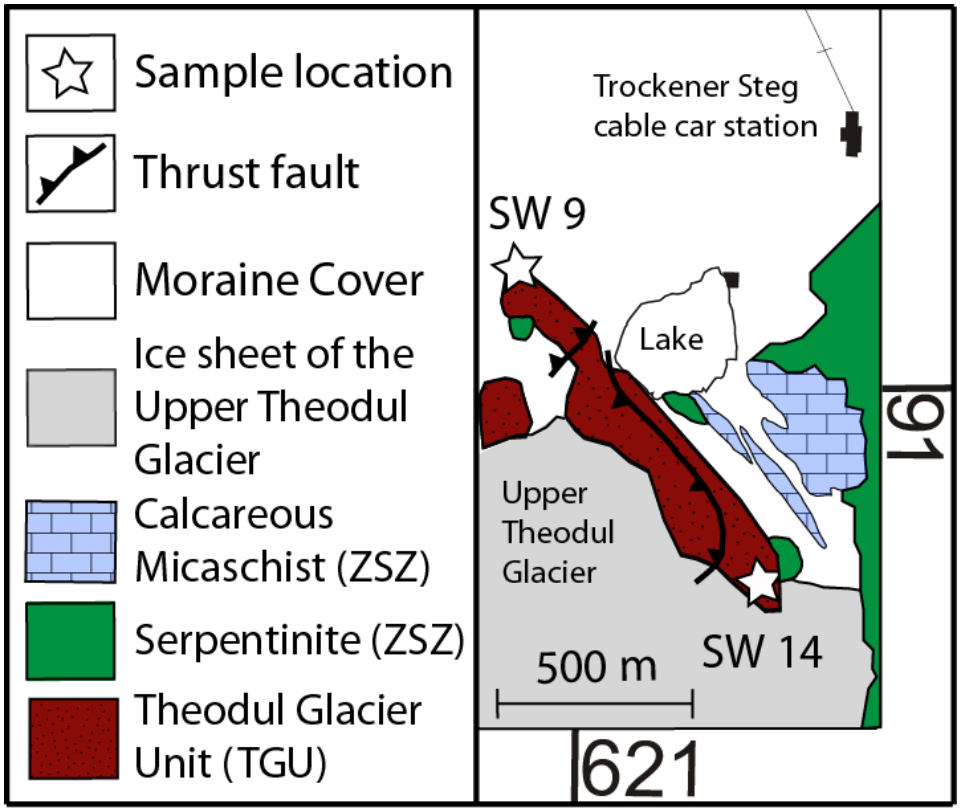

Figure 5.2: Simplified geological map of the Trockener Steg area south-west of Zermatt, with the locations of the analysed rock samples marked by white stars. The lithological units of the TGU, which consist of various HP-schists and interbedded eclogite, are shown as a single unit in brown. Note that the TGU is intimately associated with the serpentinites of the ZSZ. Easting and northing on the basis of the Swiss national coordinate system.

and rutile. During retrogression these minerals were partly replaced by calcic amphibole, epidote, chlorite, paragonite, oligoclase and quartz (Figure 5.3a). Garnet porphyroblasts are crowded with fine grained inclusions, which are mostly rutile needles, fine mica flakes and amphibole. In addition, some garnet crystals are crosscut by oligoclase veins (Figure 5.3b). In some domains, magmatic pyroxene is pseudomorphically replaced by omphacite that has later been transformed to amphibole. The former presence of magmatic phenocrysts is also indicated by parallel-elongated ore intergrowths within the large amphibole blast (Figure 5.3c). This suggests that omphacite was present in abundance during the peak metamorphism. White mica is partly aligned to the main foliation, partly randomly oriented. This shows that it formed during and after deformation (Figure 5.3d). Zircon was only observed in the matrix but not as inclusion in garnet. Zircon dominates the Hf budget of eclogite samples, which may have important consequences for the geochronological dating. Based on grain morphology both types of zircons, magmatic and metamorphic, occur in both samples.

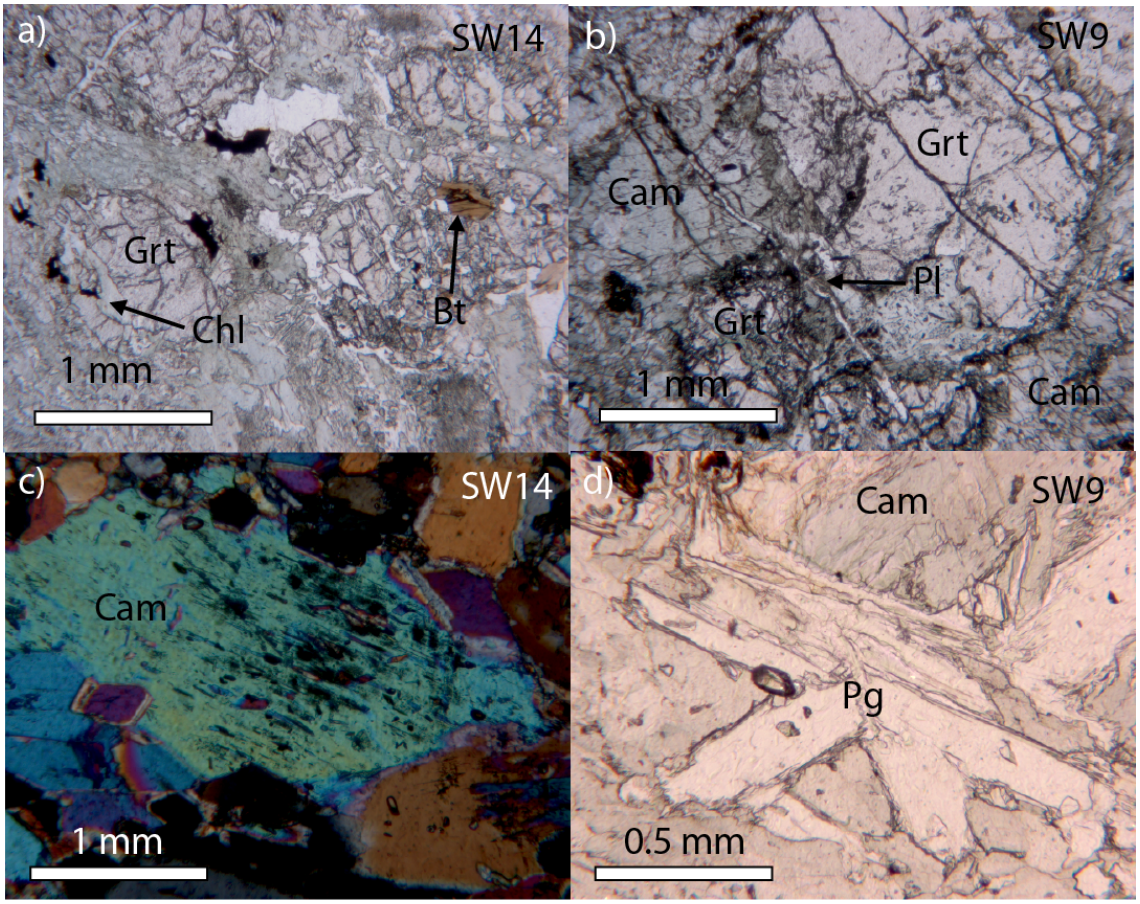

Figure 5.3: Photomicrographs of eclogite samples SW9 and SW14. a) and b) HP-paragenese of garnet and omphacite replaced by chlorite, biotite, calcic amphibole, and plagioclase veins, c) calcic amphibole pseudomorphically replacing clinopyroxene under crossed polarized light, d) randomly orientated paragonite. Grt = garnet; Bt = biotite; Chl = chlorite; Cam = calcic amphibole, Pg = paragonite.

P-T determinations from calculated assemblage stability diagrams for the eclogites of the TGU yield pressures of 18 to 22 kbar and temperatures of 500 to 600 °C (Weber, 2013). These estimates are similar to those of the Mt. Emilius klippen and the Etirol-Levaz slice, 11-13 kbar and 460-480 °C (Dal Piaz et al., 1983) and 16-17 kbar and c. 550 °C, respectively (Kienast, 1983; Ballèvre et al., 1986). The estimates for the continental outliers are in turn consistent with the eclogite metamorphism encountered in the Sesia Zone, where pressure and temperature reached 14-17 kbar and 500-600 °C (Lardeaux and Spalla, 1991). In contrast to the typical Zermatt-Saas ophiolites, which experienced HP and at least locally UHP metamorphic conditions (Reinecke, 1991; Bucher et al., 2005; Angiboust et al., 2009), these tectonic elements are clearly outside the coesite stability field and received only a "relatively high-pressure" imprint (Dal Piaz et al., 2001).

5.4 Analytical methods

5.4.1 Sample dissolution and element separation

The collected samples were crushed and divided into two splits. From one split a homogeneous powder was produced, the other was used for garnet separation. For garnet separation, crushed samples were split into grain size fractions by dry sieving. Garnet separates were then handpicked under a stereomicroscope. The separates were cleaned with 2.5 M HCl in an ultrasonic bath and rinsed twice with deionised water. A mixed ^{176}Lu-^{180}Hf tracer of was added to all samples before digestion. In order to avoid possible effects of inherited isotopic signatures in Hf-bearing phases, the "tabletop" digestion method of Lagos et al. (2007) was applied to all assays (garnet and bulk-rock). This method leaves behind refractory, Hf-bearing phases like rutile and zircon that might preserve potentially unequilibrated isotope signatures. The garnet separates were digested in Savillex screw-top PFA beakers by addition of HF-HNO_3-$HClO_4$ (4:2:1) and subsequently dried down followed by sample-spike equilibration in 6N HCl. Whole rock samples were dissolved inside steel jacketed Teflon PARR-bombs for five days at 180 °C. Subsequently Lu and Hf were separated from the matrix elements using Eichrom®Ln-Spec resin and the method described by Münker et al. (2001).

5.4.2 MC-ICPMS measurements

Lutetium and Hf measurements were performed on a Finnigan Neptune MC-ICPMS at the Steimann-Institut in Bonn. Instrumental mass bias on measured Hf isotope ratios were corrected by using the exponential law and a ^{179}Hf/^{177}Hf of 0.7325. Measured ^{176}Hf/^{177}Hf ratios presented in this work are reported relative to a ^{176}Hf/^{177}Hf ratio of 0.282160 for the Münster Ames Hf standard that is isotopically identical to the JMC-475 standard. Naturally occurring Yb in the Lu cuts was used for mass bias correction on Lu isotope ratios (Vervoort et al., 2004). Correction of the ^{176}Yb interference on ^{176}Lu was achieved by using the trend of ln (^{176}Yb/^{171}Yb) vs. ln (^{174}Yb/^{171}Yb) from Yb-only standard analyses before the Lu measurements (e.g. Vervoort et al., 2004; Lagos et al., 2007). Procedural blanks were < 24 pg for Lu and < 72 pg for Hf and were always insignificant. The effect of blank uncertainties on isochron ages is therefore insignificant. The external reproducibilities used for the isochron calculations were estimated by an empirical relationship 2σ external reproducibility $\approx 4\sigma$m (σm = standard error of a single analysis; e.g. Bizzarro et al., 2003). Regressions of isochrons and ages were calculated using ISOPLOT v. 2.49 (Ludwig, 2001) and a decay constant of $\lambda^{176}\text{Lu} = 1.867 \times 10^{-11}\text{yr}^{-1}$ (Scherer et al.,

2001; Söderlund et al., 2004).

5.4.3 Electron microprobe analysis

Electron microprobe analyses were carried out on a JEOL Superprobe JXA 8200 at the Steinmann-Institut, Bonn, using a beam current of 15 nA and an acceleration voltage of 15 kV. Elemental maps of Fe, Mg, Ca, and Mn were used to characterise the 2D distribution of major elements in single garnet grains. The dwell time of spot analysis during map scans was set to 100 msec.

5.4.4 Laser ablation analysis

Laser ablation analyses were carried out at the Steinmann-Institut in Bonn using a Resonetics M50-E ATL Excimer 193 nm laser system coupled to a Thermo-Finnigan X-series 2 quadrupole ICP-MS, following the routine described in Kirchenbaur et al. (2012). Spot sizes were set between 55 and 75 µm depending on grain size and the amount of visible inclusions. Laser fluence at the sample surface was measured at 7 J/cm^{-2}. The laser repetition rate was set to 10 Hz. Count rates were normalized using ^{29}Si as the internal standard and NIST-612 standard reference materials as external standards. The isotopes ^{29}Si, ^{43}Ca, ^{55}Mn, ^{89}Y, ^{175}Lu, and Hf were monitored. The oxide production rates were kept below 0.5 % in order to avoid the possibility of any significant oxide molecular interference on the REE isotopes that were monitored. Data reduction and evaluation was produced following the procedure of Longerich et al. (1996).

5.5 Results

As a result of crystal fractionation, nucleation and growth of garnet lead to the development of a primary growth zoning (Hollister, 1966; Atherton, 1968; Marmo et al., 2002; Konrad-Schmolke et al., 2008a). For the interpretation of Lu-Hf ages it is of fundamental interest if the observed chemical zoning represents an undisturbed prograde growth pattern. The crossing of the closure temperature (Dodson, 1973) may reset the Lu-Hf isotope system within garnet, and the ages defined by the isochrons may then reflect cooling instead of prograde crystallisation. To show that the investigated samples preserve an age linked to the prograde path, a useful proxy is the major element zoning in garnet. Major-element maps of single garnet grains of the two eclogite samples are presented in Figure 5.4. Garnet grains are mostly euhedral and show a bell-shaped distribution of Mn, Ca and Fe/(Fe+Mg) with high contents of Mn and Ca in the cores and decreasing contents towards the

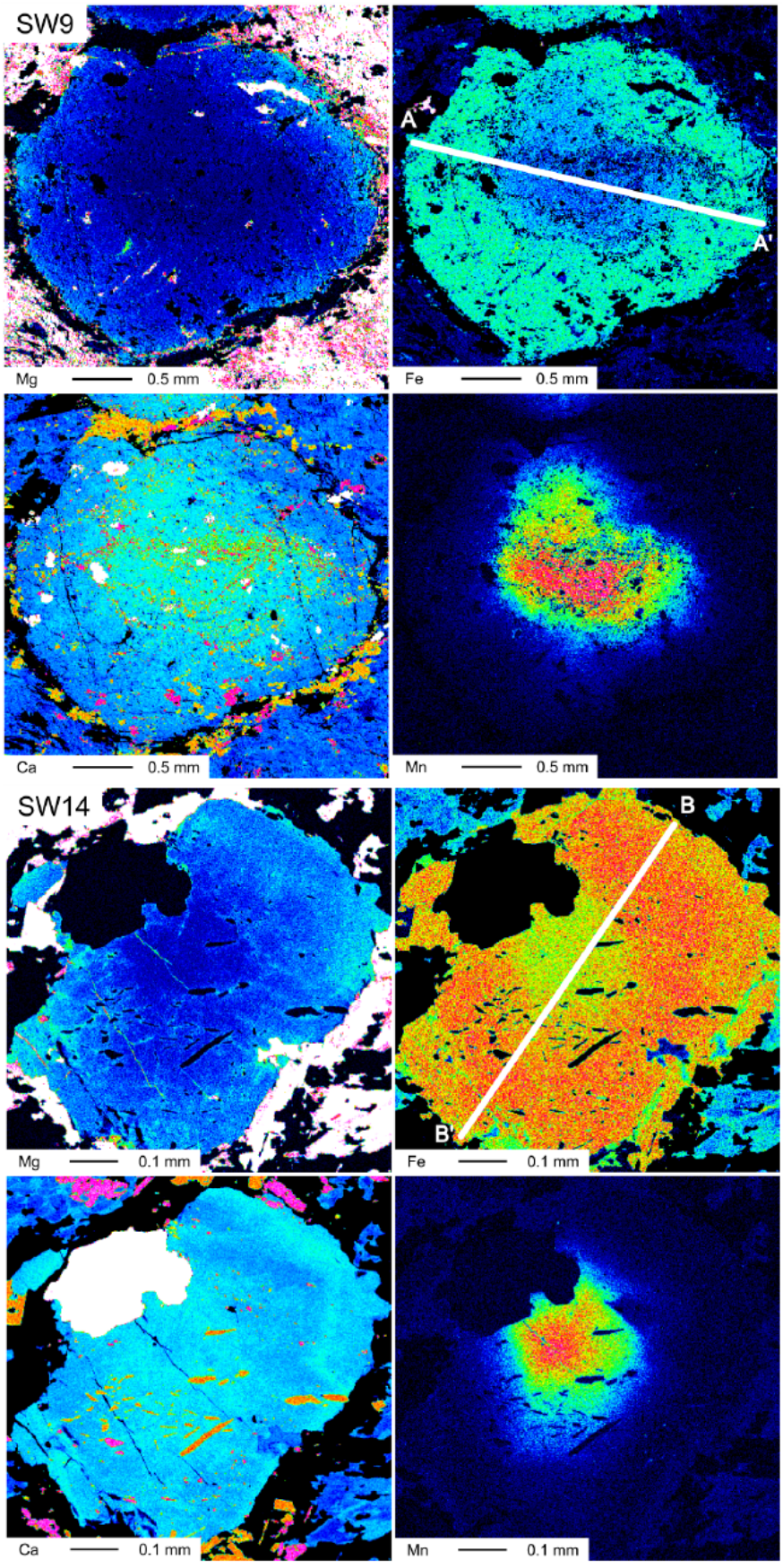

Figure 5.4: Major element distribution maps of garnets from samples SW9 and SW14. Traces AA‘ and BB‘ correspond to analyses given in Figure 5.5. Note the enrichment of Mn in the cores.

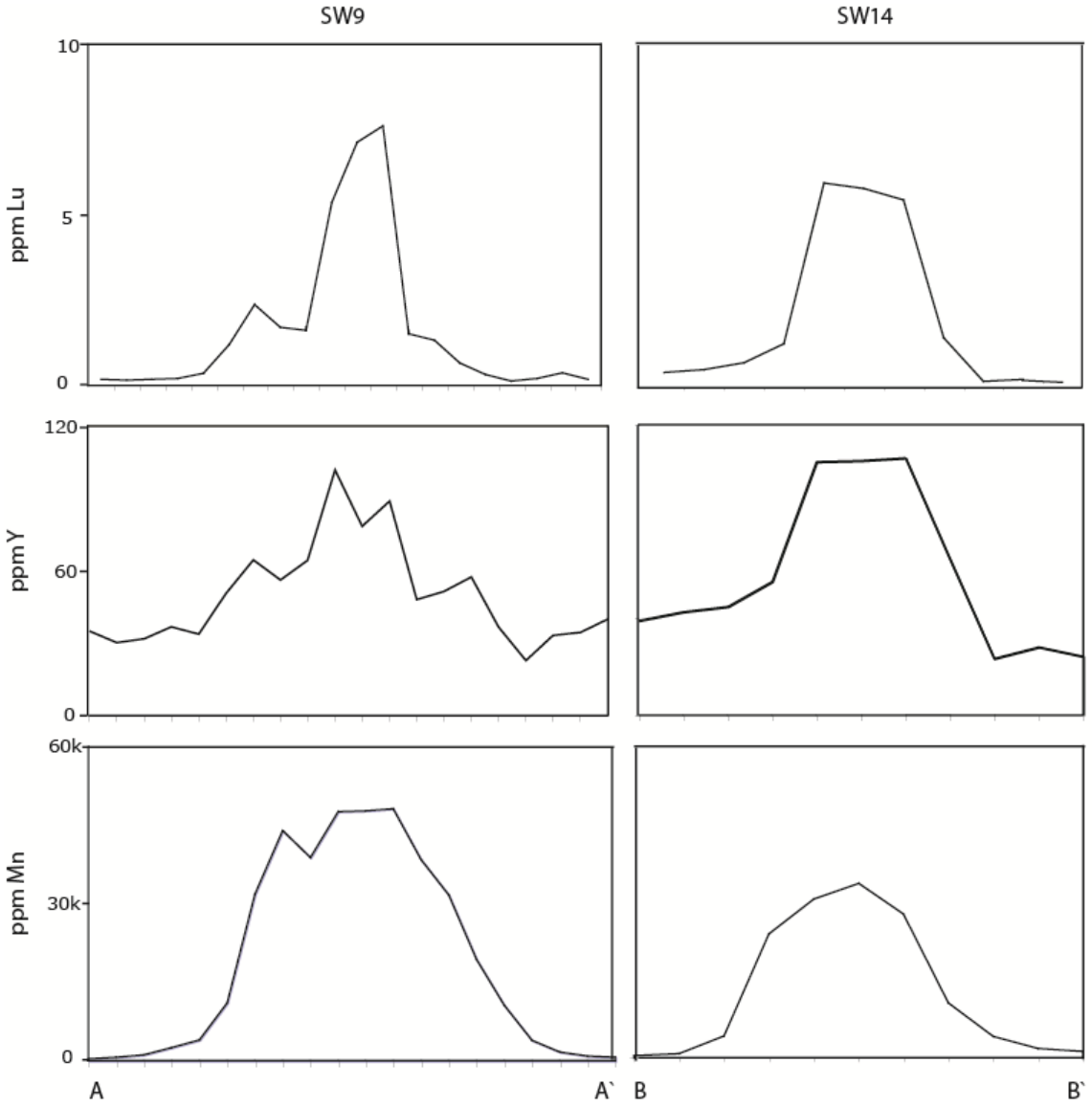

Figure 5.5: Lutetium, Y and Mn garnet zoning profiles for SW9 and SW14.

rims. Such a distribution is regarded as a preserved prograde growth-zoning pattern (Konrad-Schmolke et al., 2005; Skora et al., 2009).

Lutetium-concentration profiles of single garnet grains obtained by laser ablation analyses are presented in Figure 5.5. Both samples retained the initial pattern of garnet growth within the core and towards the rims (Skora et al., 2006). This observation is supported by the zoning patterns of Y and Mn as these elements reflect the distribution of Lu, due to analogue zoning in garnet. The distribution of Lu was not reset during peak temperature conditions. This implies that Alpine peak metamorphism did not lead to isotopic re-equilibration of the Lu-Hf system.

Concentrations of Lu and Hf and ratios of $^{176}Lu/^{177}Hf$ and $^{176}Hf/^{177}Hf$ are presented in Table 5.1. For each sample, mineral separates and whole rock aliquots

define statistically significant isochrons (MSWDs of 0.47 to 1.8). Garnet fractions and whole-rock-aliquots of sample SW9 yield a 4 point-isochron age of 56.5 ± 2.7 Ma (MSWD 0.47; Figure 5.6). For sample SW14, an isochron age of 58.2 ± 1.4 Ma was obtained (MSWD 1.8; Figure 5.7). The two ages are identical within errors. As indicated from the high Lu/Hf ratios measured for garnet separates ($^{176}Lu/^{177}Hf$ of 2 and higher), they are apparently unaffected by inherited Hf-rich phases.

Table 5.1: Lu and Hf element and isotope data of the whole rocks and garnet separates for Theodul Glacier Unit eclogite samples.

Sample		ppm Lu	ppm Hf	$^{176}Lu/^{177}Hf$	2σ	$^{176}Hf/^{177}Hf$	2σ
SW9	WR	0.319	5.90	0.007664	15	0.282798	34
	Grt1	1.76	0.135	1.852	4	0.284729	103
	Grt2	1.57	0.123	1.812	4	0.284954	570
	Grt3	1.41	0.103	1.952	4	0.284874	186
SW14	WR	0.382	9.59	0.005656	11	0.282721	13
	Grt1	1.32	0.0581	3.237	6	0.286516	335
	Grt2	1.38	0.0494	3.969	8	0.286998	107
	Grt3	1.40	0.0548	3.627	7	0.286781	430

Uncertainties on both $^{176}Lu/^{177}Hf$ and $^{176}Hf/^{177}Hf$ ratios are the estimated 2σ external reproducibilities, as discribed in the text. WR = WR (bomded).

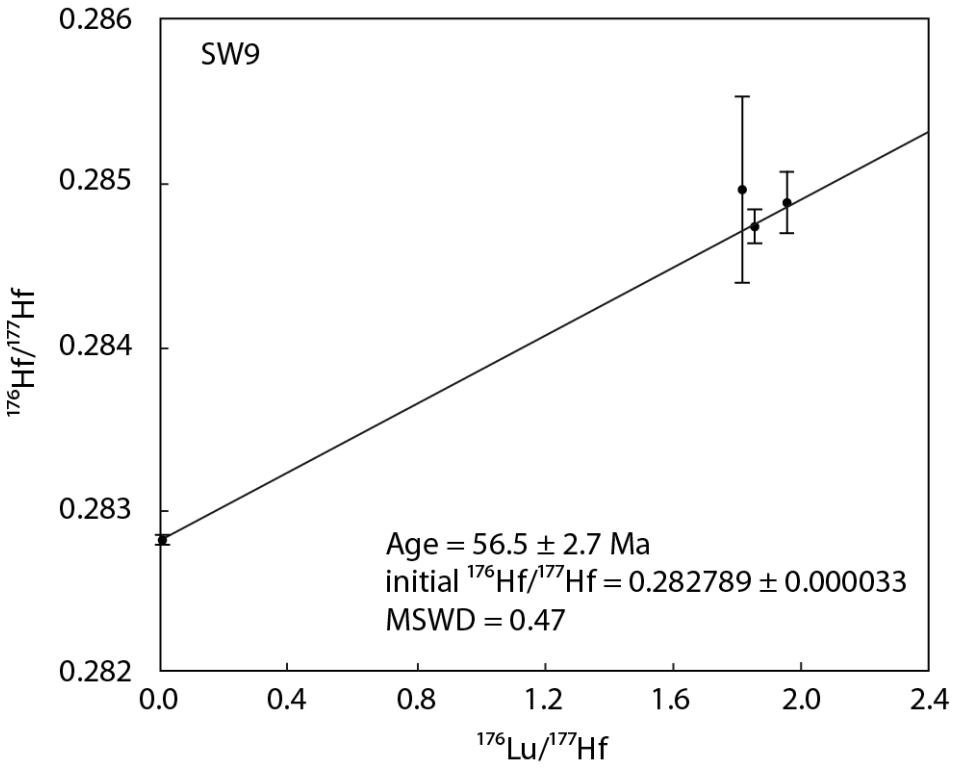

Figure 5.6: Lu-Hf garnet-whole rock isochron plot for sample SW9 from the Trockener Steg area. See Table 5.1 for data used to calculate the isochron.

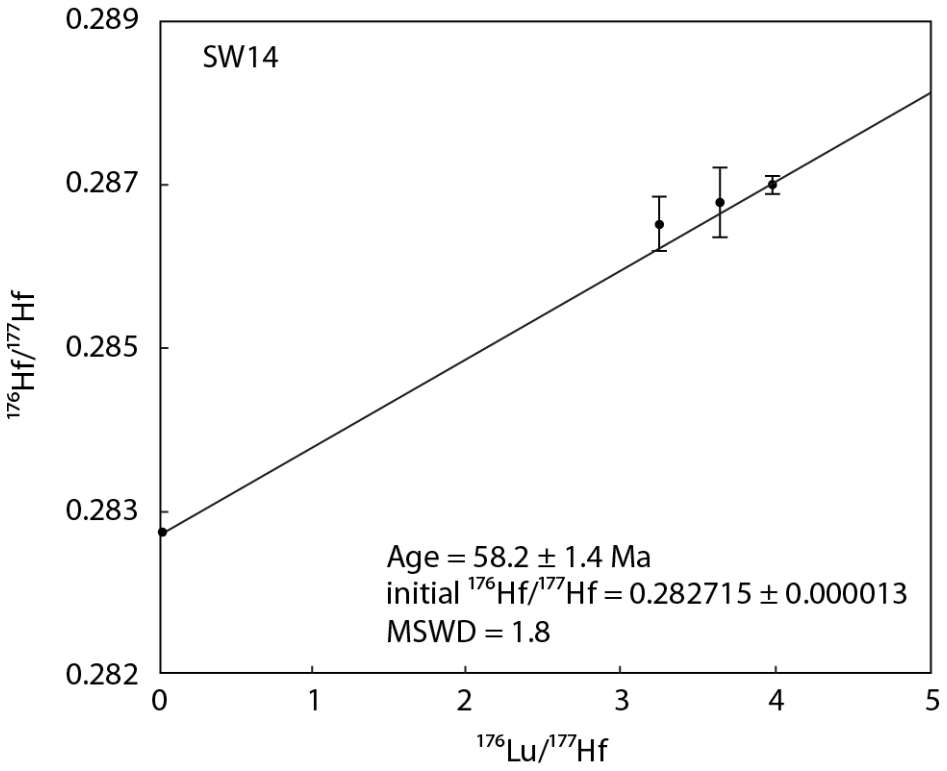

Figure 5.7: Lu-Hf garnet-whole rock isochron plot for sample SW14 from the Trockener Steg area. See Table 5.1 for data used to calculate the isochron.

5.6 Discussion

5.6.1 Geological significance of the Lu-Hf results

Various estimates have been made for the closing temperature of the Lu/Hf isotopie system (700 °C: Ganguly and Tirone, 1999; Scherer et al., 2000; 720-755 °C: Skora et al., 2006; 850 °C: Schmidt et al., 2011; 1000 °C: Shu et al., 2012). Since the eclogite samples from the TGU have experienced maximum temperatures below 700 °C, it can be assumed that they have remained below the closing temperature for the Lu-Hf system. The observed prograde garnet zoning in major elements, Mn^{2+}, Lu^{3+}, and Y^{3+}also suggests that Lu-Hf ages represent crystallization rather than cooling ages. The shape of the $Lu^{3+}$and Y^{3+} patterns presented here are similar to those reported by Skora et al. (2006) for where the authors also propose that garnet REE patterns within the ZSZ eclogites have not been reset. As a consequence, the isochron ages of 56.5 ± 2.7 Ma (MSWD 0.47) and 58.2 ± 1.4 Ma (MSWD 1.8) can confidently be interpreted as prograde crystallization ages. Since the samples studied were part of the Penninic subduction zone system, they can therefore be directly related to a subduction zone setting. Hence at around 58 to 56 Ma, the rocks of the TGU were buried to depths of 30-35 km on their way down the subduction, assuming the geochronological data refer to the beginning of garnet growth (Figure 5.8c). The fact that the two ages coincide within their errors strengthens this conclusion.

5.6.2 The Zermatt-Saas Zone – one terrane or a composite of slices?

Based on the lithological composition, the TGU is interpreted as a continental sliver comparable to Etirol-Levaz, Glacier-Rafray, Mt. Emilius, and other "Austroalpine" slivers in the Zermatt-Saas Zone. Using Rb-Sr geochronology on phengite, Dal Piaz et al. (2001) dated eclogite-facies metamorphism in some of the continental slivers - but not in the TGU - at 49-40 Ma, and in the Zermatt-Saas Zone ophiolites at 46-43 Ma. From the similarity of these age ranges they concluded that the "Austroalpine" slivers were derived from one or more intraoceanic extensional allochthon(s) that were already emplaced in the Piemonte-Liguria ocean by pre-oceanic rifting, and then subducted together with the ophiolites. In this view, the Zermatt-Saas Zone represents a coherent terrane that was subducted and exhumed in one piece. This model was supported by the finding of Jurassic zircon domains in the Etirol-Levaz sliver which were interpreted as results of melt infiltration associated with the intrusion of gabbro in the underlying ophiolite (Beltrando et al., 2010). Lutetium-Hf ages, however, which record incipient garnet growth during subduction, show a time difference of c. 8-10 Ma between the TGU (58-56 Ma) and the Zermatt-Saas Zone at

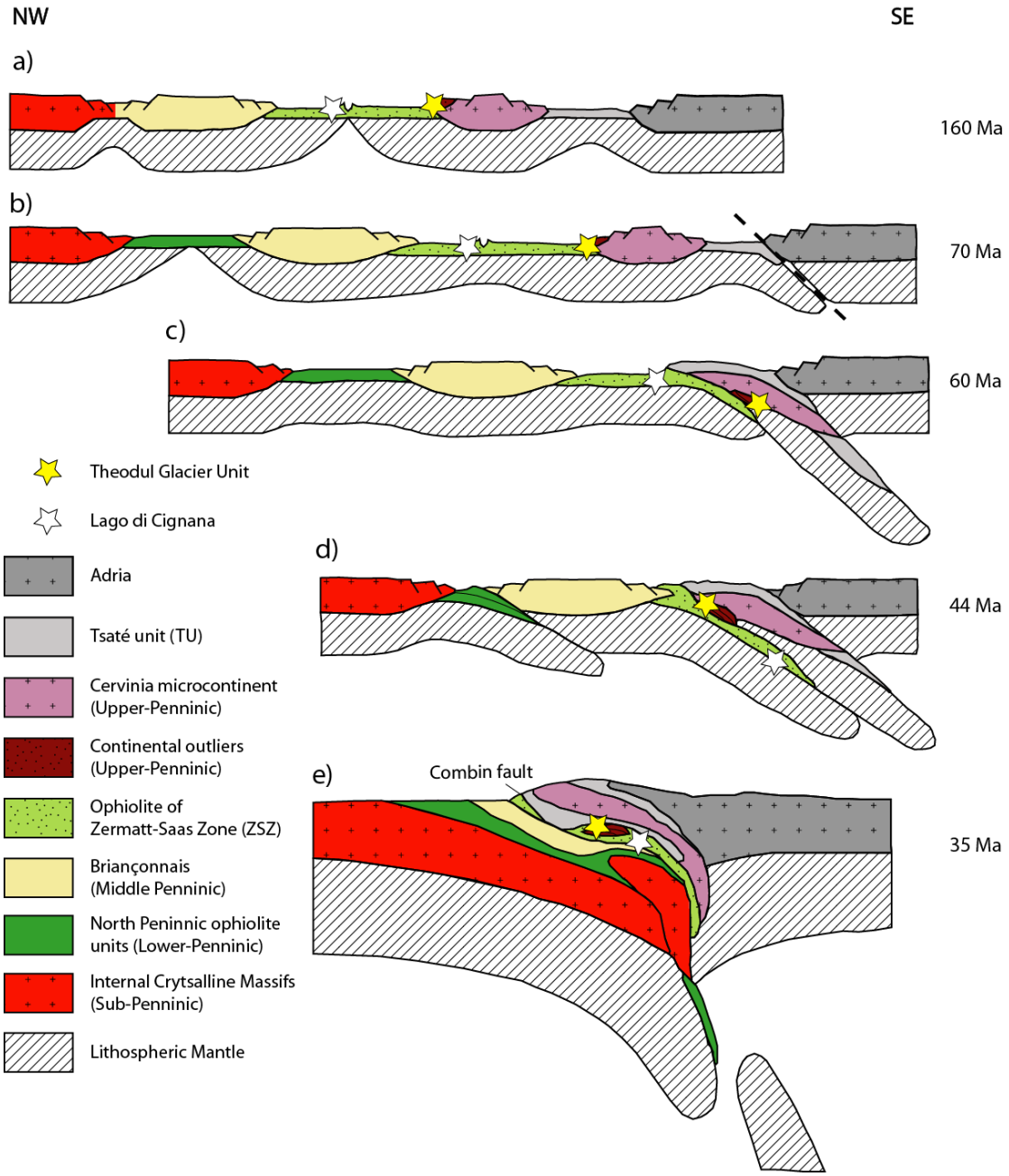

Figure 5.8: Schematic sketch, showing simplified evolution of the Western Alps in the time interval from 160 to 35 Ma. Two ocean basins existed, the Valais and the Piemonte-Liguria Ocean. (a) After the opening of the Piemonte-Liguria ocean, the TGU (yellow star) was part of the passive margin of the Cervinia microcontinent. (b) The Briançonnais terrane was separated from the European continent by rifting of the Valais Ocean in the Late Jurassic-Early Cretaceous. Subduction startet around 70 Ma at the latest. (c) TGU was subducted and accreted while other units of the Zermatt Saas Zone were still near the surface. (d) Subduction propagated continuously to the NW, while the Lago di Cignana Unit (white stars) was subducted to UHP depth. The process lasted until the arrival of the Briançonnais microcontinent which blocked the subduction zone and the subduction of the Valais ocean started. (e) Between 44 and 35 Ma, the western Alpine nappe stack was formed and the exhumation of the ZSZ and associated "Austroalpine outliers" took place. Exhumation was accompanied by thrusting along the Combin fault. In this model, the Internal Crystalline Massives are located at the European margin (Gebauer, 1999; Froitzheim, 2001). All published HP-ages are consistent with this model as discussed in the text. Sketches are not to scale.

Lago di Cignana (c. 48 Ma). As the older age is found more to the North (TGU) and the younger age to the South (Lago di Cignana), and the subduction zone which consumed the Piemonte-Liguria ocean probably dipped southeast (e.g. Dal Piaz et al., 2001), the age difference is opposite to what would be expected if the two units were parts of one coherent terrane. Consequently, at least these two parts of the Zermatt-Saas Zone were subducted independently over an age interval of nearly 10 Ma. Hence our data rather support the view that the Zermatt-Saas Zone is a composite of units with different tectonic histories (e.g. Negro et al., 2013). However, the arrangement of these units is probably not coincidental but follows the trend of decreasing metamorphic age from structurally higher to deeper tectonic units which is a general rule for high-pressure rocks in the Alps (Bearth, 1967; Berger and Bousquet, 2008), reflecting progressive accretion to the orogenic wedge: The TGU is found at the structural top of the Zermatt-Saas Zone and yielded the highest age known from this zone. More data from other parts of the ZSZ are needed to confirm this trend and to define the different tectonometamorphic units.

5.6.3 Palaeogeographic position of the TGU

The timing of eclogite-facies metamorphism in the TGU is intermediate between the Sesia nappe and the Zermatt-Saas ophiolites. As subduction generally prograded towards northwest (Laubscher, 1988, 1991; Escher et al., 1997; Rosenbaum and Lister, 2005) and the character of the TGU rocks is continental rather than oceanic (Weber, 2013), we assume that the TGU originally belonged to the northwestern continental margin of the Cervinia microcontinent or was at least located close to it (Figure 5.8).

The present-day tectonic position of the TGU is close to the boundary between two imbricated Piemont-Ligurian ophiolite units, the Zermatt-Saas Zone below and the Combin Zone on top. The Dent Blanche and Sesia nappes, which represent continental basement of the Cervinia microcontinent occupy a still higher tectonic position on top of the Combin Zone. This is interpreted in terms of out-of-sequence thrusting of Dent Blanche and Sesia over the Combin Zone between stages “d” and “e” of Figure 5.8 (Pleuger et al., 2007).

5.6.4 Implications for the “Paleocene restoration”

Our new data partly fill the Paleocene time gap in the geochronological record of high pressure metamorphism in the Central and Western Alps. So far, no evidence existed for eclogite-facies metamorphism between c. 65 Ma (Sesia Nappe) and c. 49 to 48 Ma (Lago di Cignana and Monviso; Figure 5.9). The Lu-Hf ages from the

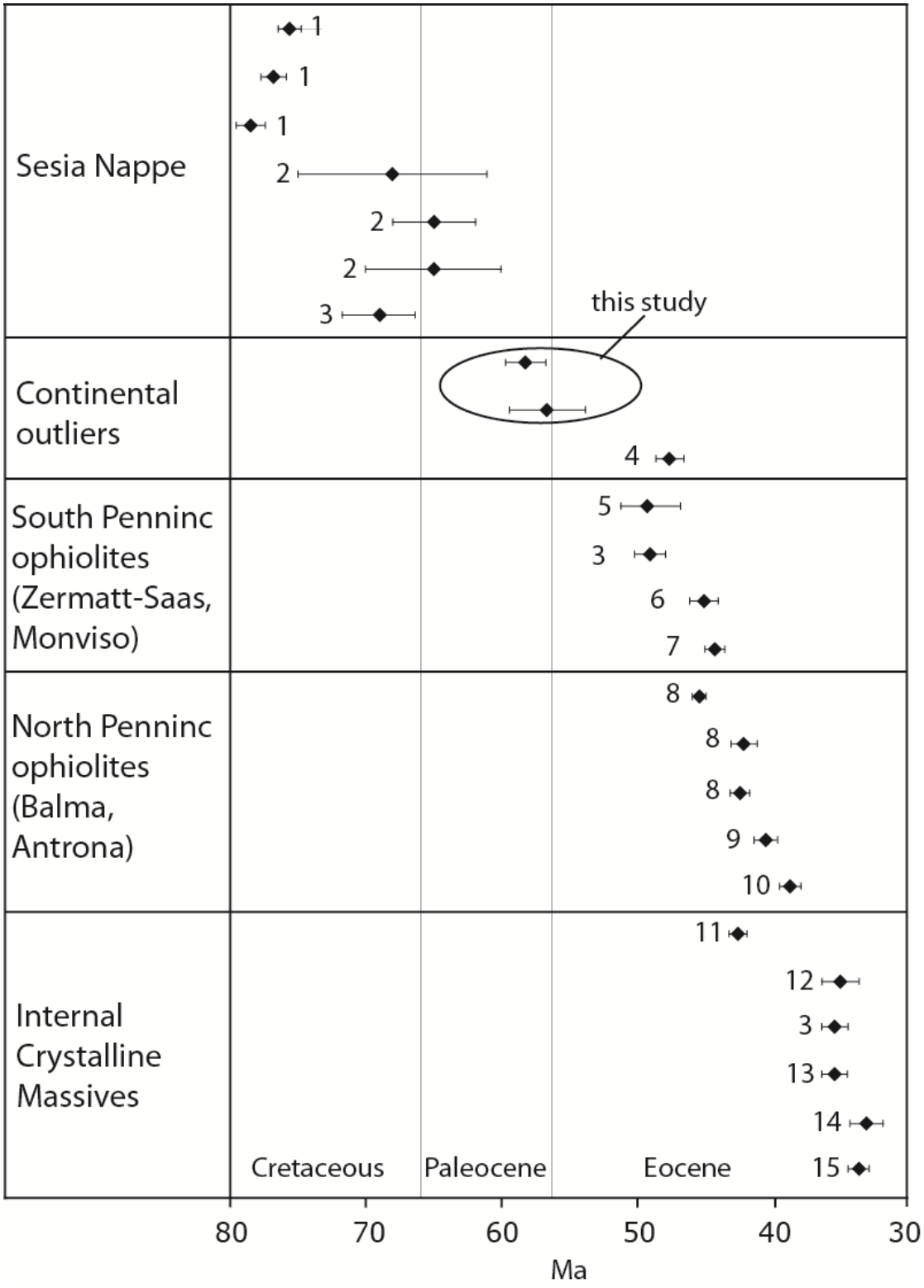

Figure 5.9: Ages of HP and UHP metamorphism in the western Alps from Lu-Hf garnet, U-Pb SHRIMP zircon, U-Pb SHRIMP allanite, and U-Pb rutile dating. (1) Rubatto et al. (2011), (2) Rubatto et al. (1999), (3) Duchêne et al. (1997), (4) Beltrando et al. (2010), (5) Lapen et al. (2003), (6) Rubatto and Hermann (2003), (7) Rubatto et al. (1998), (8) Herwartz et al. (2008), (9) Liati et al. (2005), (10) Liati and Froitzheim (2006), (11) Lapen et al. (2007), (12) Rubatto and Gebauer (1999), (13) Rubatto and Hermann (2001), (14) Gebauer et al. (1997), (15) Radulescu et al. (2009). Ages from this study, 56.5 ± 2.7 Ma and 58.2 ± 1.4 Ma, are indicated by ellipse.

TGU, c. 58-56 Ma, fall into the middle of this time span, making it very likely that subduction continued from the Late Cretaceous into the Eocene.

On the other hand, Europe-Africa convergence, as derived from the magnetic anomaly pattern in the Atlantic, almost came to a stillstand between 65 and 51 Ma (Trümpy, 1973, see also Frisch, 1979; Rosenbaum and Lister, 2005; Schettino and Turco, 2011). Therefore, subduction was probably balanced by extension of the upper plate, as is usually the case during roll-back of a subduction zone. Such roll-back extension during the Paleogene was already suggested by Rosenbaum and Lister (2005). Roll-back extension was, however, not restricted to the Paleocene but lasted from c. 80 Ma to 67 Ma in the Austroalpine (Froitzheim et al., 1997, 2012) and from 55 to 45 Ma in the Sesia Zone (Babist et al., 2006). This reflects a northwestward migration of the extensional process, in the wake of the equally northwestward-migrating subduction-related shortening.

5.6.5 Reconstruction of the tectonic evolution

Figure 5.8 attempts a reconstruction of the tectonic evolution of the western Swiss-Italian Alps, based on the existing age data and structural retrodeformation. The complicated paleogeography with continental ribbons and intervening ocean basins strongly influenced the orogenic evolution (e.g. Rosenbaum and Lister, 2005) and favoured the exhumation of HP and UHP units (Husson et al., 2009). Altogether, tectonic shortening prograded from southeast to northwest. We assume that microcontinent collisions led to the formation of new, short-lived subduction zones in more external positions (Royden and Husson, 2006, 2009). The collision of the Cervinia microcontinent at c. 70 to 65 Ma caused a new subduction zone to form in the northern sub-basin of the Piemont-Liguria ocean (Figure 5.8c). Likewise, the Brianconnais collision at c. 50 Ma started subduction in the North-Penninic (Valaisan) basin (Figure 5.8d; Herwartz et al., 2008). Between collisions, subduction of oceanic crust went on without major accretion and rollback occurred (not shown in Figure 5.8). The European continental margin started to be subducted at c. 40 Ma, which brought the Alps into a state of pure collisional orogeny (Figure 5.8e).

5.7 Conclusions

1. For the eclogites of the Theodul Glacier Unit (TGU), two Lu-Hf ages of 56.5 ± 2.7 Ma and 58.2 ± 1.4 Ma were obtained. Combined with garnet element profiles, it can be shown that these ages date the prograde growth of garnet cores. The ages can be related to a subduction-driven burial path, which implies that the TGU passed through a depth of approximately 30-35 km in the late Paleocene. Since subduction within the western Alps migrated in time from internal to external units, the TGU can be proposed to represent a fragment of the distal margin of the Cervinia microcontinent.

2. The new Lu-Hf ages fall into the Paleocene Restoration phase which separates two main orogenic events ("Eo-Alpine" and "Meso-Alpine"). Our results indicate that subduction continued throughout this period.

3. The subduction during the Paleogene occurred in a time of very low Europe-Africa convergence rates. This situation may be attributed to northwest-directed rollback, kinematically linked to extension in the upper plate.

Annotations

This chapter was submitted as an original paper to the *Swiss Journal of Geosciences*. The field work was done by S. Weber. I performed all microprobe analyses and Lu-Hf garnet dating. R. Fonseca and I carried out the LA-ICPMS analyses. S. Weber and N. Froitzheim developed the tectonic model. C. Münker and K. Bucher contributed to the manuscript. I wrote chapters 5.4 and 5.5 and further contributed to the other chapters. I produced figures 5.4, 5.5, 5.6, and 5.7.

6 Summary

Four case studies were performed on former continental margins (Chapters 2, 3, and 4) and on a continental fragment inside an ophiolitic unit (Chapter 5). The studies include Lu-Hf garnet dating, and garnet characterization by its chemical zoning. Lu zoning inside garnet was monitored by LA-ICPMS analyses in order to assign the obtained garnet ages to metamorphic stages of the individual subduction cycle.

The Adula Nappe in the Central Alps represents a coherent part of pre-Mesozoic continental basement with minor amounts of Mesozoic cover rocks from the distal European continental margin. This unit was subducted to mantle depth during the Eocene orogenic cycle but already recorded Variscan high-pressure metamorphic conditions. It shows a continuous gradient of Alpine metamorphic conditions. Variscan eclogite-facies relics are well preserved in the in the North but mainly obliterated in the South. The Adula Nappe was subducted as a cohesive body in a single event between c. 38 to 36 Ma. Subduction was short-lived as the entire nappe pile was established before 32 Ma.

The high grade metamorphic series of southeastern Pohorje in Slovenia was subjected to the highest pressure and temperature conditions during the Cretaceous Eo-Alpine metamorphic cycle. Eclogite-facies metamorphism in the ultramafic complex at the southeastern border of the Pohorje Mountains is contemporaneous with its surrounding country rocks. These rocks were subjected to eclogite facies conditions as a cohesive terrane in a single tectonic event between c. 97 and 90 Ma.

The new Lu-Hf garnet age of 5.1 $\pm$ 1.7 Ma obtained from a blueschist-facies garnet-amphibole schist, reveals that the Yuli Belt of Taiwan's Central Range was subducted after the beginning of arc-continent collision at about 6.5 Ma. Rocks from the Yuli belt remained at their maximum depth only for a very short period of time and were exhumed rapidly during ongoing convergence. Fast exhumation of these rocks can be explained by downward removal of the overlying forearc lithosphere and associated rise of deeply subducted material.

The dated eclogite samples from the Theodul Glacier Unit in the western Central Alps revealed garnet growth ages of c. 57 Ma. The unit represents a continental outlier inside the ophiolotic Zermatt-Saas Zone. Subduction was controlled by gravity acting on the downward moving slab in a setting of rollback. The differing metamorphic ages of continental occurrences inside the Zermatt-Saas Zone reveal that subduction was continuous in this unit. Thus, the Zermatt-Saas Zone was not subducted in one coherent slab but rather represents slivers subducted at different times.

The studies of the Adula Nappe, the Pohorje Nappe, and the Yuli Belt demonstrate that continental margins are subducted and exhumed to mid-crustal levels or even

to the surface within short periods of time of clearly less than 10 Ma. In the case of the Adula Nappe this timeframe is evidently just 2 Ma. The results received from investigating the Adula Nappe and the high-grade metamorphic rocks of the Pohorje Mountains further demonstrate that these continental terranes underwent subduction cycles as coherent units. In contrast, garnet dating of a continental fragment from the Zermatt-Saas Zone and its comparison with literature data lead to the conclusion that this ophiolotic unit was assembled in a long-lasting subduction event.

List of Figures

List of Tables

References

Agard, P., P. Yamato, L. Jolivet, and E. Burov: 2009, 'Exhumation of oceanic blueschists and eclogites in subduction zones: Timing and mechanisms'. *Earth-Science Reviews* **92**, 53–79.

Ague, J. J. and W. D. Carlson: 2013, 'Metamorphism as Garnet Sees It: The Kinetics of Nucleation and Growth, Equilibration, and Diffusional Relaxation'. *Elements* **9**, 439–445.

Amato, J. M., C. M. Johnson, L. P. Baumgartner, and B. L. Beard: 1999, 'Rapid exhumation of the Zermatt-Saas ophiolite deduced from high-precision Sm-Nd and Rb-Sr geochronology'. *Earth and Planetary Science Letters* **171**, 425–438.

Amelin, Y., S. L. Kamo, and D.-C. Lee: 2011, 'Evolution of early crust in chondritic or non-chondritic Earth inferred from U-Pb and Lu-Hf data for chemically abraded zircon from the Itsaq Gneiss Complex, West Greenland'. *Canadian Journal of Earth Sciences* **48**, 141–160.

Andersen, T. B., B. Jamtveit, J. F. Dewey, and E. Swensson: 1991, 'Subduction and eduction of continental crust: major mechanisms during continent-continent collision and orogenic extensional collapse, a model based on the south Norwegian Caledonides'. *Terra Nova* **3**, 303–310.

Angiboust, S., P. Agard, L. Jolivet, and O. Beyssac: 2009, 'The Zermatt-Saas ophiolite: the largest (60-km wide) and deepest (c. 70-80 km) continuous slice of oceanic lithosphere detached from a subduction zone?'. *Terra Nova* **21**, 171–180.

Arnaud, N. O. and S. P. Kelley: 1995, 'Evidence for excess argon during high pressure metamorphism in the Dora Maira Massif (western AIps, Italy), using an ultra-violet laser ablation microprobe ^{40}Ar-^{39}Ar technique'. *Contributions to Mineralogy and Petrology* **121**, 1–11.

Atherton, M. P.: 1968, 'The variation in garnet, biotite and chlorite composition in medium grade pelitic rocks from the Dalradian of Scotland, with particular reference to the zonation in garnet'. *Contributions to Mineralogy and Petrology* **18**, 347–371.

Babist, J., M. R. Handy, M. Konrad-Schmolke, and K. Hammerschmidt: 2006, 'Precollisional, multistage exhumation of subducted continental crust: The Sesia Zone, western Alps'. *Tectonics* **6**, 1–25.

Ballèvre, M., J. R. Kienast, and J. P. Vuichard: 1986, 'La 'nappe de la Dent Blanche' (Alpes occidentales): deux unitès austroalpines indèpèndantes'. *Eclogae Geologicae Helvetiae* **79**, 57–74.

Barnicoat, A. C.: 1988, 'Zoned high-pressure assemblages in pillow lavas of the Zermatt-Saas ophiolite zone, Switzerland'. *Lithos* **21**, 227–236.

Baudin, T. and D. Marquer: 1993, 'Métamorphisme et déformation dans la nappe de Tambo (Alpes centrales suisses): évolution de la substitution phengitique au cours de la déformation alpine'. *Schweizerische mineralogische und petrographische Mitteilungen* **73**, 285–299.

Baxter, E. F. and E. E. Scherer: 2013, 'Garnet Geochronology: Timekeeper of Tectonometamorphic Processes'. *Elements* **9**, 433–438.

Bearth, P.: 1963, *Contribution à la subdivision tectonique et stratigraphique du cristallin de la nappe du Grand Saint-Bernard dans le Valais (Suisse)*, pp. 407–418. In: Livre Paul Fallot 2. - Société géologique de France.

Bearth, P.: 1967, 'Die Ophiolithe der Zone von Zermatt-Saas Fee'. *Beiträge zur geologischen Karte der Schweiz* **132**, 1–130.

Becker, H.: 1993, 'Garnet peridotite and eclogite Sm-Nd mineral ages from the Lepontime dome (Swiss Alps): New evidence for Eocene high-pressure metamorphism in the central Alps'. *Geology* **21**, 599–602.

Beltrando, M., D. Rubatto, and G. Manatschal: 2010, 'From passive margins to orogens: The link between ocean-continent transition zones and (ultra)high-pressure metamorphism'. *Geology* **38**, 559–562.

Berger, A. and R. Bousquet: 2008, 'Subduction-related metamorphism in the Alps: review of isotopic ages based on petrology and their geodynamic consequences'. *Geological Society, London, Special Publications* **298**, 117–144.

Berger, A., I. Mercolli, and M. Engi: 2005, 'The central Lepontine Alps: Notes accompanying the tectonic and petrographic map sheet Sopra Ceneri (1:100'000)'. *Schweizerische mineralogische und petrographische Mitteilungen* **85**, 109–146.

Berger, A., S. M. Schmid, M. Engi, R. Bousquet, and M. Wiederkehr: 2011, 'Mechanisms of mass and heat transport during Barrovian metamorphism: A discussion based on field evidence from the Central Alps (Switzerland/northern Italy)'. *Tectonics* **30**, TC1007.

Beyssac, O., F. Negro, M. Simoes, Y.-C. Chan, and Y.-G. Chen: 2008, 'High-pressure metamorphism in Taiwan: from oceanic subduction to arc-continent collision?'. *Terra Nova* **20**, 118–125.

Biino, G. G., D. Marquer, and C. Nussbaum: 1997, 'Alpine and pre-Alpine subduction events in polycyclic basements of the Swiss Alps'. *Geology* **25**, 751–754.

Bizzarro, M., J. A. Baker, H. Haack, D. Ulfbeck, and M. Rosing: 2003, 'Early history of Earth's crust-mantle system inferred from hafnium isotopes in chondrites'. *Nature* **421**, 931–933.

Bousquet, R., M. Engi, G. Gosso, R. Oberhänsli, A. Berger, M. I. Spalla, M. Zucali, and B. Goffé: 2004, 'Transition from the Western to the Central Alps. Explanatory note to the map 'Metamorphic structure of the Alps". *Mitteilungen der Österreichischen Mineralogischen Gesellschaft* **149**, 145–156.

Bousquet, R., B. Goffé, O. Vidal, R. Oberhänsli, and M. Patriat: 2002, 'The tectonometamorphic history of the Valaisan domain from the Western to the Central Alps: New constraints on the evolution of the Alps'. *Geological Society of America Bulletin* **114**, 207–225.

Bowtell, S. A., R. A. Cliff, and A. C. Barnicoat: 1994, 'Sm-Nd isotopic evidence on the age of eclogitization in the Zermatt-Saas ophiolite'. *Journal of Metamorphic Geology* **12**, 187–196.

Bozhilov, K. N., H. W. Green, and L. Dobrzhinetskaya: 1999, 'Clinoenstatite in Alpe Arami Peridotite: Additional Evidence of Very High Pressure'. *Science* **284**, 128–132.

Brenker, F. E. and G. P. Brey: 1997, 'Reconstruction of the exhumation path of the Alpe Arami garnet-peridotite body from depths exceeding 160 km'. *Journal of Metamorphic Geology* **15**, 581–592.

Brouwer, F. M., T. Burri, M. Engi, and A. Berger: 2005, 'Eclogite relics in the Central Alps: PT - evolution, Lu-Hf ages and implications for formation of tectonic mélange zones'. *Schweizerische mineralogische und petrographische Mitteilungen* **85**, 147–174.

Bruand, E., K. Stüwe, and A. Proyer: 2010, 'Pseudosection modelling for a selected eclogite body from the Koralpe (Hohl), Eastern Alps'. *Mineralogy and Petrology* **99**, 75–87.

Brueckner, H. K., D. A. Carswell, W. L. Griffin, L. G. Medaris Jr., H. L. M. Van Roermund, and S. J. Cuthbert: 2010, 'The mantle and crustal evolution of two garnet peridotite suites from the Western Gneiss Region, Norwegian Caledonides: An isotopic investigation'. *Lithos* **117**, 1–19.

Brun, J.-P. and C. Faccenna: 2008, 'Exhumation of high-pressure rocks driven by slab rollback'. *Earth and Planetary Science Letters* **272**, 1–7.

Bruno, M., R. Compagnoni, and M. Rubbo: 2001, 'The ultra-high pressure coronitic and pseudomorphous reactions in a metagranodiorite from the Brossasco-Isasca Unit, Dora-Maira Massif, western Italian Alps: a petrographic study and equilibrium thermodynamic modelling'. *Journal of Metamorphic Geology* **19**, 33–43.

Bucher, K., Y. Fazis, C. De Capitani, and R. Grapes: 2005, 'Blueschists, eclogites, and decompression assemblages of the Zermatt-Saas ophiolite: High-pressure metamorphism of subducted Tethys lithosphere'. *American Mineralogist* **90**, 821–835.

Bucher, S. and R. Bousquet: 2007, 'Metamorphic evolution of the Briançonnais units along the ECORS- CROP profile (Western Alps): new data on metasedimentary rocks'. *Swiss Journal of Geosciences* **100**, 227–242.

Bucher, S., S. M. Schmid, R. Bousquet, and B. Fügenschuh: 2003, 'Late-stage deformation in a collisional orogen (Western Alps): nappe refolding, back-thrusting or normal faulting?'. *Terra Nova* **15**, 109–117.

Burov, E., T. Francois, P. Yamato, and S. Wolf: 2014, 'Mechanisms of continental subduction and exhumation of HP and UHP rocks'. *Gondwana Research* **25**, 464–493.

Burtman, V. S. and P. Molnar: 1993, 'Geological and Geophysical Evidence for Deep Subduction of Continental Crust Beneath the Pamir'. *Geological Society of America Special Paper* **281**, 1–76.

Caddick, M. J., J. Konopásek, and T. A. B.: 2010, 'Preservation of Garnet Growth Zoning and the Duration of Prograde Metamorphism'. *Journal of Petrology* **51**, 2327–2347.

Carlson, R. L. and G. S. Raskin: 1984, 'Density of the ocean crust'. *Nature* **311**, 555–558.

Carlson, W. and E. Schwarze: 1997, 'Petrological significance of prograde homogenization of growth zoning in garnet: an example from the Llano Uplift'. *Journal of Metamorphic Geology* **15**, 631–644.

Carlson, W. D.: 2012, 'Rates and mechanism of Y, REE, and Cr diffusion in garnet'. *American Mineralogist* **97**, 1598–1618.

Carry, N., F. Gueydan, B. J. P., and D. Marquer: 2009, 'Mechanical decoupling of high-pressure crustal units during continental subduction'. *Earth and Planetary Science Letters* **278**, 13–25.

Cavargna-Sani, M., J.-L. Epard, F. Bussy, and A. Ulianov: 2014, 'Basement lithostratigraphy of the Adula nappe: implications for Palaeozoic evolution and Alpine kinematics'. *International Journal of Earth Sciences* **103**, 61–82.

Cavargna-Sani, M., J.-L. Epard, and A. Steck: subm., 'Structure, geometry and kinematics of the northern Adula nappe (Central Alps) and its emplacement in the Lower Penninic nappe stack'. *Swiss Journal of Geosciences*.

Chemenda, A. I., M. Mattauer, J. Malavieille, and A. N. Bokun: 1995, 'A mechanism for syn-collisional rock exhumation and associated normal faulting: Results from physical modelling'. *Earth and Planetary Science Letters* **132**, 225–232.

Chemenda, A. I., R.-K. Yang, J.-F. Stephan, E. A. Konstantinovskaia, and G. M. Ivanov: 2001, 'New results from physical modelling of arc-continent collision in Taiwan: evolutionary model'. *Tectonophysics* **333**, 159–178.

Chopin, C.: 1984, 'Coesite and pure pyrope in high-grade blueschists of the Western Alps: a first record and some consequences'. *Contributions to Mineralogy and Petrology* **86**, 107–118.

Chopin, C.: 2003, 'Ultrahigh-pressure metamorphism: tracing continental crust into the mantel'. *Earth and Planetary Science Letters* **212**, 1–14.

Chopin, C. and H. Maluski: 1980, '^{40}Ar-^{39}Ar dating of high pressure metamorphic micas from the Gran Paradiso area (Western Alps): Evidence against the blocking temperature Concept'. *Contributions to Mineralogy and Petrology* **74**, 109–122.

Christensen, N. I. and W. D. Mooney: 1995, 'Seismic velocity structure and composition of the continental crust: A global view'. *Journal of Geophysical Research: Solid Earth* **100**, 9761–9788.

Ciancaleoni, L. and D. Marquer: 2006, 'Syn-extension leucogranite deformation during convergence in the Eastern Central Alps: example of the Novate intrusion'. *Terra Nova* **18**, 170–180.

Cloos, M. and R. L. Shreve: 1988, 'Subduction-Channel Model of Prism Accreation, Melange Formation, Sediment Subduction, and Subduction Erosion at Convergent Plate Margins: 2. Implications and Discussion'. *Pure and Applied Geophysics* **128**, 501–545.

Compagnoni, R., G. V. Dal Piaz, J. C. Hunziker, G. Gosso, B. Lombardo, and P. F. Williams: 1977, 'The Sesia Lanzo zone, a slice of continental crust with Alpine high pressure-low temperature assemblages in the western Italian Alps'. *Società Italiana di Mineralogia e Petrologia* **33**, 281–334.

Coward, M. and D. Dietrich: 1989, 'Alpine tectonics, an overview'. *Geological Society, London, Special Publications* **45**, 1–29.

Dal Piaz, G., B. Lombardo, and G. Gosso: 1983, 'Metamorphic evolution of the Mt. Emilius Klippe, Dent Blanche Nappe, Western Alps'. *American Journal of Science* **283**, 438–458.

Dal Piaz, G. V.: 1999, *The Austroalpine-Piedmont nappe stack and the puzzle of Alpine Tethys*, Vol. 51, pp. 155–176. In: Gosso et al. (Eds.): Third Meeting on Alpine Geol. Studies: Memorie di Scienze Geologiche.

Dal Piaz, G. V., G. Cortiana, A. Del Moro, M. S., G. Pennacchioni, and P. Tartarotti: 2001, 'Tertiary age and paleostructural inferences of the eclogitic imprint in the Austroalpine outliers and Zermatt-Saas ophiolite, western Alps'. *International Journal of Earth Sciences* **90**, 668–684.

Dale, J. and T. J. B. Holland: 2003, 'Geothermobarometry, P-T paths and metamorphic field gradients of high-pressure rocks from the Adula Nappe, Central Alps'. *Journal of Metamorphic Geology* **21**, 813–829.

Davidson, C., C. Rosenberg, and S. M. Schmid: 1996, 'Synmagmatic folding of the base of the Bergell pluton, Central Alps'. *Tectonophysics* **265**, 213–238.

De Capitani, C. and K. Petrakakis: 2010, 'The computation of equilibrium assemblage diagrams with Theriak/Domino software'. *American Mineralogist* **95**, 1006–1016.

De Hoog, J. C. M., M. Janák, M. Vrabec, and N. Froitzheim: 2009, 'Serpentinised peridotites from an ultrahigh-pressure terrane in the Pohorje Mts. (Eastern Alps, Slovenia): Geochemical constraints on petrogenesis and tectonic setting'. *Lithos* **109**, 209–222.

De Hoog, J. C. M., M. Janák, M. Vrabec, and K. H. Hatton: 2011, *Ultramafic Cumulates of Oceanic Affinity in an Intracontinental Subduction Zone: Ultrahigh-Pressure Garnet Peridotites from Pohorje (Eastern Alps, Slovenia)*, pp. 399–439. In: Dobrzhinetskaya, L., Faryad, S.W., Wallis, S., Cuthbert, S. (Eds.): Ultrahigh-Pressure Metamorphism: 25 Years after the Discovery of Coesite and Diamond. Elsevier Insights.

Dewey, J. F., M. L. Helman, E. Turco, D. H. W. Hutton, and S. D. Knott: 1989, 'Kinematics of the Western Mediterranean, in Alpine Tectonics'. *Geological Society, London, Special Publications* **45**, 265–283.

Diener, J. F. A., R. Powell, R. W. White, and H. T. J. B.: 2007, 'A new thermodynamic model for clino- and orthoamphiboles in the system Na2O-CaO-FeO-MgO-Al2O3-SiO2-H2O-O'. *Journal of Metamorphic Geology* **25**, 631–656.

Dietz, R. S.: 1961, 'Continental and ocean basin evolution by spreading of the sea floor'. *Nature* **190**, 854–857.

Dobrzhinetskaya, L., H. W. Green, and S. Wang: 1996, 'Alpe Arami: A Peridotite Massif from Depths of More Than 300 Kilometers'. *Science* **271**, 1841–1845.

Dodson, M. H.: 1973, 'Closure temperature in geochronological and petrological systems'. *Contributions to Mineralogy and Petrology* **40**, 259–274.

Duchêne, S., J. Blichert-Toft, B. Luais, P. Télouk, J.-M. Lardeaux, and F. Albarède: 1997, 'The Lu-Hf dating of garnets and the ages of the Alpine high-pressure metamorphism'. *Nature* **387**, 586–589.

Duretz, T. and T. V. Gerya: 2013, 'Slab detachment during continental collision: Influence of crustal rheology and interaction with lithospheric delamination'. *Tectonophysics* **602**, 124–140.

Duretz, T., T. V. Gerya, B. J. P. Kaus, and T. B. Andersen: 2012, 'Thermomechanical modeling of slab eduction'. *Journal of Geophysical Research* **117**, B08411.

Engi, M., A. Berger, and G. T. Roselle: 2001, 'Role of the tectonic accretion channel in collisional orogeny'. *Geology* **29**, 1143–1146.

Ernst, W. G. and J. G. Liou: 2008, 'High- and ultrahigh-pressure metamorphism: Past results and future prospects'. *American Mineralogist* **93**, 1771–1786.

Escher, A., J. C. Hunziker, M. Marthaler, H. Masson, M. Sartori, and A. Steck: 1997, *Geological framework and structural evolution of the western Swiss-Italian Alps*, pp. 205–221. In: Pfiffner et al. (Eds.): Deep Structure of the Swiss Alps: Results From NRP 20. Birkhäuser, Basel, Switzerland.

Faryad, S. W.: 2012, 'High-pressure polymetamorphic garnet growth in eclogites from the Mariánské Lázně Complex (Bohemian Massif)'. *European Journal of Mineralogy* **24**, 483–497.

Faure, M., L. Shu, B. Wang, J. Charvet, F. Choulet, and P. Monie: 2009, 'Intracontinental subduction: a possible mechanism for the Early Palaeozoic Orogen of SE China'. *Terra Nova* **21**, 360–368.

Federico, L., L. Crispini, M. Scambelluri, and G. Capponi: 2007, 'Ophiolite mélange zone records exhumation in a fossil subduction channel'. *Geology* **35**, 499–502.

Florineth, D. and N. Froitzheim: 1994, 'Transition from continental to oceanic basement in the Tasna nappe (Engadine window, Graubu?nden, Switzerland): evidence for early Cretaceous opening of the Valais ocean'. *Schweizerische mineralogische und petrographische Mitteilungen* **74**, 437–448.

Fodor, L. I., A. Gerdes, I. Dunkl, B. Koroknai, Z. Pécskay, M. Trajanova, P. Horváth, M. Vrabec, B. Jelen, K. Balogh, and W. Frisch: 2008, 'Miocene emplacement and rapid cooling of the Pohorje pluton at the Alpine-Pannonian-Dinaridic junction, Slovenia'. *Swiss Journal of Geosciences* **101**, 255–271.

Frey, M., J. Desmons, and F. Neubauer: 1999, 'The new metamorphic map of the Alps: Introduction'. *Schweizerische Mineralogische und Petrographische Mitteilungen* **79**, 1–4.

Frezzotti, M. L., J. Selverstone, Z. D. Sharp, and R. Compagnoni: 2011, 'Carbonate dissolution during subduction revealed by diamond-bearing rocks from the Alps'. *Nature Geoscience* **4**, 703–706.

Frisch, W.: 1979, 'Tectonic progradation and plate tectonic evolution of the Alps'. *Tectonophysics* **60**, 121–139.

Frischknecht, G., H. Jenny, and J. Kopp: 1923, *Geologie der Adula*. Beiträge zur Geologischen Karte der Schweiz. NF 51.

Froitzheim, N.: 2001, 'Origin of the Monte Rosa nappe in the Pennine Alps - A new working hypothesis'. *Geological Society of America Bulletin* **113**, 604–614.

Froitzheim, N., P. Conti, and M. Van Daalen: 1997, 'Late Cretaceous synorogenic, low-angle normal faulting along the Schiling fault (Switzerland, Italy, Austria) and its significance for the tectonics of the Eastern Alps'. *Tectonophysics* **280**, 260–293.

Froitzheim, N. and G. Manatschal: 1996, 'Kinematics of Jurassic rifting, mantle exhumation, and passive margin formation in the Austroalpine and Penninic nappes (eastern Switzerland)'. *Geological Society of America Bulletin* **108**, 1120–1133.

Froitzheim, N., J. Pleuger, and T. Nagel: 2006, 'Extraction faults'. *Journal of Structural Geology* **28**, 1388–1395.

Froitzheim, N., J. Pleuger, S. Roller, and T. Nagel: 2003, 'Exhumation of high- and ultrahigh-pressure metamorphic rocks by slab extraction'. *Geology* **31**, 925–928.

Froitzheim, N., S. M. Schmid, and M. Frey: 1996, 'Mesozoic paleogeography and the timing of eclogite-facies metamorphism in the Alps: A working hypothesis'. *Eclogae Geologicae Helvetiae* **89**, 81–110.

Froitzheim, N., S. Weber, T. J. Nagel, T. Ibele, and H. Furrer: 2012, 'Late Cretaceous extension overprinting a steep belt in the Northern Calcareous Alps (Schesaplana, Rätikon, Switzerland and Austria)'. *International Journal of Earth Sciences* **101**, 1315–1329.

Galli, A., B. Le Bayon, M. W. Schmidt, J.-P. Burg, E. Reusser, S. A. Sergeev, and A. Larionov: 2012, 'U-Pb zircon dating of the Gruf Complex: disclosing the late Variscan granulitic lower crust of Europe stranded in the Central Alps'. *Contributions to Mineralogy and Petrology* **163**, 353–378.

Galster, F., M. Cavargna-Sani, J.-L. Epard, and H. Masson: 2012, 'New stratigraphic data from the Lower Penninic between the Adula nappe and the Gotthard massif and consequences for the tectonics and the paleogeography of the Central Alps'. *Tectonophysics* **579**, 37–55.

Ganguly, J. and M. Tirone: 1999, 'Diffusion closure temperature and age of a mineral with arbitrary extent of diffusion: theoretical formulation and applications'. *Earth and Planetary Science Letters* **170**, 131–140.

Gasco, I., M. Gattiglio, and A. Borghi: 2013, 'Review of metamorphic and kinematic data from Internal Crystalline Massifs (Western Alps): PTt paths and exhumation history'. *Journal of Geodynamics* **63**, 1–19.

Gebauer, D.: 1996, *A P-T-t path for a (ultra?-) high-pressure ultramafic/mafic rock association and their felsic country-rocks based on SHRIMP-dating of magmatic and metamorphic zircon domains. Example: Alpe Arami (Central Swiss Alps)*, pp. 307–329. In: Basu, A. and Hart, S. (Eds.): Earth Processes: Reading the Isotopic Code. Geophysical Monograph Series, 95.

Gebauer, D.: 1999, 'Alpine geochronology of the Central and Western Alps: new constraints for a complex geodynamic evolution'. *Schweizerische Mineralogische und Petrographische Mitteilungen* **79**, 191–208.

Gebauer, D., M. Grünenfelder, G. R. Tilton, V. Trommsdorff, and S. Schmid: 1992a, 'The geodynamic evolution of garnet-peridotites, garnet-pyroxenites and eclogites of Alpe Arami and Cima di Gagnone (Central Alps) from Early Proterozoic to Oligocene'. *Schweizerische mineralogische und petrographische Mitteilungen* **72**, 107–111.

Gebauer, D., H. P. Schertl, B. M., and W. Schreyer: 1997, '35 Ma old ultrahigh-pressure metamorphism and evidence for very rapid exhumation in the Dora Maira Massif, Western Alps'. *Lithos* **41**, 5–24.

Gebauer, D., R. Schmid, A. Quadt, and P. Ulmer: 1992b, 'Oligocene, pyroxene-rich metadiorites of different ages from the Ivrea Zone and their geodynamic significance'. *Schweizerische Mineralogische und Petrographische Mitteilungen* **72**, 113–122.

Gerya, T. and B. Stöckhert: 2006, 'Two-dimensional numerical modeling of tectonic and metamorphic histories at active continental margins'. *International Journal of Earth Sciences* **95**, 250–274.

Gerya, T. V., L. L. Perchuk, and J.-P. Burg: 2008, 'Transient hot channels: Perpetrating and regurgitating ultrahigh-pressure, high-temperature crust-mantle associations in collision belts'. *Lithos* **103**, 236–256.

Gerya, T. V., B. Stöckhert, and A. L. Perchuk: 2002, 'Exhumation of high-pressure metamorphic rocks in a subduction channel: A numerical simulation'. *Tectonics* **21**, TC1056.

Giorgis, D., P. Thélin, G. Stampfli, and F. Bussy: 1999, 'The Mont-Mort metapelites: Variscan metamorphism and geodynamic context (Briançonnais basement, western Alps, Switzerland)'. *Schweizerische mineralogische und petrographische Mitteilungen* **79**, 381–398.

Goffé, B.: 1977, 'Succession de subfacies métamorphiques en Vanoise méridionale (Savoie)'. *Contributions to Mineralogy and Petrology* **62**, 23–41.

Guidotti, C. V. and F. P. Sassi: 1998, 'Petrogenetic significance of Na-K white mica mineralogy; recent advances for metamorphic rocks'. *European Journal of Mineralogy* **10**(5), 815–854.

Hacker, B. R., T. B. Andersen, S. Johnston, A. R. C. Kylander-Clark, E. M. Peterman, E. O. Walsh, and D. Young: 2010, 'High-temperature deformation during continental-margin subduction & exhumation: The ultrahigh-pressure Western Gneiss Region of Norway'. *Tectonophysics* **480**, 149–171.

Hacker, B. R. and T. V. Gerya: 2013, 'Paradigms, new and old, for ultrahigh-pressure tectonism'. *Tectonophysics* **603**, 79–88.

Hacker, B. R., P. B. Kelemen, and M. D. Behn: 2011, 'Differentiation of the continental crust by relamination'. *Earth and Planetary Science Letters* **307**, 501–516.

Hacker, B. R., L. Ratschbacher, L. Webb, M. O. McWilliams, T. Ireland, A. Calvert, S. Dong, H.-R. Wenk, and D. Chateigner: 2000, 'Exhumation of ultrahigh-pressure continental crust in east central China: Late Triassic-Early Jurassic tectonic unroofing'. *Journal of Geophysical Research* **105**, 13339–13364.

Hacker, B. R., T. Sharp, R. Y. Zhang, J. G. Liou, and R. L. Hervig: 1997, 'Determining the Origin of Ultrahigh-Pressure Lherzolites'. *Science* **278**, 702–707.

Handy, M. R., S. M. Schmid, R. Bousquet, E. Kissling, and D. Bernoulli: 2010, 'Reconciling plate-tectonic reconstructions of Alpine Tethys with the geological-geophysical record of spreading and subduction in the Alps'. *Earth-Science Reviews* **102**, 121–158.

Harley, S. L. and N. M. Kelly: 2007, 'Zircon Tiny but Timely'. *Elements* **3**, 13–18.

Harley, S. L., N. M. Kelly, and A. Möller: 2007, 'Zircon Behaviour and the Thermal Histories of Mountain Chains'. *Elements* **3**, 25–30.

Heinrich, C. A.: 1982, 'Kyanite-Eclogite to Amphibolite Facies Evolution of Hydrous Mafic and Pelitic Rocks, Adula Nappe, Central Alps'. *Contributions to Mineralogy and Petrology* **81**, 30–38.

Heinrich, C. A.: 1986, 'Eclogite Facies Regional Metamorphism of Hydrous Mafic Rocks in the Central Alpine Adula Nappe'. *Journal of Petrology* **27**, 123–154.

Hermann, J. and D. H. Green: 2001, 'Experimental constraints on high pressure melting in subducted crust'. *Earth and Planetary Science Letters* **188**, 149–168.

Hermann, J., D. Rubatto, A. Korsakov, and V. S. Shatsky: 2001, 'Multiple zircon growth during fast exhumation of diamondiferous, deeply subducted continental crust (Kokchetav Massif, Kazakhstan)'. *Contributions to Mineralogy and Petrology* **141**, 66–82.

Hermann, J., D. Rubatto, and V. Trommsdorff: 2006, 'Sub-solidus Oligocene zircon formation in garnet peridotite during fast decompression and fluid infiltration (Duria, Central Alps)'. *Mineralogy and Petrology* **88**, 181–206.

Herwartz, D., C. Münker, E. E. Scherer, T. J. Nagel, J. Pleuger, and N. Froitzheim: 2008, 'Lu-Hf garnet geochronology of eclogites from the Balma Unit (Pennine Alps): implications for Alpine paleotectonic reconstruction'. *Swiss Journal of Geosciences* **101**, 173–189.

Herwartz, D., T. J. Nagel, C. Münker, E. E. Scherer, and N. Froitzheim: 2011, 'Tracing two orogenic cycles in one eclogite sample by Lu-Hf garnet chronometry'. *Nature Geoscience* **4**, 178–183.

Hinterlechner-Ravnik, A.: 1987, 'Garnet peridotite from the Pohorje Mountains'. *Geologija* **30**, 149–181.

Hinterlechner-Ravnik, A., F. P. Sassi, and D. Visona: 1991, 'The Austridic eclogites, metabasites and metaultrabasites from the Pohorje area (Eastern Alps, Yugoslavia): 2. The metabasites and metaultrabasites, and concluding considerations'. *Rendiconti Fisiche Accademia Lincei* **2**, 175–190.

Hoinkes, G., F. Koller, G. Rantisch, E. Dachs, V. Höck, F. Neubauer, and R. Schuster: 1999, 'Alpine metamorphism of the Eastern Alps'. *Schweizerische Mineralogische und Petrographische Mitteilungen* **79**, 155–181.

Holland, T. J. B. and R. Powell: 1998, 'An internally consistent thermodynamic data set for phases of petrological interest'. *Journal of Metamorphic Geology* **16**, 309–343.

Hollister, L. S.: 1966, 'Garnet zoning: an interpretation based on the Rayleigh fractionation model'. *Science* **154**, 1647–1651.

Hunziker, J. C., J. Desmos, and A. J. Hurford: 1992, 'Thirty two years of geochronological work in the Central and Western Alps: a review on seven maps'. *Mémoires de Géologie (Lausanne)* **13**, 1–59.

Husson, L., J.-P. Brun, P. Yamato, and C. Faccenna: 2009, 'Episodic slab rollback fosters exhumation of HP-UHP rocks'. *Geophysical Journal International* **179**, 1292–1300.

Inger, S. and R. A. Cliff: 1994, 'Timing of metamorphism in the Tauern Window, eastern Alps: Rb-Sr ages and fabric formation'. *Journal of Metamorphic Geology* **12**, 695–707.

Irouschek, A.: 1985, 'Anzeichen einer alpinen Hochdruckmetamorphose in Metapeliten der Simano-Decke'. *Schweizerische mineralogische und petrographische Mitteilungen* **65**, 118–119.

Jäger, E.: 1973, 'Die alpine Orogenese im Lichte der radiometrischen Altersbestimmung'. *Eclogae Geologicae Helvetiae* **66**, 11–21.

Jäger, E.: 1979, *The Rb-Sr method*, pp. 13–26. In: Jäger E. and Hunziger J. C. (Eds.): Lectures in isotope geology. Springer, Berlin Heidelberg New York.

Jäger, E., E. Niggli, and E. Wenk: 1967, 'Rb-Sr Altersbestimmung an Glimmern der Zentralalpen'. *Beiträge zur geologischen Karte der Schweiz* **134**.

Jahn, B.-M. and J. G. Liou: 1977, 'Age and geochemical constraints of glaucophane schists of Taiwan'. *Memoir of the Geological Society of China* **2**, 129–140.

Jahn, B.-M., J. G. Liou, and H. Nagasawa: 1981, 'High-pressure metamorphic rocks of Taiwan: REE geochemistry, Rb-Sr ages and tectonic implications'. *Memoir of the Geological Society of China* **4**, 497–520.

Janák, M., D. Cornell, N. Froitzheim, J. C. M. De Hoog, I. Broska, M. Vrabec, and V. Hurai: 2009, 'Eclogite-hosting metapelites from the Pohorje Mountains (Eastern Alps): P-T evolution, zircon geochronology and tectonic implications'. *European Journal of Mineralogy* **21**, 1191–1212.

Janák, M., N. Froitzheim, B. Lupták, M. Vrabec, and E. J. Krogh Ravna: 2004, 'First evidence for ultrahigh-pressure metamorphism of eclogites in Pohorje, Slovenia: Tracing deep continental subduction in the Eastern Alps'. *Tectonics* **23**, TC5014.

Janák, M., N. Froitzheim, M. Vrabec, E. J. Krogh Ravna, and J. C. M. De Hoog: 2006, 'Ultrahigh-pressure metamorphism and exhumation of garnet peridotite in Pohorje, Eastern Alps'. *Journal of Metamorphic Geology* **24**, 19–31.

Jochum, K. P., U. Weis, B. Stoll, D. Kuzmin, Q. Yang, I. Raczek, D. E. Jacob, A. Stracke, K. Birbaum, D. A. Frick, D. Günther, and J. Enzweiler: 2011, 'Determination of Reference Values for NIST SRM 610–617 Glasses Following ISO Guidelines'. *Geostandards and Geoanalytical Research* **35**, 397–429.

Jolivet, L., C. Faccenna, B. Goffé, E. Burov, and P. Agard: 2003, 'Subduction tectonics and exhumation of high-pressure metamorphic rocks in the Mediterranean orogens'. *American Journal of Science* **303**, 353–409.

Jolivet, L., H. Raimbourg, L. Labrousse, D. Avigad, Y. Leroy, H. Austrheim, and T. B. Andersen: 2005, 'Softening trigerred by eclogitization, the first step toward exhumation during continental subduction'. *Earth and Planetary Science Letters* **237**, 532–547.

Juang, W.-S. and H. Bellon: 1986, 'Potassium-Argon ages of the Tananao Schist in Taiwan'. *Memoir of the Geological Society of China* **7**, 405–416.

Katayama, I., S. Maruyama, C. D. Parkinson, K. Terada, and Y. Sano: 2001, 'Ion micro-probe U-Pb zircon geochronology of peak and retrograde stages of ultrahigh-pressure metamorphic rocks from the Kokchetav massif, northern Kazakhstan'. *Earth and Planetary Science Letters* **188**, 185–198.

Kearey, P., K. A. Klepeis, and F. J. Vine: 2009, *Global Tectonics*. Wiley-Blackwell.

Kelly, E. D., W. D. Carlson, and J. N. Connelly: 2011, 'Implications of garnet resorption for the Lu-Hf garnet geochronometer: an example from the contact aureole of the Makhavinekh Lake Pluton, Labrador'. *Journal of Metamorphic Geology* **29**, 901–916.

Kienast, J. R.: 1983, 'Le métamorphisme de haute pression et basse température (éclogites et schistes bleus): données nouvelles sur la pétrologie des roches de la croute océanique subductée et des sédiments associés'. Ph.D. thesis, Université Paris VI.

Kirchenbaur, M., J. Pleuger, S. Jahn-Awe, T. J. Nagel, N. Froitzheim, R. O. C. Fonseca, and C. Münker: 2012, 'Timing of high-pressure metamorphic events in the Bulgarian Rhodopes from Lu-Hf garnet geochronology'. *Contributions to Mineralogy and Petrology* **163**, 897–921.

Kirst, F., S. Sandmann, T. J. Nagel, N. Froitzheim, and M. Janák: 2010, 'Tectonic evolution of the southeastern part of the Pohorje Mountains (Eastern Alps, Slovenia)'. *Geologica Carpathica* **61**, 451–461.

Kligfield, R., J. Hunziker, R. D. Dallmeyer, and S. Schamel: 1986, 'Dating of deformation phases using K-Ar and $^{40}Ar/^{39}Ar$ techniques: results from the northern apennines'. *Journal of Structural Geology* **8**, 781–798.

Kohn, M. J.: 2009, 'Models of garnet differential geochronology'. *Geochimica et Cosmochemica Acta* **73**, 170–182.

Konrad-Schmolke, M., M. R. Handy, J. Babist, and P. J. O'Brien: 2005, 'Thermodynamic modelling of diffusion-controlled garnet growth'. *Contributions to Mineralogy and Petrology* **149**, 181–195.

Konrad-Schmolke, M., P. J. O'Brien, C. De Capitani, and D. A. Carswell: 2008a, 'Garnet growth at high- and ultra-high pressure conditions and the effect of element fractionation on mineral modes and composition'. *Lithos* **103**, 309–332.

Konrad-Schmolke, M., T. Zack, P. J. O'Brien, and D. E. Jacob: 2008b, 'Combined thermodynamic and rare earth element modelling of garnet growth during subduction: Examples from ultrahigh-pressure eclogite of the Western Gneiss Region, Norway'. *Earth and Planetary Science Letters* **272**, 488–498.

Krebs, M., H.-P. Schertl, W. V. Maresch, and G. Draper: 2011, 'Mass flow in serpentinite-hosted subduction channels: P-T-t path patterns of metamorphic blocks in the Rio San Juan mélange (Dominican Republic)'. *Journal of Asian Earth Sciences* **42**, 569–595.

Kurz, W. and H. Fritz: 2003, 'Tectonometamorphic evolution of the Austroalpine nappe complex in the central Eastern Alps - consequences for the Eo-Alpine evolution of the Eastern Alps'. *International Geology Review* **45**, 1100–1127.

Kylander-Clark, A. R. C., B. R. Hacker, C. M. Johnson, B. L. Beard, and N. J. Mahlen: 2009, 'Slow subduction of a thick ultrahigh-pressure terrane'. *Tectonics* **28**, TC2003.

Kylander-Clark, A. R. C., B. R. Hacker, C. M. Johnson, B. L. Beard, N. J. Mahlen, and T. J. Lapen: 2007, 'Coupled Lu-Hf and Sm-Nd geochronology constrains prograde and exhumation histories of high- and ultrahigh-pressure eclogites from western Norway'. *Chemical Geology* **242**, 137–154.

Kylander-Clark, A. R. C., B. R. Hacker, and C. G. Mattinson: 2012, 'Size and exhumation rate of ultrahigh-pressure terranes linked to orogenic stage'. *Earth and Planetary Science Letters* **321-322**, 115–120.

Lagos, M., E. E. Scherer, F. Tomaschek, C. Münker, M. Keiter, J. Berndt, and C. Ballhaus: 2007, 'High precision Lu-Hf geochronology of Eocene eclogite-facies rocks from Syros, Cyclades, Greece'. *Chemical Geology* **243**, 16–35.

Lapen, T. J., C. M. Johnson, L. P. Baumgartner, G. V. Dal Piaz, S. Skora, and B. L. Beard: 2007, 'Coupling of oceanic and continental crust during Eocene eclogite-facies metamorphism: evidence from the Monte Rosa nappe, western Alps'. *Contributions to Mineralogy and Petrology* **153**, 139–157.

Lapen, T. J., C. M. Johnson, L. P. Baumgartner, N. J. Mahlen, B. L. Beard, and J. M. Amato: 2003, 'Burial rates during prograde metamorphism of an ultra-high-pressure terrane: an example from Lago di Cignana, western Alps, Italy'. *Earth and Planetary Science Letters* **215**, 57–72.

Lardeaux, J. M. and M. I. Spalla: 1991, 'From granulites to eclogites in the Sesia zone (Italian Western Alps): a record of the opening and closure of the Piedmont ocean'. *Journal of Metamorphic Geology* **9**, 35–59.

Laubscher, H.: 1988, 'Material balance in Alpine orogeny'. *Geological Society of America Bulletin* **100**, 1313–1328.

Laubscher, H.: 1991, 'The arc of the Western Alps today'. *Eclogae Geologicae Helvetiae* **84**, 631–659.

Li, S., E. Jagoutz, Y. Chen, and Q. Li: 2000, 'Sm-Nd and Rb-Sr isotopic chronology and cooling history of ultrahigh pressure metamorphic rocks and their country rocks at Shuanghe in the Dabie Mountains, Central China'. *Geochimica et Cosmochimica Acta* **64**, 1077–1093.

Li, S., S. Wang, Y. Chen, D. Liu, J. Qiu, Z. H., and Z. Zhang: 1994, 'Excess argon in phengite from eclogite: Evidence from dating of eclogite minerals by Sm-Nd, Rb-Sr and $^{40}Ar/^{39}Ar$ methods'. *Chemical Geology* **112**, 343–350.

Li, Z. and T. V. Gerya: 2009, 'Polyphase formation and exhumation of high- to ultrahigh-pressure rocks in continental subduction zone: Numerical modeling and application to the Sulu ultrahigh-pressure terrane in eastern China'. *Journal of Geophysical Research: Solid Earth* **114**, B9.

Liati, A. and N. Froitzheim: 2006, 'Assessing the Valais ocean, Western Alps: U-Pb SHRIMP zircon geochronology of eclogite in the Balma unit, on top of the Monte Rosa nappe'. *European Journal of Mineralogy* **18**, 299–308.

Liati, A., N. Froitzheim, and C. M. Fanning: 2005, 'Jurassic ophiolites within the Valais domain of the Western and Central Alps: geochronological evidence for re-rifting of oceanic crust'. *Contributions to Mineralogy and Petrology* **149**, 446–461.

Liati, A., D. Gebauer, and C. M. Fanning: 2003, 'The youngest basic oceanic magmatism in the Alps (Late Cretaceous; Chiavenna unit, Central Alps): geochronological constraints and geodynamic significance'. *Contributions to Mineralogy and Petrology* **146**, 144–158.

Liati, A., D. Gebauer, and C. M. Fanning: 2009, 'Geochronological evolution of HP metamorphic rocks of the Adula nappe, Central Alps, in pre-Alpine and Alpine subduction cycles'. *Journal of the Geological Society* **166**, 797–810.

Lin, A. T., A. B. Watts, and S. P. Hesselbo: 2003, 'Cenozoic stratigraphy and subsidence history of the South China Sea margin in the Taiwan region'. *Basin Research* **15**, 453–478.

Liou, J. G. and W. G. Ernst: 1984, 'Summary of Phanerozoic metamorphism in Taiwan'. *Memoir of the Geological Society of China* **6**, 133–152.

Lister, G. S., M. A. Forster, and T. J. Rawling: 2001, *Episodicity during orogenesis*, pp. 89–113. In: Miller et al. (Eds.): Continental Reactivation and Reworking. Geological Society, London, Special Publications.

Lo, C.-H. and T.-F. Yui: 1996, '$^{40}Ar/^{39}Ar$ dating of high-pressure rocks in the Tananao basement complex, Taiwan'. *Journal of the Geological Society of China* **39**, 13–30.

Longerich, H. P., S. E. Jackson, and D. Günther: 1996, 'Laser ablation inductively coupled plasma mass spectrometric transient signal data acquisition and analyte concentration calculation'. *Journal of Analytical Atomic Spectrometry* **11**, 899–904.

Louden, K. E. and D. Chian: 1999, 'The deep structure of non-volcanic rifted continental margins'. *Philosophical Transactions of the Royal Society of London* **A 357**, 767–805.

Löw, S.: 1987, 'Die tektono-metamorphe Entwicklung der Nördlichen Adula-Decke'. *Beiträge zur Geologischen Karte der Schweiz* **161**, 1–84.

Ludwig, K. R.: 2001, 'Isoplot/Ex version 2.49, Geochronological Toolkit for Microsoft Excel'. *Berkeley Geochronology Center Special Publication* **1a**.

Lundberg, N., D. L. Reed, C.-S. Liu, and J. J. Lieske: 1997, 'Forearc-basin closure and arc accretion in the submarine suture zone south of Taiwan'. *Tectonophysics* **274**, 5–23.

Majka, J., A. Rosén, M. Janák, N. Froitzheim, I. Klonowska, M. Manecki, V. Sasinková, and K. Yoshida: 2014, 'Microdiamond discovered in the Seve Nappe (Scandinavian Caledonides) and its exhumation by the "vacuum-cleaner" mechanism'. *Geology* **42**, 1107–1110.

Manatschal, G.: 2004, 'New models for evolution of magma-poor rifted margins based on a review of data and concepts from West Iberia and the Alps'. *International Journal of Earth Sciences* **93**, 432–466.

Markley, M. J., C. Teyssier, and M. Cosca: 2002, 'The relation between grain size and $^{40}Ar/^{39}Ar$ date for Alpine white mica from the Siviez-Mischabel Nappe, Switzerland'. *Journal of Structural Geology* **24**, 1937–1955.

Markley, M. J., C. Teyssier, M. A. Cosca, R. Caby, J. C. Hunziker, and M. Sartori: 1998, 'Alpine deformation and $^{40}Ar/^{39}Ar$ geochronology of synkinematic white mica in the Siviez- Mischabel Nappe, Western Pennine Alps, Switzerland'. *Tectonics* **17**, 407–425.

Marmo, B. A., G. L. Clarke, and R. Powell: 2002, 'Fractionation of bulk rock composition due to porphyroblast growth: effects on eclogite facies mineral equilibria, Pam Peninsula, New Caledonia'. *Journal of Metamorphic Geology* **20**, 151–165.

Marquer, D., N. Challandes, and U. Schaltegger: 1998, 'Early Permian magmatism in Briançonnais terranes: Truzzo granite and Roffna rhyolite (eastern Penninic nappes, Swiss and Italian Alps)'. *Schweizerische mineralogische und petrographische Mitteilungen* **78**, 397–414.

Massonne, H. J., A. P. Willner, and T. V. Gerya: 2007, 'Densities of metapelitic rocks at high to ultrahigh pressure conditions: what are the geodynamic consequences?'. *Earth and Planetary Science Letters* **256**, 12–27.

Maxelon, M. and N. S. Mancktelow: 2005, 'Three-dimensional geometry and tectonostratigraphy of the Pennine zone, Central Alps, Switzerland and Northern Italy'. *Earth-Science Reviews* **71**, 171–227.

McLennan, S. M. and S. R. Taylor: 1996, 'Heat Flow and the Chemical Composition of Continental Crust'. *The Journal of Geology* **104**, 369–377.

Meffan-Main, S., R. A. Cliff, A. C. Barnicoat, B. Lombardo, and R. Compagnoni: 2004, 'A Tertiary age for Alpine high-pressure metamorphism in the Gran Paradiso Massif, western Alps: a Rb-Sr microsampling study'. *Journal of Metamorphic Geology* **22**, 261–281.

Merrihue, C. and G. Turner: 1966, 'Potassium-argon dating by activation with fast neutrons'. *Journal of Geophysical Research* **71**, 2852–2857.

Meyre, C., C. De Capitani, and J. H. Partzsch: 1997, 'A ternary solid solution model for omphacite and its application to geothermobarometry of eclogites from the Middle Adula nappe (Central Alps, Switzerland)'. *Journal of Metamorphic Geology* **15**, 687–700.

Meyre, C., C. De Capitani, T. Zack, and M. Frey: 1999, 'Petrology of High-Pressure Metapelites from the Adula Nappe (Central Alps, Switzerland)'. *Journal of Petrology* **40**, 199–213.

Meyre, C., D. Marquer, S. M. Schmid, and L. Ciancaleoni: 1998, 'Syn-orogenic extension along the Forcola fault: Correlation of Alpine deformations in the Tambo and Adula nappes (Eastern Penninic Alps)'. *Eclogae Geologicae Helvetiae* **91**, 409–420.

Michard, A., B. Goffé, C. Chopin, and C. Henry: 1996, 'Did the Western Alps develop through an Oman-type stage? The geotectonic setting of high-pressure metamorphism in two contrasting Tethyan transects'. *Eclogae Geologicae Helvetiae* **89**, 43–80.

Miller, C., R. Mundil, M. Thöni, and J. Konzett: 2005, 'Refining the timing of eclogite metamorphism: a geochemical, petrological, Sm-Nd and U-Pb case study from the Pohorje Mountains, Slovenia (Eastern Alps)'. *Contributions to Mineralogy and Petrology* **150**, 70–84.

Missoni, S. and H.-J. Gawlick: 2011, 'Evidence for Jurassic subduction from the Northern Calcareous Alps (Berchtesgaden; Austroalpine, Germany)'. *International Journal of Earth Sciences* **100**, 1605–1631.

Monié, P. and C. Chopin: 1991, '$^{40}Ar/^{39}Ar$ dating in coesite-bearing and associated units of the Dora Maira massif, Western Alps'. *European Journal of Mineralogy* **3**, 239–262.

Müller, R. D., M. Sdrolias, C. Gaina, and W. R. Roest: 2008, 'Age, spreading rates, and spreading asymmetry of the world's ocean crust'. *Geochemistry Geophysics Geosystems* **9**, Q04006.

Münker, C., S. Weyer, E. Scherer, and K. Mezger: 2001, 'Separation of high field strength elements (Nb, Ta, Zr, Hf) and Lu from rock samples for MC-ICPMS measurements'. *Geochemistry Geophysics Geosystems* **2**, GC000183.

Nagel, T., C. De Capitani, and M. Frey: 2002a, 'Isograds and P-T evolution in the eastern Lepontine Alps (Graubünden, Switzerland)'. *Journal of Metamorphic Geology* **20**, 309–324.

Nagel, T., C. De Capitani, M. Frey, N. Froitzheim, H. Stünitz, and S. M. Schmid: 2002b, 'Structural and metamorphic evolution during rapid exhumation in the Lepontine dome (southern Simano and Adula nappes, Central Alps, Switzerland)'. *Eclogae Geologicae Helvetiae* **95**, 301–321.

Nagel, T. J.: 2008, 'Tertiary subduction, collision and exhumation recorded in the Adula nappe, central Alps'. *In: Siegesmund S, Fügenschuh B, Froitzheim N (Eds.): Tectonic Aspects of the Alpine-Dinaride-Carpathian System. Geological Society, London, Special Publications* **298**, 365–392.

Nagel, T. J., D. Herwartz, S. Rexroth, C. Münker, N. Froitzheim, and W. Kurz: 2013, 'Lu-Hf dating, petrography, and tectonic implications of the youngest Alpine eclogites (Tauern Window, Austria)'. *Lithos* **170-171**, 179–190.

Negro, F., R. Bousquet, F. Vils, C. M. Pellet, and J. Hänggi-Schaub: 2013, 'Thermal structure and metamorphic evolution of the Piemont-Ligurian metasediments in the northern Western Alps'. *Swiss Journal of Geosciences* **106**, 63–78.

Nicolaysen, L. O.: 1961, 'Graphic interpretation of discordant age measurements of metamorphic rocks'. *Annals of the New York Academy of Sciences* **91**, 198–206.

Niggli, E. and C. R. Niggli: 1965, 'Karten der Verbreitung einiger Mineralien der alpidischen Metamorphose in den Schweizer Alpen (Stilpnomelan, Alkali-Amphibol, Chloritoid, Staurolith, Disthen, Sillimanit)'. *Eclogae Geologicae Helvetiae* **58**, 335–368.

Nimis, P. and V. Trommsdorff: 2001, 'Revised Thermobarometry of Alpe Arami and other Garnet Peridotites from the Central Alps'. *Journal of Petrology* **42**, 103–115.

Oberhänsli, R., R. Bousquet, M. Engi, B. Goffé, G. Gosso, M. Handy, V. Höck, F. Koller, J. M. Lardeaux, R. Polino, P. Rossi, R. Schuster, S. Schwartz, and M. I. Spalla: 2004, *Metamorphic structure of the Alps*. Commission for the Geological Map of the World (CCGM-CGMW), UNESCO, Paris.

Ono, S.: 1998, 'Stability limits of hydrous minerals in sediment and mid-ocean ridge basalt compositions: Implications for water transport in subduction zones'. *Journal of Geophysical Research* **103**, 253–267.

Ortner, H.: 2003, 'Cretaceous thrusting in the western part of the Northern Calcareous Alps (Austria) - evidences from synorogenic sedimentation and structural data'. *Mitteilungen der Österreichischen Geologischen Gesellschaft* **94**, 63–77.

Ota, T. and Y. Kaneko: 2010, 'Blueschists, eclogites, and subduction zone tectonics: Insights from a review of Late Miocene blueschists and eclogites, and related young high-pressure metamorphic rocks'. *Gondwana Research* **18**, 167–188.

Paquette, J. L., C. Chopin, and J. J. Peucat: 1989, 'U-Pb zircon, Rb-Sr and Sm-Nd geochronology of high to very high pressure metaacidic rocks from the Western Alps'. *Contributions to Mineralogy and Petrology* **101**, 280–289.

Paquin, J. and R. Altherr: 2001, 'New Constraints on the P-T Evolution of the Alpe Arami Garnet Peridotite Body (Central Alps, Switzerland)'. *Journal of Petrology* **42**(6), 1119–1140.

Partzsch, J. H.: 1998, 'The tectono-metamorphic evolution of the middle Adula nappe'. Ph.D. thesis, Univ. Basel, Switzerland.

Peterman, E. M., B. R. Hacker, and E. F. Baxter: 2009, 'Phase transformations of continental crust during subduction and exhumation: Western Gneiss Region, Norway'. *European Journal of Mineralogy* **21**, 1097–1118.

Pleuger, J., R. Hundenborn, K. Kremer, S. Babinka, W. Kurz, E. Jansen, and N. Froitzheim: 2003, 'Structural evolution of Adula nappe, Misox zone, and Tambo nappe in the San Bernardino area: Constraints for the exhumation of the Adula eclogites'. *Mitteilungen der Österreichischen Geologischen Gesellschaft* **94**, 99–122.

Pleuger, J. and Y. Y. Podladchikov: 2014, 'A purely structural restoration of the NFP20-East cross section and potential tectonic overpressure in the Adula nappe'. *Tectonics* **10.1002/2013TC003409**.

Pleuger, J., S. Roller, J. M. Walter, E. Jansen, and N. Froitzheim: 2007, 'Structural evolution of the contact between two Penninic nappes (Zermatt-Saas zone and Combin zone, Western Alps) and implications for the exhumation mechanism and palaeogeography'. *International Journal of Earth Sciences* **96**, 229–252.

Qiu, Y. M., S. Gao, N. J. McNaughton, D. I. Groves, and W. Ling: 2000, 'First evidence of >3.2 Ga continental crust in the Yangtze craton of south China and its implications for Archean crustal evolution and Phanerozoic tectonics'. *Geology* **28**, 11–14.

Radulescu, I. G., D. Rubatto, C. Gregory, and R. Compagnoni: 2009, 'The age of HP metamorphism in the Gran Paradiso Massif, Western Alps: A petrological and geochronological study of 'silvery micaschists''. *Lithos* **110**, 95–108.

Raimbourg, H., L. Jolivet, and Y. Leroy: 2007, 'Consequences of progressive eclogitization on crustal exhumation, a mechanical study'. *Geophysical Journal International* **168**, 379–401.

Raith, M., P. Raase, H. Kreuzer, and P. Müller: 1978, *The age of the Alpidic metamorphism in the western Tauern Window, Austrian Alps, according to radiometric dating*, pp. 140–148. In: Cloos, H., Roeder, D. and Schmidt, K. (Eds.): Alps, Apennines, Hellenides. Schweizerbart, Stuttgart.

Ratschbacher, L., C. Dingeldey, C. Miller, B. R. Hacker, and M. O. McWilliams: 2004, 'Formation, subduction, and exhumation of Penninic oceanic crust in the Eastern Alps: time constraints from $^{40}Ar/^{39}Ar$ geochronology'. *Tectonophysics* **394**, 155–170.

Rebay, G., M. I. Spalla, and D. Zanoni: 2012, 'Interaction of deformation and metamorphism during subduction and exhumation of hydrated oceanic mantle: Insights from the Western Alps'. *Journal of Metamorphic Geology* **30**, 687–702.

Reddy, S. M., J. Wheeler, and R. A. Cliff: 1999, 'The geometry and timing of orogenic extension: an example from the Western Italian Alps'. *Journal of Metamorphic Geology* **17**, 573–589.

Reinecke, T.: 1991, 'Very-high-pressure metamorphism and uplift of coesite-bearing metasediments from the Zermatt-Saas zone, Western Alps'. *European Journal of Mineralogy* **3**, 7–17.

Risold, A.-C., V. Trommsdorff, and B. Grobéty: 2001, 'Genesis of ilmenite rods and palisades along humite-type defects in olivine from Alpe Arami'. *Contributions to Mineralogy and Petrology* **140**, 619–628.

Rosenbaum, G. and G. S. Lister: 2005, 'The Western Alps from the Jurassic to Oligocene: spatio-temporal constraints and evolutionary reconstructions'. *Earth-Science Reviews* **69**, 281–306.

Rosenbaum, G., G. S. Lister, and C. Duboz: 2002, 'Relative motions of Africa, Iberia and Europe during Alpine orogeny'. *Tectonophysics* **359**, 117–129.

Rosenberg, C. L., A. Berger, and S. M. Schmid: 1995, 'Observations from the floor of a granitoid pluton: Inferences on the driving force of final emplacement'. *Geology* **23**, 443–446.

Royden, L. H. and L. Husson: 2006, 'Trench motion, slab geometry and viscous stresses in subduction systems'. *Geophysical Journal International* **167**, 881–905.

Royden, L. H. and L. Husson: 2009, 'Subduction with Variations in Slab Buoyancy: Models and Application to the Banda and Apennine Systems'. *Subduction Zone Geodynamics, Frontiers in Earth Sciences* pp. 35–45.

Rubatto, D.: 2002, 'Zircon trace element geochemistry: partitioning with garnet and the link between U-Pb ages and metanorphism'. *Chemical Geology* **184**, 123–138.

Rubatto, D. and D. Gebauer: 1999, 'Eo/Oligocene (35 Ma) high-pressure metamorphism in the Gornergrat Zone (Monte Rosa, Western Alps): implications for paleogeography'. *Schweizerische Mineralogische und Petrographische Mitteilungen* **79**, 353–362.

Rubatto, D., D. Gebauer, and R. Compagnoni: 1999, 'Dating of eclogite-facies zircons: the age of Alpine metamorphism in the Sesia-Lanzo Zone (Western Alps)'. *Earth and Planetary Science Letters* **167**, 141–158.

Rubatto, D., D. Gebauer, and M. Fanning: 1998, 'The youngest basic oceanic magmatism in the Alps (Late Cretaceous; Chiavenna unit, Central Alps): geochronological constraints and geodynamic significance'. *Contributions to Mineralogy and Petrology* **132**, 269–287.

Rubatto, D. and J. Hermann: 2001, 'Exhumation as fast as subduction?'. *Geology* **29**, 3–6.

Rubatto, D. and J. Hermann: 2003, 'Zircon formation during fluid circulation in eclogites (Monviso, Western Alps): Implications for Zr and Hf budget in subduction zones'. *Geochimica et Cosmochimica Acta* **67**, 2173–2187.

Rubatto, D. and J. Hermann: 2007, 'Zircon behaviour in deeply subducted rocks'. *Elements* **3**, 31–35.

Rubatto, D., D. Regis, J. Hermann, K. Boston, M. Engi, M. Beltrando, and S. R. B. McAlpine: 2011, 'Yo-yo subduction recorded by accessory minerals in the Italian Western Alps'. *Nature Geoscience* **4**, 338–342.

Rubatto, D., I. S. Williams, and I. S. Buick: 2001, 'Zircon and monazite response to prograde metamorphism in the Reynolds Range, central Australia'. *Contributions to Mineralogy and Petrology* **140**, 458–468.

Ruffet, G., G. Féraud, M. Balèvre, and J.-R. Kiénast: 1995, 'Plateau ages and excess argon in phengites: an $^{40}Ar/^{39}Ar$ laser probe study of Alpine micas (Sesia Zone, Western Alps, northern Italy)'. *Chemical Geology* **121**, 327–343.

Ruffet, G., G. Gruau, M. Ballevre, G. Feraud, and P. P.: 1997, 'Rb-Sr and ^{40}Ar-^{39}Ar laser probe dating of high-pressure phengites from the Sesia zone (Western Alps): underscoring of excess argon and new age constraints on the high-pressure metamorphism'. *Chemical Geology* **141**, 1–18.

Rumble, D.: 1998, *Stable isotope geochemistry of ultrahigh-pressure rocks*, pp. 241–259. In: Hacker, B. R. and Liou, J. G. (Eds.): When Continents Collide: Geodynamics and Geochemistry of Ultrahigh-Pressure Rocks. Kluwer.

Rütti, R., M. Maxelon, and N. S. Mancktelow: 2005, 'Structure and kinematics of the northern Simano Nappe, Central Alps, Switzerland'. *Eclogae Geologicae Helvetiae* **98**, 63–81.

Sachsenhofer, R. F., I. Dunkl, C. Hasenhüttl, and B. Jelen: 1998, 'Miocene thermal history of the southwestern margin of the Styrian Basin: vitrinite reflectance and fission-track data from the Pohorje/Kozjak area (Slovenia)'. *Tectonophysics* **297**, 17–29.

Sassi, R., C. Mazzoli, C. Miller, and J. Konzett: 2004, 'Geochemistry and metamorphic evolution of the Pohorje Mountain eclogites from the easternmost Austroalpine basement of the Eastern Alps (Northern Slovenia)'. *Lithos* **78**, 235–261.

Scaillet, S.: 1996, 'Excess ^{40}Ar transport scale and mechanism in high-pressure phengites: A case study from an eclogitized metabasite of the Dora-Maira nappe, western Alps'. *Geochimica et Cosmochimica Acta* **60**, 1075–1090.

Scherer, E. E., K. L. Cameron, and J. Blichert-Toft: 2000, 'Lu-Hf garnet geochronology: Closure temperature relative to the Sm-Nd system and the effects of trace mineral inclusions'. *Geochimica et Cosmochimica Acta* **64**, 3413–3432.

Scherer, E. E., C. Münker, and K. Mezger: 2001, 'Calibrating the Lu-Hf clock'. *Science* **293**, 683–686.

Schettino, A. and E. Turco: 2011, 'Tectonic history of the western Tethys since the Late Triassic'. *Geological Society of America Bulletin* **123**, 89–105.

Schmädicke, E., K. Mezger, M. A. Cosca, and M. Okrusch: 1995, 'Variscan Sm-Nd and Ar-Ar ages of eclogite facies rocks from the Erzgebirge, Bohemian Massif'. *Journal of Metamorphic Geology* **13**, 537–552.

Schmid, S. M., B. Fügenschuh, E. Kissling, and R. Schuster: 2004, 'Tectonic map and overall architecture of the Alpine orogen'. *Eclogae Geologicae Helvetiae* **97**, 93–117.

Schmid, S. M. and E. Kissling: 2000, 'The arc of the western Alps in the light of geophysical data on deep crustal structure'. *Tectonics* **19**, 62–85.

Schmid, S. M., O. A. Pfiffner, N. Froitzheim, G. Schönborn, and E. Kissling: 1996, 'Geophysical-geological transect and tectonic evolution of the Swiss-Italian Alps'. *Tectonics* **15**, 1036–1064.

Schmid, S. M., A. Zingg, and M. Handy: 1987, 'The kinematics of movements along the Insubric Line and the emplacement of the Ivrea Zone'. *Tectonophysics* **135**, 47–66.

Schmidt, A., K. Mezger, and P. J. O'Brien: 2011, 'The time of eclogite formation in the ultrahigh pressure rocks of the Sulu terrane Constraints from Lu-Hf garnet geochronology'. *Lithos* **125**, 743–756.

Schuster, R. and K. Stüwe: 2008, 'Permian metamorphic event in the Alps'. *Geology* **36**, 603–606.

Sherlock, S., S. Kelley, S. Inger, N. Harris, and A. Okay: 1999, '^{40}Ar-^{39}Ar and Rb-Sr geochronology of high-pressure metamorphism and exhumation history of the Tavsanli Zone, NW Turkey'. *Contributions to Mineralogy and Petrology* **137**, 46–58.

Shu, Q., G. P. Brey, A. Gerdes, and H. Hoefer: 2014, 'Mantle eclogites and garnet pyroxenites - the meaning of two-point isochrons, Sm-Nd and Lu-Hf closure temperatures and the cooling of the subcratonic mantle'. *Earth and Planetary Science Letters* **389**, 143–154.

Shu, Q., G. P. Brey, A. Gerdes, H. E. Höfer, and H. M. Seitz: 2012, 'Eclogites and garnet pyroxenites from the mantle: their age and ageing- two point isochrons, Sm-Nd and Lu-Hf closure temperatures, model ages'. In: *European Mineralogical Conference: Vol. 1*.

Shyu, J. B. H., Y.-M. Wu, C.-H. Chang, and H.-H. Huang: 2011, 'Tectonic erosion and the removal of forearc lithosphere during arc-continent collision: Evidence from recent earthquake sequences and tomography results in eastern Taiwan'. *Journal of Asian Earth Sciences* **42**, 415–422.

Skora, S., L. P. Baumgartner, N. J. Mahlen, C. M. Johnson, S. Pilet, and E. Hellebrand: 2006, 'Diffusion-limited REE uptake by eclogite garnets and its consequences for Lu-Hf and Sm-Nd geochronology'. *Contributions to Mineralogy and Petrology* **152**, 703–720.

Skora, S., L. P. Baumgartner, N. J. Mahlen, C. M. Lapen, T. J.and Johnson, and F. Bussy: 2008, 'Estimation of a maximum Lu diffusion rate in natural eclogite garnet'. *Swiss Journal of Geosciences* **101**, 637–650.

Skora, S., T. J. Lapen, L. P. Baumgartner, C. M. Johnson, E. Hellebrand, and N. J. Mahlen: 2009, 'The duration of prograde garnet crystallization in the UHP eclogites at Lago di Cignana, Italy'. *Earth and Planetary Science Letters* **287**, 402–411.

Smit, M. A., E. E. Scherer, and K. Mezger: 2013, 'Lu-Hf and Sm-Nd garnet geochronology: Chronometric closure and implications for dating petrological processes'. *Earth and Planetary Science Letters* **381**, 222–233.

Söderlund, U., P. J. Patchett, J. D. Vervoort, and C. E. Isachsen: 2004, 'The ^{176}Lu decay constant determined by Lu-Hf and U-Pb isotope systematics of Precambrian mafic intrusions'. *Earth and Planetary Science Letters* **219**, 311–324.

Spandler, C., G. Yaxley, D. H. Green, and D. Scott: 2010, 'Experimental phase and melting relations of metapelite in the upper mantle: implications for the petrogenesis of intraplate magmas'. *Contributions to Mineralogy and Petrology* **160**, 569–589.

Spear, F. S. and C. G. Daniel: 2001, 'Diffusion control of garnet growth, Harpswell Neck, Maine, USA'. *Journal of Metamorphic Geology* **19**, 179–195.

Spear, F. S., J. Selverstone, D. Hickmott, P. Crowley, and K. V. Hodges: 1984, 'P-T paths from garnet zoning: A new technique for deciphering tectonic processes in crystalline terranes'. *Geology* **12**, 87–90.

Spicher, A.: 1980, *Tektonische Karte der Schweiz*. Schweizerische Geologische Komission.

Stampfli, G. M.: 1993, 'Le Briançonnais, terrain exotique dans le Alpes?'. *Eclogae Geologicae Helvetiae* **86**, 1–45.

Stampfli, G. M., G. D. Borel, R. Marchant, and J. Mosar: 2002, *Western Alps geological constraints on western Tethyan reconstructions*, pp. 75–104. In: Rosenbaum, G. and Lister, G. S. (Eds.): Reconstruction of the evolution of the Alpine-Himalayan Orogen. Journal of the Virtual Explorer, 7.

Stampfli, G. M., J. Mosar, D. Marquer, R. Marchant, T. Baudin, and G. Borel: 1998, 'Subduction and obduction processes in the western Alps'. *Tectonophysics* **296**, 159–204.

Staub, R.: 1938, 'Einige Ergebnisse vergleichender Studien zwischen Wallis und Bünden'. *Eclogae Geologicae Helvetiae* **31**, 345–353.

Steinmann, M.: 1994, 'Ein Beckenmodell für das Nordpenninikum der Ostschweiz'. *Jahrbuch der Geologischen Bundesanstalt* **137**, 675–721.

Stern, R. J.: 2002, 'Subduction Zones'. *Reviews of Geophysics* **40**, 3–1–3–38.

Stucki, A., D. Rubatto, and V. Trommsdorff: 2003, 'Mesozoic ophiolite relics in the Southern Steep Belt of the Central Alps'. *Schweizerische mineralogische und petrographische Mitteilungen* **83**, 285–299.

Stüwe, K. and R. Schuster: 2010, 'Initiation of subduction in the Alps: Continent or ocean?'. *Geology* **38**, 175–178.

Suppe, J.: 1984, 'Kinematics of arc-continent collision, flipping of subduction, and back-arc spreading near Taiwan'. *Memoir of the Geological Society of China* **6**, 21–33.

Tenczer, V. and K. Stüwe: 2003, 'The metamorphic field gradient in the eclogite type locality, Koralpe region, Eastern Alps'. *Journal of Metamorphic Geology* **21**, 377–393.

Thöni, M.: 2002, 'Sm-Nd isotope systematics in garnet from different lithologies (Eastern Alps): age results, and an evaluation of potential problems for garnet Sm-Nd chronometry'. *Chemical Geology* **185**, 255–281.

Thöni, M.: 2006, 'Dating eclogite-facies metamorphism in the Eastern Alps - approaches, results, interpretations: a review'. *Mineralogy and Petrology* **88**, 123–148.

Thöni, M., C. Miller, J. Blichert-Toft, M. J. Whitehouse, J. Konzett, and A. Zanetti: 2008, 'Timing of high-pressure metamorphism and exhumation of the eclogite type-locality (Kupplerbrunn-Prickler Halt, Saualpe, south-eastern Austria): constrains from correlations of the Sm-Nd, Lu-Hf, U-Pb and Rb-Sr isotopic systems'. *Journal of Metamorphic Geology* **26**, 561–581.

Tilton, G. R., W. Schreyer, and H.-P. Schertl: 1991, 'Pb- Sr- Nd isotopic behavior of deeply subducted crustal rocks from the Dora Maira Massif, Western Alps, Italy-ll: what is the age of the ultrahigh-pressure metamorphism?'. *Contributions to Mineralogy and Petrology* **108**, 22–33.

Todd, C. S. and M. Engi: 1997, 'Metamorphic field gradients in the Central Alps'. *Journal of Metamorphic Geology* **15**, 513–530.

Todt, W. A., U. Altenberger, and J. F. Von Raumer: 1995, 'U-Pb data on zircons for the thermal peak of metamorphism in the Variscan Odenwald, Germany'. *Geologische Rundschau* **84**, 466–472.

Toth, T. M., V. Grandjean, and M. Engi: 2000, 'Polyphase evolution and reaction sequence of compositional domains in metabasalt: a model based on local chemical equilibrium and metamorphic differentiation'. *Geological Journal* **35**, 163–183.

Trajanova, M., Z. Pécskay, and T. Itaya: 2008, 'K-Ar geochronology and petrography of the Miocene Pohorje Mountains batholith (Slovenia)'. *Geologica Carpathica* **59**, 247–260.

Treloar, P. J., D. C. Rex, P. G. Guise, M. P. Coward, M. P. Searle, B. F. Windley, M. G. Petterson, M. Q. Jan, and I. W. Luff: 1989, 'K-Ar and Ar-Ar geochronology of the Himalayan collision in NW Pakistan: Constraints on the timing of suturing, deformation, metamorphism and uplift'. *Tectonics* **8**, 881–909.

Trommsdorff, V.: 1990, 'Metamorphism and tectonics in the Central Alps: The Alpine lithospheric mélange of Cima Lunga and Adula'. *Memorie della Società Geologica Italiana* **45**, 39–49.

Trümpy, R.: 1973, *The timing of orogenic events in the Central Alps*, pp. 229–251. In: DeJong, K. A. and Scholten,R. (Eds.): Gravity and Tectonics. Wiley, London.

Trümpy, R.: 1975, 'Penninic-Austroalpine boundary in the Swiss Alps: A presumed former continental margin and its problems'. *American Journal of Science* **275-A**, 209–238.

Trümpy, R.: 1980, *Geology of Switzerland. A guide book. Part A: An outline of the Geology of Switzerland*. Wepf & Co. Publishers, Basel, New York.

Trümpy, R.: 1992, 'Ostalpen und Westalpen - Verbindendes und Trennendes'. *Jahrbuch der Geologischen Bundesanstalt, Wien* **135**, 875–882.

Tsai, C.-H., Y. Iizuka, and W. G. Ernst: 2013, 'Diverse mineral compositions, textures, and metamorphic P-T conditions of the glaucophane-bearing rocks in the Tamayen mélange, Yuli belt, eastern Taiwan'. *Journal of Asian Earth Sciences* **63**, 218–233.

Tsao, S., E. Law, H.-C. Ho, Y.-H. Lee, W. T. Jiang, and C. H. Chen: 1996, 'The geological significance of K-Ar ages of metapelites from the Central Range, Taiwan'. *Bulletin of the Central Geological Survey* **11**, 37–84.

Ustaszewski, K., Y.-M. Wu, J. Suppe, H.-H. Huang, C.-H. Chang, and S. Carena: 2012, 'Crust-mantle boundaries in the Taiwan-Luzon arc-continent collision system determined from local earthquake tomography and 1D models: Implications for the mode of subduction polarity reversal'. *Tectonophysics* **578**, 31–49.

Van Blanckenburg, F.: 1992, 'Combined high-precision chronometry and geochemical tracing using accessory minerals: applied to the Central-Alpine Bergell intrusion (central Europe)'. *Chemical Geology* **100**, 19–40.

van Huene, R., C. R. Ranero, and P. Vannucchi: 2004, 'Generic model of subduction erosion'. *Geology* **32**, 913–916.

van Hunen, J. and M. B. Allen: 2011, 'Continental collision and slab break-off: A comparison of 3-D numerical models with observations'. *Earth and Planetary Science Letters* **302**, 27–37.

Van Roermund, H. L. M. and M. R. Drury: 1998, 'Ultra-high pressure (P > 6 GPa) garnet peridotites in Western Norway: exhumation of mantle rocks from > 185 km depth'. *Terra Nova* **10**, 295–301.

Vervoort, J. D., P. J. Patchett, U. Söderlund, and M. Baker: 2004, 'Isotopic composition of Yb and the determination of Lu concentrations and Lu/Hf ratios by isotope dilution using MC-ICPMS'. *Geochemistry Geophysics Geosystems* **5**, Q11002.

Visona, D., A. Hinterlechner-Ravnik, and F. P. Sassi: 1991, 'Geochemistry and crustal P-T polymetamorphic path of the mantle-derived rocks from the Pohorje area (Austrides, Eastern Alps, Slovenia)'. *Mineralia Slovaca* **23**, 515–525.

Vogt, K. and T. V. Gerya: 2014, 'From oceanic plateaus to allochthonous terranes: Numerical modelling'. *Gondwana Research* **25**, 494–508.

Vrabec, M., M. Janák, N. Froitzheim, and J. C. M. De Hoog: 2012, 'Phase relations during peak metamorphism and decompression of the UHP kyanite eclogites, Pohorje Mountains (Eastern Alps, Slovenia)'. *Lithos* **144**, 40–55.

Warren, C. J.: 2013, 'Exhumation of (ultra-)high-pressure terranes: concepts and mechanisms'. *Solid Earth* **4**, 75–92.

Warren, C. J., C. Beaumont, and R. A. Jamieson: 2008, 'Modelling tectonic styles and ultra-high pressure (UHP) rock exhumation during the transition from oceanic subduction to continental collision'. *Earth and Planetary Science Letters* **267**, 129–145.

Warren, C. J., S. P. Kelley, S. C. Sherlock, and C. S. McDonald: 2012, 'Metamorphic rocks seek meaningful cooling rate: Interpreting $^{40}Ar/^{39}Ar$ ages in an exhumed ultra-high pressure terrane'. *Lithos* **155**, 30–48.

Weber, S.: 2013, 'Untersuchung von Subduktionsprozessen anhand Eklogitfazieller Gesteine des Zermatt-Saas-Ophiolith-Komplexes'. Ph.D. thesis, University of Freiburg.

Whitehead, J. A., H. J. B. Dick, and H. Schouten: 1984, 'A mechanism for magmatic accretion under spreading centres'. *Nature* **312**, 146–148.

Whitney, D. and N. C. A. Seaton: 2010, 'Garnet polycrystals and the significance of clustered crystallization'. *Contributions to Mineralogy and Petrology* **160**, 591–607.

Whitney, D. L. and B. W. Evans: 2010, 'Abbreviations for names of rock-forming minerals'. *American Mineralogist* **95**, 185–187.

Wiederkehr, M., R. Bousquet, M. A. Ziemann, A. Berger, and S. M. Schmid: 2011, '3-D assessment of peak-metamorphic conditions by Raman spectroscopy of carbonaceous material: an example from the margin of the Lepontine dome (Swiss Central Alps)'. *International Journal of Earth Sciences* **100**, 1029–1063.

Willet, S. D., D. Fisher, C. Fuller, E.-C. Yeh, and C.-Y. Lu: 2003, 'Erosion rates and orogenic-wedge kinematics in Taiwan inferred from fission-track thermochronometry'. *Geology* **31**, 946–949.

Wilson, M.: 2000, *Active continental margins*, pp. 191–225. In: Wilson, M. (Ed): Igneous Petrogenesis. Springer, Netherlands.

Yue, L.-F., J. Suppe, and J.-H. Hung: 2005, 'Structural geology of a classic thrust belt earthquake: the 1999 Chi-Chi earthquake Taiwan (Mw=7.6)'. *Journal of Structural Geology* **27**(11), 2058–2083.

Yui, T.-F. and C.-H. Lo: 1989, 'High-pressure metamorphosed ophiolitic rocks from the Wanjung area, Taiwan'. *Proceedings of the Geological Society of China* **32**, 47–62.

Zhang, S.-B., Y.-F. Zheng, Y.-B. Wu, Z.-F. Zhao, S. Gao, and F.-Y. Wu: 2006, 'Zircon U-Pb age and Hf isotope evidence for 3.8 Ga crustal remnant and episodic reworking of Archean crust in South China'. *Earth and Planetary Science Letters* **252**, 56–71.

Zhou, B. and B. J. Hensen: 1995, 'Inherited isotope components preserved in monazite inclusions within garnets in leucogneiss from East Antarctica and implications for closure temperature studies'. *Chemical Geology* **121**, 317–326.

Ziegler, W.: 1956, 'Geologische Studien in den Flyschgebieten des Oberhalbsteins (Graubünden)'. *Eclogae Geologicae Helvetiae* **49**, 1–78.

Zulbati, F.: 2008, 'Structural and metamorphic evolution of the phengite-bearing schists of the northern Adula Nappe (Central Alps, Switzerland)'. *Geological Journal* **43**, 33–57.

Zulbati, F.: 2010, 'Multistage metamorphism and deformation in high-pressure metabasites of the northern Adula Nappe Complex (Central Alps, Switzerland)'. *Geological Journal* **46**, 82–103.

Acknowledgements

First of all, I thank Thorsten Nagel who gave me the opportunity to become a "Doctor". You were always helpful, encouraging, and patient. I really enjoyed working with you.

I also thank Niko Froitzheim and Carsten Münker who were always willing to share their extensive knowledge with me.

And I thank Prof. Beck for becoming a member of my examination board.

I acknowledge the funding that I received from the Deutsche Forschungsgemeinschaft (DFG grant TN401/3-1).

A special thanks goes to Daniel Herwartz for all the enlightening and encouraging discussions about Lu-Hf systematics and the improvements you contributed to the manuscripts.

I further thank Maria Kirchenbaur, Elis Hoffmann, Raúl Fonseca, Frederik Kirst, Alex Heuser, Irena Miladinova, Robert Kurzawski, Jacek Kossak, Frank Wombacher, Ambre Luguet, and all the staff working at the Poppelsdorfer Schloss (currently and in the past years). I appreciated every fruitful discussion and the pleasant atmosphere at "the Schloss".

Hugs, waves, and kisses go out to Nadine Pickarski. Thanks for being there.

I dedicate this work to my friend, Sebastian Bernhardt.

7 Appendix

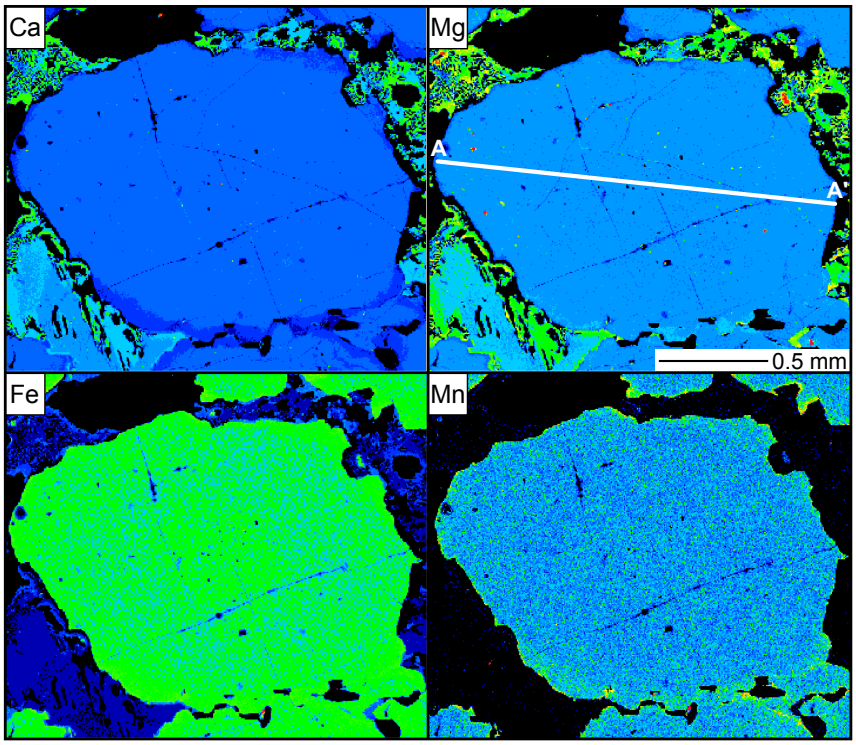

Figure 7.1: Element distribution maps of garnet from eclogite sample SADU22 from Alpe Arami.

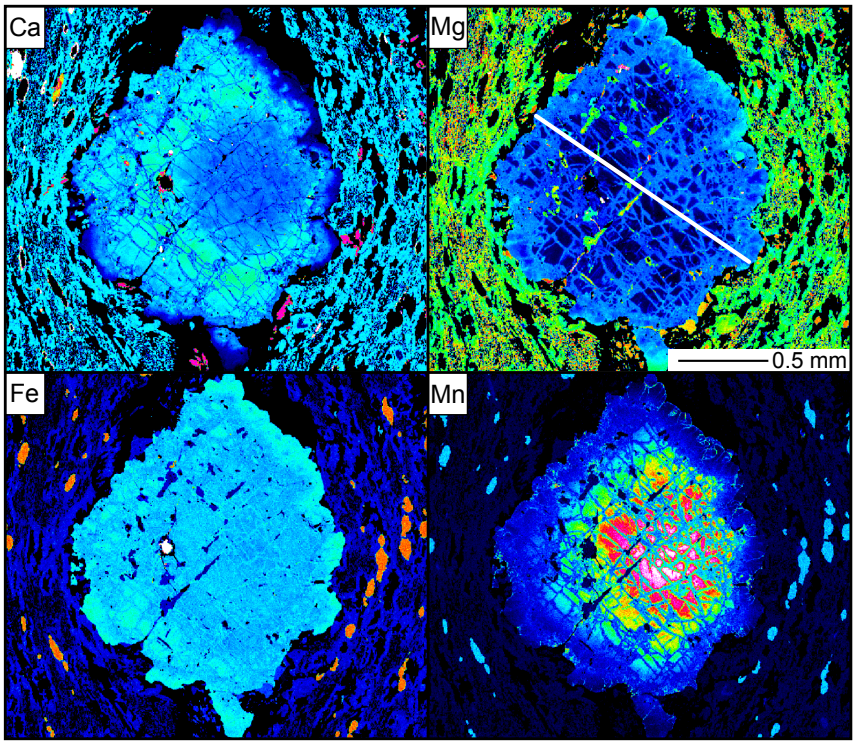

Figure 7.2: Element distribution maps of garnet from eclogite sample SADU52 from Piz d'Arbeola.

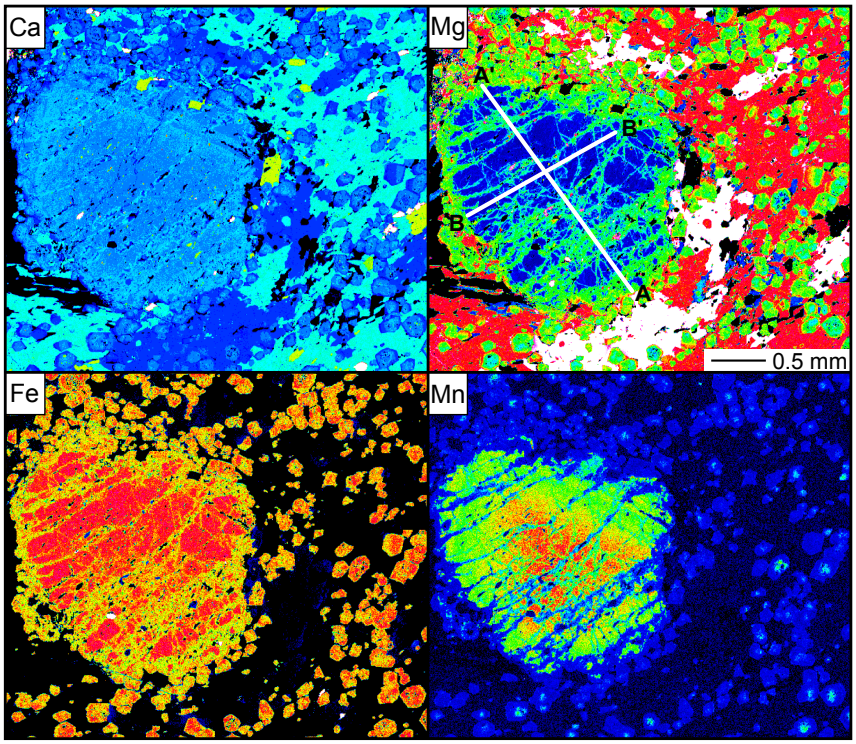

Figure 7.3: Element distribution maps of garnet from eclogite sample B15 from Passo del San Bernardino.

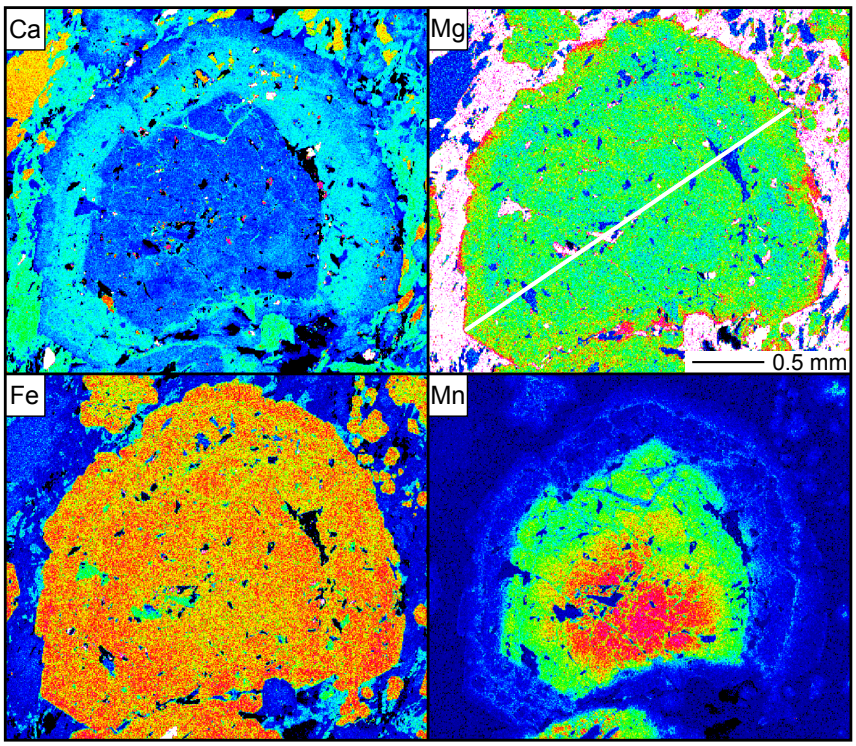

Figure 7.4: Element distribution maps of garnet from eclogite sample SADU33 from the Fanellahorn.

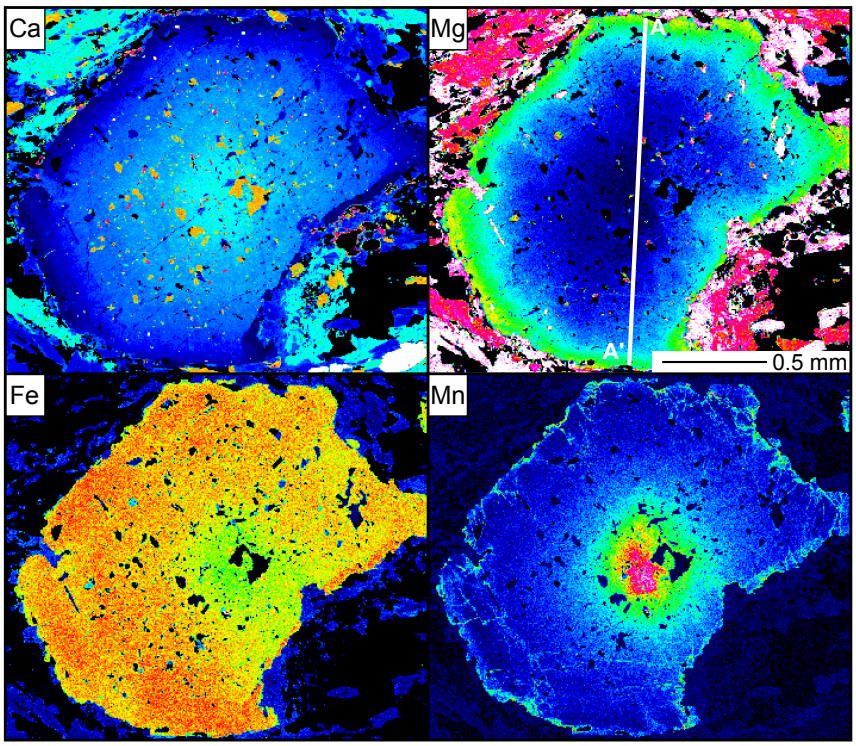

Figure 7.5: Element distribution maps of garnet from eclogite sample SADU40 from Lake Zervreila.

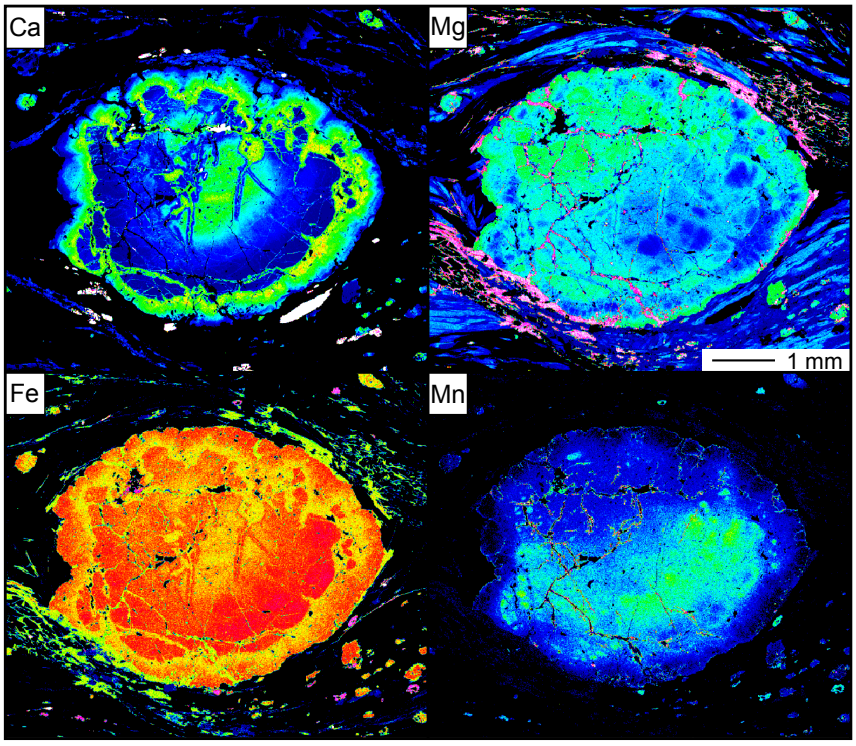

Figure 7.6: Element distribution maps of garnet from garnet-mica schist sample SADU8 from Passo del San Bernardino.

Table 7.1: Representative microprobe analyses of HP mineral phases from samples B15, SADU8, and SADU22 in wt% and p.f.u. Fe is calculated as FeO.

Sample	B15	B15	B15	B15	B15	B15	SADU8	SADU8	SADU8	SADU22	SADU22	SADU22
Mineral	small Grt	large Grt outer rim	large Grt rim	large Grt core	Omp	Phengite	large Grt outer rim	large Grt rim	large Grt core	Grt rim	Grt core	Omp
SiO_2	39.0	39.0	38.4	38.7	55.8	52.0	37.7	38.2	38.3	39.5	39.5	53.9
Al_2O_3	22.0	21.9	21.6	21.1	10.7	30.2	21.3	21.6	21.6	22.7	22.8	12.6
MgO	6.00	6.30	2.82	2.31	8.97	3.16	2.39	4.49	3.18	7.98	8.01	8.55
FeO	22.6	21.5	25.4	24.7	3.73	1.35	31.0	33.2	29.7	18.9	19.2	3.73
CaO	9.76	10.7	9.80	9.93	14.1	0.02	5.95	0.86	5.13	11.2	10.7	14.2
MnO	0.46	0.48	2.37	3.59	<DL	<DL	0.32	1.15	1.13	0.41	0.39	0.03
Na_2O	0.09	0.06	0.01	0.02	6.46	0.85	0.06	0.06	0.07	0.02	0.05	5.99
K_2O	0.01	0.03	<DL	0.04	<DL	9.08	0.03	<DL	<DL	<DL	0.01	<DL
TiO_2	<DL	0.096	0.06	0.18	<DL	<DL	0.19	<DL	0.07	0.02	0.12	0.26
Cr_2O_3	<DL	0.036	0.03	<DL	<DL	<DL	0.03	0.03	<DL	<DL	0.04	<DL
Total	**99.90**	**100.08**	**100.55**	**100.57**	**99.68**	**96.56**	**99.00**	**99.55**	**99.18**	**100.74**	**100.79**	**99.30**
Si	6.01	5.99	6.01	6.08	1.99	6.74	6.04	6.07	6.09	5.95	5.94	1.93
Al	3.99	3.96	4.00	3.91	0.45	4.61	4.03	4.05	4.05	4.04	4.05	0.53
Mg	1.38	1.44	0.66	0.54	0.48	0.61	0.57	1.06	0.75	1.79	1.80	0.46
Fe	2.92	2.76	3.33	3.24	0.11	0.15	4.16	4.41	3.95	2.38	2.42	0.11
Ca	1.61	1.77	1.64	1.67	0.54	0.00	1.02	0.15	0.87	1.81	1.72	0.55
Mn	0.06	0.06	0.31	0.48	0.00	0.00	0.04	0.16	0.15	0.05	0.05	0.00
Na	0.03	0.02	0.00	0.01	0.45	0.21	0.02	0.02	0.02	0.01	0.01	0.42
K	0.00	0.01	0.00	0.01	0.00	1.50	0.01	0.00	0.00	0.00	0.00	0.00
Ti	0.00	0.01	0.01	0.02	0.00	0.00	0.02	0.00	0.01	0.00	0.01	0.01
Cr	0.00	0.00	0.00	0.00	0.00	0.00	0.00	0.00	0.00	0.00	0.01	0.00
Total	**16.01**	**16.02**	**15.98**	**15.95**	**4.01**	**13.82**	**15.93**	**15.91**	**15.89**	**16.03**	**16.02**	**4.00**
O	24.00	24.00	24.00	24.00	6.00	22.00	24.00	24.00	24.00	24.00	24.00	6.00

Table 7.2: Representative microprobe analyses of HP mineral phases from samples SADU33, SADU40, and SADU52 in wt% and p.f.u. Fe is calculated as FeO.

Sample	SADU33	SADU33	SADU33	SADU33	SADU40	SADU40	SADU40	SADU40	SADU40	SADU52	SADU52	SADU52	SADU52
Mineral	small Grt	large Grt outer rim	large Grt rim	large Grt core	Grt outer rim	Grt rim	Grt core	Omp	Amp	small Grt	large Grt outer rim	large Grt rim	large Grt core
SiO_2	38.7	38.6	38.5	37.9	39.0	39.5	38.2	55.9	46.4	38.7	38.9	38.6	38.0
Al_2O_3	21.8	21.9	21.5	21.3	22.2	22.2	21.8	11.4	14.5	21.7	21.7	21.7	21.3
MgO	3.69	3.99	2.57	1.65	6.30	7.06	1.77	8.67	11.2	4.40	4.42	1.94	1.75
FeO	26.2	26.3	26.4	24.1	26.8	26.4	24.7	3.59	11.9	22.9	23.5	25.2	23.8
CaO	10.2	9.59	9.25	8.89	6.30	6.29	12.7	13.3	8.09	11.7	11.5	11.9	10.1
MnO	0.29	0.10	2.75	6.33	1.10	0.33	1.68	<DL	0.10	0.86	1.08	2.10	6.57
Na_2O	<DL	<DL	0.04	0.06	0.04	0.04	0.09	6.87	4.30	0.03	<DL	<DL	0.05
K_2O	<DL	0.02	<DL	0.02	<DL	<DL	<DL	0.01	0.46	0.02	<DL	<DL	<DL
TiO_2	0.05	0.10	0.09	0.20	0.09	0.03	0.15	0.05	0.53	0.08	0.09	0.10	0.09
Cr_2O_3	0.03	0.05	0.10	0.05	0.03	0.07	0.02	0.02	0.07	<DL	0.06	0.01	<DL
Total	**100.93**	**100.65**	**101.20**	**100.36**	**101.94**	**101.91**	**100.99**	**99.81**	**97.56**	**100.37**	**101.20**	**101.55**	**101.64**
Si	6.01	6.00	6.02	6.01	5.96	6.00	5.97	1.99	6.64	6.00	6.00	6.00	5.97
Al	3.99	4.01	3.96	3.98	4.00	3.97	4.01	0.48	2.45	3.96	3.93	3.97	3.94
Mg	0.85	0.92	0.60	0.39	1.44	1.60	0.41	0.46	2.40	1.02	1.01	0.45	0.41
Fe	3.40	3.42	3.46	3.19	3.43	3.36	3.23	0.11	1.43	2.97	3.03	3.29	3.13
Ca	1.70	1.60	1.55	1.51	1.03	1.02	2.12	0.51	1.24	1.94	1.89	1.99	1.70
Mn	0.04	0.01	0.36	0.85	0.14	0.04	0.22	0.00	0.01	0.11	0.14	0.28	0.87
Na	0.00	0.00	0.01	0.02	0.01	0.01	0.02	0.47	1.19	0.01	0.00	0.00	0.02
K	0.00	0.00	0.00	0.00	0.00	0.00	0.00	0.00	0.08	0.00	0.00	0.00	0.00
Ti	0.01	0.01	0.01	0.02	0.01	0.00	0.02	0.00	0.06	0.01	0.01	0.01	0.01
Cr	0.00	0.00	0.01	0.00	0.00	0.01	0.00	0.00	0.01	0.00	0.01	0.00	0.00
Total	**15.99**	**15.98**	**15.97**	**15.98**	**16.03**	**16.00**	**16.01**	**4.01**	**15.52**	**16.02**	**16.02**	**16.00**	**16.05**
O	24.00	24.00	24.00	24.00	24.00	24.00	24.00	6.00	23.00	24.00	24.00	24.00	24.00

Table 7.3: Representative microprobe analyses of HP mineral phases from samples S34 and S89 in wt% and p.f.u. Fe is calculated as FeO.

Sample	S34	S34	S34	S34	S34	S89	S89	S89	S89	S89
Mineral	Grt rim	Grt core	Grt rim	Omph	Zo	Grt rim	Grt core	Grt rim	Omph	Zo
SiO_2	40.07	39.98	40.12	54.57	39.92	40.73	40.52	40.59	53.94	39.16
Al_2O_3	23.23	23.33	22.96	9.81	32.57	22.77	23.10	22.49	8.60	32.15
MgO	10.15	10.15	10.03	10.23	0.08	13.26	13.18	13.46	12.00	0.12
FeO	17.68	17.86	18.12	3.27	2.00	15.38	15.52	15.54	2.39	1.36
CaO	9.22	9.00	9.07	16.23	24.63	7.78	7.79	7.70	18.25	24.84
MnO	0.36	0.35	0.30	0.06	<DL	0.46	0.39	0.38	0.05	0.06
Na_2O	0.04	0.02	0.06	5.36	0.03	<DL	<DL	0.05	4.39	0.05
K_2O	<DL	<DL	<DL	0.03	<DL	<DL	<DL	0.01	<DL	<DL
TiO_2	0.02	0.02	0.09	0.12	0.07	0.04	<DL	0.05	0.16	0.03
Cr_2O_3	0.02	<DL	0.01	<DL	0.04	0.27	0.10	0.28	0.05	0.16
Total	**100.78**	**100.71**	**100.76**	**99.69**	**99.36**	**100.68**	**100.59**	**100.56**	**99.82**	**97.92**
Si	5.96	5.95	5.98	1.96	3.01	5.98	5.96	5.97	1.94	3.00
Al	4.07	4.09	4.03	0.41	2.89	3.94	4.00	3.90	0.36	2.90
Mg	2.25	2.25	2.23	0.55	0.01	2.90	2.89	2.95	0.64	0.01
Fe	2.20	2.22	2.26	0.10	0.13	1.89	1.91	1.91	0.07	0.09
Ca	1.47	1.43	1.45	0.62	1.99	1.22	1.23	1.21	0.70	2.04
Mn	0.05	0.04	0.04	0.00	0.00	0.06	0.05	0.05	0.00	0.00
Na	0.01	0.01	0.02	0.37	0.00	0.00	0.00	0.02	0.31	0.01
K	0.00	0.00	0.00	0.00	0.00	0.00	0.00	0.00	0.00	0.00
Ti	0.00	0.00	0.01	0.00	0.00	0.00	0.00	0.00	0.00	0.00
Cr	0.00	0.00	0.00	0.00	0.00	0.03	0.01	0.03	0.00	0.01
Total	**16.00**	**16.00**	**16.00**	**4.02**	**8.04**	**16.00**	**16.03**	**16.03**	**4.03**	**8.04**
O	24.00	24.00	24.00	6.00	12.00	24.00	24.00	24.00	6.00	12.00

Table 7.4: Representative microprobe analyses of HP mineral phases from samples FK99 and S119 in wt% and p.f.u. Fe is calculated as FeO.

Sample	FK99	FK99	FK99	FK99	FK99	FK99	S119	S119	S8119	S119	S119
Mineral	Grt rim	Grt core	Grt rim	Cpx	Opx	OI	Grt rim	Grt core	Grt rim	Cpx	OI
SiO_2	41.30	41.13	41.17	52.83	56.89	40.43	41.67	41.89	41.71	53.34	39.90
Al_2O_3	23.56	23.49	23.76	0.87	0.80	<DL	24.18	23.87	23.93	1.48	0.01
MgO	16.22	16.61	16.36	17.29	32.73	44.77	17.94	18.05	18.26	17.91	49.78
FeO	13.37	13.54	13.66	2.61	8.29	14.91	10.30	10.10	10.58	1.77	9.99
CaO	5.80	5.36	5.39	24.96	0.13	0.01	6.46	6.36	5.98	23.97	<DL
MnO	0.30	0.35	0.51	0.01	0.12	0.16	0.28	0.21	0.33	0.02	0.03
Na_2O	<DL	<DL	<DL	0.45	0.02	0.02	0.04	<DL	0.01	0.66	<DL
K_2O	0.02	0.01	<DL	<DL	0.01	<DL	0.02	<DL	0.02	<DL	<DL
TiO_2	0.07	0.03	<DL	0.05	0.01	<DL	0.05	0.04	0.02	0.08	<DL
Cr_2O_3	0.06	0.18	0.11	0.11	<DL	<DL	<DL	0.04	0.04	0.62	<DL
Total	**100.68**	**100.71**	**100.95**	**99.19**	**98.99**	**100.30**	**100.92**	**100.55**	**100.87**	**99.84**	**99.72**
Si	5.96	5.94	5.93	1.95	1.99	2.02	5.93	5.97	5.94	1.94	1.97
Al	4.01	4.00	4.04	0.04	0.03	0.00	4.05	4.01	4.02	0.06	0.00
Mg	3.49	3.58	3.51	0.95	1.71	3.33	3.80	3.83	3.88	0.97	3.66
Fe	1.61	1.64	1.65	0.08	0.24	0.62	1.22	1.20	1.26	0.05	0.41
Ca	0.90	0.83	0.83	0.99	0.00	0.00	0.98	0.97	0.91	0.94	0.00
Mn	0.04	0.04	0.06	0.00	0.00	0.01	0.03	0.02	0.04	0.00	0.00
Na	0.00	0.00	0.00	0.03	0.00	0.00	0.01	0.00	0.00	0.05	0.00
K	0.00	0.00	0.00	0.00	0.00	0.00	0.00	0.00	0.00	0.00	0.00
Ti	0.01	0.00	0.00	0.00	0.00	0.00	0.00	0.00	0.00	0.00	0.00
Cr	0.01	0.02	0.01	0.00	0.00	0.00	0.00	0.00	0.00	0.02	0.00
Total	**16.02**	**16.03**	**16.03**	**4.04**	**3.99**	**5.98**	**16.05**	**16.02**	**16.05**	**4.02**	**6.03**
O	24.00	24.00	24.00	6.00	6.00	8.00	24.00	24.00	24.00	6.00	8.00

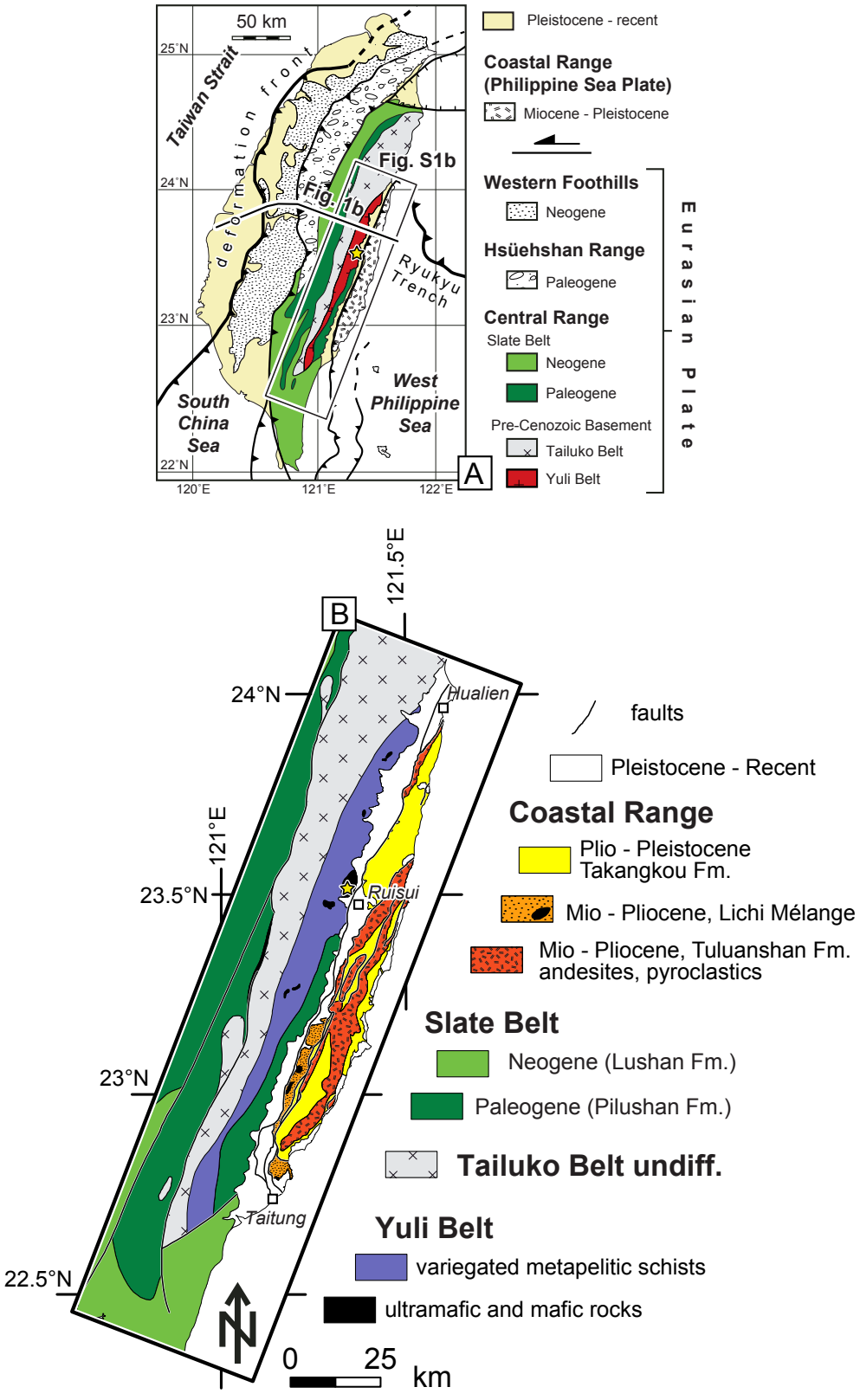

Figure 7.7: Tectonic overview of Taiwan. B: Geologic map of central eastern Taiwan (inset in A) showing the main lithologic units within the Yuli Belt and the adjacent units.

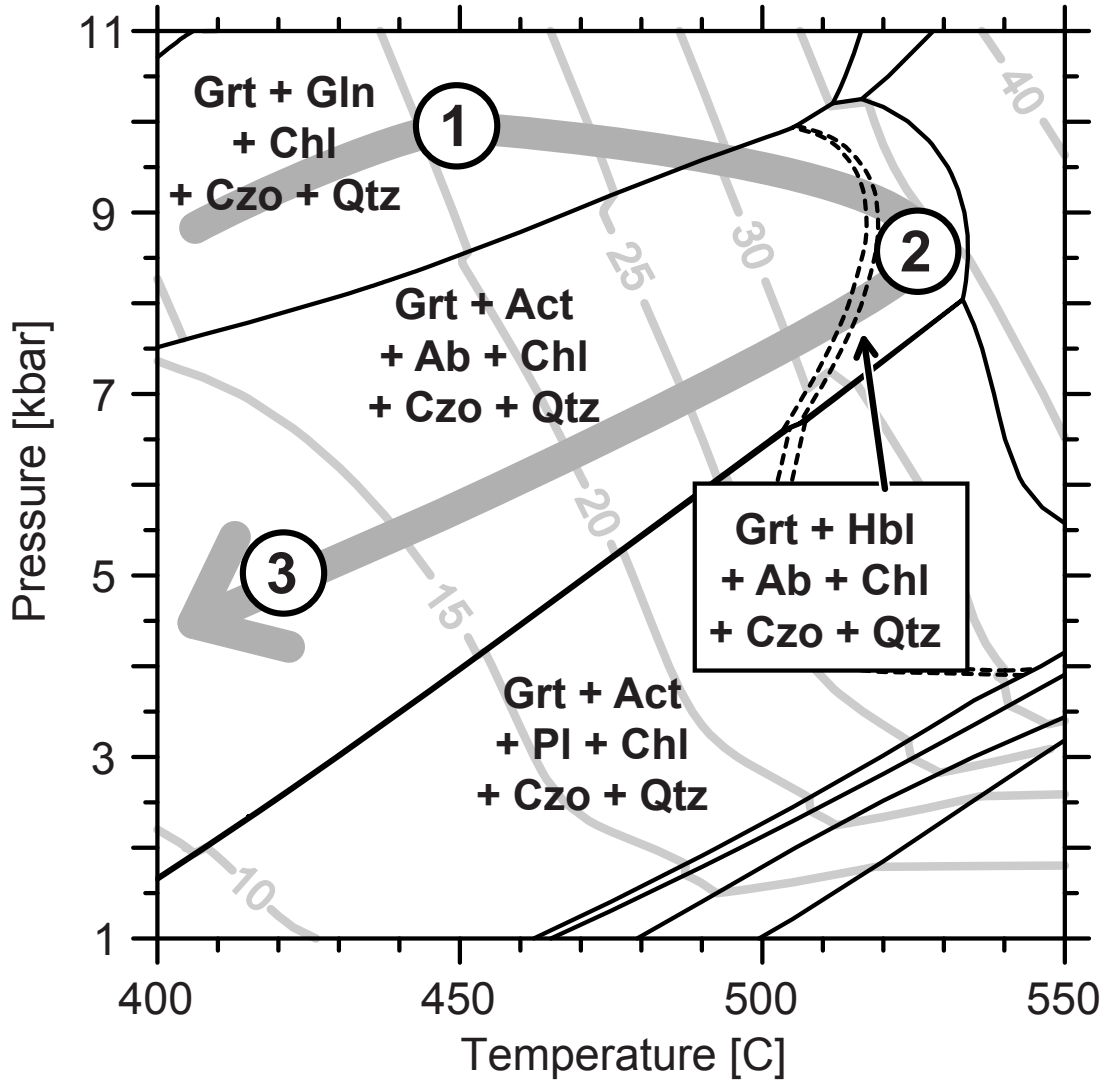

Figure 7.8: Phase diagram calculated for very slightly oxidized Si-Al-Fe-Mn-Mg-Ca-Na bulk composition of sample TW1 (Table 7.5). For the calculation, we used the program Domino (De Capitani and Petrakakis, 2010) and the thermodynamic database of Holland and Powell (1998) updated with non-ideal solid solution models designed for this database, in particular for amphibole (Diener et al., 2007). The diagram shows a large stability field for the observed paragenesis grt + amp + czo + qtz + chl + tit ± ab. Modeled compositions of amphibole, however, vary considerably through pressure-temperature (P-T) space and confirm a clockwise P-T path. Predicted compositions reproduce the three observed generations of amphibole at 450 °C/1 GPa (Am_1), 525 °C/0.85 GPa (Am_2), and 420 °C/0.5 GPa, respectively (Table 7.5). At peak pressures of 1 GPa outside the albite stability field, amphibole rich in glaucophane component contains the Na budget if the rock. The subsequent peak-temperature conditions at around 525 °C/0.8 GPa are well-constrained through the coexistence of albite and hornblende (Am_2). The stability field of the latter is illustrated by dashed lines in Figure 4.2B illustrating major uptake of Al on the tetrahedral site and, thus, the stability of hornblende on the high-temperature side. The inferred conditions agree with published estimations for identical samples from Tsai et al. (2013). Along the retrograde P-T path tremolite-actinolite-rich amphibole (Am_3) coexists with albite. Isopleths for volume percent garnet (solid grey isopleths in Fig. 4.2B) show that garnet largely grows along the prograde P-T path, which accords with the observation in thin section that at least some of the garnet predeates glaucophane and garnet generally predates hornblende.

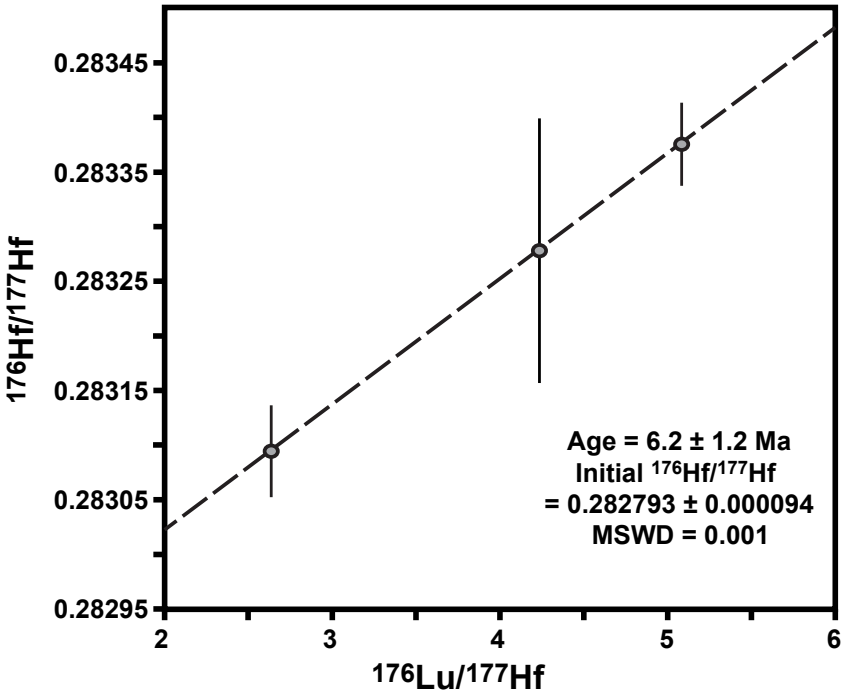

Figure 7.9: Lu–Hf isochron plot for garnet separates of sample TW1 only. Plotting routine and parameters are the same as in Fig. 4.3.

Analytical details

Mineral compositions and bulk compositions (Table 7.5) were determined using a JEOL-JXA-8900 microprobe and PANalytical-Axios XRF analyzer, respectively.

For the isotopic analysis, a mixed ^{176}Lu-^{180}Hf tracer was added to the samples before digestion. Garnet separates were digested by a method that leaves behind refractory, Hf-rich phases like zircon that might preserve inherited isotope signatures (Lagos et al., 2007). Whole rock powder was fully digested inside steal mantled pressure bombs. Lutetium and Hf were separated from the matrix elements using the method of Münker et al. (2001). Hafnium cuts were additionally purified by repeating the Ln-spec column chemistry using 48 ml of 6N HCl to remove remaining matrix elements and Lu. Subsequently, Hf was eluted using 2N HF. Measurements were obtained on a Thermo Neptune MC-ICPMS at the Steinmann-Institut. Naturally occurring Yb in the Lu cuts was used for mass bias correction on Lu isotope ratios (Lagos et al., 2007; Vervoort et al., 2004) and interferences on ^{176}Lu were corrected by monitoring ^{173}Yb and ^{177}Hf and the natural isotope compositions. Instrumental mass bias on Hf isotope ratios were corrected by using the exponential law and a ^{179}Hf/^{177}Hf of 0.7325. Measured ^{176}Hf/^{177}Hf ratios are calculated relative to a ^{176}Hf/^{177}Hf ratio of 0.282160 for the Münster Ames Hf standard, which is isotopically identical to the JMC-475 standard. Isobaric interferences on ^{176}Hf and ^{180}Hf were corrected by monitoring ^{173}Yb, ^{175}Lu, ^{181}Ta, and ^{183}W and their natural isotope compositions. Hafnium compositions were calculated using both the tracers and the natural Lu compositions (Amelin et al., 2011). The difference between the two was then added to the external reproducibilities used for the isochron calculations, which were estimated by the empirical relationship 2σ external reproducibility $\approx 4\sigma$m (σm = standard error of a single analysis; Bizzarro et al., 2003). For further details of the analytical treatment we also refer to Herwartz et al. (2008) and Kirchenbaur et al. (2012).

Table 7.5: Bulk rock RXA-data and selected microprobe analyses from sample TW1. Weight percents for iron oxides are given as Fe_2O_3 for the bulk analyses and as FeO for mineral compositions. Ca and Fe in the input composition for the phase diagram calculation are very slightly adjusted considering S as pyrite, P as apatite, and the ignition loss as CO_2 in calcite (Si: 52.54, Al: 18.04, Fe: 12.88, Mn: 1.76, Mg: 5.01, Ca: 8.78, Na: 1.04). The composition is normalized to 100 cations and oxygen calculated assuming bivalent iron (O: 161.04). Finally, 0.2 oxygen are added to account for some trivalent iron, e.g. in clinozoisite/ epidote. In Italics are three amphibole compositions predicted by the thermodynamic calculations in Figure 4.2 for the three indicated metamorphic stages (450 °C/1 GPa, 525 °C/0.85 GPa, and 420 °C/0.5 GPa, respectively).

	Bulk rock	Amp_1		Amp_2		Amp_3		Grt core	Grt int	Grt rim	Ab	Chl	Chl	Phe	Czo	Tit
SiO_2	51.11	55.98		41.67		54.51		37.53	37.87	37.90	68.29	27.34	26.74	50.93	38.44	31.07
TiO_2	0.53	<DL		0.52		0.14		0.43	0.08	<DL	<DL	<DL	<DL	0.17	0.12	37.64
Al_2O_3	14.89	10.33		15.50		1.75		19.43	21.26	21.91	19.82	20.66	19.87	25.90	27.16	0.90
FeO/Fe_2O_3	16.93	13.53		17.15		13.22		26.78	25.65	25.13	0.20	19.88	23.43	4.77	8.00	0.44
MnO	2.02	0.19		0.31		0.80		6.16	5.69	5.51	0.05	0.48	1.16	0.07	0.31	0.18
MgO	3.27	8.91		8.05		14.67		1.94	2.73	2.46	<DL	18.81	15.05	2.97	0.05	<DL
CaO	8.76	1.08		9.68		11.36		8.23	7.18	8.16	0.19	0.01	0.04	0.01	23.51	29.45
Na_2O	0.52	6.96		3.62		0.94		0.04	0.05	0.03	11.88	0.02	0.01	0.12	<DL	0.06
K_2O	0.15	0.01		0.58		0.08		<DL	0.01	0.02	0.08	<DL	<DL	11.29	0.03	0.01
Cr_2O_3	<DL	0.03		<DL		<DL		0.03	0.01	0.02	0.01	<DL	<DL	<DL	<DL	0.01
Total	**98.18**	**97.00**		**97.08**		**97.46**		**100.56**	**100.53**	**101.13**	**100.51**	**87.19**	**86.30**	**96.21**	**97.61**	**99.76**
			Model 450°C/1GPa		Model 525°C/0.85GPa		Model 420°C/0.5GPa									
Si	51.32	7.83	8.00	6.23	6.64	7.85	8.00	6.03	6.00	5.96	2.96	2.81	2.84	6.84	3.05	1.02
Ti	0.40	0.00	-	0.06	-	0.01	-	0.05	0.01	0.00	0.00	0.00	0.00	0.02	0.01	0.93
Al	17.62	1.70	1.80	2.73	2.64	0.30	0.14	3.68	3.97	4.06	1.01	2.50	2.49	4.10	2.54	0.03
Fe	12.79	1.58	2.38	2.14	1.98	1.59	3.47	3.60	3.40	3.30	0.01	1.71	2.08	0.54	0.53	0.01
Mn	1.72	0.02	-	0.04	-	0.10	-	0.84	0.76	0.73	0.00	0.04	0.10	0.01	0.02	0.01
Mg	4.89	1.86	0.82	1.79	1.78	3.15	1.39	0.46	0.64	0.58	0.00	2.88	2.38	0.59	0.01	0.00
Ca	9.42	0.16	0.10	1.55	1.52	1.75	1.80	1.42	1.22	1.37	0.01	0.00	0.00	0.00	2.00	1.03
Na	1.01	1.89	1.99	1.05	0.94	0.26	0.26	0.01	0.02	0.01	1.00	0.00	0.00	0.03	0.00	0.00
K	0.19	0.00	-	0.11	-	0.02	-	0.00	0.00	0.00	0.00	0.00	0.00	1.94	0.00	0.00
Cr	-	0.00	-	0.00	-	0.00	-	0.00	0.00	0.02	0.00	0.00	0.00	0.00	0.00	0.00
O	**161.24**	**23.00**	**23.00**	**23.00**	**23.00**	**23.00**	**23.00**	**24.00**	**24.00**	**24.00**	**8.00**	**14.00**	**14.00**	**22.00**	**12.50**	**5.00**

Table 7.6: Lu–Hf concentrations and isotopic compositions of sample TW1. Uncertainties are estimated 2σ external reproducibilities. The isochron in Figure 4.3 was calculated using the $^{176}Hf/^{177}Hf$ errors in the last column, which also account for uncertainties resulting from the unknown Lu composition in the measured Hf cuts.

Sample	ppm Lu	ppm Hf	$^{176}Lu/^{177}Hf$	Error	$^{176}Hf/^{177}Hf$	Error
Whole rock	0.787	2.66	0.04193	0.00008	0.282898	0.000038
Garnet1	18.5	1.00	2.624	0.005	0.283095	0.000042
Garnet2	14.9	0.500	4.230	0.008	0.283279	0.000121
Garnet3	34.3	0.956	5.083	0.010	0.283377	0.000038

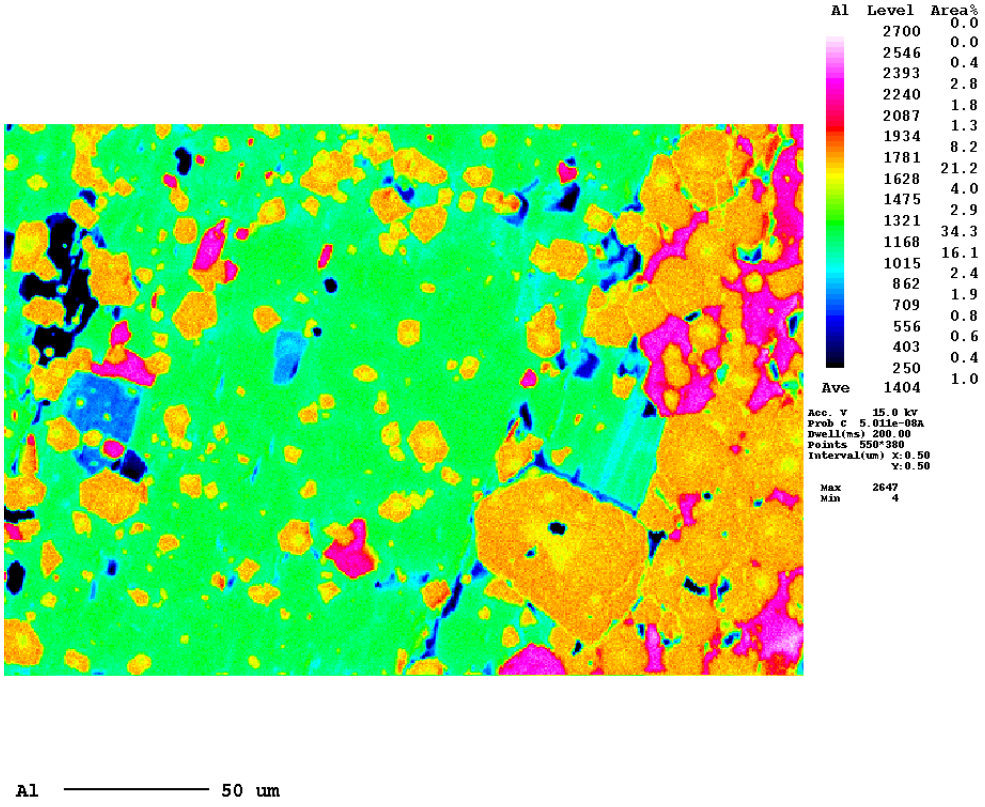

Figure 7.10: Al distribution map of sample TW1 from Taiwan.

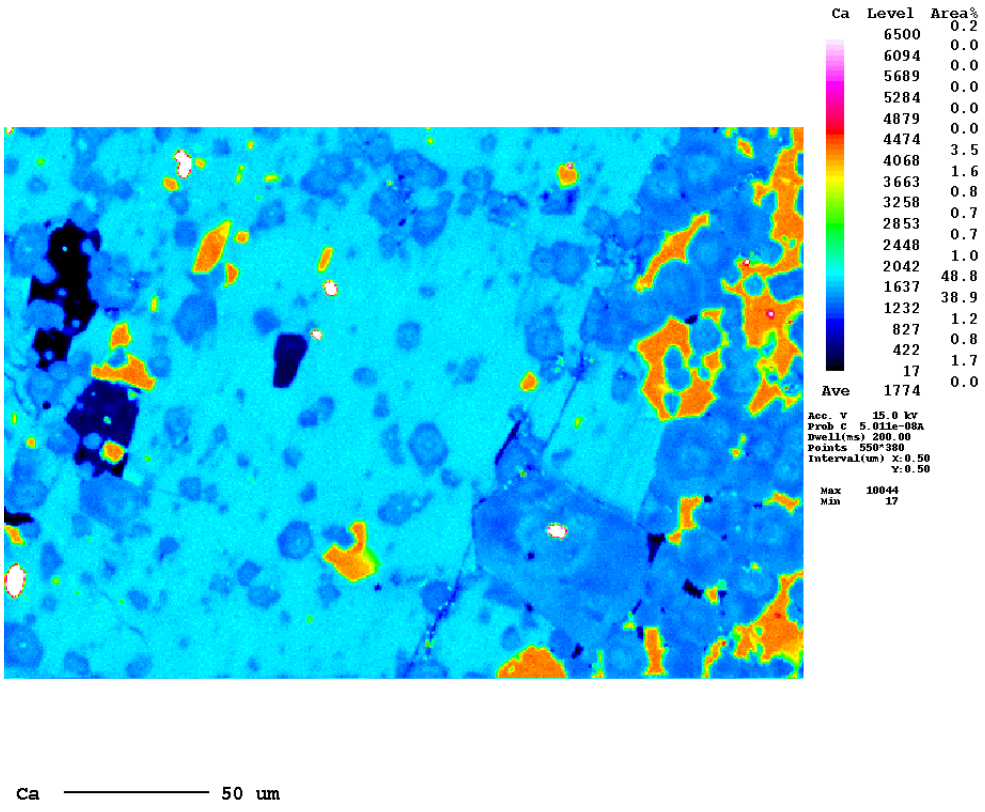

Figure 7.11: Ca distribution map of sample TW1 from Taiwan.

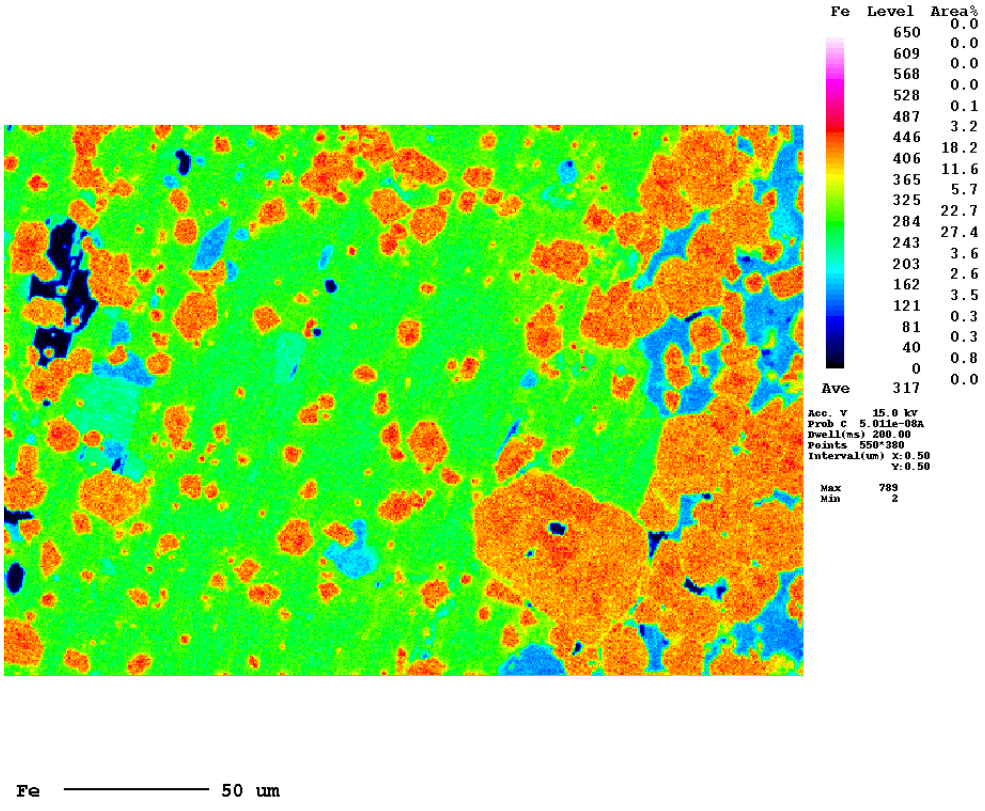

Figure 7.12: Fe distribution map of sample TW1 from Taiwan.

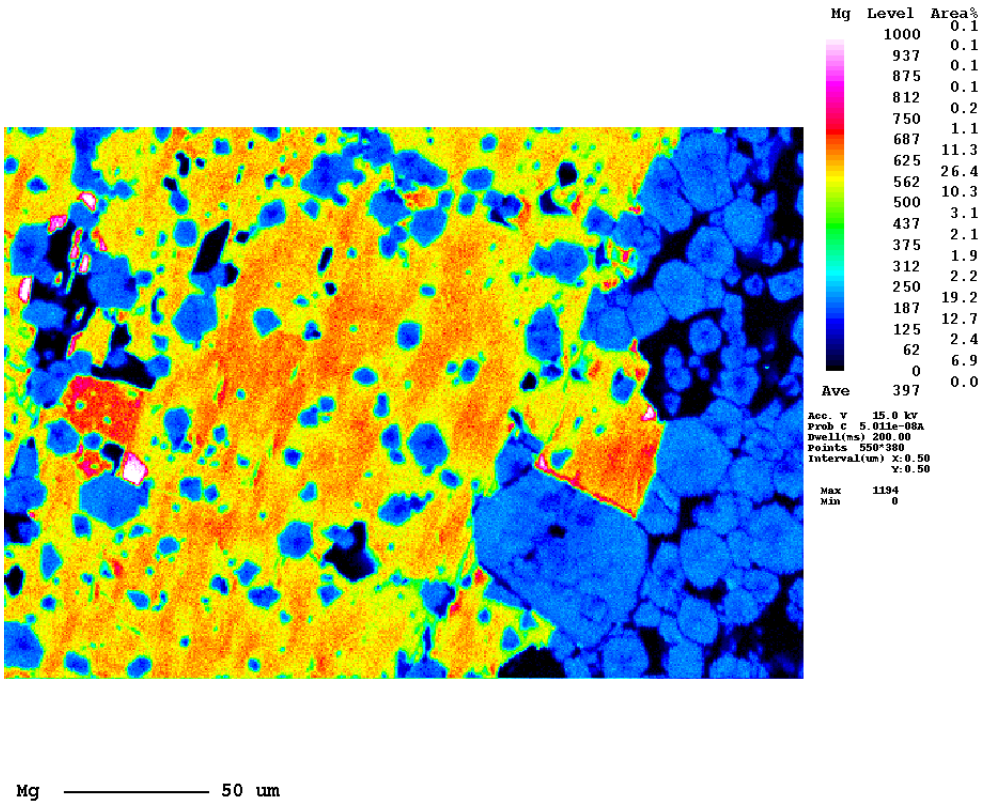

Figure 7.13: Mg distribution map of sample TW1 from Taiwan.

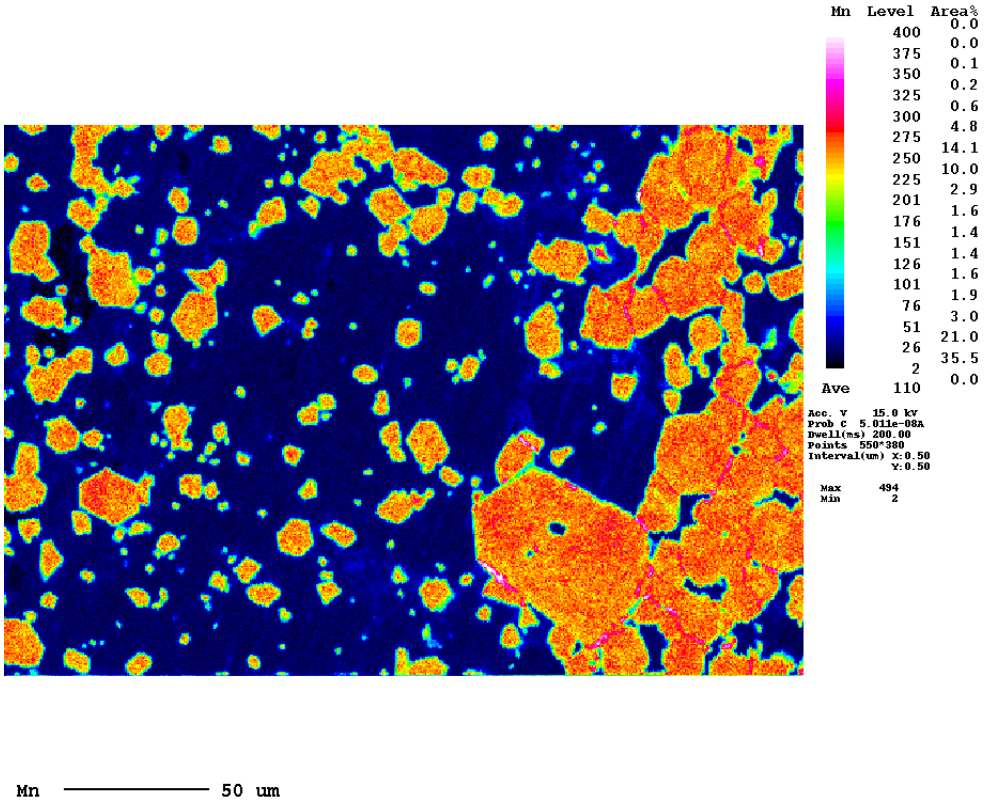

Figure 7.14: Mn distribution map of sample TW1 from Taiwan.

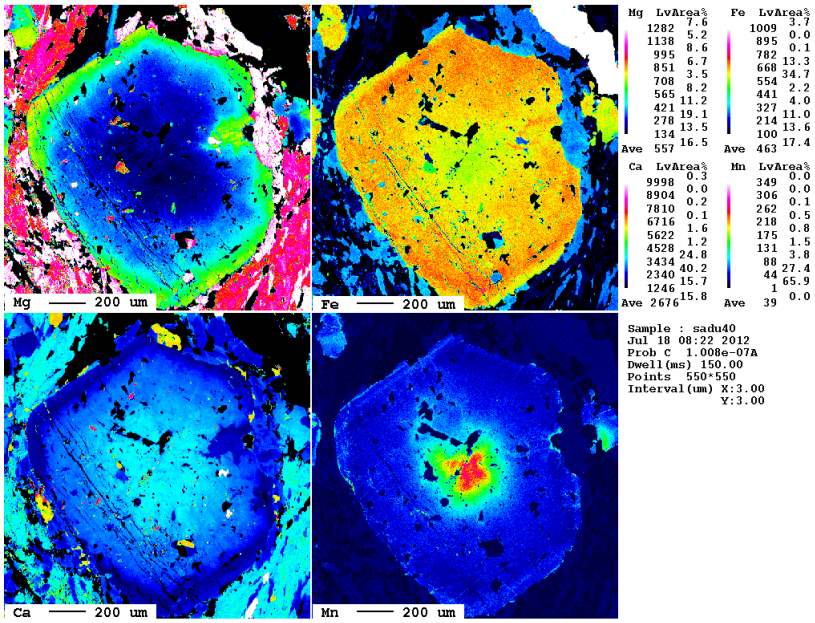

Figure 7.15: Element distribution maps of sample SADU40 from Lake Zerfreiler (northern Adula Nappe).

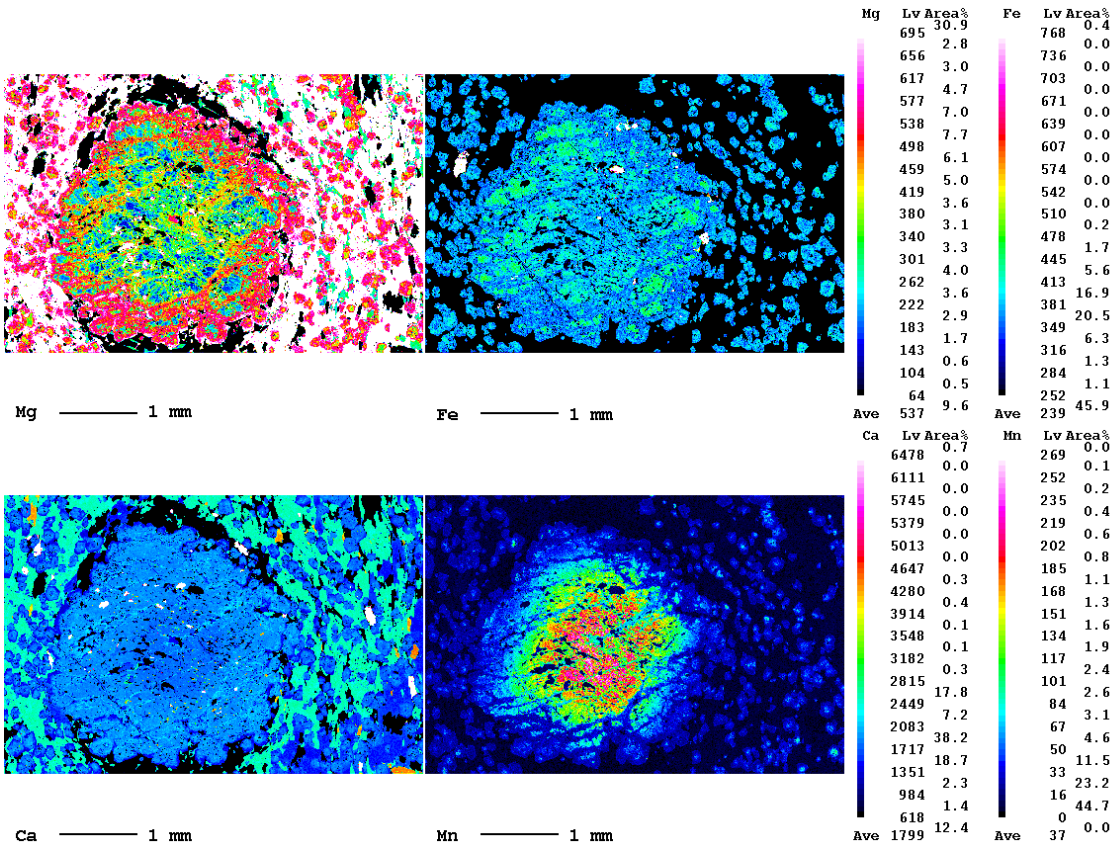

Figure 7.16: Element distribution maps of sample B15 from Passo del San Bernardino (central Adula Nappe).

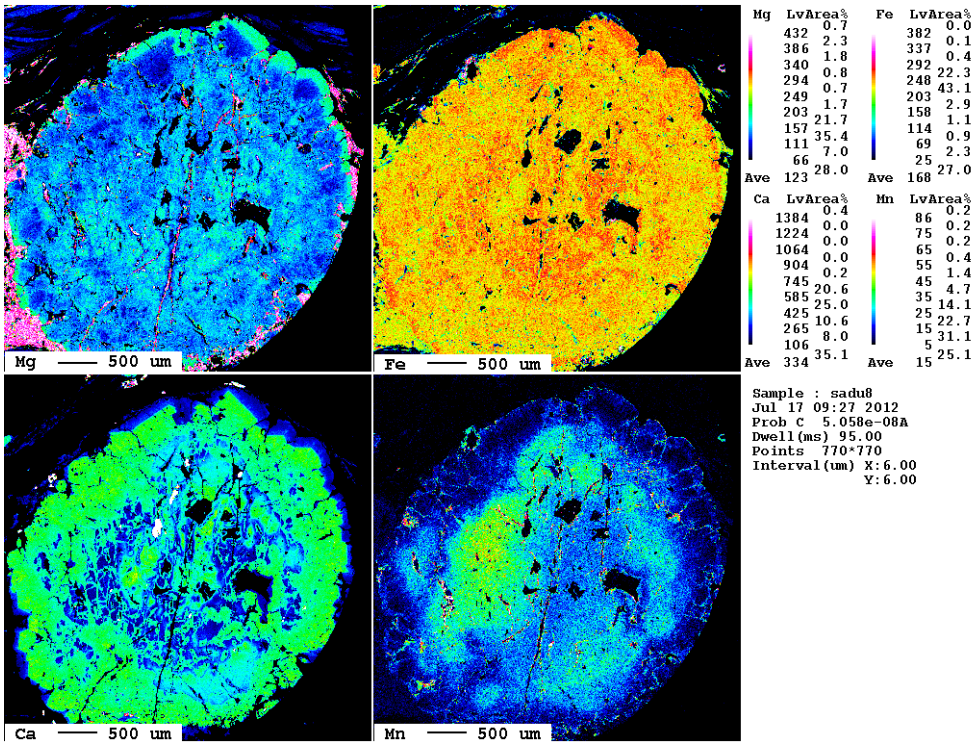

Figure 7.17: Element distribution maps of sample SADU8 from Passo del San Bernardino (central Adula Nappe).

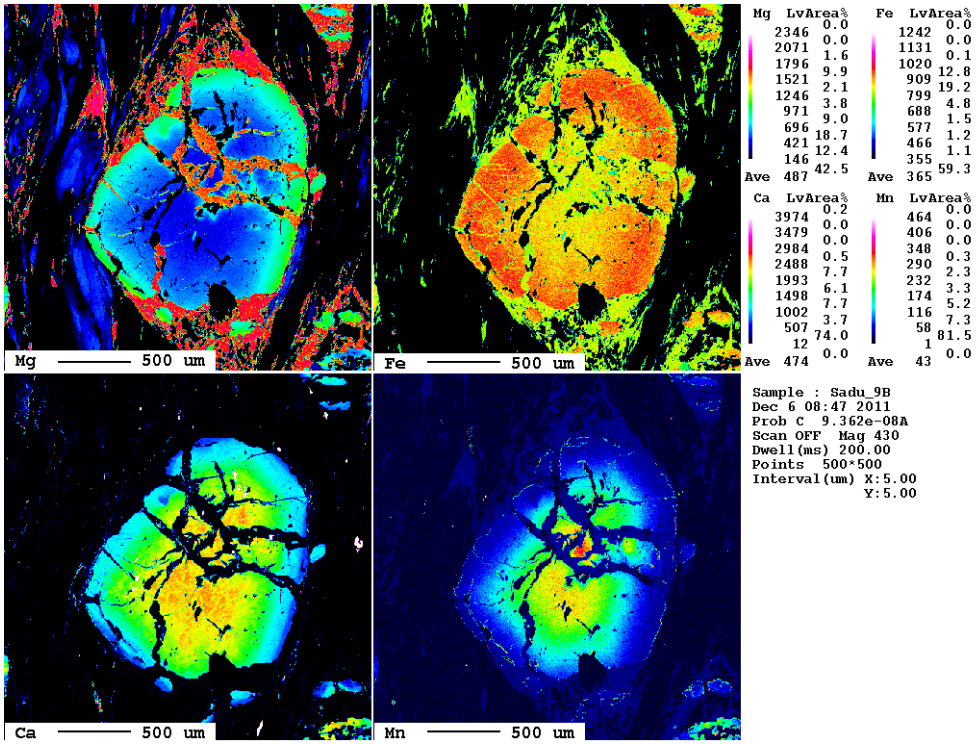

Figure 7.18: Element distribution maps of sample SADU9B from Passo del San Bernardino (central Adula Nappe).

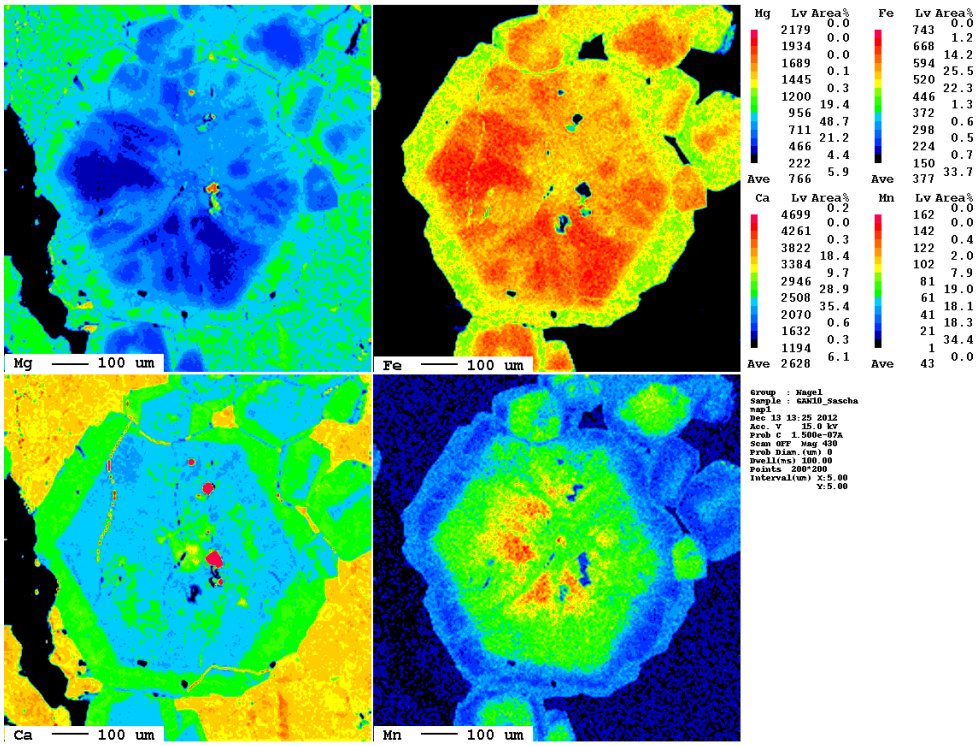

Figure 7.19: Element distribution maps of sample Gan10 from Ganan (central Adula Nappe). This sample was provided by R. Kurzawski.

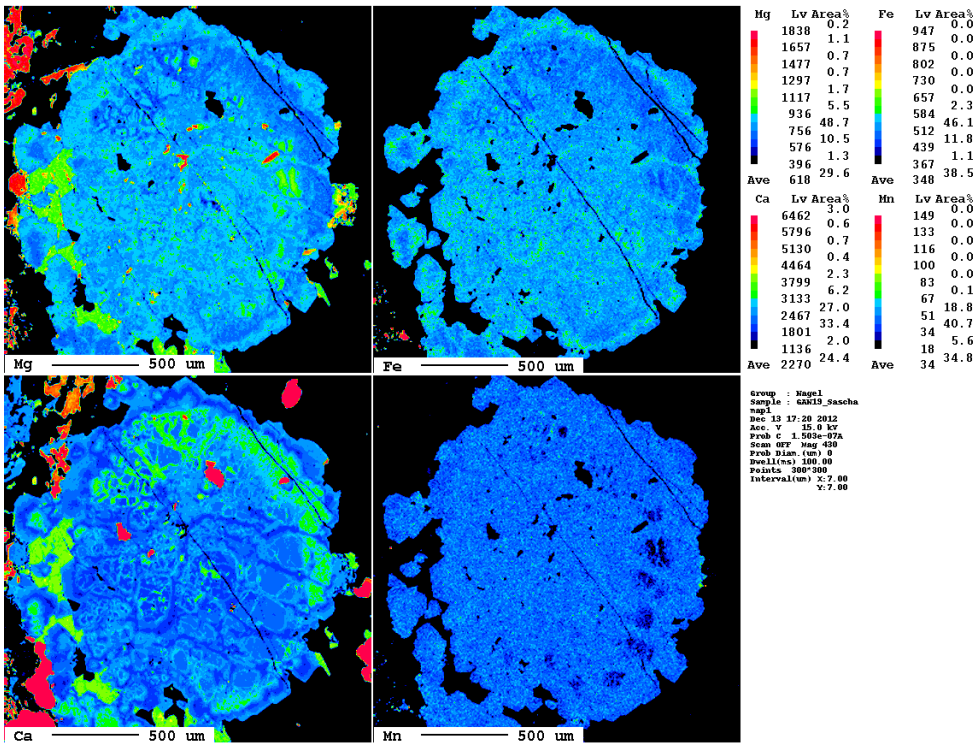

Figure 7.20: Element distribution maps of sample Gan19 from Ganan (central Adula Nappe). This sample was provided by R. Kurzawski.

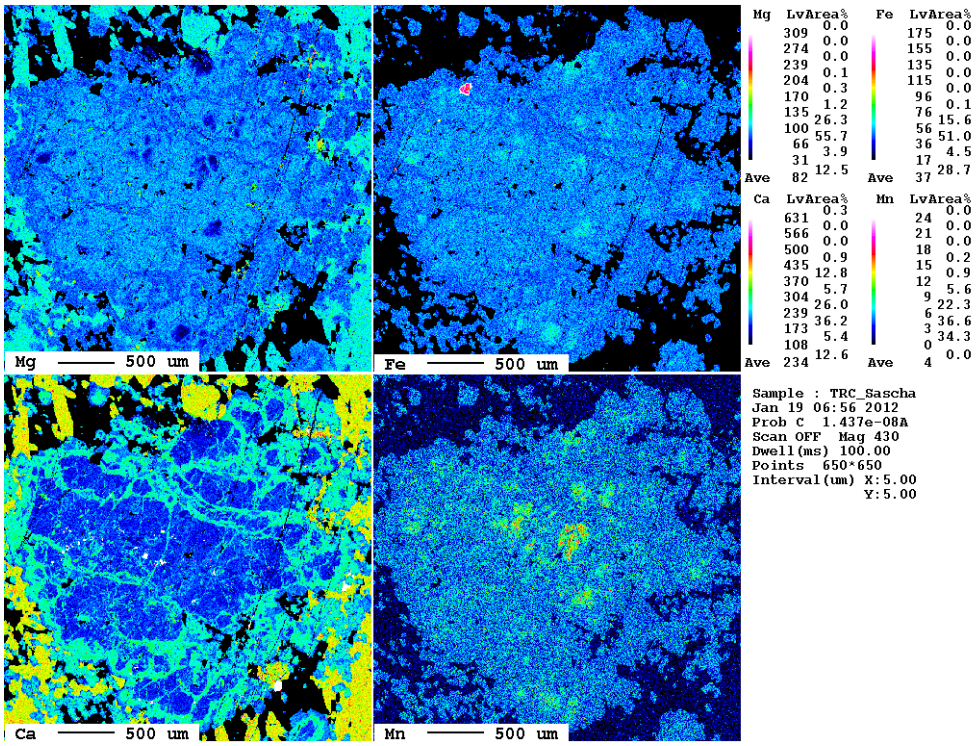

Figure 7.21: Element distribution maps of sample TRC1 from Trescolmen (central Adula Nappe).

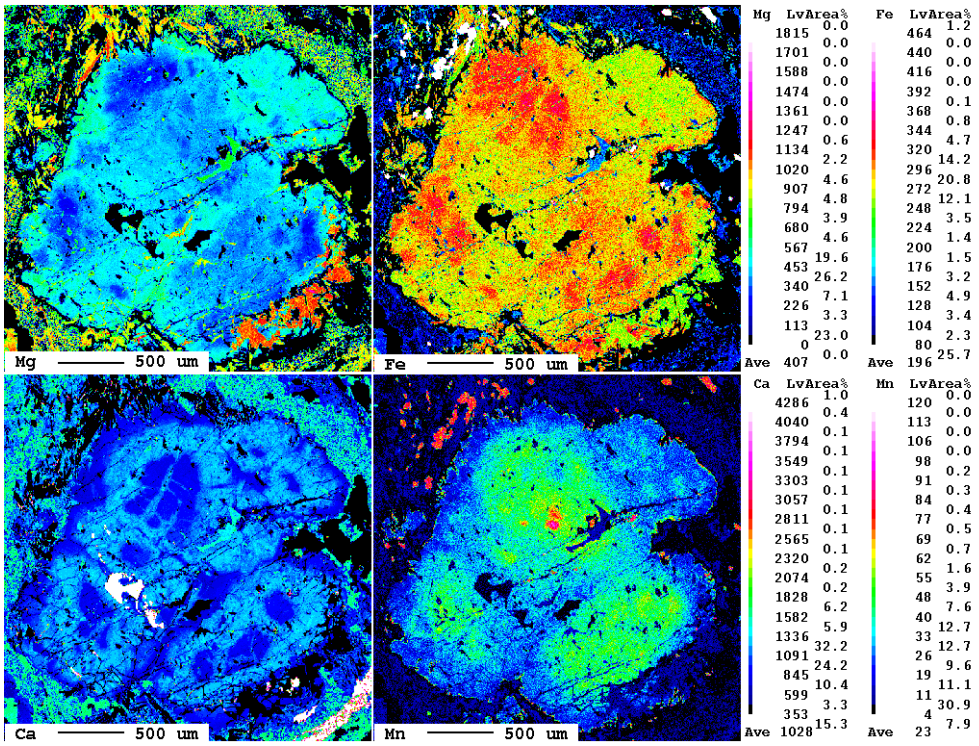

Figure 7.22: Element distribution maps of sample SADU15B from I Corn de Golin (central Adula Nappe).

Table 7.7: List of samples

Sample	Lithology	Location	Coordinates
B15	eclogite	Passo del San Bernardino	32T 513968 5149671
SADU5	eclogite	Passo del San Bernardino	32T 513984 5148029
SADU6	eclogite	Passo del San Bernardino	32T 513971 5148065
SADU7A	eclogite	Passo del San Bernardino	32T 514111 5149176
SADU7B	eclogite	Passo del San Bernardino	32T 514111 5149176
SADU8	grt-mica schist	Passo del San Bernardino	32T 513994 5149074
SADU9A	grt-mica schist	Passo del San Bernardino	32T 512916 5148339
SADU9B	grt-mica schist	Passo del San Bernardino	32T 512916 5148339
SADU10	eclogite	Passo del San Bernardino	32T 513968 5149672
SADU11	grt-mica schist	Passo del San Bernardino	32T 513968 5149672
SADU12	amphibolite in micaschist	Passo del San Bernardino	32T 514062 5149777
SADU13	amphibolie	Passo del San Bernardino	32T 514099 5149925
SADU14	gneiss	Passo del San Bernardino	32T 514047 5149873
SADU15A	eclogite	I Corn de Golin	32T 512458 5133071
SADU15B	eclogite	I Corn de Golin	32T 512458 5133071
SADU16	grt-mica schist	I Corn de Golin	32T 512458 5133071
SADU17	grt-mica schist	I Corn de Golin	32T 512458 5133071
SADU18	mylonite	Laura	32T 507749 5117842
SADU19	grt-mylonite	Laura	32T 507749 5117842
SADU20	grt-amphibolite	Gorduno	32T 502241 5118385
SADU21	eclogite	Gorduno	32T 502241 5118385
SADU22	eclogite	Alpe Arami	32T 498728 5119544
SADU23	eclogite	Pass de Ganan	
SADU24	eclogite	Pass de Ganan	
SADU25	eclogite	Pass de Ganan	
SADU26	grt-mica schist	Pass de Ganan	
SADU27	grt-mica schist	Pass de Ganan	
SADU28	eclogite/ amphibolite	Pass de Ganan	
SADU30	gneiss	Vals	32T 512357 5160927
SADU31	grt-amphibolite	Vals	32T 511423 5160354
SADU32	grt-amphibolite	Vals	32T 511605 5160379
SADU33	eclogite	Fanellahorn	32T 510726 5155408
SADU34	grt-amphibolite	Fanellahorn	32T 510415 5155151
SADU35	grt-mica schist	Fanellahorn	32T 510784 5155829
SADU36	grt-mica schist	Zapport	32T 506379 5149965
SADU37	grt-mica schist	Alp de Trescolmen	32T 513611 5137971
SADU38	eclogite	Alp de Trescolmen	32T 513654 5137902
SADU39	grt-mica schist	Alp de Trescolmen	32T 513602 5137983
SADU40	eclogite	Zerfreiler	32T 508957 5158701
SADU41	grt-amphibolite	Val Grono	32T 514075 5119861
SADU42	eclogite	Alta Burasca	32T 512848 5139592
SADU43	grt-mica schist	Alta Burasca	32T 512839 5139514
SADU44	grt-mica schist	Confin Basso	32T 513127 5145021
SADU45	grt-mica schist	Confin Basso	32T 513127 5145021
SADU47	eclogite	Confin Basso	32T 513006 5145388
SADU48	eclogite	Confin Basso	32T 513006 5145388
SADU49	eclogite	Confin Basso	32T 513006 5145388
SADU50	grt-mica schist	Alp de Confin	32T 512007 5144349
SADU51	grt-amphibolite	Piz d'Arbeola	32T 512444 5141964
SADU52	grt-amphibolite	Piz d'Arbeola	32T 512444 5141964
SADU53	grt-mica schist	Piz d'Arbeola	32T 513189 5143218

(continues on next page)

Table 7.7: continued from previous page

Sample	Lithology	Location	Coordinates
SADU54	grt-mica schist	Piz d'Arbeola	32T 513189 5143218
TRC1	eclogite	Alp de Trescolmen	32T 513654 5137902
S34	eclogite	Radkovec	33T 536612 5139064
S89	eclogite	Jurisna Vas	33T 540062 5140956
S119	grt-websterite	Radkovec	33T 536667 5138931
FK99	grt-lherzolite	Kostanjevec	33T 539820 5138338
Gr1	amphibolite	Val Bregaglia	32T 535930 5129519
Gr2	serpentinite	Val Bregaglia	32T 536069 5128834
Gr3A	bt-orthogneiss	Val Bregaglia	32T 536152 5128729
Gr3B	bt-orthogneiss	Val Bregaglia	32T 536152 5128729
Gr3C	bt-orthogneiss	Val Bregaglia	32T 536152 5128729
Gr4A	gneiss/ mica schist	Val Bregaglia	32T 536420 5128761
Gr4B	gneiss/ mica schist	Val Bregaglia	32T 536420 5128761
Gr5A	migmatic bt-gneiss	Val Bregaglia	32T 537131 5127542
Gr6	serpentinite	Val Bregaglia	32T 535517 5128856
Gr7	mica schist	Val Bregaglia	32T 543150 5129895
Gr7B	mica schist	Val Bregaglia	32T 543150 5129895
Gr8	mica schist	Val Bregaglia	32T 543058 5129809
Gr9	orthogneiss	Val Bregaglia	32T 542788 5129632
Gr10	mica schist	Val Bregaglia	32T 542617 5129509
Gr11	serpentinite	Val Bregaglia	32T 542579 5129291
Gr12	gneiss	Val Bregaglia	32T 542551 5129005
Gr13	granodiorite (Bergell)	Valle dei Ratti	32T 542173 5117724
Gr13B	granodiorite (Bergell)	Valle dei Ratti	32T 542173 5117724
Gr14	gneiss	Valle dei Ratti	32T 542181 5118011
Gr15	mica schist	Valle dei Ratti	32T 542127 5118132
Gr16	migmatic gneiss	Valle dei Ratti	32T 542162 5118311
Gr17	migmatic gneiss	Valle dei Ratti	32T 542154 5118552
Gr18	gneiss	Valle dei Ratti	32T 541925 5118613
Gr19	migmatic gneiss with grt	Valle dei Ratti	32T 542385 5118626
Gr20	gneiss	Valle dei Ratti	32T 542764 5117903
Gr21	vein of qz	Valle dei Ratti	32T 542744 5117912
Gr22	vein of qz	Valle dei Ratti	32T 542721 5117909
Gr23	bt-orthogneiss	Valle dei Ratti	32T 542721 5117909
Gr24	migmatic orthogneiss	Valle dei Ratti	32T 541454 5118237
Gr25	orthogneiss	Valle dei Ratti	32T 541199 5117875
Gr26	orthogneiss	Val Codera	32T 541516 5122354
Gr27	orthogneiss	Val Codera	32T 540996 5122363
Gr28	orthogneiss	Val Codera	32T 540770 5122517
Gr29	migmatic bt-gneiss	Val Codera	32T 541367 5122824
Gr31	orthogneiss	Val Codera	
Gr32	migmatic orthogneiss	Val Codera	
Gr33	migmatic orthogneiss	Val Codera	
Gr34	migmatic gneiss	Val Codera	
Gr35	migmatic gneiss	Val Codera	
Gr36	migmatic orthogneiss	Val Schiesone	32T 533960 5126585
Gr37	migmatic orthogneiss	Val Schiesone	32T 534014 5126493
Gr38	migmatic orthogneiss	Val Schiesone	32T 534014 5126493
Gr39	gneiss	Val Schiesone	32T 531589 5126713